Title	Catalytic Reactions Driven Under Aerobic Conditions Using Gold Nanoparticles Deposited on Citric Acid-Modified Cellulose
Author(s)	Suwattananuruk, Butsaratip
Citation	大阪大学, 2024, 博士論文
Version Type	VoR
URL	https://doi.org/10.18910/101451
rights	
Note	

Doctoral Dissertation

**Catalytic Reactions Driven Under Aerobic Conditions
Using Gold Nanoparticles
Deposited on Citric Acid-Modified Cellulose**

(クエン酸変性セルロース担持金ナノ粒子を用いる

大気雰囲気下で駆動する触媒反応)

Suwattananuruk Butsaratip

August 2024

Department of Applied Chemistry
Graduated School of Engineering
Osaka University

Table of content

General Introduction

1. Introduction to gold nanoparticles

Gold has been considered one of the most inert metals due to the fact that it is the only metal with endothermic chemisorption energy, which prevents it from bonding with oxygen (**Figure 1**).[1] This can be explained by considering the interaction between the oxygen valence states and the metal d-states, as described in the d-band model.[2,3] In the case of gold, its d-states are at such a low energy level that the interaction with oxygen 2p-states results in net repulsion. Consequently, it is unlikely that gold would serve effectively as a catalyst for oxidation reactions.
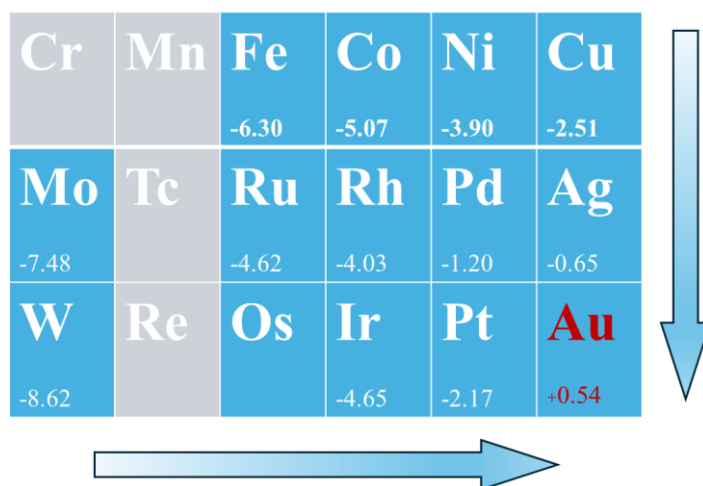

Figure 1. The energies for dissociative chemisorption of oxygen on transition metal surfaces, relative to a molecule in vacuum calculated by density functional theory (DFT). All results are for adsorption at either a body-centered cubic (210) surface (for Fe, Mo, W) or a face-centered cubic (211) surface (other metals)[3,4]

For a long time, the catalytic activity of gold was not well understood. However, in the late 1980s, Haruta made a groundbreaking discovery by identifying that gold particles at the nanometer scale, known as gold nanoparticles (AuNPs), are highly efficient catalysts. Haruta and co-workers found that AuNPs were surprisingly active, even at low temperatures, for many kinds of reactions such as CO oxidation and propylene epoxidation.[5–6] Since then, reports on gold-based catalysts have garnered significant attention in recent years because they function well under mild conditions in a variety of organic transformations with good regio- and chemo-selectivity.[7–8] Unlike bulk gold, which is generally considered inactive, gold in the form of nanometer-sized particles exhibits a high corner-to-surface ratio (**Figure 2**).[3b] Additionally, significant quantization of the conduction band occurs

when AuNPs become exceedingly small. These quantum-sized display multiple optical absorption peaks in their spectra and often have non-face-centered cubic (non-fcc) atomic packing structures, unlike larger nanocrystals which typically have fcc structures.[9] Consequently, AuNPs exhibit unique fluorescent[10], chiral[11], and magnetic properties[12] as well as high chemical reactivities.[5–6] Therefore, it is clear that the catalytic activity is highly dependent on the size of AuNPs.
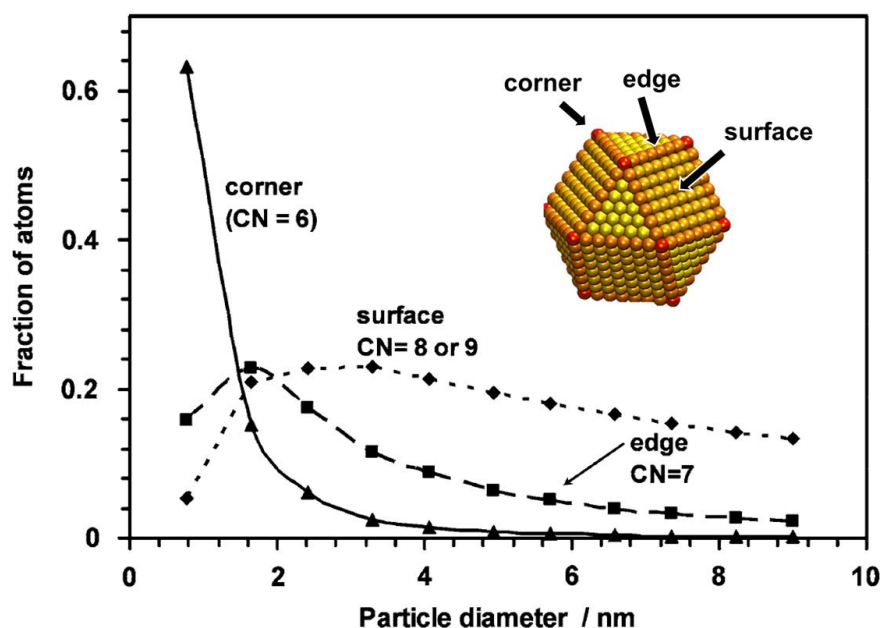

Figure 2. Calculated fractions of Au atoms at corners, edges, and crystal faces in uniform nanoparticles consisting of the top half of a truncated octahedron as a function of the AuNPs diameter.[3b]

Catalysts commonly contain very small size of metal particles, typically in the nanometer range, dispersed onto a solid support to stabilize them.[13] Haruta found that differently supported AuNPs exhibit different catalytic activity for low-temperature CO oxidation.[5] Hutchings predicted and proved that supported gold is the preferred catalyst for synthesizing vinyl chloride monomer through the acetylene hydrochlorination reaction.[14] Since then, solid-supported gold catalysis has garnered significant attention from both academic and industrial research communities.[15,16] It has become evident that the nature of the support material and the interaction of gold-support interfacial sites are crucial not only for stabilizing AuNPs but also for influencing the catalytic behavior of supported AuNPs.[17] Up to the present, a significant part of the research on nanocatalysis has been focused on AuNPs, owing to their simple and well-known fabrication methods as well as on the intriguing synergistic effect of support on a variety of reactions.[18]

2. Size-dependent catalytic activity

The catalytic activity of AuNPs is influenced by several factors, with particle size being one of the most crucial.[19] This is because the surface area of nanoparticles, which is inversely proportional to their size, plays a key role. For instance, Tsunoyama and colleagues discovered that smaller AuNPs stabilized by poly(*N*-vinyl-2-pyrrolidone) (PVP) exhibited significantly higher catalytic activity in the oxidation of p-hydroxybenzyl alcohol.[20] Jawale et al. investigated the catalytic activity of small (3 nm) and larger (20 nm) AuNPs supported on carbon nanotubes across a range of chemical reactions, including silane oxidation, alcohol oxidation, and reductive amination. In all cases, the reaction rates observed for the smaller AuNPs were at least 5.5 times higher than those for the larger ones.[21]

The nitroaromatic reduction is a common model reaction for determining the catalytic activity of metal nanoparticles.[22] Aromal and coworkers found a full reduction of 4-nitrophenol in the presence of 20 nm AuNPs after 30 minutes, but the reaction took only 15 min when 15 nm AuNPs were used.[23]
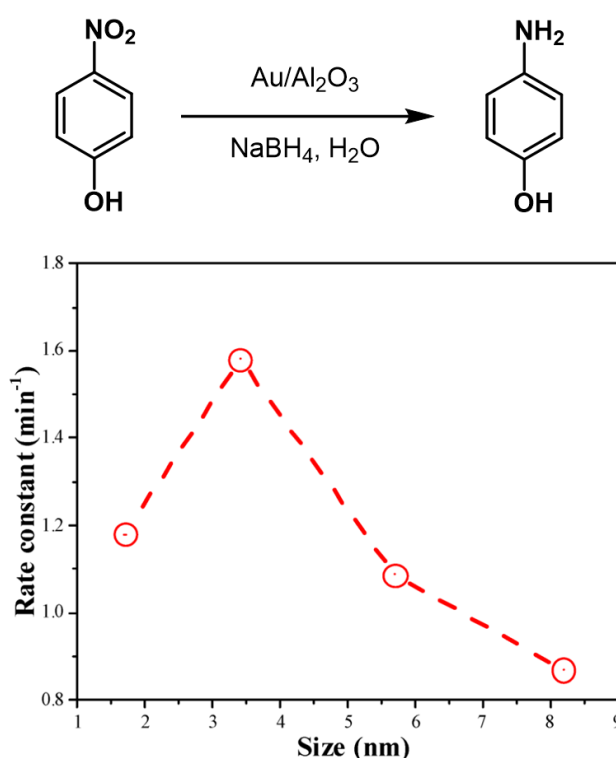

Figure 3 The correlation between the rate constants and the Au particle sizes of AuNPs.[25]

Although extremely small nanoparticles with dimensions in the nanometer range, or even smaller down to sub-nanometer size,[24] can be synthesized, it has been observed that the catalytic activity of AuNPs does not always increase proportionally with particle size reduction. For instance, Lin et al.

found that the highest catalytic activity in the reduction of 4-nitrophenol with Au/Al_2O_3 was not achieved with the smallest NPs of 1.7 nm, but rather with larger nanoparticles measuring 3.4 nm in diameter (**Figure 3**).[25] This suggests that, for this reaction, the facet atoms (surface) exhibit higher activity compared to the edge and corner atoms of the particles.[26]

Corma et al. demonstrated that the geometric and electronic differences between small (< 2 nm) and large AuNPs significantly influence their activity and selectivity. Their theoretical and experimental studies showed that small planar particles are highly active in reactions involving Lewis acid-base interactions to activate C–C multiple bonds in alkenes and alkynes.[27]

Since the catalytic activity of different-sized AuNPs is dependent on their size, a robust and reliable process for size-selective production of AuNPs, especially with a limited size distribution, is required.

3. Size-controlled preparation of gold nanoparticle and Trans-deposition method

The catalytic activity of metal nanoparticles activity is known to be substantially influenced by their particle sizes.[26] As a result, developing a method for size-controlled metal nanoparticles synthesis is a promising way to fine-tune their catalytic activity. Former research groups have developed procedures for size-selective preparation of AuNPs using poly(*N*-vinyl-2-pyrrolidone) (PVP) as a stabilizing matrix.[28] Furthermore, using PVP(K-15) as a transient matrix, size-selectively synthesized AuNPs can be transported from PVP to other solid supports, such as hydroxyapatite, while retaining their particle size. Haesuwannakij and coworkers proposed a new method for size-controlled synthesis of AuNPs on metal oxide supports (hydroxyapatite, HAP).[28b–c] This method is called trans-deposition process (**Figure 4**). The PVP-stabilized AuNPs with different particle sizes were used as Au precursors. The AuNPs, protected by the hydrophilic polymer PVP, were successfully transferred to HAP without a substantial size change. The method facilitated the preparation of Au:HAP with a wide range of diameters, from 1 to 8 nm It is a practical and reproducible approach for the size-controlled preparation of metal nanoparticles.[28]
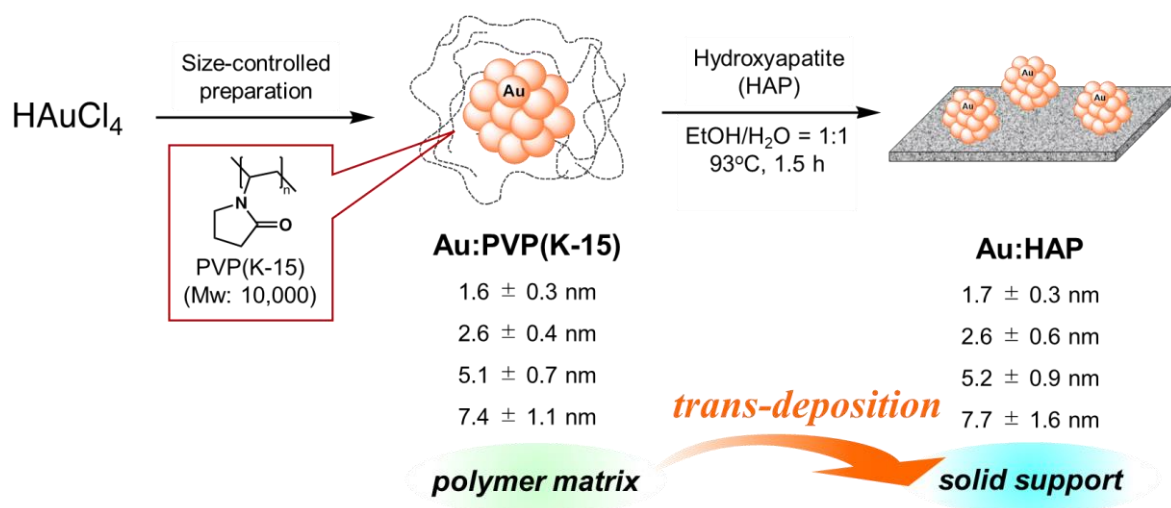
Figure 4. Size-controlled synthesis of AuNPs on PVP and transfer to hydroxyapatite via trans-deposition process.[28c]

4. Supported gold nanoparticles

In the field of supported metal catalysts, support materials were traditionally viewed as inert, primarily functioning to enhance the stability of small metal particles by anchoring them. In the beginning, traditional impregnation techniques were used to manufacture AuNPs on supported substrates utilizing chloroauric acid ($HAuCl_4$) as the gold precursor. After the calcination step, comparatively large AuNPs (i.e., >30 nm) were typically produced, and the resulting catalysts were eventually inactive.[29] Subsequent investigation determined that the inefficiency of impregnation method was caused by (i) the weak interaction between $[AuCl_4]^-$ ion and metal oxide surface in an acidic (pH ~ 1) environment, (ii) particle growth during the calcination step when the catalyst's chlorine content is high,[30] possibly as a result of a weak bond between the hard base of chloride ion and soft acid of cationic Au, and (iii) poisoning of the active areas with chlorine.[30,31] As a result, many techniques for producing AuNPs catalysts were created to counteract these negative effects. One of the primary methods for producing supported AuNPs is deposition-precipitation. This technique was first successfully employed in the early 1990s by Haruta and colleagues to produce active AuNP catalysts.[32,33] Preformed TiO_2 particles are initially combined with $HAuCl_4$, followed by the deposition-precipitation method. Using similar techniques, AuNPs have been deposited on various oxide supports, including Fe_2O_3,[34] Al_2O_3,[32] and MgO.[33] In this thesis, the author also applied this method to deposit AuNPs on solid support.

After established of deposition-precipitation method, Haruta investigated catalytic activity of AuNPs on difference solid support and found that differently supported AuNPs exhibit different catalytic activity for low-temperature CO oxidation.[5] In 1987, Tauster introduced the concept of

strong metal-support interaction (SMSI) to explain the unusual H_2 chemisorption properties observed in noble metal NPs supported on TiO_2.[35] Following this, the potential roles of support materials were investigated at a fundamental level, mostly using model catalysts.[36]

Supports can influence catalytic reactions either directly or indirectly through various mechanisms. The support can significantly affect the electronic structure of nanoparticles, particularly through charge transfer between the support and the nanoparticles (**Figure 5a**). This interaction can influence the stability, shape, and chemical reactivity of the nanoparticles.[37] For example, charge transfer in the metal close to the Au-CeO_x interface facilitated CO_2 adsorption and activation for CO_2 hydrogenation to methanol.[38] The support can also influence the reactivity of metal nanoparticles (NPs) by altering their chemical properties. One key mechanism responsible for such chemical modifications is Strong Metal-Support Interaction (SMSI). For example, metal clusters supported on TiO_2 may experience deactivation of NPs at high temperatures in a reducing environment. This deactivation occurs because the NPs become encapsulated, with their active sites covered by substrate atoms, leading to their inactivity (**Figure 5b**).[39] Another possible interaction is the combined role of NPs and their support through the process of spillover. Spillover refers to the migration of an adsorbate molecule or atom from one surface to another (from substrate to NPs, or vice versa) where it would not adsorb individually. This migration can be a crucial step in a chemical reaction. For instance, hydrogen and oxygen spillover have a significant impact on catalytic processes, facilitating reactions by efficiently transferring reactants between the support and the NPs (**Figure 5c**).[40] Moreover, support can provide specific defect sites that anchor and stabilize metal NPs, including metastable particles. Supports also facilitate electron transfer to or from the metal particles and contribute additional functionalities such as acidity or basicity to the overall supported metal catalyst. These factors can significantly affect the catalytic properties of supported metal materials, a phenomenon particularly evident in supported Au-based nanoparticle catalysts.[41] Despite these studies, the role of supports in practical catalysts remains complex and is not fully understood in many cases.[42]
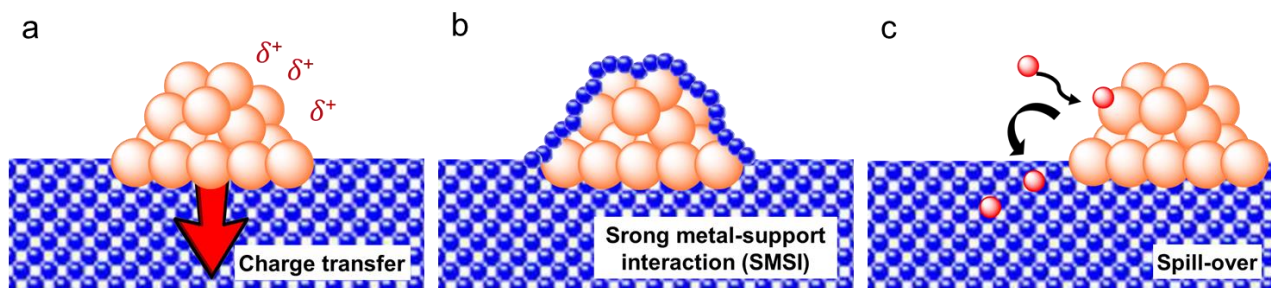

Figure 5. Example of possible effects of the support on the deposited nanoparticles.[41]

5. Polymer supported gold nanoparticles

Among several types of supported AuNPs, hybrid composites of polymeric supports with metal nanoparticles have garnered significant attention. This is because they can be easily functionalized with organic groups such as thiols, phosphines, carboxylic acids, and amines.[5,43] In addition to the aforementioned advantages, the ease of preparation in desired shapes and sizes makes polymers a unique choice for supporting the immobilization of metal nanoparticles in catalytic applications.[36] Polymer-protected AuNPs, in which AuNPs are dispersed quasi-homogeneously in a liquid such as poly(N-vinyl-2-pyrrolidone) (PVP), can be used to catalyze various chemical transformations.[44] As well as in the case of other solid supports, the polymer matrixes can control the reactivity and selectivity of the catalytic reaction. In addition, it can also stabilize and regulate the size of the AuNPs. For example, PVP can enhance catalytic activity in the aerobic oxidation of alcohols by donating electron density to the gold surface. As a result of that, PVP-supported AuNPs have higher catalytic activity than AuNPs supported on other protective polymers, such as poly(vinyl alcohol) or poly(allylamine).[45]
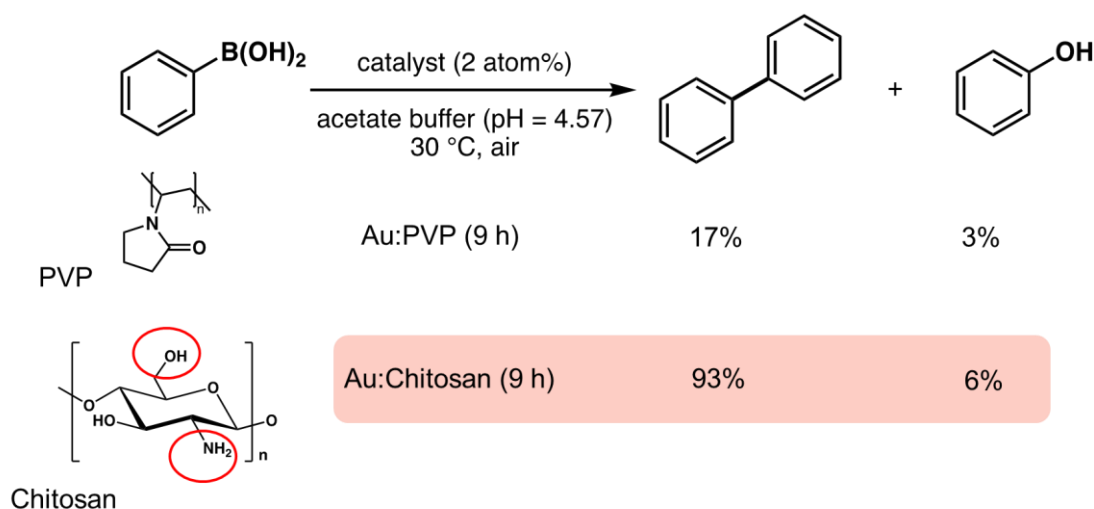

Figure 6. The homocoupling reaction of phenylboronic acids catalyzed by AuNPs.

Other polymer supports have also been explored. For instance, Dhital and co-workers proposed that AuNPs stabilized by polyhydroxylated biopolymer matrices such as chitosan exhibit significantly enhanced catalytic activity in the homocoupling reaction of phenylboronic acids compared to AuNPs supported on PVP (**Figure 6**). This is because the reaction requires basic conditions for the formation of tetra-coordinated boronate intermediates, and acidic conditions are necessary to suppress the formation of peroxyboronate intermediates to prevent phenol formation. The hydroxy groups in chitosan play a crucial role by directing the boronic acid towards the gold surface and the amine

groups create a basic environment conducive to forming tetra-coordinated boronate intermediates, enabling the reaction under aqueous acidic conditions (**Figure 7**). Thus, polymer not only stabilizes AuNPs but also regulates their catalytic activity through its functional groups.[46]
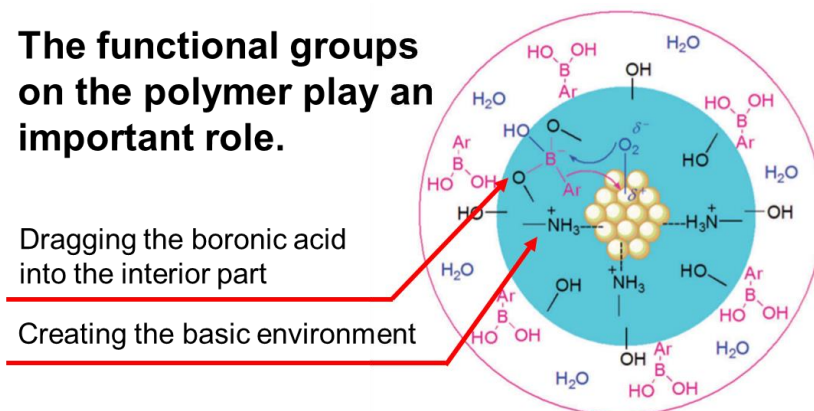

Figure 7. Dual roles polyhydroxylated biopolymer matrices

6. Cellulose and Fibrillated-Citric Acid Modified Surface Cellulose (F-CAC)

Bioresource-based functional materials, such as wood and crustacean shells, have garnered significant attention over the decades due to their contributions to sustainable development and environmentally friendly science. Among these materials, cellulose stands out as the most common macromolecule. Cellulose offers several advantages as a metal catalyst support compared to other heterogeneous supports. These benefits include a higher absorption capacity and a large number of hydroxyl groups, which provide opportunities for functionalization to various functional groups.[47] In 1982, Turbak and coworkers extracted nano cellulose such as cellulose nanofibrils (CNFs), from eucalyptus pulp using a high-pressure homogenizer.[48] As research progresses, CNFs have demonstrated high strength, flexibility, high surface area, and tunable surface chemistry, allowing for controlled interactions with polymers, nanoparticles, small molecules, and biological material.[49] CNF has been widely used in recent years owing to pioneering work by Isogai[50] and Yano[51] in a wide range of scientific and industrial sectors, including their use as a solid support for heterogeneous catalyst systems. One of the first examples of CNFs-supported AuNPs was reported by Kitaoka. The catalyst exhibited excellent catalytic efficiency, with a turnover frequency up to 840 times higher than that of conventional polymer-supported AuNPs in the reduction reaction of 4-nitrophenol.[52] Following this, Zhang and coworkers presented a green, one-pot synthesis of AuNPs on nanocellulose under hydrothermal conditions. The abundant electron-rich hydroxyl groups on the surface of nanocellulose played a key role in both the reduction and immobilization of AuNPs. Compared to unsupported AuNPs and other Au-containing catalysts, the resulting nanohybrid catalyst demonstrated

9

significantly higher catalytic activity and stability for the reduction of 4-nitrophenol.[53] Recently, Córdova and colleagues reported on a cellulose-supported AuNPs catalyst by functionalizing cellulose with mercaptopropyl silane or aminopropyl silane groups to immobilize the AuNPs. This catalyst effectively promotes the cycloisomerization of alkynoic acids and allenynamides to enol lactones and dihydropyrroles, respectively, achieving high yields. The cellulose-supported AuNPs exhibit recyclability, maintaining their efficiency and selectivity over 9 cycles. A significant discovery is that the AuNPs supported on cellulose serve as highly efficient catalysts for these transformations.[54]

The surface of cellulose has been subjected to chemical alterations to improve its physical attributes and/or provide additional functionality. Thus, research has focused on surface and chemical modification of cellulose to enhance its physical characteristics and incorporate additional features. Uyama and coworkers have developed a scalable and straightforward method for producing surface-fibrillated cellulose by modifying cellulose hydroxyl groups with citric acid (F-CAC). This method enables easy manipulation of cellulose and allows to produce large quantities of fibrillated cellulose, approximately 100 g per batch (**Figure 8**).[55] While CNFs and cellulose microfibrils prepared by physical fibrillation methods using a grinding mill often suffer from fibril agglomeration at high concentrations, the electrostatic repulsion between citric acid moieties on each cellulose fibril prevents such agglomeration. This retention of their fibrillated state ensures the stability and effectiveness of the fibrillated cellulose.[56]

F-CAC is particularly intriguing due to its derivation from cellulose which is abundant on Earth and the method for functionalizing is simply making it very easy to prepare. This material exhibits high resistance to organic solvents and a large surface area, making it an excellent candidate for solid support of nanoparticles. The presence of carboxylic groups enables immobilization of metal ions and provides Brønsted acidity. Its dispersibility allows for use as a heterogeneous catalyst, and its intrinsic chirality offers the potential for stereoselective catalysis. These advantageous properties make F-CAC a promising solid support material for various catalytic applications.
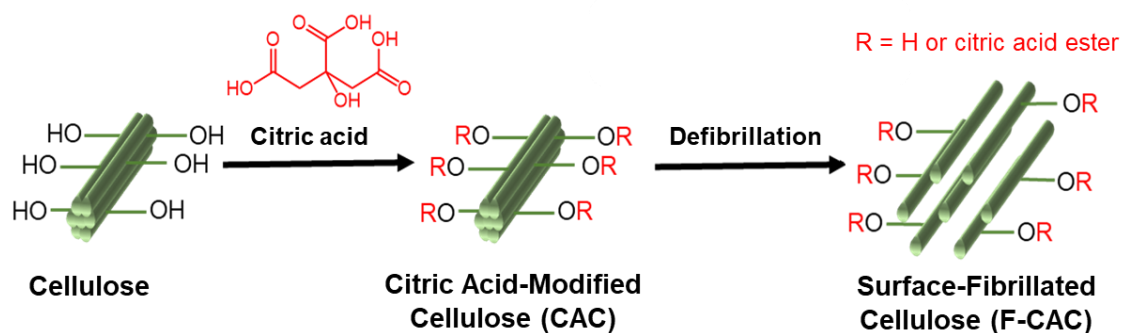

Figure 8. Fibrillated-citric acid modified surface cellulose

7. Introduction to the present work

Previous studies have demonstrated that PVP stabilized AuNPs (Au:PVP) exhibited excellent catalytic activity toward the oxidation of alcohols.[45] AuNPs stabilized by biopolymers, such as chitin and/or chitosan, show higher catalytic activity toward aerobic homocoupling of phenylboronic acid than Au:PVP.[46] In this context, functional groups on chitosan play an important role in regulating and improving the catalytic activity of AuNPs. In this thesis, the use of F-CAC as a solid support was researched. Unlike chitosan, F-CAC features acidic functional groups instead of basic ones, which may lead to novel catalytic properties. In addition, cellulose is abundant on Earth, and its functionalization is simple. Moreover, it is resistant to organic solvents, which is perceived as a good property for solid support of nanoparticles. Size-selective Au:PVP was transferred to F-CAC via trans-deposition method.[28c] The thus-prepared Au:F-CAC was successfully applied to the aerobic oxidation of benzyl alcohol. The Au:F-CAC catalyst was found to be reusable for at least six cycles without a significant loss of catalytic activity. Additionally, the particle size of Au:F-CAC remained unchanged even after the sixth cycle, demonstrating the stability of the composite.[57]

In this doctoral thesis, the author expanded the unique applications of Au:F-CAC. Previously studies have demonstrated the use of F-CAC in the oxidation of indanol in basic conditions. However, citric acid on the cellulose surface can serve as a solid Brønsted acid, leading to base consumption through neutralization with the solid support, necessitating an excess of base. The author aims to leverage the utility of this catalyst for other reactions that proceed under acidic or neutral conditions to highlight the merit of the solid Brønsted acid functional group on F-CAC, potentially leading to novel catalytic activities in various organic transformations.
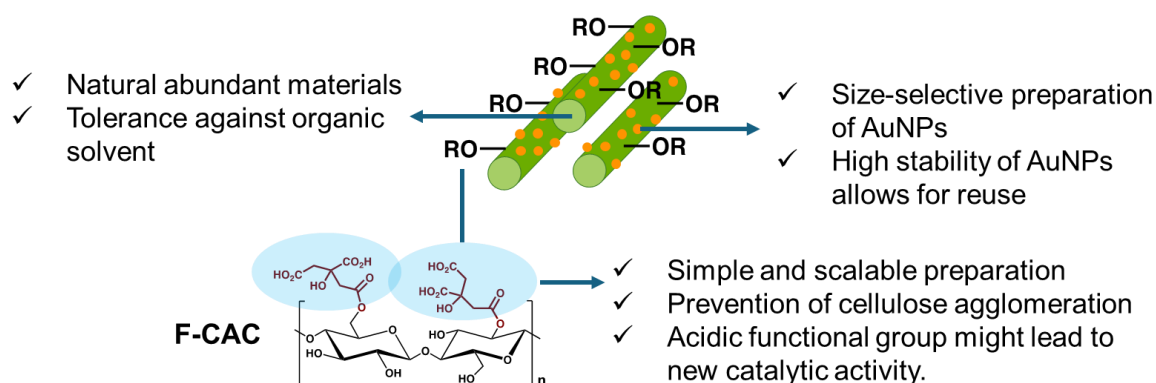

Figure 9. Advantages of Au:F-CAC

Chapter 1: Preparation of Au:F-CAC

In chapter 1, the author details the preparation of Au:F-CAC and addresses significant issues with reproducibility. Although Au:F-CAC was successfully prepared, achieving consistent results proved challenging, particularly in the reproducibility of the F-CAC preparation process. The efficiency of transferring AuNPs to F-CAC varied from 90% to 40%. Thus, establishing a reproducible method to synthesize Au:F-CAC was crucial. The reasons for irreproducibility were narrowed down to 4 main factors. The first one was the amount of citric acid on the surface of F-CAC. This could be controlled by the temperature and time to bake the F-CAC. The second factor was the carboxylic group on citric acid could be in either sodium salt form or acid form. Another factor is surface morphology which was altered by changing the machine used to fibrillate F-CAC. The fibrillation time was also taken into consideration. The final factor was the method of transferring AuNPs. The amount of F-CAC, solvent, and gold was optimized. All these factors were studied and optimized to establish a reproducible procedure for synthesizing Au:F-CAC.

Chapter 2: Intramolecular hydroamination catalysed by gold nanoparticles deposited on fibrillated cellulose

In chapter 2, the author describes intramolecular hydroamination, which has been found to yield good results under slightly acidic conditions. Au:F-CAC was explored for its ability to create an acidic environment and its reusability. The Au:F-CAC catalyst facilitates the intramolecular cycloamination of amines with unactivated alkenes under aerobic conditions, yielding pyrrolidine derivatives. A minimal loading of just 0.2 atom% Au:F-CAC is sufficient for complete conversion. The catalyst's remarkable sensitivity to the alkene's substitution pattern enables a distinctive chemoselective cycloamination, yielding novel compounds.
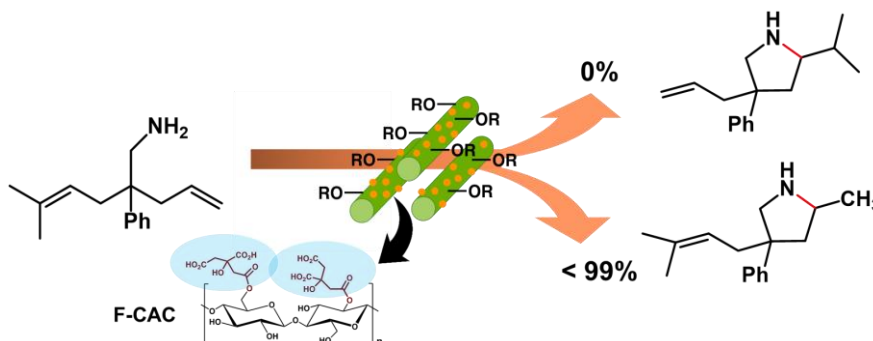

Figure 10. Chemoselective cycloamination by Au:F-CAC

Chapter 3: Dehydrogenative Oxidation of Hydrosilanes Using Gold Nanoparticle Deposited on Citric Acid-Modified Fibrillated Cellulose: Unveiling the Role of Molecular Oxygen

In chapter 3, the author discusses the dehydrogenative oxidation of hydrosilanes, a reaction typically performed in water. The study investigated the possibility of using the catalyst in organic solvents, capitalizing on the high tolerance of F-CAC towards such solvents. This reaction proceeded under neutral conditions, with the carboxylic group on F-CAC helping stabilize the AuNPs. The stability of Au:F-CAC in the reaction provides the possibility for kinetic studies on size dependency of AuNPs. Au:F-CAC catalysts of varying particle sizes (1.7 nm, 4.9 nm, and 7.7 nm) were synthesized using the trans-deposition method, a technique previously developed. These catalysts demonstrated remarkable catalytic activity for producing silanols with high turnover frequencies. Mechanistic studies, including isotope labeling experiments, kinetics, and spectroscopic analyses, enabled to elucidate that catalytically active cationic Au sites form on the surface through the adsorption of molecular oxygen. These findings provide novel insights into the reaction mechanism.
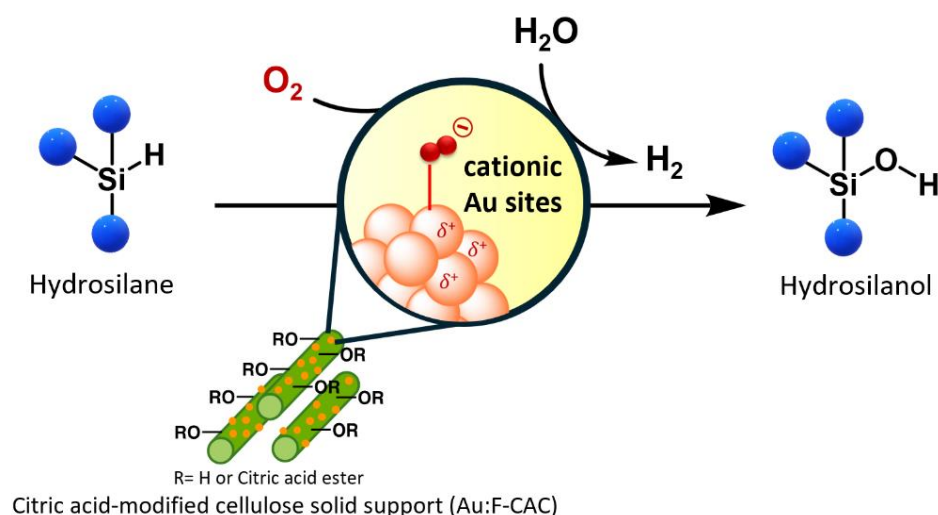
Figure 11. Oxidation of hydrosilanes through cationic Au sites on F-CAC

Chapter 4: Dehydrosilylation of Alcohols Using Gold Nanoparticles Deposited on Citric Acid-modified Fibrillated Cellulose

In chapter 4, the author extended the work from chapter 3 to the dehydrosililation of alcohols, due to the similarity of reaction mechanism. The catalyst exhibited remarkable catalytic activity under mild conditions with 0.01–0.05 mol% of Au loading, facilitating the formation of silyl ethers with excellent yield. The study found that the high catalytic activity of Au:F-CAC can overcome the limitation of requiring excess alcohol for silly alcohol protection applications. This work presents a

significant advancement in the field of dehydrosilylation catalysis, offering a sustainable, efficient, and environmentally friendly approach for the synthesis of functional silanol-based materials and alcohol protection applications. The scope of substrates and the utility of the catalyst have been thoroughly studied.
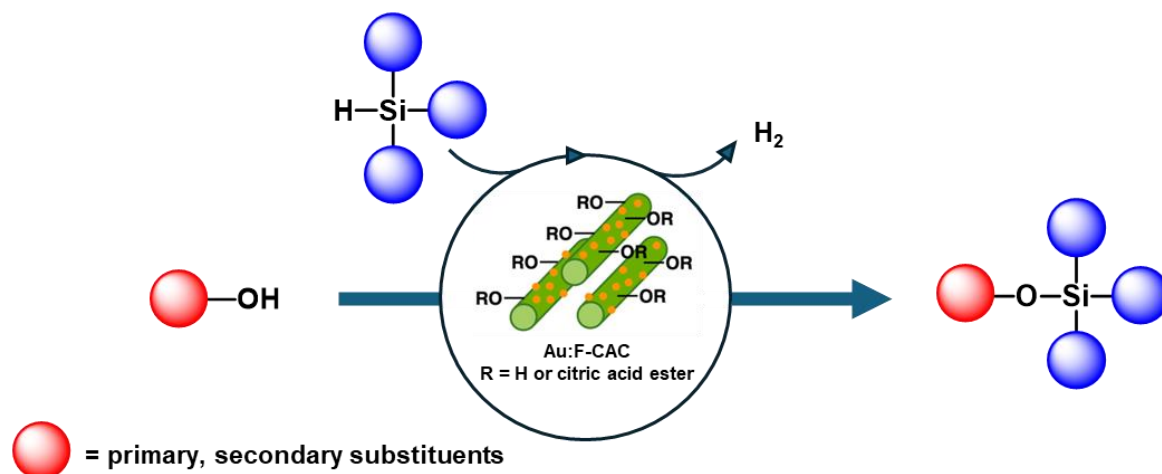

Figure 12. Dehydrosililation of alcohols by Au:F-CAC

References

1. J. Kim, E. Samano, B. E. Koel, *Surf. Sci.* **2006**, *600*, 4622.

2. B. Hammer, J. Norskov, *Nature* **1995**, *376*, 238.

3. (a) B. Hvolbæk, T. V. W. Janssens, B. S. Clausen, H. Falsig, C. H. Christensen, J. K. Nørskov, *Nano Today* **2007**, *2*, 14. (b) T. V. W. Janssens, B. S. Clausen, B. Hvolbæk, H. Falsig, C. H. Christensen, T. Bligaard, J. K. Nørskov, *Top. Catal.* **2007**, *44*, 15.

4. T. Bligaard, J. K. Nørskov, S. Dahl, J. Matthiesen, C. H. Christensen, J. Sehested, *J. Catal.* **2004**, *224*, 206.

5. M. Haruta, T. Kobayashi, H. Sano, N. Yamada, *Chem. Lett.* **1987**, 405.

6. M. Haruta, *Chem. Rec.* **2003**, *3*, 75.

7. B. S. Takale, M. Bao, Y. Yamamoto, *Org. Biomol. Chem.* **2014**, *12*, 2005.

8. Q.-Y. Yang, Y. Zhu, L. Tian, S.-H. Xie, Y. Pei, H. Li, H.-X. Li, M.-H. Qiao, K.-N. Fan, *Appl. Catal., A* **2009**, *369*, 67.

9. (a) H. Qian, M. Zhu, Z. Wu, R. Jin, *Acc. Chem. Res.* **2012**, *45*, 1470.

10. (a) J. Heng, J. T. Petty, R. M. Dickson, *J. Am. Chem. Soc.* **2003**, *125*, 7780. (b) Z. Wu, R. Jin, *Nano Lett.* **2010**, *10*, 2568.

11. (a) H. Yao, K. Miki, N. Nishida, A. Sasaki, K. Kimura. *J. Am. Chem. Soc.* **2005**, *127*, 15536. (b) M. Zhu, H. Qian, X. Meng, S. Jin, Z. Wu, R. Jin, *Nano Lett.* **2011**, *11*, 3963.

12. (a) M. Hu, C. M. Aikens, M. P. Hendrich, R. Gupta, H. Qian, G. C. Schatz, R. Jin, *J. Am. Chem. Soc.* **2009**, *131*, 2490. (b) Y. Negishi, H. Tsunoyama, M. Suzuki, N. Kawamura, M. M. Matsushita, K. Maruyama, T. Sugawara, T. Yokoyama, T. Tsukuda, *J. Am. Chem. Soc.* **2006**, *128*, 12034.

13. M. Sankar, Q. He, R. V. Engel, M. A. Sainna, A. J. Logsdail, A. Roldan, D. J. Willock, N. Agarwal, C. J. Kiely, G. J. Hutchings, *Chem. Rev.* **2020**, *120*, 3890.

14. G. J. Hutchings, *J. Catal.* **1985**, *96*, 292.

15. X. Y. Liu, A. Wang, T. Zhang, C.-Y. Mou, *Nano Today* **2013**, *8*, 403.

16. R. Ciriminna, E. Falletta, C. Della Pina, J. H. Teles, M. Pagliaro, *Angew. Chem., Int. Ed.* **2016**, *55*, 14210.

17. A. Corma, H. Garcia, *Chem. Soc. Rev.* **2008**, *37*, 2096.

18. (a) J. Kimling, M. Maier, B. Okenve, V. Kotaidis, H. Ballot, A. Plech, *J. Phys. Chem., B* **2006**, *110*, 15700. (b) C. Daruich De Souza, B. Ribeiro Nogueira, M. E. C. M. Rostelato, *J. Phys. Chem. Solids* **2019**, *798*, 714.

19. (a) P. Freund, M. Spiro, *J. Phys. Chem.* **1985**, *89*, 1074. (b) C. Burda, X. Chen, R. Narayanan, M. A. El-Sayed, *Chem. Rev.* **2005**, *105*, 1025. (c) O. M. Wilson, M. R. Knecht, J. C. Garcia-Martinez, R. M. Crooks, *J. Am. Chem. Soc.* **2006**, *128*, 4510. (d) G. L. Bezemer, J. H. Bitter, H. P. C. E. Kuipers, H. Oosterbeek, J. E. Hollewijn, X. Xu, F. Kapteijn, A. J. van Dillen, K. P. de Jong, *J. Am. Chem. Soc.* **2006**, *128*, 3956.

20. H. Tsunoyama, H. Sakurai, H. Tsukuda, *Chem. Phys. Lett*. **2006**, *429*, 528.

21. V. Jawale, E. Gravel, V. Geertsen, H. Li, N. Shah, R. Kumar, J. John, I. N. Namboothiri, E. Doris, *Tetrahedron*. **2014**, *70*, 6140.

22. M. Q. Yang, X. Pan, N. Zhanga, Y. J. Xu, *CrystEngComm*. **2013**, *15*, 6819.

23. S. A. Aromal, K. D. Babu, D. Philip, *Spectrochim. Acta A Mol. Biomol. Spectrosc*. **2012**, *96*, 1025.

24. S. Lin, N. Chen, S. Sun, J. C. Chang, Y. Wang, C. Yang, L. Lo, *J. Am. Chem. Soc.* **2010**, *132*, 8309.

25. C. Lin, K. Tao, D. Hua, Z. Ma, S. Zhou, *Molecules*. **2013**, *18*, 12609.

26. M. Valden, X. Lai, D. W. Goodman. *Science*. **1998**, *281*, 1647.

27. M. Boronat, A. Pérez, A.Corma, *Acc. Chem. Res*. **2014**, *47*, 834.

28. (a) H. Tsunoyama, H. Sakurai, H. Negishi, Y. Tsukuda, *J. Am. Chem. Soc.* **2005**, *127*, 9374. (b) S. Haesuwannakij, W. Karuehanon, V. L. Mishra, H. Kitahara, H. Sakurai, S. Kanaoka, S. Aoshima, *Monatsh. Chem.* **2014**, *145*, 23. (c) S. Haesuwannakij, T. Poonsawat, M. Noikham, E. Somsook, Y. Yakiyama, R. N. Dhital, H. Sakurai, *Nanosci. Nanotechnol*. **2017**, *17*, 4649.

29. M. Haruta, *CATTECH* **2002**, *6*, 102.

30. H. Oh, *J. Catal.* **2002**, *210*, 375.

31. C. K. Costello, M. C. Kung, H.-S. Oh, Y. Wang, H. H. Kung, *Appl. Catal., A* **2002**, *232*, 159.

32. M. Haruta, S. Tsubota, T. Kobayashi, H. Kageyama, M. J. Genet, B. Delmon, *J. Catal.* **1993**, *144*, 175.

33. S. Tsubota, M. Haruta, T. Kobayashi, A. Ueda, Y. Nakahara, *Stud. Surf. Sci. Catal.* **1991**, *63*, 695.

34. D. Andreeva, T. Tabakova, V. Idakiev, P. Christov, R. Giovanoli, *Appl. Catal., A* **1998**, *169*, 9.

35. S. J. Tauster, *Acc. Chem. Res.* **1987**, *20*, 389.

36. P. Priecel, H. Adekunle, S. Romen, H. Padilla, Z. Zhong, J. A. Sancheza, *Chin. J. Catal.* **2016**, *37*, 1619.

37. (a) A. M. Venezia, V. L. Parola, B. Pawelec, J. L. G. Fierro, *Appl. Catal., A* **2004**, *264*, 43. (b) N. Lopez, *J. Catal.* **2004**, *223*, 232. (c) J. A. Rodriguez, X. Wang, P. Liu, W. Wen, J. C.

Hanson, J. Hrbek, M. Perez, J. Evans, *Top. Catal.* **2007**, *44*, 73. (d) H. Häkkinen, S. Abbet, A. Sanchez, U. Heiz, U. Landman, *Angew. Chem., Int. Ed.* **2003**, *42*, 1297.

38. X. Yang, S. Kattel, S. D. Senanayake, J. A. Boscoboinik, X. Nie, J. Graciani, J. A. Rodriguez, P. Liu, D. J. Stacchiola, J. G. Chen, *J. Am. Chem. Soc.* **2015**, *137*, 10104.

39. (a) Q. Fu, T. Wagner, *Surf. Sci. Rep.* **2007**, *62*, 431. (b) F. Pesty, H.-P. Steinrück, T. E. Madey, *Surf. Sci.* **2001**, *487*, 269.

40. (a) V. V. Rozanov, O. V. Krylov, *Usp. Khim.* **1997**, *66*, 117. (b) W. C. Conner, J. L. Falconer, *Chem. Rev.* **1995**, *95*, 759. (c) S. J. Teichner, *Appl. Catal.* **1990**, *62*, 1.

41. M. Ahmadi, H. Mistry, B. Roldan Cuenya, *J. Phys. Chem. Lett.* **2016**, *7*, 3519.

42. M. Sankar, Q. He, R. V. Engel, M. A. Sainna, A. J. Logsdail, A. Roldan, D. J. Willock, N. Agarwal, C. J. Kiely, G. J. Hutchings, *Chem. Rev.* **2020**, 120, 3890.

43. P. Claus, A. Brückner, C. Mohr, H. Hofmeister, *J. Am. Chem. Soc.* **2000**, *122*, 11430.

44. (a) A. S. K. Hashmi, G. J. Hutchings, *Angew. Chem.* **2006**, *118*, 8064. (b) A. S. K. Hashmi, *Chem. Rev.* **2007**, *107*, 3180.

45. H. Tsunoyama, N. Ichikuni, H. Sakurai, T. Tsukuda, *J. Am. Chem. Soc.* **2009**, *131*, 7086.

46. R. N. Dhital, A. Murugadoss, H. Sakurai, *Chem. Asian. J.* **2012**, *7*, 55.

47. (a) J. Liu, A. Plog, P. Groszewicz, L. Zhao, Y. Xu, H. Breitzke, A. Stark, R. Hoffmann, T. Gutmann, K. Zhang, G. Buntkowsky, *Chem. Eur. J.* **2015**, *21*, 12414. (b) O. Levy-Ontman, B. Biton, S. Shlomov, A. Wolfson, *Polymers* **2018**, *10*, 659.

48. A. F. Turbak, A. El-Kafrawy, F. W. Snyder, A. B. Auerbach (ITT Corp.), *US-A 4352770*, **1982**.

49. (a) K. J. De France, T. Hoare, E. D. Cranston, *Chem. Mater.* **2017**, *29*, 4609.
(b) B. Thomas, M. C. Raj, K. B. Athira, M. H. Rubiyah, J. Joy, A. Moores, G. L. Drisko, C. Sanchez, *Chem. Rev.* **2018**, *118*, 11575.

50. T. Saito, S. Kimura, Y. Nishiyama, A. Isogai, *Macromolecules.* **2007**, *8*, 2485.

51. H. Yano, S. Nakahara, *J. Mater. Sci.* **2004**, *39*, 1635.

52. H. Koga, E. Tokunaga, M. Hidaka, Y. Umemura, T. Saito, A. Isogai, T. Kitaoka, *Chem. Commun.* **2010**, *46*, 8567.

53. X. Wu, C. Lu, Z. Zhou, G. Yuan, R. Xiong, X. Zhang, *Environ. Sci.: Nano* **2014**, *1*, 71.

54. L. Deiana, E. Badali, A. A. Rafi, C.-W. Tai, J.-E. Bäckvall, A. Córdova, *ACS Catal.* **2023**, *13*, 10418.

55. (a) X. Cui, T. Honda, T.-A. Asoh, H. Uyama, *Carbohydr. Polym.* **2020**, *230*, 115662. (b) X. Cui, A. Ozaki, T.-A. Asoh, H. Uyama, *Polym. Degrad. Stab.* **2020**, *175*, 109118.

17

56. (a) G. Sinawang, T. Asoh, M. Osaki, H. Yamaguchi, A. Harada, H. Uyama, Y. Takashima, *ACS Appl. Polym. Mater.* **2020**, *2*, 2274. (b) A. Sugawara, T.-A. Asoh, Y. Takashima, A. Harada, H. Uyama, *Polym. Degrad. Stab.* **2020**, *177*, 109157. (c) H. Tsuchiya, G. Sinawang, T.-A. Asoh, M. Osaki, Y. Ikemoto, Y. Higuchi, H. Yamaguchi, A. Harada, H. Uyama, Y. Takashima, *Biomacromolecules* **2020**, *21*, 3936.

57. T. Chutimasakul, Y. Uetake, J. Tantirungrotechai, T. Asoh, H. Uyama, H. Sakurai, *ACS Omega*. **2020**, *5*, 33206

Chapter 1: Preparation of Au:F-CAC

1.1   Introduction

In this chapter, the author attempted to reproduce the preparation of Au:F-CAC. Although Au:F-CAC had been prepared, the author faced a serious problem with reproducibility. In particular, the process of preparing F-CAC was found unreproducible. The method to transfer gold nanoparticles (AuNPs) to F-CAC dropped from 90% to 40%. Thus, establishing a reproducible method to synthesize Au:F-CAC is crucial. The inability to replicate the catalyst was attributed to four main factors. First, the amount of citric acid on the surface of F-CAC must be within the range of 0.8–1 mmol/g. This can be controlled by adjusting the baking temperature and time for the F-CAC. The second factor is that the carboxylic groups on the citric acid must be in the sodium form. Therefore, after synthesizing F-CAC, the pH should be adjusted to 9 to ensure the conversion of all carboxylic acid groups to their sodium form, which also affects the surface properties of F-CAC. Another factor is surface morphology, which can be altered by changing the machine used for fibrillation. The fibrillation time was also carefully considered. The final factor involves the method of transferring AuNPs, where the quantities of F-CAC, solvent, and gold were optimized.

1.2   Result and discussion
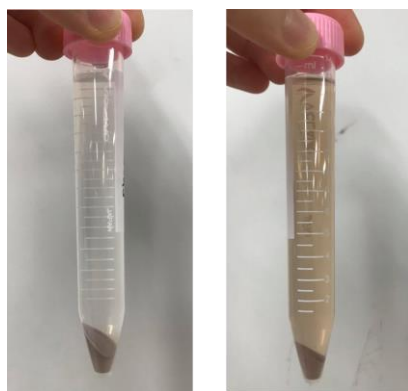
Figure 1-1. Trans-deposition with previous lot of F-CAC and second lot of F-CAC

The author followed the procedure established by a previous lab member. However, as shown in **Figure 1-1**, the color of the supernatant differed, indicating that AuNPs were not fully transferred onto F-CAC after the trans-deposition method. The gold content in the prepared Au:F-CAC was further analyzed using inductively coupled plasma atomic emission spectroscopy (ICP-AES). The results revealed that only 40% of AuNPs were transferred from PVP to F-CAC, compared to 90% in the previous sample. The primary difference between the previous procedure and the current one is

the use of a different F-CAC. Consequently, the author hypothesized that the main issue was related to the solid support (F-CAC) and began re-optimizing the preparation method. Three factors were considered: the amount of citric acid, pH adjustment, and the fibrillation method.

1.2.1. Deposition efficiency effects by amount of citric acid

Table 1-1. Effect of time and temperature toward amount of citric acid

conditions	introduction amount of citric acid (mmol/g)	deposition efficiency (%)
110 °C, 13 h	0.5	24
110 °C, 24 h	1.7	22
120 °C, 13 h	0.7	28
130 °C, 13 h	0.9	29
130 °C, 15 h	1.5	25
130 °C, 18 h	2.0	14
140 °C, 24 h	2.8	10

The general method for preparing F-CAC begins with dispersing 30 g of cellulose in 300 mL of distilled water and stirring for 5 minutes at room temperature. Then, 90 g of citric acid (CA) is added to the dispersion, followed by an additional 5 minutes of stirring. The mixture is incubated in an oven at various times and temperatures. These different times and temperatures affect the amount of citric acid incorporated into F-CAC, as shown in **Table 1-1**. This is considered the primary factor influencing the percentage deposition of AuNPs on F-CAC. The citric acid content in F-CAC was determined using a titration experiment with NaOH. The target value of citric acid content is 0.9 mmol/g, based on the citric acid percentage in the previous batch. The loading citric amount of 0.9 mmol/g was also tested for its effect on trans-deposition. Although the best deposition efficiency was observed within the range of 0.8–1 mmol/g of citric acid, it did not match the efficiency seen in previous results. Therefore, the citric acid loading was fixed at approximately 0.8–1 mmol/g. Subsequently, other factors were considered.

1.2.2. Deposition efficiency effects by pH adjustment

The next factor to be optimized was the pH adjustment during the construction of F-CAC. To assess the impact of pH on the chemical properties of the F-CAC surface, infrared (IR) spectroscopy was

employed. The results indicated that pH adjustment plays a crucial role. Esterification by citric acid was confirmed by the appearance of new peaks corresponding to carboxylic acid and ester carbonyl functionalities around 1730 cm^{-1}, along with an increase in the O-H stretching band of carboxylic acid (2800–2950 cm^{-1}). Upon deprotonation with NaOH, the ester carbonyl band formed during esterification became more distinct. Additionally, a new absorption band was observed at 1590 cm^{-1}, attributed to the sodium carboxylate of the grafted citric acid, as shown in **Figure 1-2**. The IR spectrum of F-CAC from the previous batch showed peaks corresponding to F-CAC that had been deprotonated with NaOH. Therefore, NaOH aqueous solution was added to the CAC dispersion in water to adjust the pH values to 7, 7.5, and 9, respectively. At pH levels above 7, the carboxylic acid groups are theoretically deprotonated. The pH was adjusted to 7.8 consistent with the pH used in a previous batch of F-CAC.
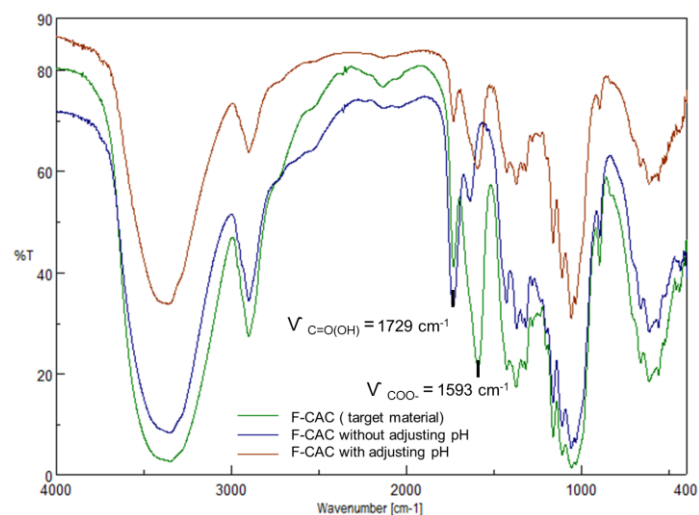
Figure 1-2. IR spectrums compare F-CAC before, after deprotonated with NaOH and previous lot of F-CAC

Table 1-2. Effect of time and temperature toward amount of citric acid

pH	deposition (%)
None	29
7	38
7.8	39
9	43

Based on previous findings, pH 9 was selected because the rod-shaped structure of cellulose is rarely

observed under these conditions. The deprotonation of carboxyl groups by NaOH produced stronger electrostatic repulsion[1] and promoted the disruption of hydrogen bonding[2] which led to the disintegration of the cellulose during mechanical fibrillation in water. Then each pH sample was used to conduct trans-deposition method, and it was found that the pH 9 sample showed the highest efficiency of 43% (**Table 1-2**).

1.2.3. Deposition efficiency effects by ratio of Au and F-CAC

The fibrillation method was optimized using three different machines. The first machine, the Starburst Mini (**Figure 1-3**), is a wet jet milling device that disperses, emulsifies, pulverizes, and exfoliates particles by colliding them into a ceramic ball under high pressure. F-CAC was fibrillated using two pressure levels: 130 Pa and 230 Pa.
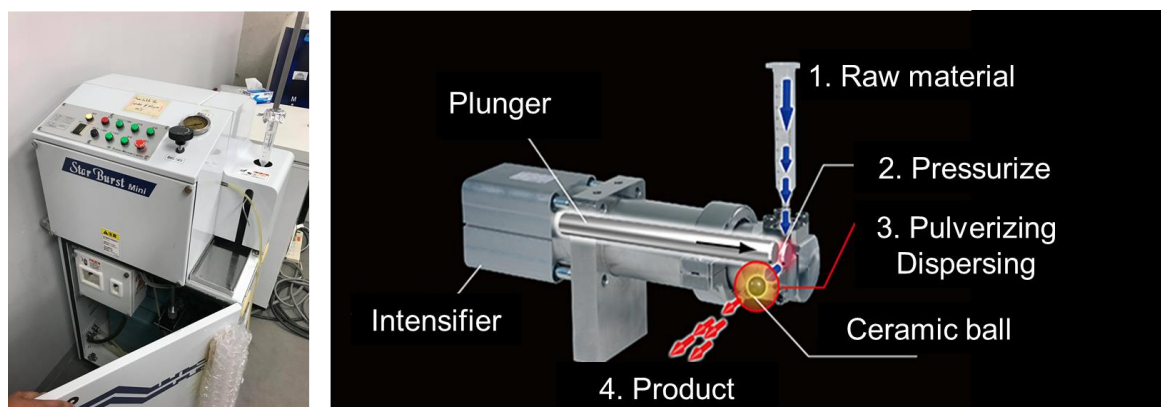
Figure 1-3. Picture of a Starburst Mini and its internal mechanism

The sample was passed through the syringe (Figure 1-3, number 1), pressurized in the machine, and then exited at number 4, completing one cycle. Gel formation was observed in the sample subjected to low-pressure fibrillation (130 Pa) for 3 cycles and high-pressure fibrillation (230 Pa) for 2 and 3 cycles. As a result, this sample was not used as a solid support. Only samples treated at 130 Pa for 1 or 2 cycles and 230 Pa for 1 cycle were freeze-dried and crushed into powder.

Trans-deposition was also conducted with these samples obtained from the Starburst Mini. F-CAC subjected to 130 Pa for 1 or 2 cycles, as well as F-CAC subjected to 230 Pa for 1 cycle, successfully completed the trans-deposition process, achieving deposition efficiencies of 92%, 90%, and 89% (**Tables 1-3**), respectively. However, instead of forming a fine powder, the obtained catalyst turned into a compact mass of F-CAC. Additionally, the gold solution was not fully dispersed on F-CAC. Some white spots were observed in the compact mass. The reason why the deposition efficiency is high might come from the fact that mild gel formation was formed and AuNPs were taped into a gel.

However, these results indicate that this machine is not suitable for constructing F-CAC as a solid support.

Table 1-3. Trans-deposition efficiency by Starburst Mini

sample	%deposition
130 Pa, 1cycle	92%
130 Pa, 2cycles	90%
230 Pa1cycle	89%
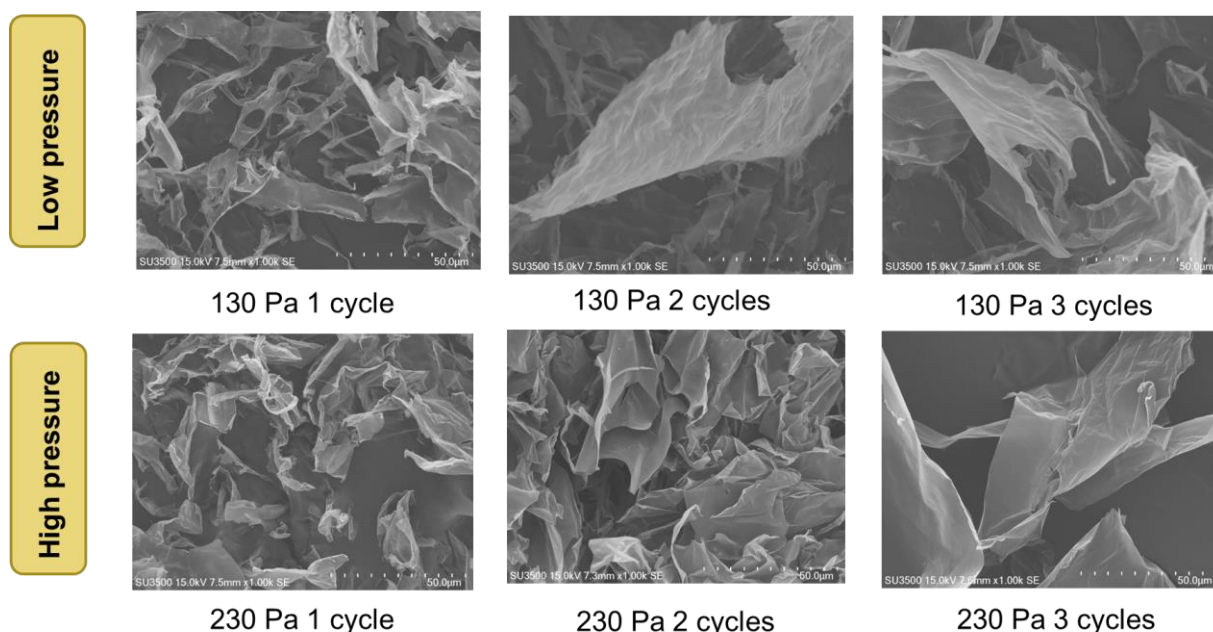
Figure 1-4. TEM picture of F-CAC fibrillated by Starburst Mini

The other two machines used for fibrillating F-CAC were the experimental blender (MRC 8010G) and the juice mixer (Vitamix, TNC5200; Entrex Incorporated, Tokyo, Japan). Both machines operate on similar principles, employing a specialized stainless steel 4-blade mechanism. The key differences between these two machines are their sample loading capacities and their rpm.

The author started with the experimental blender, loading 20 mL of the sample and fibrillating it at 22,000 rpm. The duration of the fibrillation method was varied to achieve different surface morphologies, as shown in **Figure 1-5**. The samples were then freeze-dried and crushed into powder. Each sample was also applied for deposition, with the results shown in **Table 1-4**. The deposition efficiency remained low for all these samples. Consequently, the author proceeded to the next machine, the juice mixer.

Table 1-4. Trans-deposition efficiency by Experimental blender

fibrillation time (min)	deposition (%)
9	49
12	42
15	48
21	40

F-CAC with experimental blender 3 cycles (9 min)

F-CAC with experimental blender 4 cycles (12 min)

F-CAC with experimental blender 5 cycles (15 min)
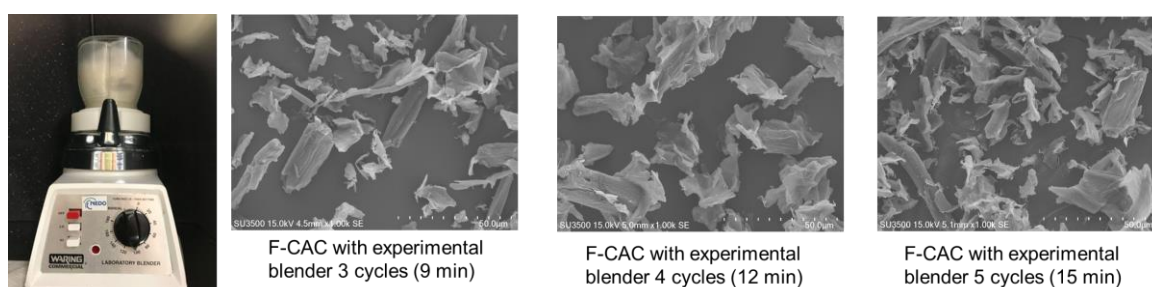
Figure 1-5. Picture of experimental blender and TEM picture of F-CAC fibrillated by this machine Starburst Mini fibrillated by Starburst Mini

Juice mixer machine used for large-scale preparation of F-CAC. The sample loading per time for this machine is up to 400 mL. Then, the sample was fibrillated at 37,000 rpm. Samples were dried with a freeze-dry machine and crushed into powder (**Figure 1-6**). Each sample was also used for deposition. The result is shown in **Table 1-5**. The highest deposition efficiency was observed in the sample that was fibrillated with a Juice mixer for 12.5 minutes. Then, conditions to prepare this F-CAC are fixed with 0.9% citric acid, pH 9, and fibrillation with a juice mixer for 12.5 minutes.

Table 1-5. Trans-deposition efficiency by Juice mixer

fibrillation time (min)	deposition (%)
0	43
12.5	60
25	58

Non-Fibrillated | Fibrillated 50 times (12.5 min) | Fibrillated 100 times (25 min)
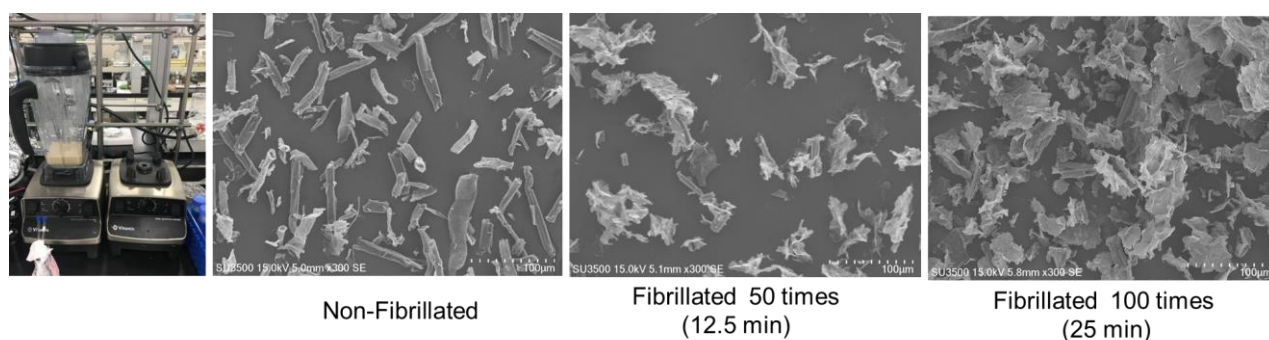
Figure 1-6. Picture of juice mixer blender and TEM picture of F-CAC fibrillated by this machine Starburst Mini fibrillated by Starburst Mini

1.2.4. Deposition efficiency effects by ration of Au and F-CAC

The amount of F-CAC was carefully considered. The author experimented with increasing the F-CAC quantity while maintaining a constant gold concentration of 8.5×10^{-4} mmol. This adjustment improved the deposition efficiency of gold in F-CAC to 84%. Although this result did not reach the previous level of 90%, it represents the best outcome achieved by the author. Additionally, this result demonstrated good reproducibility.

Table 1-6. Trans-deposition efficiency by increasing weight Ratio of F-CAC

amount of F-CAC (mg)	deposition (%)
25	60
30	66
50	72
100	84
150	85

1.3 Conclusion

The author successfully prepared Au:F-CAC with reproducibility. The inconsistency was narrowed down to four main factors:

1. The amount of citric acid on the surface of F-CAC should be within the range of 0.8–1 mmol/g, controlled by the baking temperature at 130 °C. for 13 hours.

2. The carboxylic groups on citric acid must be in sodium form, necessitating a pH adjustment to 9 after synthesizing F-CAC, which also affects the surface properties.

3. Surface morphology, which is altered by the fibrillation process, is dependent on the machine and fibrillation time. The F-CAC was optimized to be fibrillated with a juice mixer for 12.5 minutes.

4. The method of transferring AuNPs, involving the optimization of F-CAC amount, solvent, and gold. The concentration of gold was optimized to 8.5×10^{-4} mmol.

A novel optimization method was established, achieving an 85% deposition efficiency.

1.4 Experimental detail

1.4.1 Procedure for Preparation of F-CAC (previous method)[3]

30 g of cellulose was dispersed in 300 mL of distilled water and stirred for 5 minutes at room temperature. 90 g of CA was added to the dispersion, followed by 5 minutes of further stirring. The mixture was incubated in an oven for 15 h and the reaction began with the evaporation of water under high temperature. To investigate the effect of temperature on the esterification between CA and hydroxyls of cellulose, the mixture was incubated at 110 °C, 120 °C, 130 °C, and 145 °C, separately. After the reaction, the residual CA was removed by washing thoroughly with water until the pH of the filtrate was approximately pH 7. After CA was removed, the modified cellulose was washed with 300 mL methanol, and 300 mL acetone, and then dried under vacuum. The introduced carboxylic acid groups were confirmed by Fourier transform-infrared spectroscopy (FT-IR; Spectrum One, PerkinElmer Co., Ltd., Japan) and the carboxylic acid group content of the cellulose was evaluated via conductometric titration (LAQUA F-74, HORIBA, Ltd., Kyoto, Japan).
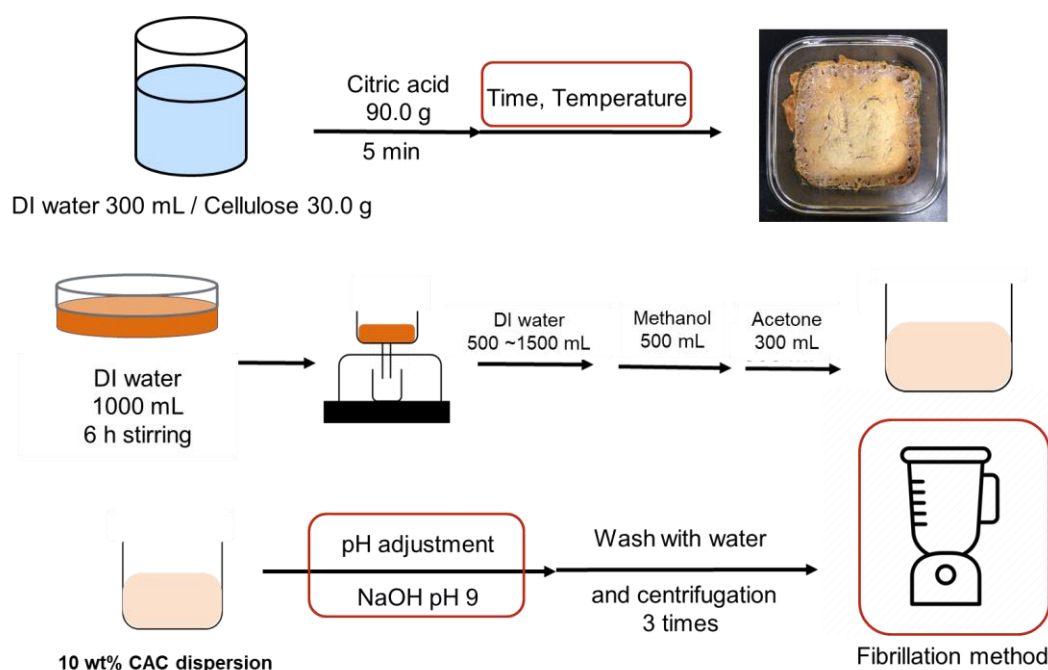
Figure 1-7. General procedure for preparation F-CAC

1.4.2 Procedure for Preparation of F-CAC (vary Citric Acid Loading)

To a 500 mL round-bottomed flask were added cellulose (30 g), and distilled water (300 mL). To the dispersion was added citric acid (90 g), and then the mixture was stirred for 5 min at room temperature. The mixture was transferred to a heat-resistant dish and incubated in an oven at different times and temperatures. After cooling to room temperature, the residual citric acid was removed by washing with water until the pH of the filtrate was approximately pH 7. After that, the modified cellulose was successively washed with methanol (300 mL), and acetone (300 mL), and then dried under vacuum to give F-CAC (ca. 0.9 wt% citric acid loading) as a colorless powder. The loading amount of citric acid was determined by titration using aqueous HCl and NaOH solutions (**Figure 1-7**).

1.4.3 Procedure for Preparation of F-CAC (ca. 0.9 wt %Citric Acid Loading), pH of carboxylic acid deprotonation

To a 500 mL round-bottomed flask were added cellulose (30 g), and distilled water (300 mL). To the dispersion was added citric acid (90 g), and then the mixture was stirred for 5 min at room temperature. The mixture was transferred to a heat-resistant dish and incubated in an oven at different times and temperatures. After cooling to room temperature, the residual citric acid was removed by washing with water until the pH of the filtrate was approximately pH 7. After that, the modified cellulose was successively washed with methanol (300 mL), and acetone (300 mL), and then dried under vacuum to give F-CAC (ca. 0.9 wt% citric acid loading) as a colorless powder. Then the F-CAC powder (20 g) was dispersed in water 200 mL and was adjusted pH in to 7, 7.8, and 9 with NaOH (1 mol/L). Then the residual NaOH was removed by washing with water until the pH of the filtrate was approximately pH 7. The carboxylic acid deprotonation was confirmed by IR

1.4.4 Procedure for Preparation of F-CAC (ca. 0.9 wt% citric acid loading), changing surface morphology

To a 500 mL round-bottomed flask were added cellulose (30 g), and distilled water (300 mL). To the dispersion was added citric acid (90 g), and then the mixture was stirred for 5 min at room temperature. The mixture was transferred to a heat-resistant dish and incubated in an oven at 130 °C for 13 h. After cooling to room temperature, the residual citric acid was removed by washing with water until the pH of the filtrate was approximately pH 7. After that, the modified cellulose was successively washed with methanol (300 mL), and acetone (300 mL), and then dried under vacuum to give F-CAC (ca. 0.9 wt% citric acid loading) as a colorless powder. Then the F-CAC powder (20 g) was dispersed in water 200 ml and was adjusted pH to 9 with NaOH (1 mol/L). Then the residual

NaOH was removed by washing with water until the pH of the filtrate was approximately pH 7. Then fibrillated using a different machine. The surface morphology of cellulose before and after fibrillation was compared by SEM observation. The surface morphology of cellulose and F-CAC is shown in **Figures 1-4**, **1-5**, and **1-6**.
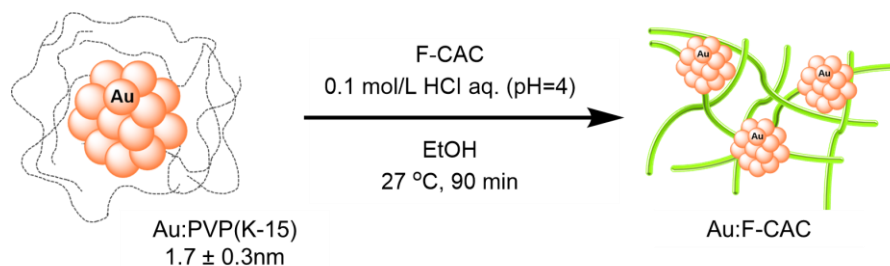
Figure 1-8. General procedure for preparation F-CAC

1.4.5   General Procedure for Preparation Au:F-CAC (Previous method) [4]

In a reaction tube (φ = 10 mm) equipped with a magnetic stir bar, Au:PVP(K-15) and F-CAC (25 mg) were mixed in solvent (2 mL), and then pH value was adjusted using an aqueous hydrochloric acid solution (0.1 mol/L). After stirring at 1300 rpm for 90 min, the solid was separated from the supernatant by centrifugation at 7500 rpm at room temperature and washed with ethanol (ca. 10 mL) three times. The remaining powder was dried under vacuum at 45 °C for 12 h to afford Au:F-CAC as a powder.

1.4.6   General Procedure for Preparation Au:F-CAC (vary solid support Loading)

Through trans-deposition method. In a reaction tube (φ = 10 mm) equipped with a magnetic stir bar, Au:PVP(K-15) and F-CAC (25, 30, 50, 100, and 150 mg) were mixed in solvent (2 mL), and then pH value was adjusted using an aqueous hydrochloric acid solution (0.1 mol/L). After stirring at 1300 rpm for 90 min, the solid was separated from the supernatant by centrifugation at 7500 rpm at room temperature and washed with ethanol (ca. 10 mL) three times. The remaining powder was dried under vacuum at 45 °C for 12 h to afford Au:F-CAC as a powder.

1.5 References

1. G. Bali, X. Meng, J. I. Deneff, Q. Sun, A. J. Ragauskas, *ChemSusChem* **2015**, *8*, 275.

2. M. Cheng, Z. Qin, Y. Chen, J. Liu, Z. Ren, *Cellulose* **2017**, *24*, 3243.

3. X. Cui, T. Honda, T. Asoh, H. Uyama*, Carbohydr. Polym.* **2020**, *230*, 115662.

4. T. Chutimasakul, Y. Uetake, J. Tantirungrotechai, T. Asoh, H. Uyama, H. Sakurai, *ACS Omega*. **2020**, *5*, 33206.

Chapter 2: Intramolecular hydroamination catalysed by gold nanoparticles deposited on fibrillated cellulose

2.1   Introduction

Cyclic amines are important intermediates in the pharmaceutical and chemical industries.[1] One effective method for their synthesis is hydroamination. Hydroamination of unactivated olefins, or the direct addition of an amine's N-H bond to an unactivated carbon-carbon multiple bonds is a widely used synthetic technique due to its efficiency in providing pathways to nitrogen heterocycles and complex compounds. Although hydroamination of olefins is thermodynamically feasible under normal conditions and the reactions are exothermic, there is a high reaction barrier. The reactions are nearly ergoneutral due to a large negative entropy.[2] Therefore, a catalyst is required to achieve the reaction with high yield

Over the past 20 years, several research projects have concentrated on the development of catalysts, including group IV metals, organolanthanides, alkali metals, and transition metals. Among these, transition-metal-catalyzed amination of alkenes is a promising catalytic cycle for hydroamination. Cationic Au(I) complexes, in particular, are notable for their highly carbophilic Lewis acidic nature, which effectively activates C–C multiple bonds.[3] This is because of their electron deficient and low oxophilicity, showing good functional group compatibility, and low air and moisture sensitivity.[4] Moreover, it has been reported that the distinct Lewis acid property of Au(I) significantly contributes to its high catalytic activity toward olefins.

This property allows Au(I) to activate inert olefins via π-bonding, facilitating the nucleophilic addition of toluenesulfonate to produce the anti-addition product. Density functional theory (DFT) studies of the hydroamination of alkenes and dienes by Au(I) revealed that the reaction proceeds through a stepwise mechanism. Additionally, cationic Au(I) complexes have been investigated and established as efficient catalysts for intra- and intermolecular hydroamination of olefins under mild conditions, due to their unique Lewis acid character.[5] Toste et al. combined experimental and theoretical investigation of intramolecular aminoauration revealed that the anti-addition mechanism plays a preferential role in the Au(I) complexes-promoted nucleophilic addition to an alkene.[5b]

In contrast to homogeneous Au(I) complexes, zero-valent AuNP catalysts also exhibit a Lewis acidic nature under oxygen atmosphere. It is well established that superoxide-like species are formed during the absorption of oxygen. These species are beneficial for catalytic aerobic oxidation reactions.[6] Simultaneously, the surface of the gold near the absorption site becomes positively charged, leading to Lewis acid property.[7] Previous research has demonstrated that intermolecular hydroamination[8] occurs with Au:PVP [PVP: poly(N-vinyl-2-pyrrolidone)] under aerobic conditions.[9]

In this process, terminal and/or internal alkenes are activated at positively charged sites with the assistance of molecular oxygen, resulting in the production of cyclic amines. These compounds are prevalent in natural products and pharmaceuticals. The study also investigated alternative stabilizing supports, particularly polymer-based matrices, known for their superior catalytic activity and ease of use.

Previous studies in the author group have shown that AuNPs stabilized by biomacromolecules like chitin and chitosan exhibit superior catalytic activity compared to those stabilized by PVP in certain cases.[10] As mentioned in the introduction, AuNPs stabilized by chitin or chitosan have proven effective for the homocoupling reaction of phenylboronic acids due to the presence of functional groups such as amine and amide.[11] These groups create a localized basic environment near the reaction site, which prevents unwanted oxidation pathways and enhances the chemoselectivity of the reaction. This indicates that the functional group on polymer matrix can effectively control the catalytic activity. Recently, Uyama et al. developed a simple method to create fibrillated cellulose through chemical modification with citric acid (F-CAC).[12] Additionally, The author group devised a size-selective method to produce AuNPs stabilized on F-CAC (Au:F-CAC), which were used for the aerobic oxidation of 1-indonol to yield 1-indanone quantitatively.[13] Au:F-CAC were recyclable at least six times. This shows high stability of AuNPs on F-CAC. Given that the AuNPs-catalyzed hydroamination reaction occurs under slightly acidic conditions (**Figure 2-1**), the author considered F-CAC, which contains carboxylic acid groups, to be a suitable matrix for facilitating this reaction. Moreover, its excellent tolerance to organic solvents and ability to be reused make the reaction highly practical. In this context, the author employed Au:F-CAC for the intramolecular hydroamination reaction and investigated the influence of the F-CAC matrix on the reaction.
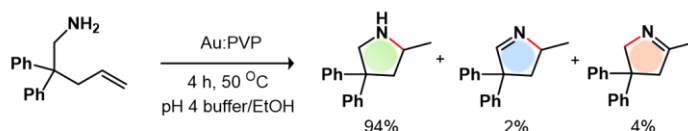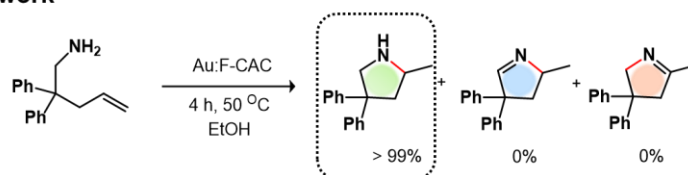
Figure 2-1. Hydroamination of primary amines

2.2 Result and discussions

2.2.1 Optimization of reaction conditions

The catalytic activity of Au:F-CAC (particle size of Au: 1.7 ± 0.2 nm, 1.7×10^{-3} wt%), prepared by trans-deposition method,[13a,14,15]was compared with the result obtained using Au:PVP from previous work (**Table 2-1**, entry 1). In the presence of 5 mol% of Au:F-CAC, the reaction was conducted in a buffer/EtOH solution under aerobic conditions, yielding pyrrolidine **2a** quantitatively and without any side products such as **3a** or **4a** (entry 2). It should be noted that the intermolecular addition of ammonia did not occur due to its low nucleophilicity. In contrast, the intramolecular reaction, which is entropically favorable, proceeded much more rapidly. In experiments conducted without additional formic acid, which acts as a reducing agent, the reaction did not proceed. This suggests that the citric acid moiety in F-CAC does not serve as a reducing agent (entry 3).

Table 2-1. Hydroamination of primary amines in various condition

entry	catalyst (atom%)	additive	solvent	time (h)	%yield			
					1a	2a	3a	4a
1	Au:PVP (5)	1000 mol% HCO_2H 500 mol% NH_3	pH 4.01 buffer/EtOH	4	-	94	2	4
2	Au:F-CAC (5)	1000 mol% HCO_2H 500 mol% NH_3	pH 4.01 buffer/EtOH	4	-	99	-	-
3	Au:F-CAC (5)	500 mol% NH_3	pH 4.01 buffer/EtOH	4	100	-	-	-

The ratio of formic acid to liquid ammonia was optimized (**Table 2-2**). The optimal condition for using Au:F-CAC was found to be a ratio of HCO_2H to NH_3 at 1:2 which is the reverse ratio in the case of using Au:PVP. This difference may be attributed to the presence of citric acid on the surface of F-CAC. Further studies on the reaction with a reduced amount of catalyst showed that the reaction proceeded successfully with 2 mol% of Au:F-CAC without any loss in the yield of **2a**, although the reaction time needed to be slightly extended (**Table 2-3**, entry 1).

Table 2-2: Optimization of the ratio between HCO$_2$H and NH$_3$
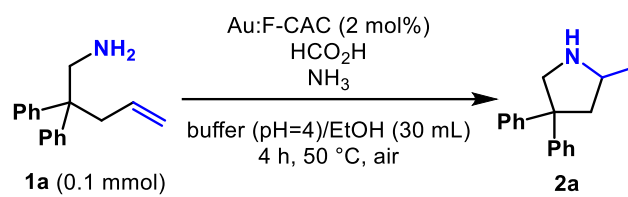
HCO$_2$H (mol%)	aq. NH$_3$ (mol%)	yield (%)^a	
		1a	2a
1000	500	64	32
1000	1500	58	40
1000	2000	48	53
1000	4000	43	50
1000	6000	68	30
2000	4000	42	53
4000	8000	68	34

^{a}Determined by ^{1}H NMR analysis.

Table 2-3: Optimization of the amount of HCO_2NH_4
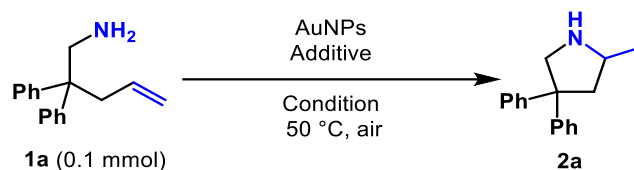
entry	catalyst (atom%)	additive	solvent	time (h)	%yield [a] 1a	%yield [a] 2a	Leaching (%)
1	Au:F-CAC (2)	1000 mol% HCO_2H 2000 mol% NH_3	pH 4.01 buffer/EtOH	10	-	99	45
2	Au:F-CAC (2)	1000 mol% HCO_2H 2000 mol% NH_3	EtOH	4	-	99	25
3	Au:F-CAC (2)	500 mol% HCO_2NH_4	EtOH	4	-	99	0
4	Au:F-CAC (0.5)	500 mol% HCO_2NH_4	EtOH	4	-	99	n.d.
5	Au:F-CAC (0.2)	500 mol% HCO_2NH_4	EtOH	8	-	99	n.d.
6	Au:F-CAC (0.5)	500 mol% HCO_2NH_4	EtOH	2	13	85	n.d.
7	Au:PVP (0.5)	500 mol% HCO_2NH_4	EtOH	2	47	45	n.d.
8	Au:PVP (0.2)	500 mol% HCO_2NH_4	EtOH	8	52	46	n.d.
9	Au:PVP (0.2)	500 mol% HCO_2NH_4	EtOH	24	43	55	n.d.

[a]Determined by ^1H NMR analysis.

A kinetic study on this reaction revealed that the reaction rate was 1.5×10^{-2} mmol/h during the first 2 h; however, decreased to 1.1×10^{-2} mmol/h over the subsequent 2 hours (**Figure 2-2**). A significant drop in the reaction rate was observed at 8 hours, reducing to 0.4×10^{-2} mmol/h. This reduction in reaction rate is likely due to two main factors. Firstly, agglomeration of AuNPs was observed. The particle size of AuNPs on F-CAC increased from 1.6 ± 0.4 nm to 1.9 ± 0.7 nm within 2 h and further grew to 5.7 ± 1.4 nm after 10 h (**Figure 2-3**). To investigate the effect of size-dependent catalytic activity, larger AuNPs were prepared and tested. Freshly prepared catalysts with 8.7 ± 1.0 nm Au:F-CAC were used; however, no reaction occurred, confirming the size dependency of AuNPs catalytic activity.
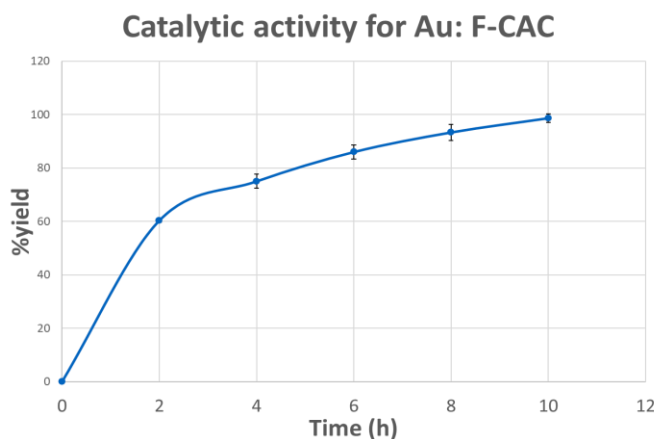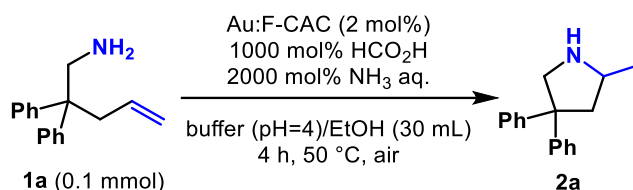
Figure 2-2. kinetic study on reaction of Au:F-CAC in pH 4.01 buffer/EtOH
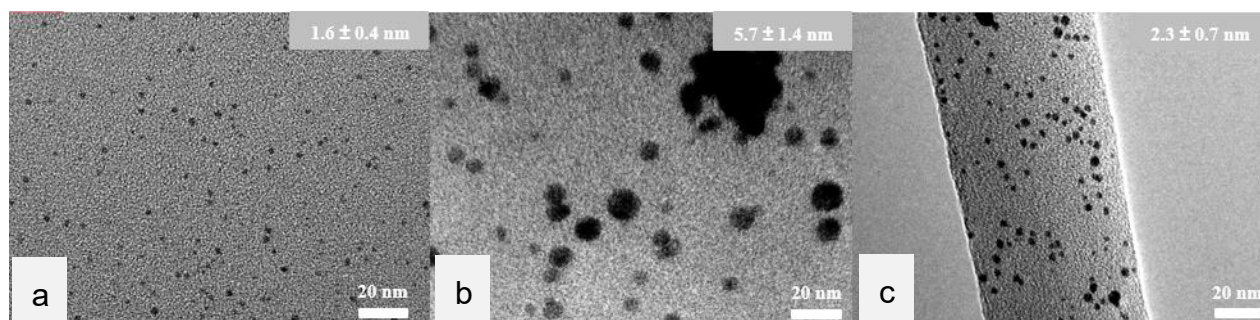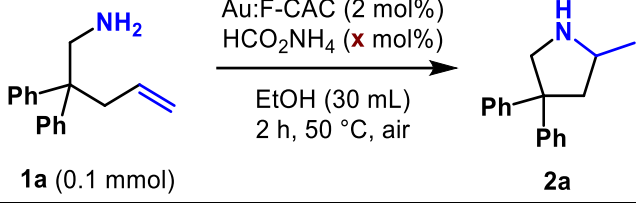
Figure 2-3. TEM images and their size distribution of Au:F-CAC (a) before the reaction, (b) after reaction (Table 2-2, entry 1) and (c) after reaction (Table 2-2, entry 2)

The second factor involves the leaching of gold into the solvent. Inductively coupled plasma-atomic emission spectroscopy (ICP-AES) analysis conducted with the Au:F-CAC after the reaction. The results revealed significant gold leaching from F-CAC, resulting in a 45% loss of gold. This phenomenon of gold leaching has been previously reported to occur particularly with polar solvents such as water, DMF, and DMSO.[13a] To minimize the water content in the solvent, the solvent system was optimized using 2 mol% of Au:F-CAC. The reaction did not proceed in toluene; however, using absolute ethanol (EtOH) significantly improved the outcome, reducing gold loss to 25% compared to the buffer/EtOH system (Table 2-3, entry 2). Ammonium formate was optimized to 500 mol% and used in place of liquid ammonia and formic acid in EtOH. (Table 2-4). The use of ammonium formate completely prevented gold leaching while maintaining high catalytic activity (entry 3). The use of an

excess amount of ammonium formate would also accelerate the cleavage of the Au–C bond, expelling the cyclized product. Under these reaction conditions, the amount of gold can be reduced to 0.2 mol% by extending the reaction time to 8 hours. (**Table 2-3**, entries 4 and 5).

Table 2-4: Optimization of the amount of HCO_2NH_4

Au:F-CAC (2 mol%)
HCO_2NH_4 (**x** mol%)

EtOH (30 mL)
2 h, 50 °C, air

1a (0.1 mmol)

2a

x	yield (%)[a]	
	1a	**2a**
1000	7	90
500	8	85
400	20	79
200	55	44

[a]Determined by ^{1}H NMR analysis.

For comparison, using Au:PVP under the same conditions resulted in a lower yield (45%) after 2 hours, whereas Au:F-CAC achieved a significantly higher yield (85%) (**Table 2-3**, entries 6 and 7). The difference in catalytic activity was more pronounced at 0.2 mol% of Au:F-CAC (**Table 2-3**, entries 5 and 8), with the reaction using Au:PVP not completing even after 24 hours (**Table 2-3**, entry 9). These findings highlight the excellent stability of AuNPs under these reaction conditions. Although reducing the gold amount to 0.2 mol% extended the reaction time by 8 hours, the substrate scope was limited to **1a**. Therefore, the reaction conditions of entry 4 were selected as the optimal conditions due to the need for additional catalyst in substrates with substituents at the alkene position (**Figure 2-5**).

2.2.2 The durability and reusability of Au:F-CAC

To understand the catalytic activity of Au:F-CAC, transmission electron microscopy (TEM) was conducted to observe AuNPs on F-CAC after the reaction compared with Au:PVP. Similar to previous study, severe aggregation of Au:PVP was noted under aqueous conditions (**Table 2-5**, entry C).[9c] In contrast, the aggregation of AuNPs in Au:F-CAC was partially suppressed (entry A). Utilizing solid ammonium formate in absolute ethanol further suppressed aggregation in both cases.

However, the particle size of Au:F-CAC remained significantly smaller than that of Au:PVP (entries B and D), resulting in the high catalytic activity of the Au:F:CAC catalyst.

Table 2-5. TEM images and particle sizes of Au:F-CAC and Au:PVP after reaction. [a] 2 mol% of AuNPs was used. [b] entry 2 in **Table 2-3** [c] entry 3 in **Table 2-3** [d] Au:PVP(K-30) (1.5 ± 0.2 nm) was used.
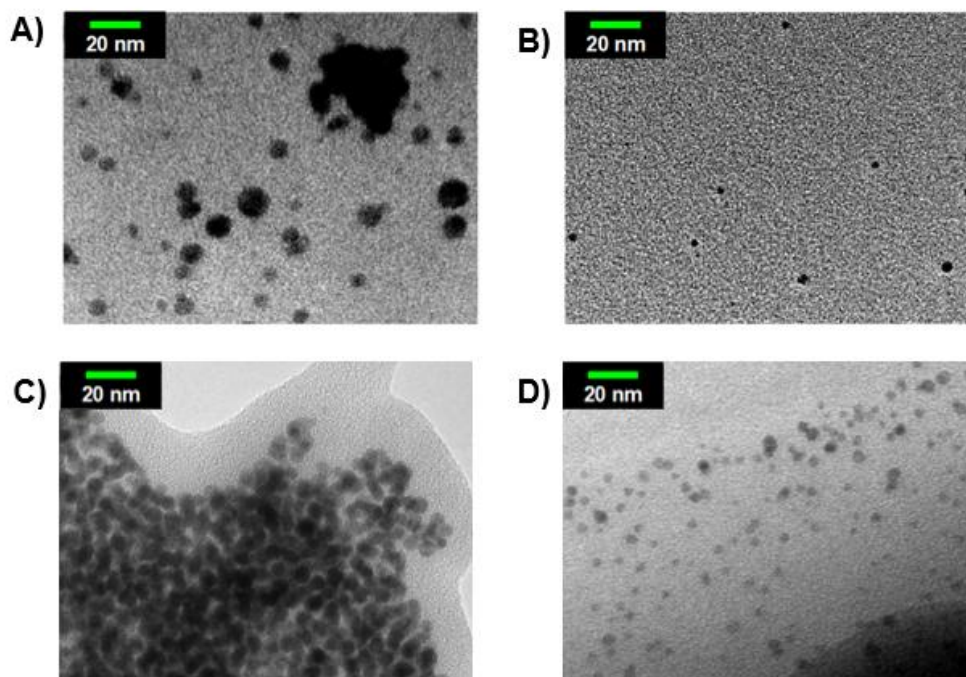
	catalyst	solvent	particle size (nm)
A[a]	Au:F-CAC	buffer/EtOH	5.7 ± 1.8
B[b]	Au:F-CAC	EtOH	2.3 ± 0.7
C[c]	Au:PVP	buffer/EtOH	Aggregate
D[d]	Au:PVP	EtOH	3.2 ± 0.7

Subsequently, the durability of the Au:F-CAC catalyst was investigated through a reusability test (**Figure 2-4**). After each reaction cycle, the catalyst was filtered, washed with ethanol, and dried overnight before reuse. In the second cycle, the hydroamination of **1a** yielded nearly quantitative results after 4 hours. Although there was a noticeable decline in catalytic activity after the third cycle, **2a** was still produced in moderate yields (59–71%). Transmission electron microscopy (TEM) analysis of the spent catalyst after six cycles revealed slightly aggregated Au:F-CAC (3.2 ± 0.2 nm), suggesting that the reduced catalytic activity could be attributed to the decreased surface area of the AuNPs.
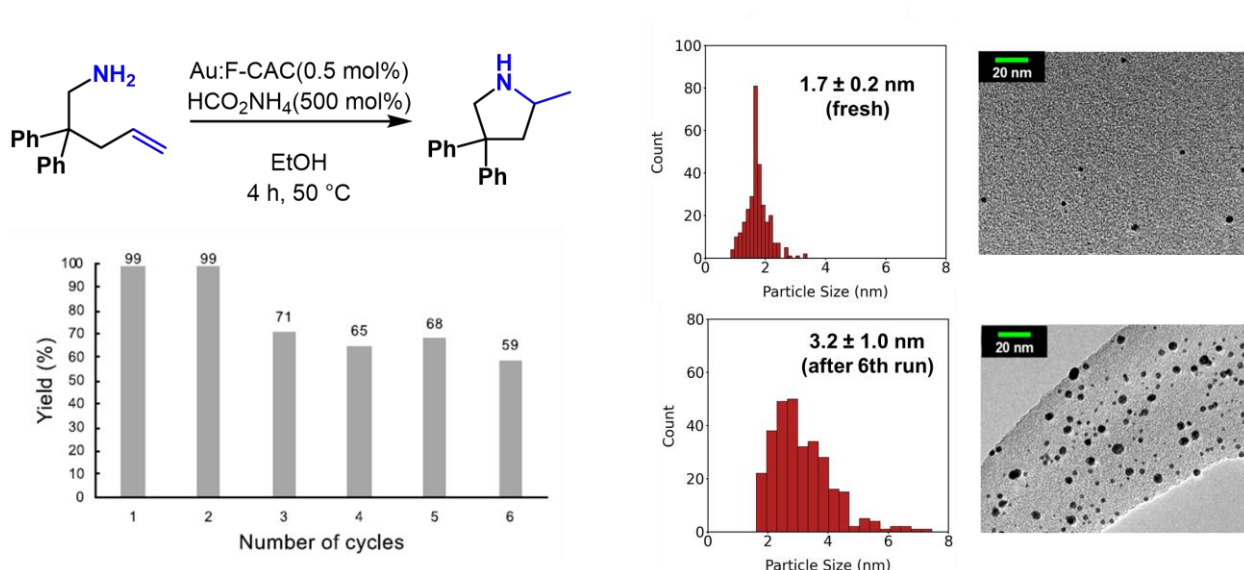
Figure 2-4. Reusability test of Au:F-CAC

2.2.3 The effect of the reaction atmosphere

The reaction was examined using 0.5 mol% Au:F-CAC under various atmospheric conditions. The yield of **2a** remained nearly unchanged in both aerobic and oxygen atmospheres, indicating that the partial pressure of oxygen does not affect the reaction rate (**Table 2-6**, entries 1 and 2). This suggests that the absorption of oxygen atoms is not involved in the rate-determining step. Consistent with previous theoretical findings using density functional theory (DFT), which identified reductive elimination as the rate-determining step, these experimental results align well with previous report.[16] As expected, the cyclization did not occur in a nitrogen atmosphere, confirming the essential role of oxygen in this reaction (entry 3).

Table 2-6. Effect of the reaction atmosphere

entry	atmosphere	time (h)	recovery of 1a (%)[a]	yield of 2a (%)[a]
1	Air	1	44	53
2	O_2	1	43	56
3	N_2	4	100	0

[a]Determined by ^{1}H NMR analysis.

2.2.3 Substrate scope

The reaction was tested with substrates having various substituents and protecting groups (**Figure 2-5**). A primary amine with a β-methallyl group did not react under the optimized conditions (**Table 2-3**, entry 5). However, using 0.5 mol% of Au:F-CAC, the cyclization produced pyrrolidine **2b** with an 83% yield. When the Au:F-CAC catalyst concentration was increased to 1.0 mol%, **2b** was obtained in quantitative yield. Primary amines with crotyl (**1c**) and prenyl groups (**1d**) did not react, even with extended reaction times or higher catalyst amounts, likely due to steric hindrance from the di- or tri-substituted alkenes. Unlike cationic gold complexes, reaction conditions involving AuNPs are highly sensitive to steric factors because there are gold species adjacent to the cationic Au site activated by oxygen. Therefore, these conditions are anticipated to facilitate the selective hydroamination of terminal alkenes. However, when using benzyl-protected amine (**1e**), the starting material decomposed, likely due to the instability of benzylamine under the oxidizing conditions of AuNPs and molecular oxygen.

	2b	2c	2d	2e
$x = 0.2$	0% (24 h)	0% (24 h)	0% (24 h)	0% (24 h)
$x = 0.5$	83% (4 h)	0% (24 h)	0% (24 h)	0% (24 h)
$x = 1.0$	99% (4 h)	0% (24 h)	0% (24 h)	0% (24 h)
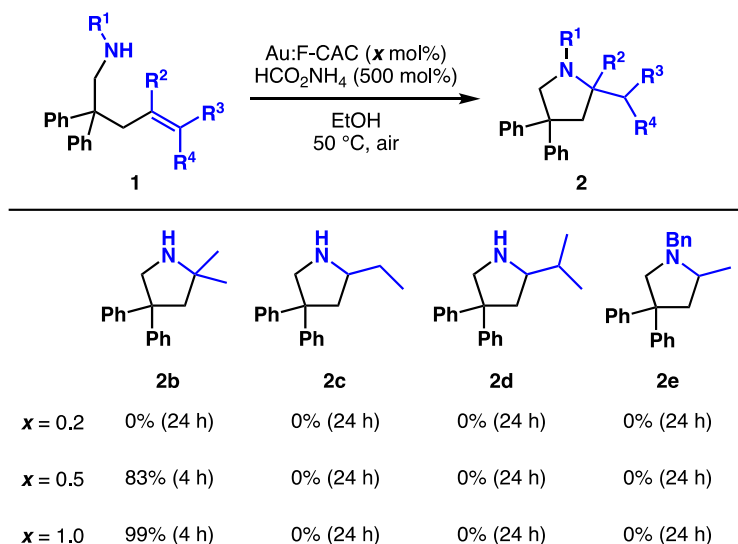
Figure 2-5. Scope of alkenes

The author investigated substrates with different substituents at the β-position of the amino group (**Figure 2-6**). Given the sensitivity of the reaction conditions to steric hindrance in the alkene moiety, the chemoselective cyclization of amines with secondary olefins showcase the unique efficiency of this system. For instance, the cyclization of an amine with both allyl and prenyl groups (**1f**) resulted in selective cyclization at the allyl site, producing **2f** in 89% yield with complete chemoselectivity (dr = 1:1). Similarly, an amine with a diallyl group (**1g**) yielded the desired product **2g** (85%) within 4

hours. The reaction also proceeded smoothly with an amine-bearing homoallyl group (**1h**), affording piperazine 2 h in 79% yield.
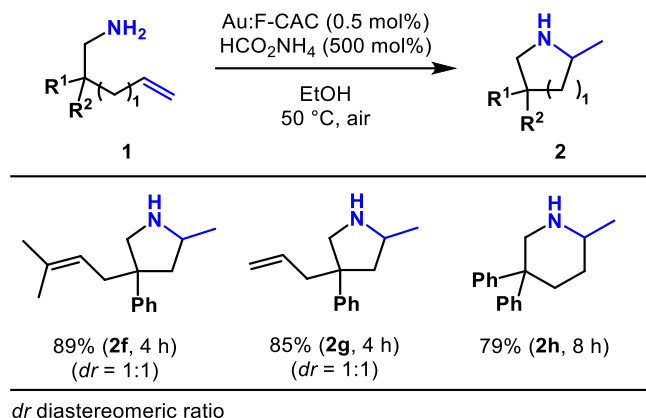
Figure 2-6. The substrate scope of intramolecular cyclisation of primary amine

Then, this reaction condition was applied to amines with protecting groups, such as toluenesulfonyl (**1j**) and benzoyl (**1k**) groups; however, the cyclization reaction did not occur. After several attempts, cesium carbonate (Cs$_2$CO$_3$) was found to be effective for the intermolecular cyclization reaction by increasing the nucleophilicity of amides. When sulfonimines **1j** were treated with 0.5 mol% of Au:F-CAC and 300 mol% of Cs$_2$CO$_3$ under an aerobic atmosphere at 50 °C for 30 hours , the Pyrrolidine (**2j**) was obtained in quantitative yield (**Figure 2-7**). Although amide (**1k**) participated in this reaction, the yield was low (12%). The reaction with benzylamine **1e** did not proceed under these optimized conditions.
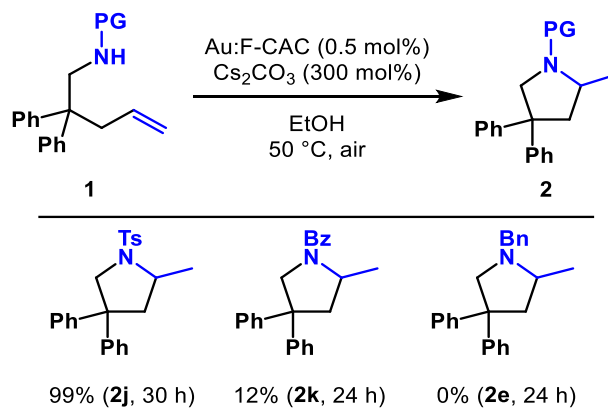
Figure 2-7. The substrate scope of protected amines

2.3 Conclusion

Au:F-CAC exhibits exceptional catalytic activity in hydroamination reactions, with the gold content reduced to 0.2 atom%. The choice of the sacrificial reductant as well as the basicity of the reaction conditions are important for successfully promoting the formal Lewis acid reaction because the redox reaction between O_2 and the solvent occurs after the main addition reaction. The catalytic of Au:F-CAC shows higher activity than Au:PVP. This is due to the stabilization of gold on F-CAC. By focusing on the fact that this catalyst is substantially affected by the substitution pattern of alkene moiety, unprecedented chemoselective cyclization was achieved. This cyclization, which has been challenging with conventional cationic Au-catalyzed reactions, enabled the synthesis of novel compounds, highlighting the unique capabilities of Au:F-CAC.

2.4 Experimental details

2.4.1 General method for hydroamination reaction with mixture of pH 4 buffer and ethanol

To a reaction tube equipped with a magnetic stir bar were added Au:F-CAC, amine (**1**) (0.10 mmol), additive, and EtOH (10 mL) with pH 4 buffer (20 ml). The mixture was stirred at 50 °C under an ambient atmosphere. After stirring for a specific time, the catalyst was removed by filtration and washed with diethyl ether (ca. 5 mL × 3). To the filtrate was added 1,1,2,2-tetrachloroethane (10.2 μL, 0.10 mmol) as an internal standard, and then the mixture was agitated. NMR measurements were performed to determine the yields.

2.4.2 General method for hydroamination reaction with pure ethanol

To a reaction tube equipped with a magnetic stir bar were added Au:F-CAC, amine (**1**) (0.10 mmol), additive, and EtOH (10 mL). The mixture was stirred at 50 °C under an ambient atmosphere. After stirring for a specific time, the catalyst was removed by filtration and washed with diethyl ether (ca. 5 mL × 3). To the filtrate was added 1,1,2,2-tetrachloroethane (10.2 μL, 0.10 mmol) as an internal standard, and then the mixture was agitated. NMR measurements were performed to determine the yields.

2.4.3 Synthetic procedure and compound data

2-Phenylpent-4-enenitrile (1f-1)
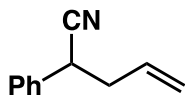
1f-1 was prepared according to the literature procedure.[17]

To a solution of *N,N*-diisopropylamine (3.1 mL, 22 mmol) in THF (12.5 mL) was added *n*-BuLi (8.0 mL, 21 mmol, 2.6 mol/L in *n*-hexane) at –78 °C. After stirring for 2 h, to this was added benzyl cyanide (2.1 mL, 18 mmol, 1 equiv) and the mixture was stirred for 3 h at the same temperature. To this was added 3-bromo-1-propene (1.7 mL, 20 mmol), and the reaction mixture was warmed to room temperature and stirred for 12 h at the same temperature. To this was added saturated aqueous NH_4Cl solution (50 mL) and the resulting mixture extracted with dichloromethane (50 mL × 3). The combined organic extract was dried over Na_2SO_4. After filtration, the filtrate was concentrated under reduced pressure. The residue was purified by column chromatography (*n*-hexane/EtOAc = 20:1) to give **1f-1** (2.6 g, 16.5 mmol, 82%);

R_f = 0.45 (*n*-hexane/EtOAc = 9:1);

^1H NMR (CDCl$_3$) δ 7.41−7.31 (m, 5H), 5.84–5.75 (m, 1H), 5.21–5.20 (m, 1H), 5.17–5.16 (m, 1H), 3.87 (dd, *J* = 7.8, 6.4 Hz, 1H), 2.66–2.62 (m, 2H);

^{13}C NMR (CDCl$_3$) δ 135.1 (1C), 132.5 (1C), 128.9 (2C), 128.0 (1C), 127.2 (2C), 120.2 (1C), 119.2 (1C), 39.7 (1C), 37.3 (1C);

The chemical shifts were consistent with those reported in the literature.[17]

2-Allyl-5-methyl-2-phenylhex-4-enenitrile (1f-2)
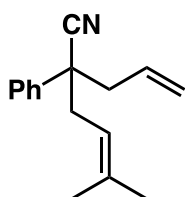
To a solution of *N,N*-diisopropylamine (2.9 mL, 21 mmol) in THF (50 mL) was added *n*-BuLi (8.0 mL, 21 mmol, 2.6 mol/L in *n*-hexane) at –78 °C. After stirring for 2 h, to this was added **1f-1** (2.75 g, 17.5 mmol, 1 equiv) and the mixture was stirred for 3 h at the same temperature. To this was added 1-chloro-3-methyl-but-2-ene (2.4 mL, 21 mmol, 1.2 equiv), and the reaction mixture was warmed to room temperature and stirred for 12 h at the same temperature. To this was added saturated aqueous NH_4Cl (50 mL) and the resulting mixture extracted with dichloromethane (50 mL × 3). The combined organic extract was dried over Na_2SO_4. After filtration, the filtrate was concentrated under reduced

pressure. The residue was purified by silica-gel column chromatography (*n*-hexane/EtOAc = 4:1) to give **1f-2** (3.09 g, 13.7 mmol, 78%);

TLC R_f = 0.67 (*n*-hexane/EtOAc = 4:1);

^{1}H NMR (CDCl$_3$) δ 7.42–7.35 (m, 3H), 7.33–7.27 (m, 2H), 5.71–5.62 (m, 1H), 5.17–5.10 (m, 2H), 5.09–5.03 (m, 1H), 2.75–2.64 (m, 3H), 2.59–2.54 (dd, J = 14.6, 6.9 Hz, 1H), 1.67 (s, 3H), 1.55 (s, 3H);

^{13}C NMR (CDCl$_3$) δ: 138.1 (1C), 136.8 (1C), 131.9 (1C), 128.7 (2C), 127.6 (1C), 126.3 (2C), 122.1 (1C), 119.9 (1C), 117.4 (1C), 48.0 (1C), 43.8 (1C), 38.7 (1C), 25.8 (1C), 18.1 (1C);

IR (diamond, cm^{-1}) 3059, 2980, 2913, 2235, 1671, 1642, 1600, 1494, 1451, 1377, 1111;

HRMS (EI) *m/z* 226.1593 (226.1551 calcd for C$_{16}$H$_{19}$N, [M+H]$^+$).

2-Allyl-5-methyl-2-phenylhex-4-en-1-amine (1f)
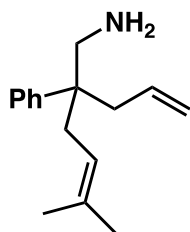
To a suspension of lithium aluminum hydride (0.65 g, 17 mmol) in Et$_2$O (30 mL) was slowly added a solution of **1f-2** (2.9 g, 13 mmol) in Et$_2$O (10 mL) at 0 °C under nitrogen atmosphere. The reaction mixture was allowed to warm to room temperature and stirred for 12 h at the same temperature. To the mixture were added Et$_2$O (30 mL), water (1.6 mL), 15% aqueous NaOH solution (1.6 mL), and water (5.0 mL). The combined organic extract was dried over Na$_2$SO$_4$. After filtration, the filtrate was concentrated under reduced pressure. The residue was purified by silica-gel column chromatography (CH$_2$Cl$_2$/MeOH/Et$_3$N = 49/49/2) to give **1f** (2.71 g, 11.8 mmol, 90%);

TLC R_f = 0.75 (CH$_2$Cl$_2$/MeOH/Et$_3$N = 49/49/2);

^{1}H NMR (CDCl$_3$) δ 7.38–7.29 (m, 4H), 7.24–7.18 (m, 1H), 5.67–5.56 (m, 1H), 5.10–4.93 (m, 3H), 2.91 (s, 2H), 2.53–2.31 (m, 4H), 1.65 (s, 3H), 1.58 (s, 3H);

^{13}C NMR (CDCl$_3$) δ: 144.6 (1C), 134.7 (1C), 133.3 (1C), 128.1(2C), 126.7(2C), 125.7 (1C), 119.6 (1C), 117.2 (1C), 48.9 (1C), 46.1 (1C), 39.8 (1C), 33.8 (1C), 25.9 (1C), 17.9 (1C);

IR (diamond, cm^{-1}); 3058, 2972, 2912, 2855, 1637, 1598, 1494, 1444, 1375, 1033;

HRMS (EI) *m/z* 229.1829 (229.1830 calcd for C$_{16}$H$_{23}$N, [M+H]$^+$).

2-Methyl-4,4-diphenylpyrrolidine (2a)
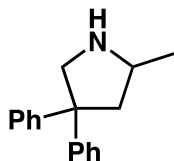
To a reaction tube equipped with a magnetic stir bar were added Au:F-CAC (0.5 mol%), amine (**1a**) (23.7 mg, 0.10 mmol), HCO$_2$NH$_4$ (31.5 mg, 500 mol%), and EtOH (10 mL). The mixture was stirred under air for 3 h at 50 °C. After cooling to room temperature, to the mixture was added saturated aqueous NaHCO$_3$ (ca. 5 mL), and the mixture was extracted with EtOAc. The combined organic extract was dried over Na$_2$SO$_4$. After filtration, the filtrate was concentrated under reduced pressure. The residue was purified by preparative TLC to give **2a** (23.5 mg, 0.99 mmol, 99%);

TLC R_f = 0.37 (CH$_2$Cl$_2$/MeOH/Et$_3$N = 49/49/2);

^{1}H NMR (CDCl$_3$) δ 7.31–7.15 (m, 10H), 3.68 (d, J = 11.4 Hz, 1H), 3.47 (d, J = 11.4 Hz, 1H), 3.38 (ddd, J = 8.9, 6.5, 6.4 Hz, 1H), 2.75 (dd, J = 12.7, 6.5 Hz, 1H), 2.04 (dd, J =12.7, 8.9 Hz, 1H), 1.66 (s, 1H), 1.21 (d, J = 6.4 Hz, 3H);

^{13}C NMR (CDCl$_3$) δ 147.7 (1C), 147.0 (1C), 128.31 (2C), 128.27 (2C) 127.0 (2C), 126.9 (2C), 126.0 (2C), 57.8 (1C), 57.3 (1C), 53.1, (1C), 47.0 (1C), 22.4 (1C);

The chemical shifts were consistent with those reported in the literature.[17]

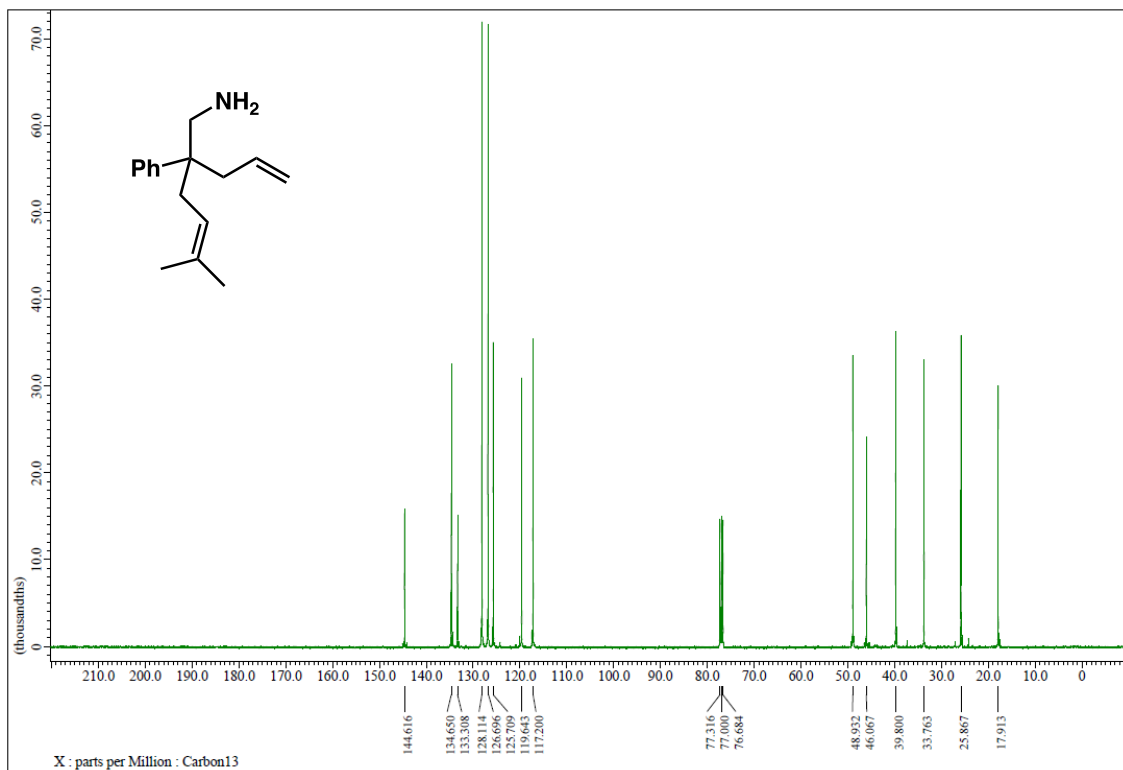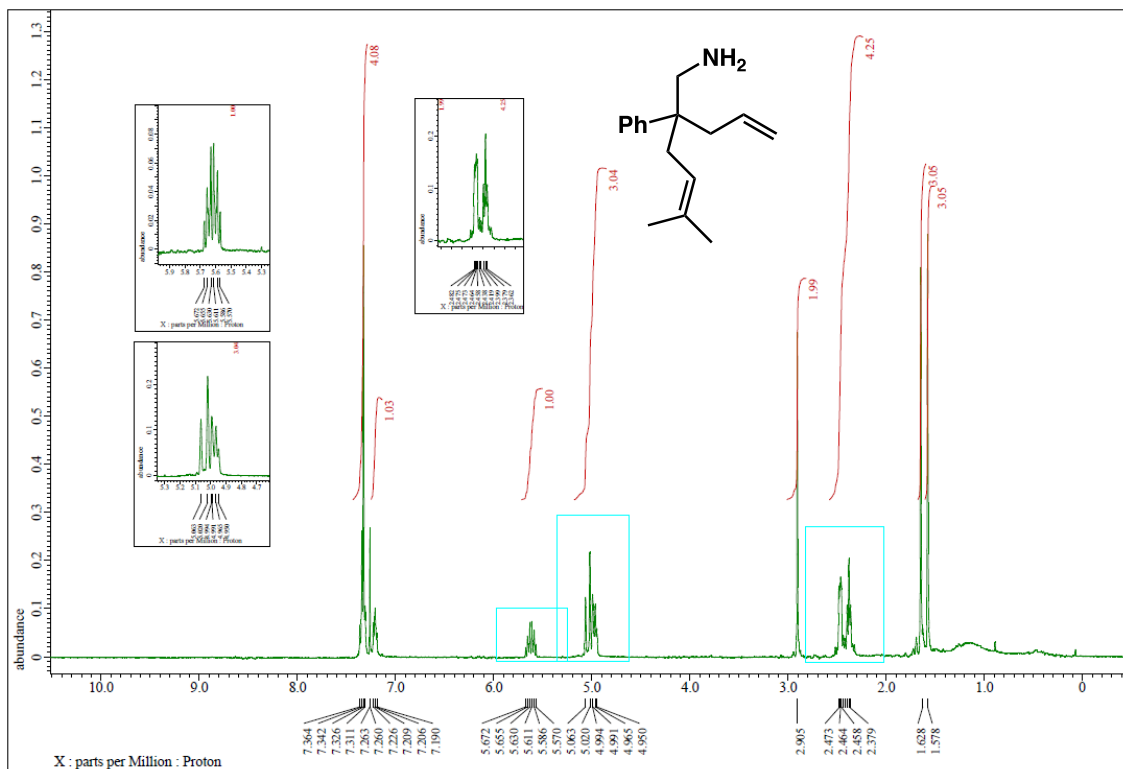## 2,2-Dimethyl-4,4-diphenylpyrrolidine (2b)
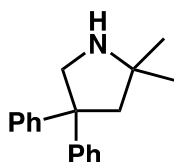
To a reaction tube equipped with a magnetic stir bar were added Au:F-CAC (1 mol%), amine (**2b**) (25.1 mg, 0.10 mmol), HCO$_2$NH$_4$ (31.5 mg, 500 mol%), and EtOH (10 mL). The mixture was stirred under air for 4 h at 50 °C. After cooling to room temperature, to the mixture was added saturated aqueous NaHCO$_3$ (ca. 5 mL), and the mixture was extracted with EtOAc. The combined organic extract was dried over Na$_2$SO$_4$. After filtration, the filtrate was concentrated under reduced pressure. The residue was purified by preparative TLC to give **2b** (24.8 mg, 0.99 mmol, 99%);

TLC R_f = 0.66 (CH$_2$Cl$_2$/MeOH/Et$_3$N = 70/38/2);

^{1}H NMR (CDCl$_3$) δ 7.32–7.24 (m, 8H), 7.18–7.12 (m, 2H), 3.66 (s, 2H), 2.55 (s, 2H), 1.84 (1s), 1.16 (s, 6H);

^{13}C NMR (CDCl$_3$) δ 147.5 (2C), 128.4 (4C), 126.9 (4C), 125.9 (2C), 59.3 (1C), 58.3 (1C), 57.2 (1C),

52.0 (1C), 30.7 (2C);

The chemical shifts were consistent with those reported in the literature.[18]

2-Methyl-4-(3-methylbut-2-en-1-yl)-4-phenylpyrrolidine (2f)
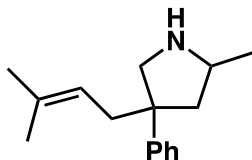
To a reaction tube equipped with a magnetic stir bar were added Au:F-CAC (0.5 mol%), amine (**2f**) (22.9 mg, 0.10 mmol), HCO_2NH_4 (31.5 mg, 500 mol%), and EtOH (10 mL). The mixture was stirred under air for 4 h at 50 °C. After cooling to room temperature, to the mixture was added saturated aqueous $NaHCO_3$ (ca. 5 mL), and the mixture was extracted with EtOAc. The combined organic extract was dried over Na_2SO_4. After filtration, the filtrate was concentrated under reduced pressure. The residue was purified by preparative TLC to give **2f** (20.4 mg, 0.89 mmol, 89%, dr = 1:1) as a diastereomeric mixture (dr = 1:1);

TLC R_f = 0.73 (CH_2Cl_2/MeOH/Et_3N = 90/8/2);

^{1}H NMR ($CDCl_3$) δ 7.32–7.15 (m, 5 H), 4.94–4.83 (m, 1H), 3.50 (ddd, J = 8.9, 6.5, 6.4 Hz, 0.5H), 3.30–3.12 (m, 2.5H), 2.44–2.24 (m, 3H), 1.61 (s, 3H), 1.58–1.49 (m, 1H), 1.44 (s, 1.5H), 1.41 (s, 1.5H), 1.24 (d, J = 6.4 Hz, 1.5H), 1.19 (d, J = 6.4 Hz, 1.5H);

^{13}C NMR ($CDCl_3$) δ 147.6 (0.5C), 147.3 (0.5C), 133.8 (0.5C), 133.6 (0.5C), 127.9 (0.5C+0.5C), 127.8 (0.5C+0.5C), 126.9 (1C+1C), 125.6 (0.5C+0.5C), 120.6 (0.5C), 120.4 (0.5C), 57.9 (0.5C), 57.1 (0.5C), 54.1 (0.5C), 53.3 (0.5C), 52.63 (0.5C), 52.57 (0.5C), 45.8 (0.5C), 45.2 (0.5C), 40.9 (0.5C), 39.3 (0.5C), 25.8 (0.5C+0.5C), 22.0 (0.5C), 21.9 (0.5C), 17.8 (0.5C), 17.7 (0.5C);

IR (diamond, cm^{-1}) 2960, 2922, 2854, 1605, 1496, 1442, 1401, 1222, 1111, 1074, 1029;

HRMS (EI) m/z 229.1822 (229.1830 calcd for $C_{16}H_{23}N$, [M+H]$^+$).

4-Allyl-2-methyl-4-phenylpyrrolidine (2g)
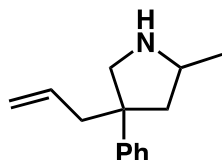
To a reaction tube equipped with a magnetic stir bar were added Au:F-CAC (0.5 mol%), amine (**2g**) (20.1 mg, 0.10 mmol), HCO_2NH_4 (31.5 mg, 500 mol%), and EtOH (10 mL). The mixture was stirred under air for 4 h at 50 °C. After cooling to room temperature, to the mixture was added saturated

aqueous $NaHCO_3$ (ca. 5 mL), and the mixture was extracted with EtOAc. The combined organic extract was dried over Na_2SO_4. After filtration, the filtrate was concentrated under reduced pressure. The residue was purified by preparative TLC to give **2g** (17.1 mg, 0.85 mmol, 85%) as a diastereomeric mixture (dr = 1:1);

TLC R_f = 0.62 (CH_2Cl_2/MeOH/Et_3N = 88/10/2);

^{1}H NMR (400 MHz, $CDCl_3$) δ 7.31–7.28 (m, 2H), 7.24–7.17 (m, 3H), 5.50–5.43 (m, 1H), 4.96–4.92 (m, 2H), 3.51–3.40 (m, 0.5H), 3.32–3.12 (m, 2.5H), 2.52–2.34 (m, 2.5H), 2.29 (dd, J = 12.4, 6.4 Hz, 0.5H), 1.61 (dd, J = 12.4, 9.2 Hz, 0.5H), 1.54 (dd, J = 13.3, 8.2 Hz, 0.5H), 1.23 (d, J = 6.4 Hz, 1.5H), 1.17 (d, J = 6.0 Hz, 1.5H);

^{13}C NMR ($CDCl_3$) δ 147.2 (0.5C), 147.0 (0.5C), 135.1 (0.5C), 134.9 (0.5C), 128.1 (1C), 128.0 (1C), 126.8 (2C), 125.9 (0.5C), 125.8 (0.5C), 117.4 (0.5C), 117.3 (0.5C), 57.9 (0.5C), 57.0 (0.5C), 54.1 (0.5C), 53.1 (0.5C), 52.0 (0.5C+0.5C, two signals overlapped), 47.3 (0.5C), 45.8 (0.5C), 45.6 (0.5C), 45.1 (0.5C), 22.3 (0.5C), 22.1 (0.5C);

The chemical shifts were consistent with those reported in the literature.[19]

2-Methyl-5,5-diphenylpiperidine (2h)
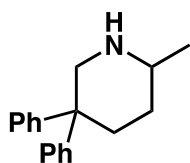
To a reaction tube equipped with a magnetic stir bar were added Au:F-CAC (0.5 mol%), amine (**2h**) (25.1 mg, 0.10 mmol), HCO_2NH_4 (31.5 mg, 500 mol%), and EtOH (10 mL). The mixture was stirred under air for 8 h at 50 °C. After cooling to room temperature, to the mixture was added saturated aqueous $NaHCO_3$ (ca. 5 mL), and the mixture was extracted with EtOAc. The combined organic extract was dried over Na_2SO_4. After filtration, the filtrate was concentrated under reduced pressure. The residue was purified by preparative TLC to give **2h** (19.8 mg, 0.79 mmol, 79%);

TLC R_f = 0.43 (CH_2Cl_2/MeOH/Et_3N = 88/10/2);

^{1}H NMR (400 MHz, $CDCl_3$) δ 7.41 (d, J = 7.32 Hz, 2H), 7.35 (t, J = 7.8 Hz, 2H), 7.24–7.01 (m, 6H), 3.92 (dd, J = 13.6, 3.0 Hz, 1H), 3.11 (d, J = 13.6 Hz, 1H), 2.83–2.73 (m, 1H), 2.71 (ddd, J = 13.5, 6.6, 3.4 Hz, 1H), 2.22 (ddd, J = 13.5, 13.5, 3.4 Hz, 1H), 1.64 (ddd, J = 13.5, 6.6, 3.4 Hz, 1H), 1.23–1.08 (m, 1H), 1.01 (d, J = 6.4 Hz, 1H);

^{13}C NMR ($CDCl_3$) δ 148.8 (1C), 144.7 (1C), 128.6 (2C), 128.2 (4C), 126.4 (2C), 125.78 (1C), 125.76 (1C), 55.7 (1C), 52.3 (1C), 45.2 (1C), 35.4 (1C), 31.4 (1C), 22.5 (1C);

The chemical shifts were consistent with those reported in the literature.[20]

2-Methyl-4,4-diphenyl-1-tosylpyrrolidine (2j)
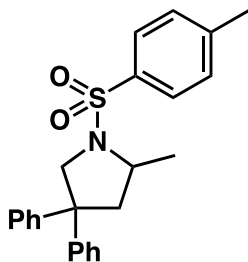
To a reaction tube equipped with a magnetic stir bar were added Au:F-CAC (0.5 mol%), amine (**2j**) (39.1 mg, 0.10 mmol), Cs_2CO_3 (97.7 mg, 300 mol%), and EtOH (10 mL). The mixture was stirred under air for 30 h at 50 °C. After cooling to room temperature, to the mixture was added saturated aqueous $NaHCO_3$ (ca. 5 mL), and the mixture was extracted with EtOAc. The combined organic extract was dried over Na_2SO_4. After filtration, the filtrate was concentrated under reduced pressure. The residue was purified by preparative TLC to give **2j** (38.6 mg, 0.99 mmol, 99%);

TLC R_f = 0.64 (CH_2Cl_2/MeOH/Et_3N = 67/30/3);

^{1}H NMR (CDCl$_3$) δ 7.62–7.60 (AA'BB', 2H), 7.33–7.01 (m, 12H), 4.17 (d, J = 10.5 Hz, 1H), 3.94 (d, J = 10.5 Hz, 1H), 3.78 (qdd, J = 7.3, 6.9, 6.4 Hz, 1H), 2.79 (dd, J = 12.3, 7.3 Hz, 1H), 2.39 (s, 3H), 2.26 (dd, J = 12.3, 6.9 Hz, 1H), 1.24 (d, J = 6.4 Hz, 3H);

^{13}C NMR (CDCl$_3$) δ 145.5 (1C), 144.8 (1C), 142.9 (1C), 135.3 (1C), 129.5 (2C), 128.4 (4C), 127.1 (2C), 126.7 (2C), 126.44 (2C), 126.41 (1C), 126.2 (1C), 58.4 (1C), 55.4 (1C), 52.2 (1C), 46.0 (1C), 22.1 (1C), 21.4 (1C);

The chemical shifts were consistent with those reported in the literature.[21]

¹H NMR (400 MHz) and ¹³C NMR (100 MHz) spectra of **1f-1** (CDCl₃)
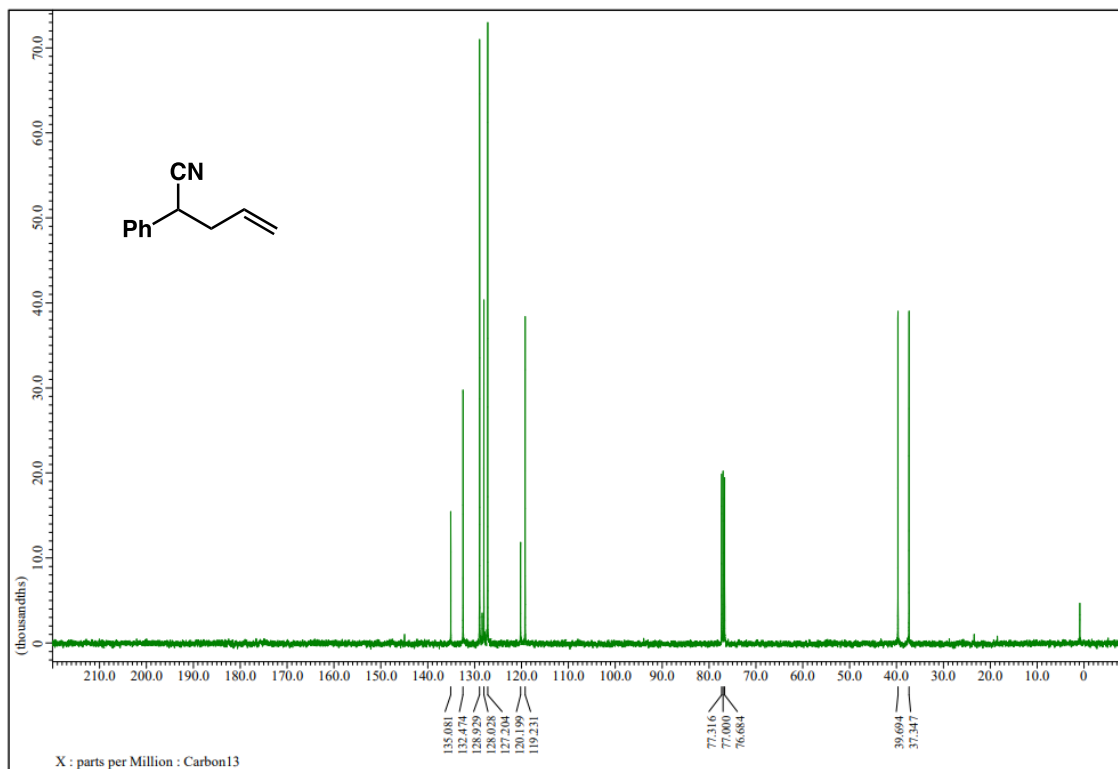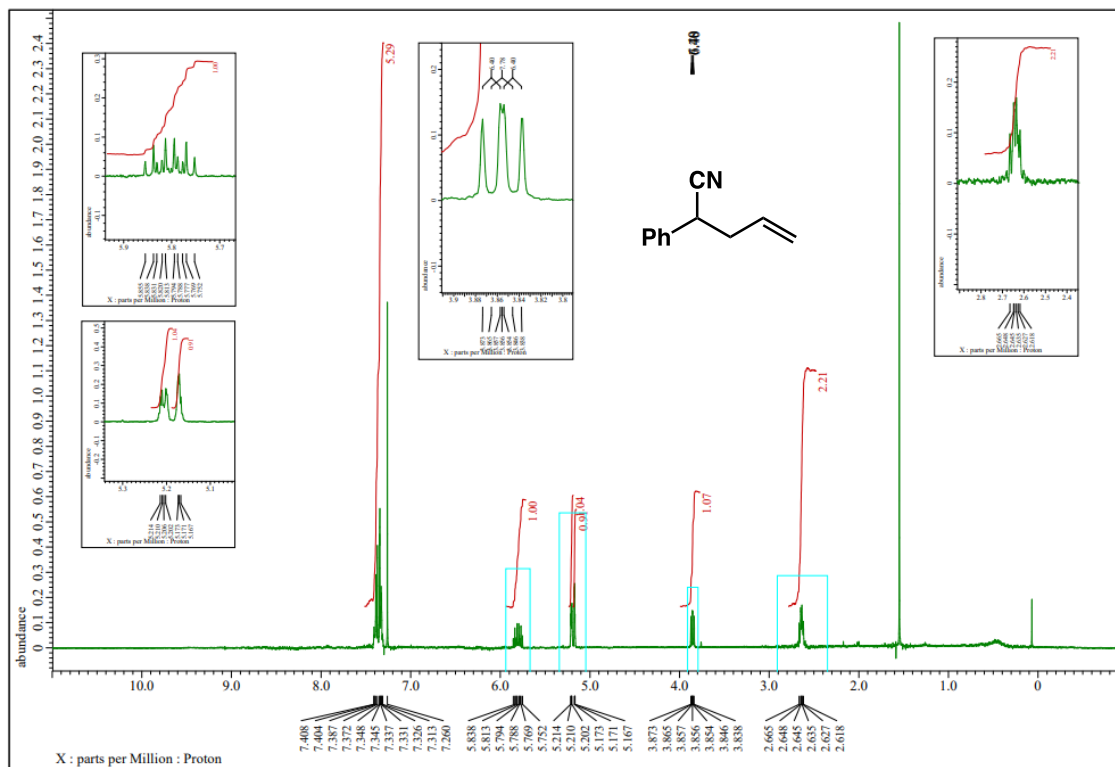
^{1}H NMR (400 MHz) and ^{13}C NMR (100 MHz) spectra of **1f-2**(CDCl$_3$)

¹H NMR (400 MHz) and ¹³C NMR (100 MHz) spectra of **2a** (CDCl₃)
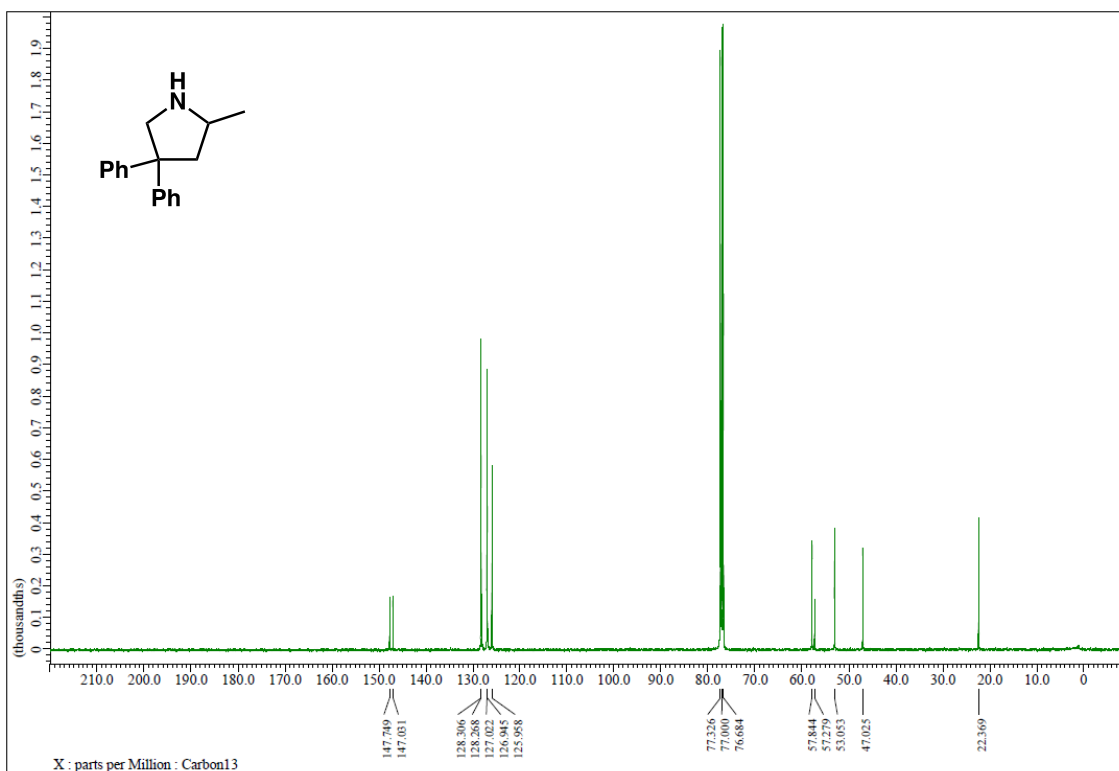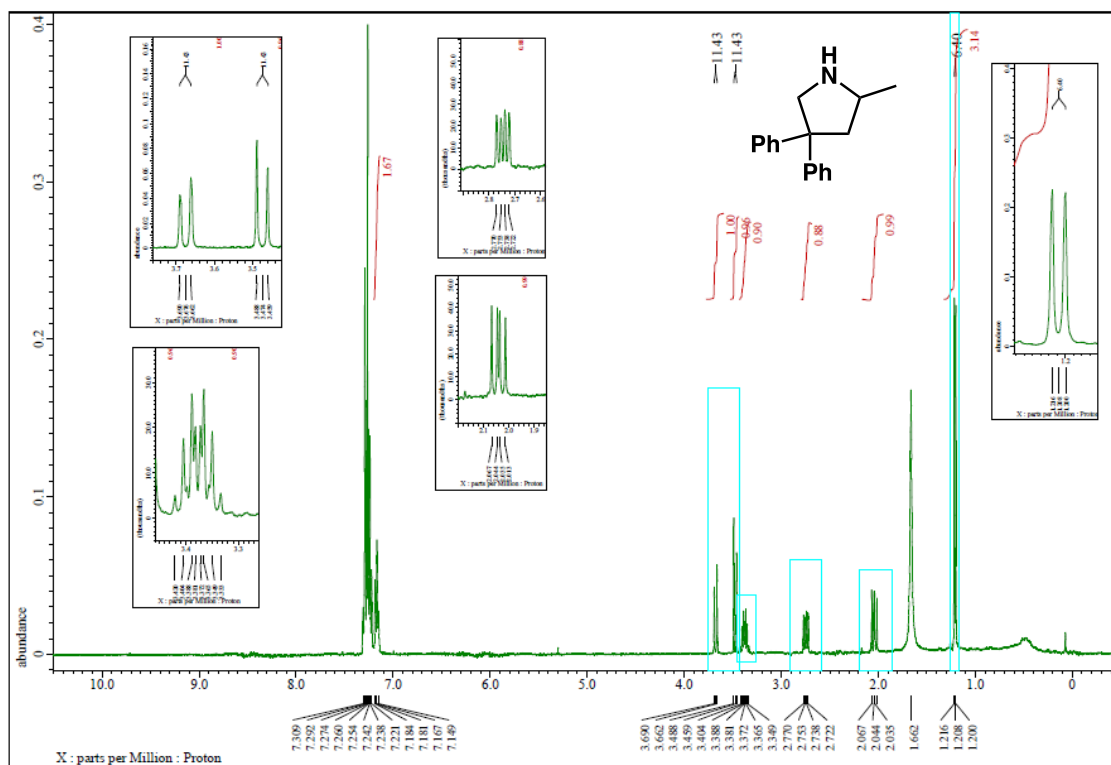
^{1}H NMR (400 MHz) and ^{13}C NMR (100 MHz) spectra of **2b**(CDCl$_3$)
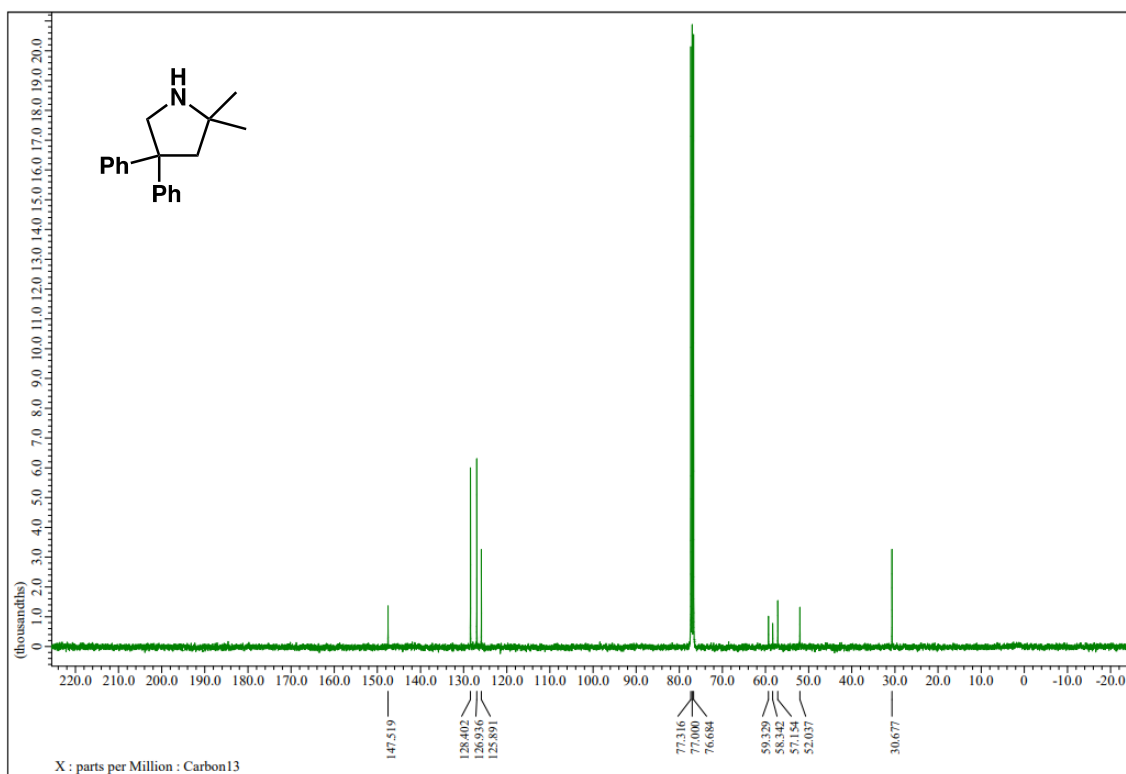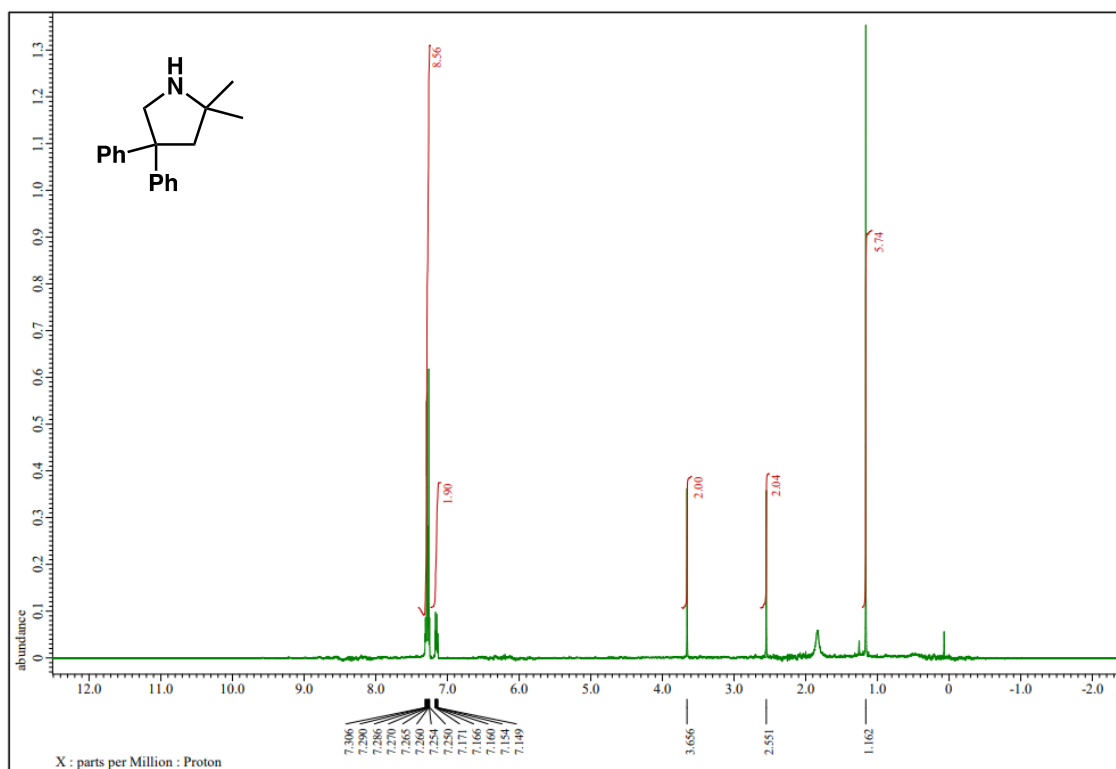
¹H NMR (400 MHz) and ¹³C NMR (100 MHz) spectra of **2f** (CDCl₃)
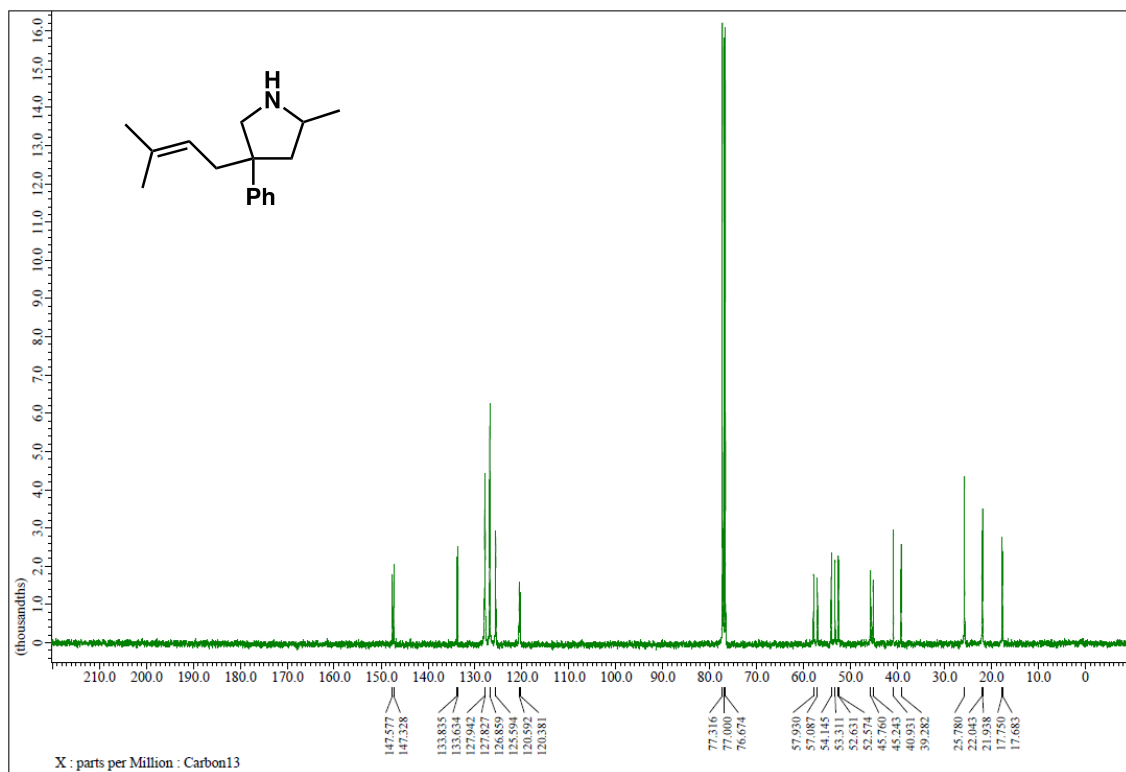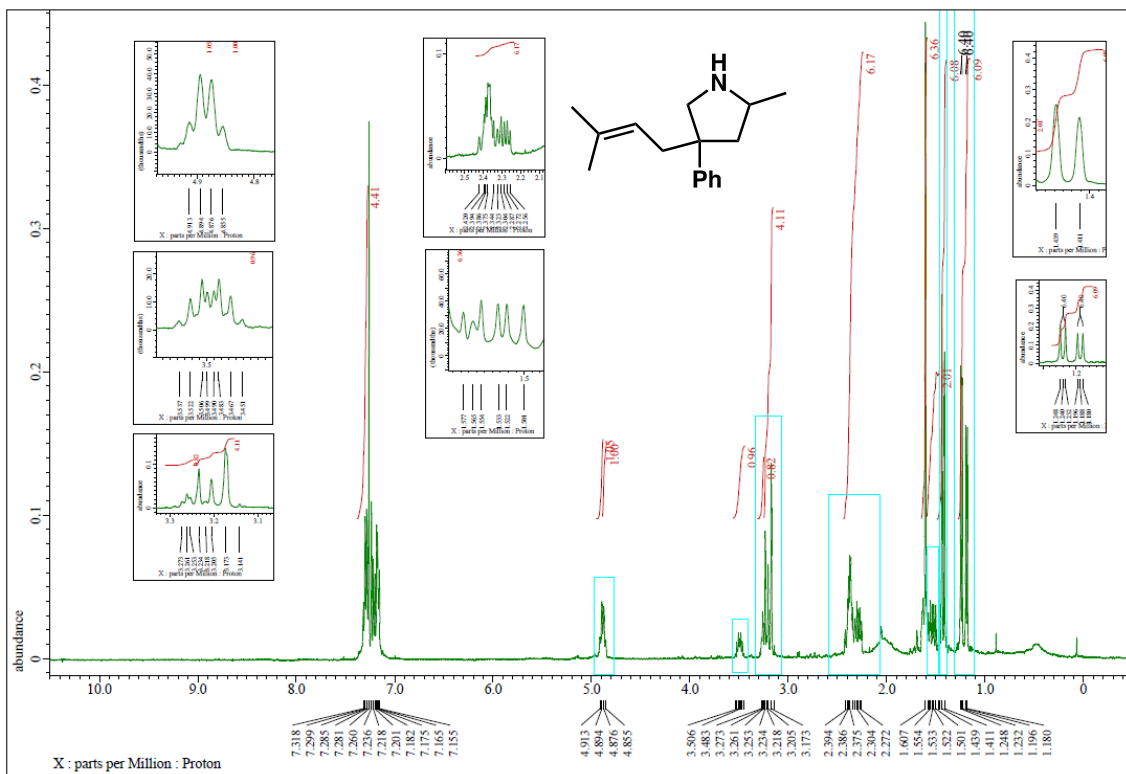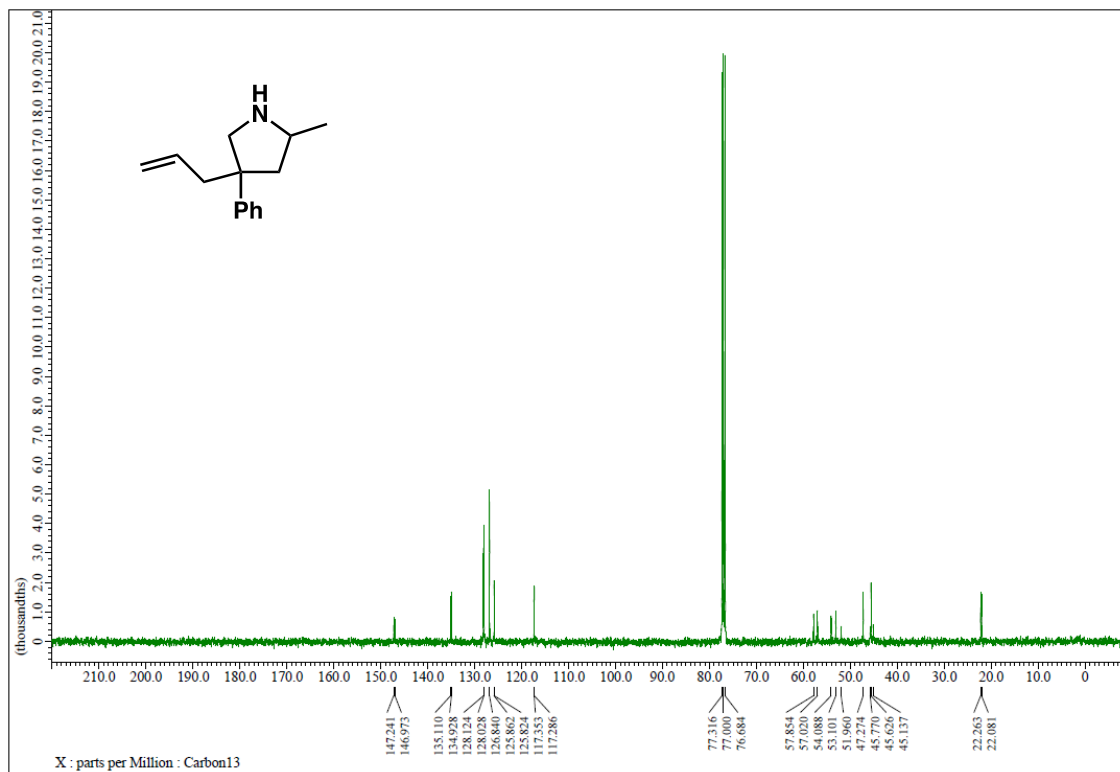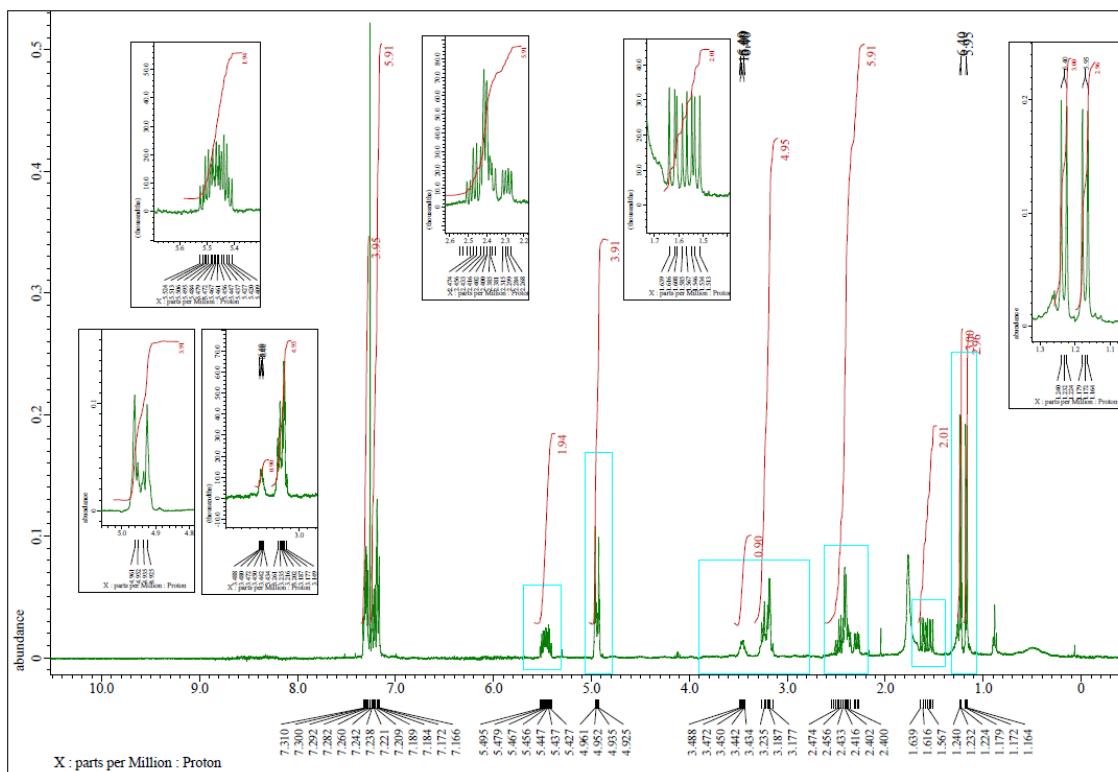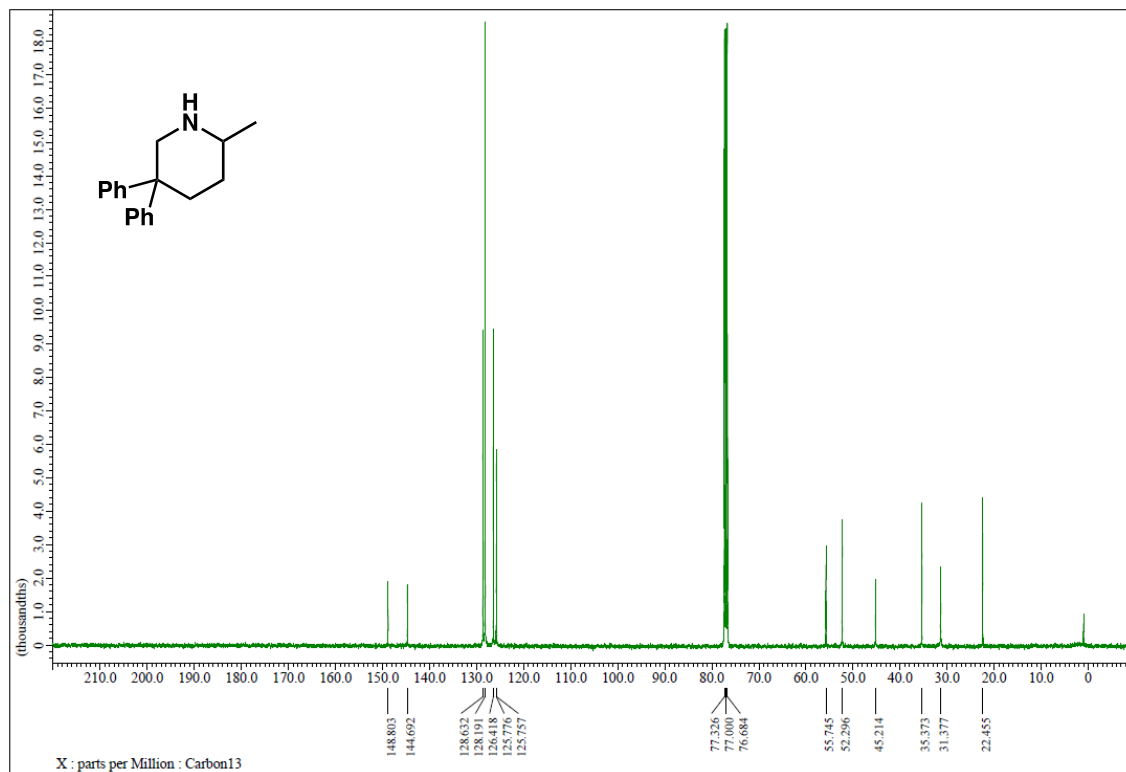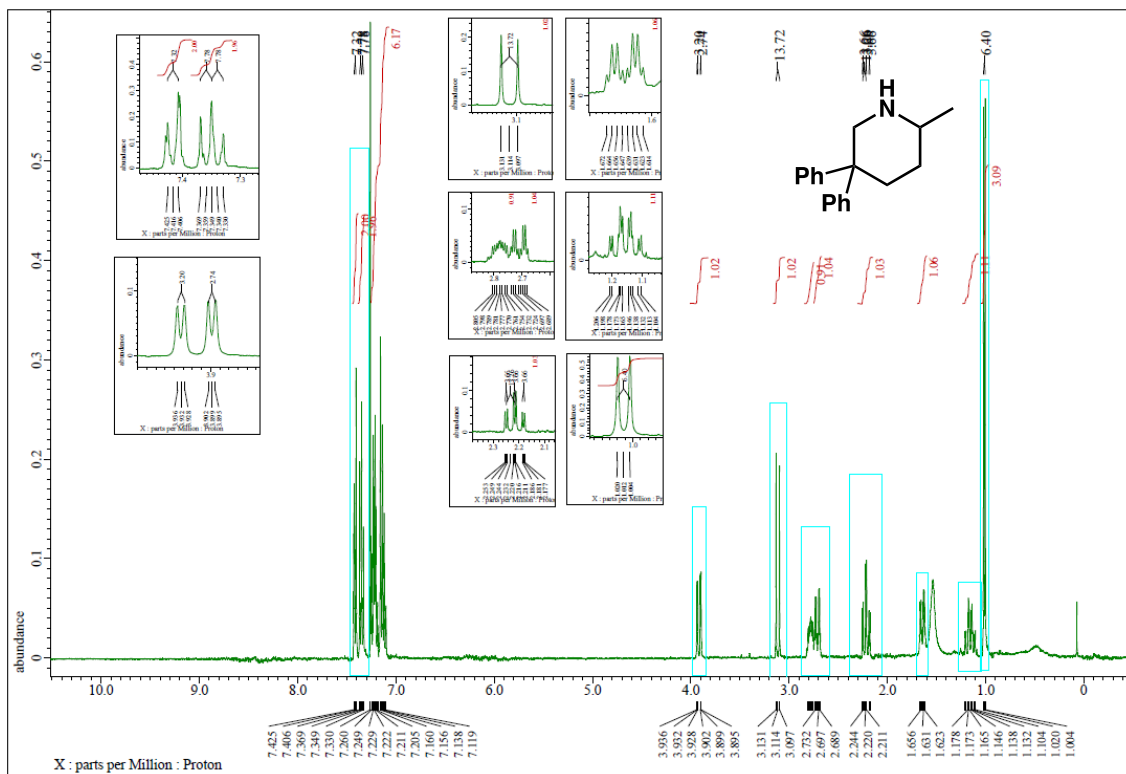
¹H NMR (400 MHz) and ¹³C NMR (100 MHz) spectra of **2g** (CDCl₃)

2.5 References

1. T. E. Müller, K. C. Hultzsch, M. Yus, F. Foubelo, M. Tada, *Chem. Rev.* **2008**, *108*, 3795.

2. (a) A. M. Johns, N. Sakai, A. Ridder, J. F. Hartwig, *J. Am. Chem. Soc.* **2006**, *128*, 9306. (b) J. J. Brunet, D. Neibecker, F. Niedercorn, *J. Mol. Catal.* **1989**, *49*, 235.

3. (a) D. Campeau, D. F. León Rayo, A. Mansour, K. Muratov, F. Gagosz, *Chem. Rev.* **2021**, *121*, 8756. (b) D. J. Gorin, F. D. Toste, *Nature* **2007**, *446*, 395. (c) A. S. K. Hashmi, *Acc. Chem. Res.* **2014**, *47*, 864.

4. R. A. Widenhoefer, X. Han, *Eur. J. Org. Chem.* **2006**, *20*, 4555.

5. (a) J. Zhang, C.-G. Yang, C. He, *J. Am. Chem. Soc.* **2006**, *128*, 1798. (b) R. L. LaLonde, W. E. Brenzovich, D. Benitez, E. Tkatchouk, K. Kelley, W. A. Goddard III, F. D. Toste, *Chem. Sci.* **2010**, *1*, 226.

6. G. Bistoni, P. Belanzoni, L. Belpassi, F. Tarantelli, *J. Phys. Chem. A* **2016**, *120*, 5239.

7. (a) I. Kamiya, H. Tsunoyama, T. Tsukuda, H. Sakurai, *Chem. Lett.* **2007**, *36*, 646. (b) H. Tsunoyama, N. Ichikuni, H. Sakurai, T. Tsukuda, *J. Am. Chem. Soc.* **2009**, *131*, 7086. (c) M. Palashuddin, S. K. Jana, C. K. Chattopadhyay, *Chem. Commun.* **2013**, *49*, 8235.

8. (a) J. Huang, M. Arndt, K. Gooßen, H. Heydt, L. J. Gooßen, *Chem. Rev.* **2015**, *115*, 2596. (b) M. Sengupta, S. Das, S. M. Islam, A. Bordoloi, *ChemCatChem* **2021**, *13*, 1089.

9. (a) H. Kitahara, I. Kamiya, H. Sakurai, *Chem. Lett.* **2009**, *38*, 908–909. (b) H. Kitahara, H. Sakurai, *Chem. Lett.* **2009**, *39*, 46. (c) H. Kitahara, H. Sakurai, *Chem. Lett.* **2012**, *41*, 1328.

10. (a) C. P. Jiménez-Gómez, J. A. Cecilia, *Molecules* **2020**, *25*, 3981. (b) H. Shaghaleh, X. Xu, S. Wang, *RSC Adv.* **2018**, *8*, 825.

11. R. N. Dhital, A. Murugadoss, H. Sakurai, *Chem. Asian J.* **2012**, *7*, 55.

12. (a) X. Cui, T. Honda, T.-A. Asoh, H. Uyama, *Carbohydr. Polym.* **2020**, *230*, 115662. (b) G. Sinawang, T. A. Asoh, M. Osaki, H. Yamaguchi, A. Harada, H. Uyama, Y. Takashima, *ACS Appl. Polym. Mater.* **2020**, *2*, 2274.

13. (a) T. Chutimasakul, Y. Uetake, J. Tantirungrotechai, T.-A. Asoh, H. Uyama, H. Sakurai, *ACS Omega* **2020**, *5*, 33206. (b) S. Haesuwannakij, T. Kimura, Y. Furutani, K. Okumura, K. Kokubo, T. Sakata, H. Yasuda, Y. Yakiyama, H. Sakurai, *Sci. Rep.* **2017**, *7*, 9579.

14. H. Tsunoyama, H. Sakurai, Y. Negishi, T. Tsukuda, *J. Am. Chem. Soc.* **2005**, *127*, 9374.

15. H. Tsunoyama, H. Sakurai, T. Tsukuda, *Chem. Phys. Lett.* **2006**, *429*, 528.

16. K. Bobuatong, H. Sakurai, M. Ehara, *ChemCatChem* **2017**, *9*, 4490.

17. A. Horn, P. H. Dussault, *J. Org. Chem.* **2019**, *84*, 14611.

18. M. R. Crimmin, M. Arrowsmith, A. G. M. Barrett, I. J. Casely, M. S. Hill, P. A. Procopiou, *J. Am. Chem. Soc.* **2009**, *131*, 9670.

19. L. Ferrand, Y. Tang, C. Aubert, L. Fensterbank, V. Mouriès-Mansuy, M. Petit, M. Amatore, *Org. Lett.* **2017**, *19*, 2062.

20. H. Ohmiya, T. Moriya, M. Sawamura, *Org. Lett.* **2009**, *11*, 2145.

21. G.-Q. Liu, W. Li, Y.-M. Li, *Adv. Synth. Catal.* **2013**, *355*, 395.

Chapter 3: Dehydrogenative Oxidation of Hydrosilanes Using Gold Nanoparticle Deposited on Citric Acid-Modified Fibrillated Cellulose: Unveiling the Role of Molecular Oxygen

3.1   Introduction

Silanols have a wide range of applications. They are excellent building blocks for silicon-based polymeric materials[1], serve as pharmacological functional groups[2], and act as coupling reagents[3] as well as protecting groups in organic synthesis.[4] Traditionally, oxidizing silanes required a stoichiometric amount of oxidants such as permanganate, osmium tetroxide, peroxide, peracid and ozone (**Figure 3-1A**).[5] These methods inevitably produced a corresponding amount of by-products. As a result, catalytic dehydrogenative oxidation of hydrosilanes has garnered attention due to its use of non-toxic reactants, with hydrogen being the sole by-product, rendering these processes clean and environmentally friendly.
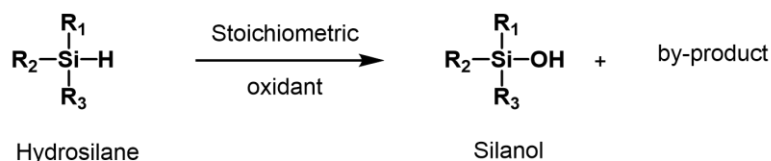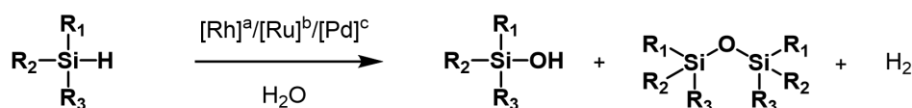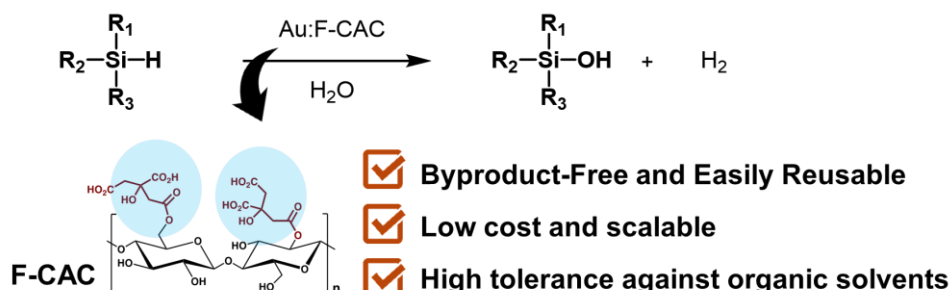
Figure 3-1. Oxidation of hydrosilane in various methods

On the other hand, noble metal catalysts, such as Rh,[6a] Ru,[6b] and Pd,[6c] were proposed to overcome these drawbacks. These catalytic systems involving water and oxygen have been recently devised. They offer the advantage of cleanly producing silanols along with hydrogen gas as the only by-product.[7] However, the removal of water easily occurs in molecules containing Si-OH groups to engage in an intermolecular condensation process, resulting in undesired siloxanes (**Figure 3-1B**).[6] The selective formation of silanols can be potentially difficult. Thus, it is crucial to seek processes that are more environmentally favorable and provide products selectively.

Gold nanoparticles (AuNPs) are renowned catalysts for aerobic oxidation reactions.[8] Kaneda et al. initially reported on AuNP-catalyzed oxidation of hydrosilanes under aerobic conditions at 80 °C. The oxidation of various silanes into silanols in water can be facilitated by hydroxyapatite-supported gold nanoparticles (AuHAP). This is the first catalytic technique for the selective production of aliphatic silanols. The AuHAP can function as extremely effective and reusable catalysts.[8a, 8b] Then various solid-supported AuNPs catalysts have been explored, including those stabilized on carbon nanotubes (CNT)[9], cellulose,[10] and manganese oxide (MnO_2).[11] These studies have highlighted the critical role of solid supports in catalytic activity especially in MnO_2. The enhanced catalytic activity of MnO_2-AuNPs can be attributed to the solid support. The interactions between AuNPs and the MnO_2 support by charge transfer facilitate oxidative processes, yielding excellent results in the oxidation of hydrosilanes. Additionally, a high concentration of Au^+ species and oxygen vacancies on the catalyst surface creates highly active sites for oxidation reactions. Furthermore, the ultrasmall size of AuNPs on the MnO_2 surface exposes high-energy Au facets, increases the surface-to-volume ratio, and ensures uniform dispersion. The synthesis of MnO_2-AuNPs is straightforward, utilizing MnO_2 nanowires as physical templates for AuNPs deposition without requiring any prior surface modification or functionalization. This report underscores the importance of developing novel supports to enhance catalytic activity.

In aspect of sustainable and environmentally friendly science, cellulose-based materials, abundant in nature, hold considerable promise. The previous report has devised a straightforward and scalable approach to produce citric acid-modified cellulose (F-CAC), which can be easily defibrated into a fluffy nanostructure using a commercially available mixer.[12] The fluffy nanostructure and excellent tolerance to organic solvents make F-CAC well-suited as a heterogeneous catalyst for reactions conducted in organic solvents. The earlier research showcased the size-selective preparation of Au:F-CAC catalysts using the trans-deposition method. By using size-selectively prepared Au:PVP (K-15) (PVP: poly(*N*-vinyl-2-pyrrolidone)), the Au:F-CAC was able to prepare with particle sizes ranging from 1.7 to 8.2 nm, enabling the investigation of size effects. These Au:F-CAC catalysts have shown good catalytic activity in the oxidation of alcohols and the intramolecular cyclization of amines.

Furthermore, the AuNPs in Au:F-CAC are stable under reaction conditions, likely due to the introduced coordinative carboxy groups, which facilitate size-selective preparation and recyclability.

In this chapter, the author explored the catalytic activity of Au:F-CAC in the dehydrogenative oxidation of hydrosilane. Size-selectively prepared Au:F-CAC catalysts underwent kinetic studies, uncovering size effects that had not been previously explored. Furthermore, labeling experiments and comprehensive spectroscopic analyses, including near-ambient pressure X-ray photoelectron spectroscopy (NAP-XPS) and solution-state X-ray absorption spectroscopy (XAS), were conducted on the model AuNPs catalyst to investigate the influence of molecular oxygen under aerobic conditions.

3.2 Result and discussions

3.2.1 Optimization of reaction conditions

The preparation of catalyst Au:F-CAC (particle size of Au: 1.7 ± 0.2 nm, 1.7×10^{-3} wt%) is well studied and the optimization condition for preparing is already established.[13] With the catalyst in hand, its application to silane oxidation was explored. The triphenylsilanol (**1a**) was selected as a model substrate. In the presence of Au:F-CAC (0.5 atom%) and H_2O (1000 mol%) in n-hexane, the oxidation of hydrosilane resulted in a 58% yield of triphenylsilanol (**2a**) after 15 minutes (**Table 3-1**, entry 1), with no detection of hexaphenyldisiloxane (**3a**). Utilizing polar solvents such as EtOAc and tetrahydrofuran (THF) slightly increased the yield (entries 2 and 3). Complete conversion of **1a** to **2a** was achieved by extending the reaction time to 120 minutes, resulting in a quantitative yield (entry 4). The Au loading could be reduced to 0.01 atom% without compromising the yield of **2a**, although a slight increase in reaction time was necessary (entries 5–7). The reaction did not occur in the absence of Au:F-CAC (entry 8). Additionally, decreasing the amount of water required a longer reaction time (entries 6 and 7).

Table 3-1. Optimization of the reaction conditions
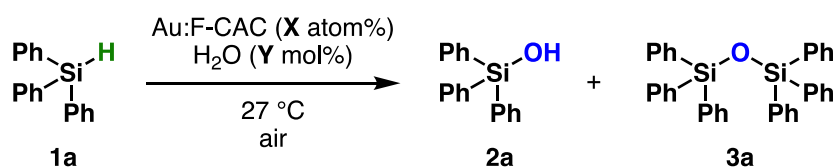
entry	X (atom%)	Y (mol%)	solvent	time (min)	yield of 2a (%)[a]	yield of 3a (%)[a]
1	0.5	1000	*n*-hexane	15	58	0
2	0.5	1000	EtOAc	15	62	0
3	0.5	1000	THF	15	64	0
4	0.5	1000	THF	120	99	0
5	0.07	1000	THF	300	99	0
6	0.01	400	THF	300	99	0
7	0.01	200	THF	360	99	0
8	–	200	THF	360	0	0

[a]Determined by GC.

3.2.2 The durability and reusability of Au:F-CAC

Recycling experiments were conducted to evaluate the durability of the Au:F-CAC catalyst. **Figure 3-2a** shows the results of experiments using 0.01 atom% of Au:F-CAC in THF, along with its reusability tests. The spent catalyst was easily recovered by filtration and reused without additional treatment, maintaining consistently high activity up to the sixth recycling cycle. Transmission electron microscopy (TEM) images of fresh and reused Au:F-CAC, shown in **Figure 3-2b**, revealed slight aggregation of AuNPs after the sixth cycle. However, the mean diameter of Au NPs was 2.5 ± 1.0 nm, which is within the error range of the fresh catalyst (1.7 ± 0.8 nm). The sustained catalytic activity suggests high stability of the catalyst, likely due to the carboxylic acid groups attached to the cellulose. This notable stability allowed to investigate the size dependency in this reaction (vide infra). A hot filtration test was conducted to separate the Au:F-CAC from the reaction mixture when the yield of **2a** reached 56% (approximately after 3 hours, **Figure 3-3**). The filtrate, subjected to identical conditions without the catalyst, exhibited no increase in the yield of **2a**. Inductively coupled plasma spectroscopy-atomic emission spectroscopy (ICP-AES) analysis of the filtrate confirmed the absence of Au species (detection limit: 10 ppb). These findings suggest that the reaction occurs in heterogeneous manner on the surface of AuNPs.[14]
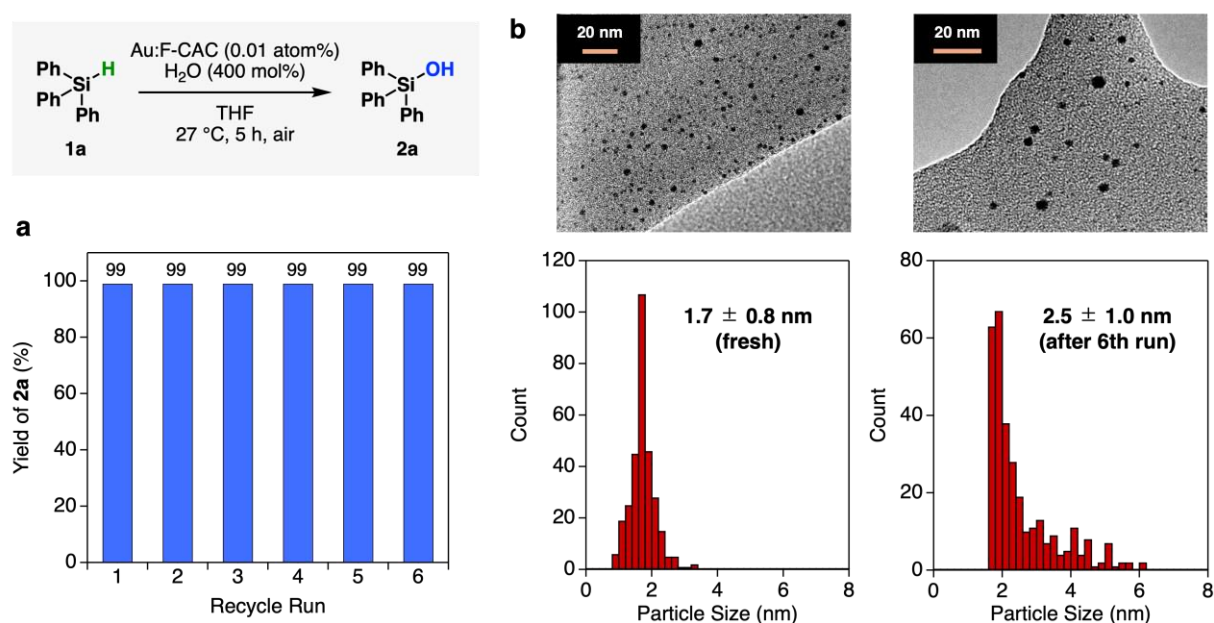
Figure 3-2. Catalytic performance of Au:F-CAC catalyst for oxidation of hydrosilane. (a) Recycling run experiment. (b) TEM images of the fresh and spent catalyst after the sixth run. Mean diameter and standard deviation are based on the average 300 particles.
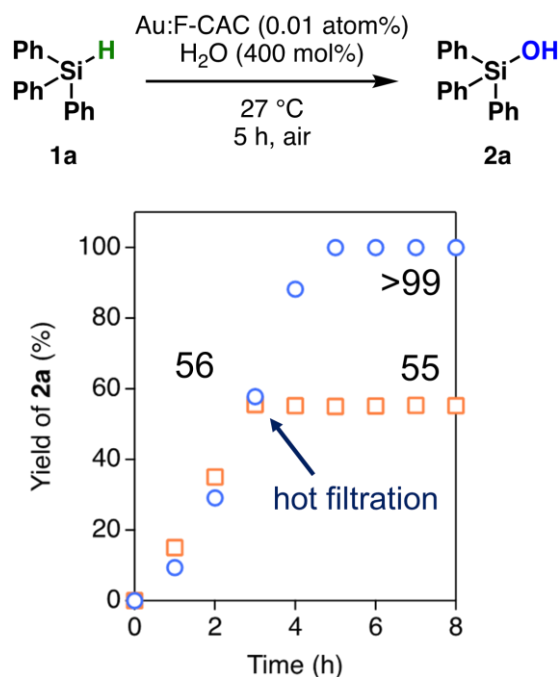
Figure 3-3. Hot filtration experiment

Additionally, other substrates, such as methyldiphenylsilane (**1b**) and dimethylphenylsilane (**1c**), were tested under the same reaction conditions, resulting in the quantitative formation of the corresponding silanols **2b** and **2c** (**Figure 3-4**).

99% (**2a**, 4 h)   99% (**2b**, 2 h)   99% (**2c**, 2 h)
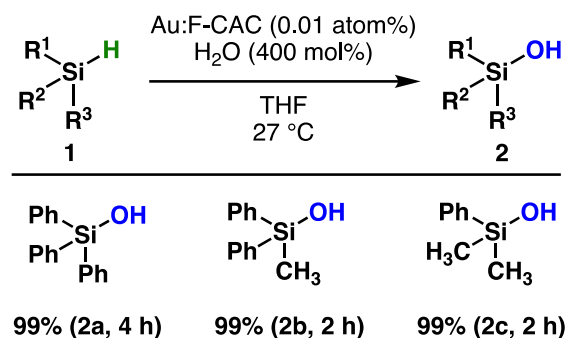
[a]Determined by ^{1}H NMR analysis.

Figure 3-4. Substrate scope

3.2.3 Size dependency of Au:F-CAC and kinetic study

Due to the robust durability of the Au:F-CAC catalyst under reaction conditions, the size dependency was able to investigate. Au:F-CAC catalysts sized at 1.7 ± 0.8 nm, 4.9 ± 0.7 nm, and 7.7 ± 1.4 nm were prepared using the trans-deposition method tailored for F-CAC. Kinetic studies were conducted using 0.01 atom% catalysts at 27 °C, and in all cases, the oxidation reaction successfully

yielded 2a. Notably, there was no significant aggregation of AuNPs observed post-reaction, even for the 4.9 nm and 7.7 nm particles. (**Figure 3-4**).
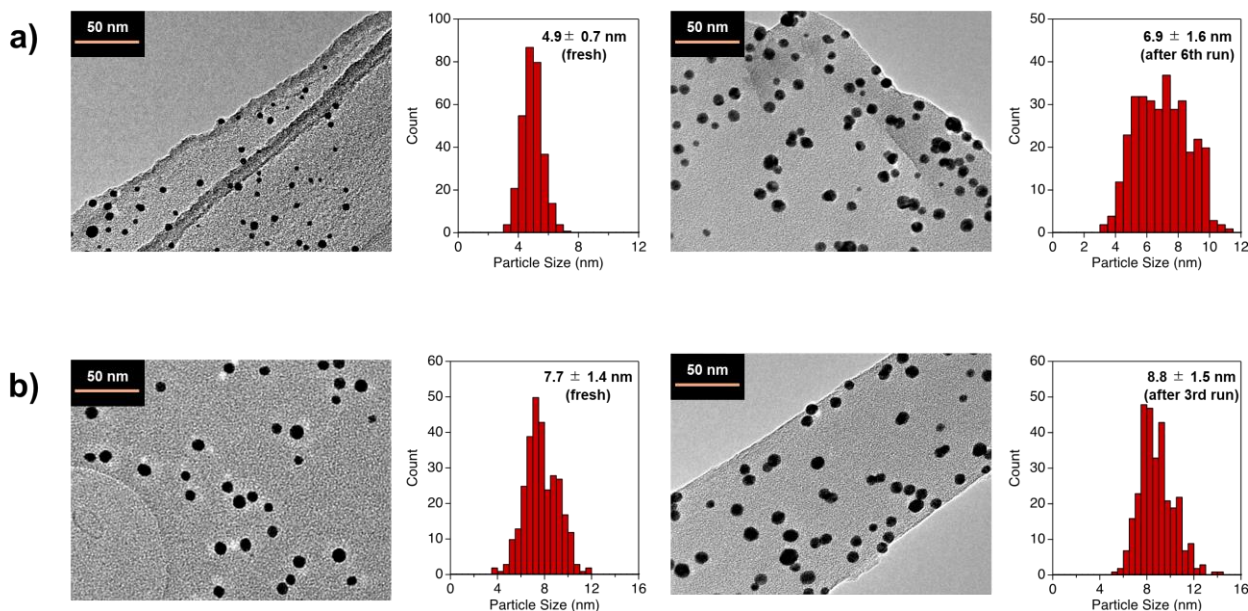
Figure 3-4. TEM images and size distribution of Au:F-CAC. (a) Au:F-CAC (4.9 nm): fresh (left) and spent catalyst after sixth run (right). (b) Au:F-CAC (7.7 nm): fresh (left) and spent catalyst after third run (right).

Figure 3-5 presents time-course plots of the concentration of **1a**, showing that the reaction rate order was 1.7 nm > 4.9 nm > 7.7 nm. An induction period of approximately 2 hours was observed for Au:F-CAC with a size of 7.7 nm. Despite this, the plots fit linear functions, indicating zeroth-order kinetics for 1a. This zeroth-order kinetics suggests that the catalytically active surface of Au was thoroughly saturated with reactants, attributed to the small amount of Au used ([**1a**]/[$N_{surface\ Au}$] > 14,000). Therefore, the zeroth-order kinetic constant (k, mmol L^{-1} h^{-1}) and turnover frequency (TOF) based on total loaded Au atoms (TON$_{total\ Au}$, h^{-1}) were evaluated using the data after the induction period (**Table 3-2**) as follows,

$$\text{TOF}_{\text{total Au}} = \frac{k}{C_{\text{Au}}}$$

where C_{Au} signifies the initial concentration of Au. The TOF$_{total\ Au}$ values of Au:F-CAC of 1.7 nm, 4.9 nm, and 7.7 nm were 3060 h^{-1}, 2160 h^{-1}, and 1200 h^{-1}, respectively. In addition, the

TOF based on the surface Au atoms (TON$_{\text{surface Au}}$) was calculated based on the assumption that AuNPs are spherical with a diameter determined by TEM (d$_{\text{TEM}}$) as follows,

$$TOF_{\text{surface Au}} = TOF_{\text{total Au}} \cdot \left(\frac{N_{\text{surface Au}}}{N_{\text{total Au}}}\right)^{-1} = TOF_{\text{total Au}} \cdot \frac{(d_{\text{TEM}})^3}{(d_{\text{TEM}})^3 - (d_{\text{TEM}} - 0.576)^3}$$

The distance between Au atoms in the particles is assumed to be 0.288 nm from the crystal structure of Au. The TOF$_{\text{surface Au}}$ values of Au:F-CAC of 1.7 nm, 4.9 nm, and 7.7 nm were calculated to be 4304 h^{-1}, 7028 h^{-1}, and 5976 h^{-1}, respectively. These findings indicate that Au:F-CAC with a size of 4.9 nm exhibited the highest catalytic activity, demonstrating clear size dependency in the oxidation of hydrosilane (**Table 3-2**).
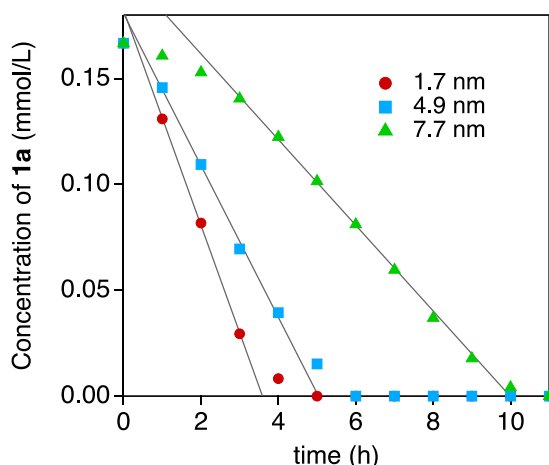
Figure 3-5. Plots of the concentration of **1a** after the specific time. The reaction was performed under air using 0.01 atom% Au:F-CAC and H$_2$O (400 mol%) in THF (3 mL) at 27 °C.

Table 3-2. Kinetic parameters and catalytic activity

d$_{\text{TEM}}$ (nm)	k (mmol L^{-1} h^{-1})	TOF$_{\text{total Au}}$ (h^{-1})[a]	TOF$_{\text{surface Au}}$ (h^{-1})[b]
1.7	0.051	3060	4304
4.9	0.036	2160	7028
7.7	0.020	1200	5976

[a]Based on the total Au atoms. [b]Based on the surface Au atoms.

The catalytic activity of reported AuNP catalysts, including Au:F-CAC was summarised in **Table 3-3**. Although the catalytic activity based on TON was moderate among these catalysts, Au:F-CAC does not require expensive materials and complicated synthetic procedures. In fact, F-CAC can be prepared in a 30 g scale through easy protocols from low-cost and naturally derived starting materials, rendering Au:F-CAC an easy-to-access nanomaterial.

Table 3-3. Summary of the reported catalytic activity on dehydrogenative oxidation of dimethylphenylsilane[8e,15]

catalyst	Au loading (mol%)	time (min)	solvent	TOF (h⁻¹)	reuse (times)	ref.
Au/AlO(OH)	0.1	30	EtOAc	1960	10	8e[a]
AuNPore	1	60	Acetone	10700	5	7[b]
AuCNT	0.001	360	THF–H_2O	9100	5	8a[a]
Au(ONT)	0.05	150	THF	768	4	16[a]
Au(o-CNTs)	0.1	40	H_2O	1477	3	9a[a]
AuHAP	0.83	180	H_2O	40	4	8b[a]
MnO_2-Au	0.001	10	H_2O	590000	10	11a[a]
Au-SiO_2	0.4	1	THF	59400	5	17[b]
SBA–PIL–Au	0.4	180	H_2O	83	3	8c[a]
AuHAP	0.04	5	Acetone	29711	-	18[a]
KCC-1-APTS/Au	0.05	1320	THF–H_2O	-	10	19
Au-MPBen	52μ	30	THF	1475	4	20[b]
Au_1/mpg-C_3N_4	0.004	30	Acetone	50200	10	21[a]
Au/TiO_2	0.003	30	H_2O	-	10	22
Au:F-CAC	**0.01**	**120**	**THF**	**7028**	**5**	**This work**

[a]Based on the gold loading. [b]Based on the surface gold atoms.

3.2.4 Reaction mechanism study

The effect of the reaction atmosphere was investigated using 0.01 atom% of Au:F-CAC at 27 °C, evaluating the yield of **2a** after 2 hours. The yields of **2a** were 93% in oxygen, 29% in air, and 6% in an argon atmosphere (**Table 3-4**). This result clearly indicates that the oxygen partial pressure influences the reaction rate, suggesting that the adsorption of molecular oxygen on the surface of AuNPs and/or such adsorbed Au species is involved in the rate-determining step.

Table 3-4. Effect of oxygen partial pressure

entry	atmosphere	yield of 2a (%)[a]
1	O_2	93
2	air	29
3	Ar	6

[a]Determined by GC

To elucidate the reaction mechanism of hydrosilane oxidation, isotope labeling experiments and theoretical calculations were conducted. The reaction was conducted using $[^{18}O]H_2O$ under ambient aerobic conditions to trace the origin of the oxygen atom in silanol. Using the optimized reaction conditions, the reaction was completed within 4 hours. Fourier transform infrared (FT-IR) absorption spectroscopy of the synthesized **2a** revealed a peak corresponding to the Si−O vibration at 845 cm^{-1}, which was red-shifted by 12 cm^{-1} compared to non-labeled **2a** (857 cm^{-1}) (**Figure 3-6**). This outcome confirmed the formation of $[^{18}O]$**2a**, indicating that the oxygen atom in **2a** originated from H_2O rather than molecular oxygen. Theoretical calculations using density functional theory (DFT) at the B3LYP-D3BJ/6-31G(d) level in the gas phase assigned the vibration mode, showing the Si−^{18}O vibration shifted by 11 cm^{-1} from the Si−^{16}O vibration, aligning well with the experimental data. Therefore, molecular oxygen accelerates the reaction by adsorbing onto the surface of AuNPs. Previous studies have shown that AuNPs-catalyzed intramolecular cyclization of amines and/or alcohols proceeds under an aerobic atmosphere using AuNPs catalysts such as Au:PVP[24] and Au:F-CAC.[25] Moreover, theoretical calculations suggest that cationic Au sites, which catalyze intramolecular cyclization, form by the adsorption of molecular oxygen on the surface.[8,26] Based on this, the acceleration effect of oxygen in this reaction is attributed to the efficient formation of cationic Au species. Camargo et al. reported that the formation of a higher number of cationic Au sites facilitated by Au-support interactions is critical for achieving high catalytic activity in hydrosilane oxidation, which aligns closely with the author findings.[9,11a,27]
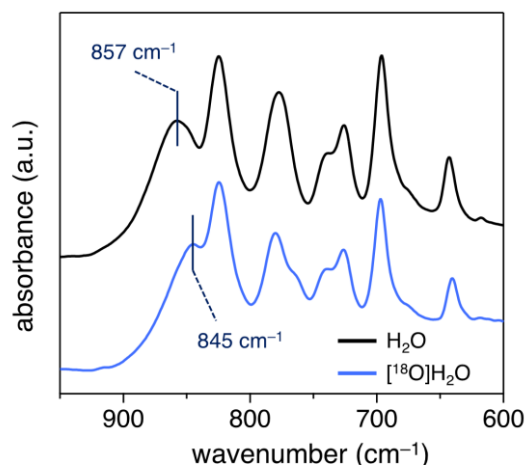
Figure 3-6. Isotope labeling experiment using $[^{18}O]H_2O$ and FT-IR spectra of **2a**. Au:F-CAC (0.01 atom%), $[^{18}O]H_2O$ (400 mol%), and THF (3 mL) were used.

In order to confirm the formation of cationic Au sites, NAP-XPS experiments were conducted using Au:PVP (K-30, 1.7 nm) as a model catalyst (**Figure 3-7**). Au 4f NAP-XPS measurements were performed at an oxygen partial pressure (p_{oxygen}) of 0.1 Torr and under ultrahigh vacuum conditions (6.8×10^{-9} Torr) using the same sample. The NAP-XP spectra at the Au 4f core level are shown in **Figure 3-8**. Under ultrahigh vacuum conditions, peaks corresponding to Au $4f_{7/2}$ and Au $4f_{5/2}$ core levels were observed at 83.7 eV and 87.4 eV, respectively, indicating a shift towards lower binding energy compared to bulk Au (84.0 eV for Au $4f_{7/2}$ and 87.7 eV for Au $4f_{5/2}$).[28] This shift suggests the formation of slightly anionic Au(0) species.
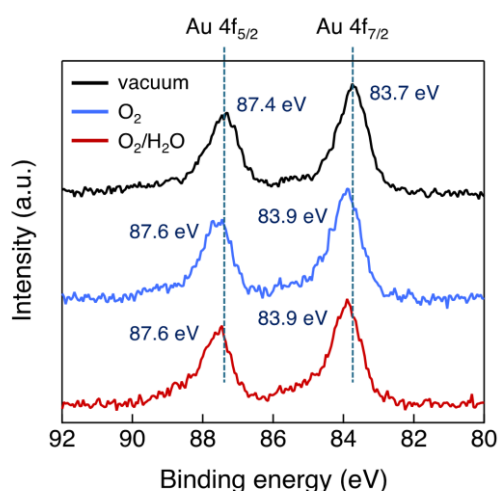
Figure 3-7. Au 4f NAP-XPS data of Au:PVP under vacuum (black line), p_{oxygen} = 0.1 Torr (bule line), and p_{oxygen} = 0.1 Torr, p_{water} = 0.1 Torr (red line)
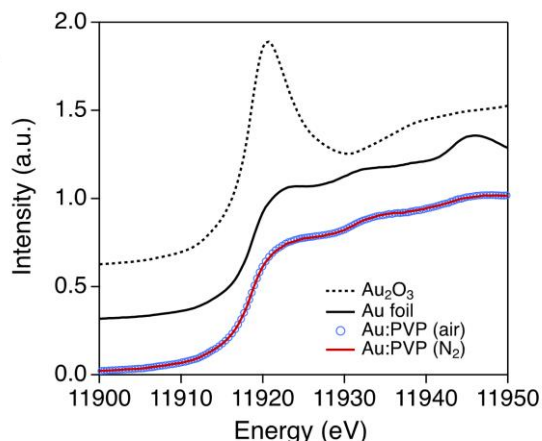
Figure 3-8. Au L$_3$-edge XAS data of Au:PVP in H$_2$O

In addition to the NAP-XPS experiment, Au L$_3$-edge solution state XAS experiments were conducted to gain further experimental insight into the electronic state of AuNPs. Au:PVP (K-30) was dissolved in H$_2$O at an Au concentration of 8.0 mmol/L, and the solution was bubbled with N$_2$ gas for 15 minutes. The prepared solution was then packed in a gas barrier bag and subjected to the XAS experiment using the fluorescence method. However, the XAS spectra remained almost unchanged before and after bubbling N$_2$ gas. This was likely due to the presence of a significant amount of H$_2$O, which adsorbs onto the Au surface, preventing the gaseous oxygen from influencing the electronic state of AuNPs (**Figure 3-8**).

In contrast, under an O$_2$ atmosphere (p_{oxygen} = 0.1 Torr), the Au 4f XPS signals shifted to 83.9 eV and 87.6 eV. The 0.2 eV shift is attributed to the adsorption of molecular oxygen on the surface of the AuNPs, providing experimental evidence for the formation of cationic Au sites. Additionally, NAP-XPS experiments were conducted under conditions where both gaseous O$_2$ and H$_2$O co-existed (p_{oxygen} = 0.1 Torr, p_{water} = 0.1 Torr), but no further peak shift was observed. These results suggest that molecular oxygen significantly influences the electronic state of AuNPs, while the effect of water is minimal. In summary, the NAP-XPS results clearly demonstrate that molecular oxygen plays a crucial role in generating active cationic Au sites, explaining the effect of the atmosphere on the reaction. This finding offers a new perspective on the generally accepted reaction mechanism for the oxidation of hydrosilane.[8b]
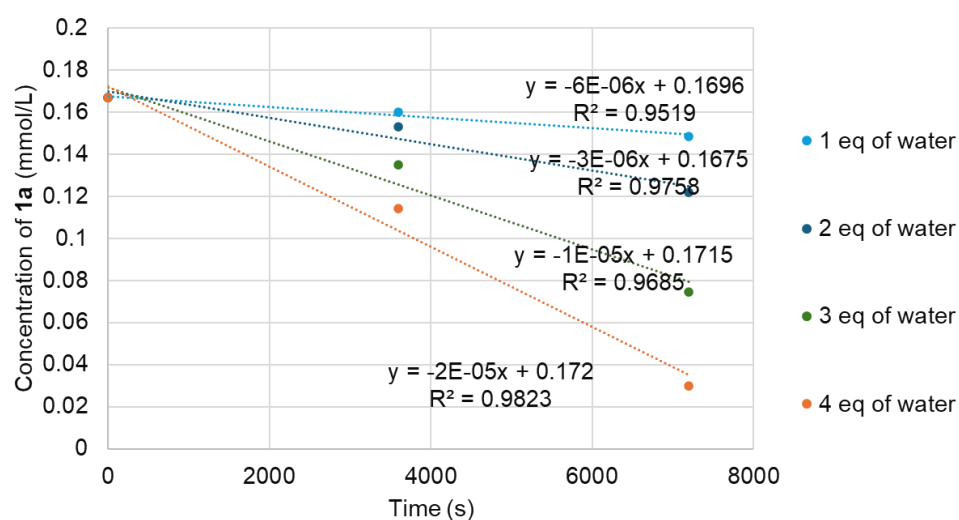
Figure 3-9. Plots of the concentration of **1a**
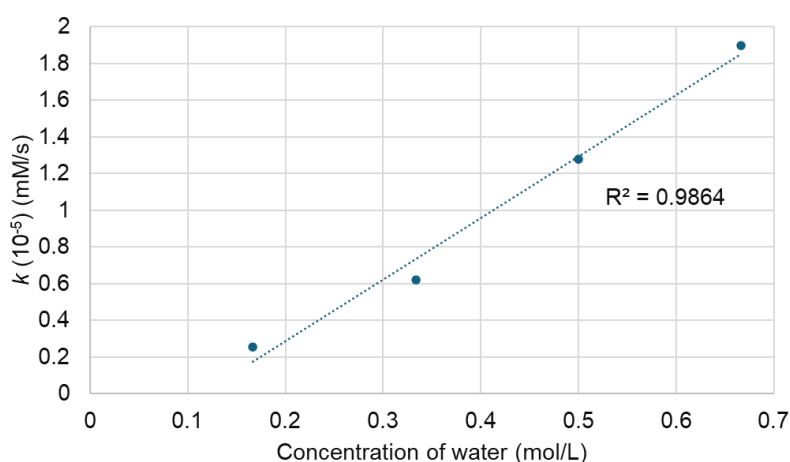
Figure 3-10. Plots of the reaction rate against the water concentration

To further clarify the detailed reaction mechanism, a kinetic study was conducted where the reaction rate was plotted against the concentration of H_2O, revealing an increase in reaction rate with higher H_2O concentration. This indicates that H_2O participates in the rate-determining step (RDS) (**Figures 3-9** and **3-10**). Additionally, the reaction rate was measured using D_2O instead of H_2O, revealing a secondary kinetic isotope effect (KIE) with $k_H/k_D = 1.17$ (n = 3), suggesting that O–H bond cleavage occurs as a pre-equilibrium process before the RDS (**Figure 3-11**).[29] This identifies that processes such as dissociative adsorption of H_2O or proton transfer are not part of the mechanism.
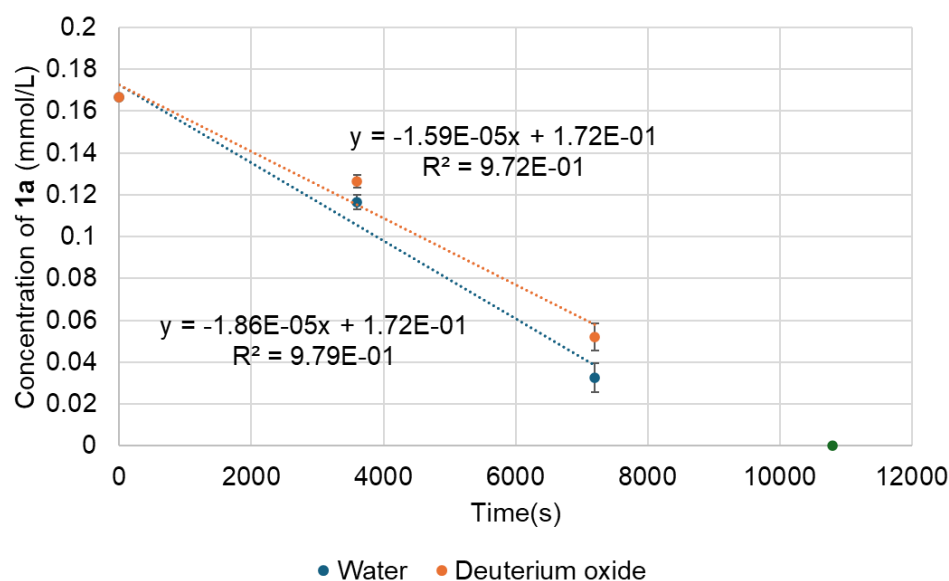
Figure 3-11. Plots of the concentration of **1a** using H_2O and D_2O

According to the experimental data, a proposed reaction mechanism is illustrated in **Figure 3-12**. The process begins with the adsorption of oxygen to create cationic Au surface species (labeled as **A**). Subsequently, H_2O and hydrosilane undergo dissociative adsorption, possibly involving Si–H and/or O–H bond cleavage, forming intermediates **B** and/or **C**, which are in equilibrium. Following this, Si–O bond formation likely proceeds through an S_N2 type mechanism, similar to that observed in previous studies of PdNP-catalyzed dehydrogenative oxidation of hydrosilane,[30] resulting in the formation of silanol and intermediate **D**. Finally, reductive elimination from **D** on the Au surface regenerates species **A** or **B**, releasing H_2 and completing the catalytic cycle. It should be noted that while the exact role of cationic Au sites formed via O_2 adsorption remains uncertain, further theoretical calculations are needed to provide more detailed insights into the reaction mechanism. Additionally, the actual mechanism in practice is likely more complex than the proposed model due to the presence of multiple interacting molecules on the catalyst surface under experimental conditions.
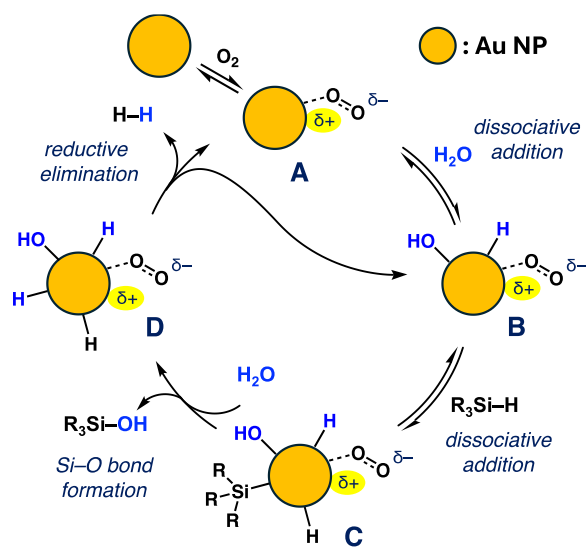
Figure 3-12. Possible reaction mechanism

3.3   Conclusion

In this chapter, the dehydrogenative oxidation of hydrosilane was investigated using size-selectively prepared Au:F-CAC catalysts. These catalysts displayed remarkable catalytic activity in terms of turnover frequency (TOF) and exhibited high stability under the reaction conditions, allowing for the exploration of size-dependency effects. Since the initial discovery of Au nanoparticle-catalyzed oxidation of hydrosilanes in 2009, the role of oxygen has remained unclear despite its significant impact on facilitating the reaction. This study, particularly the mechanistic investigations, highlights a new aspect of oxygen's role: the formation of cationic Au sites through adsorption. It is well established that under aerobic conditions, AuNPs demonstrate high catalytic activity in various oxidation reactions. Concurrently, they also exhibit cationic properties, which is another critical factor in reaction development and mechanistic studies.

3.4 Experimental details

3.4.1 General method for oxidation of hydrosilane

To a reaction tube equipped with a magnetic stir bar was added Au:F-CAC, hydrosilane (0.50 mmol), water, and solvent (3 mL). The mixture was stirred at 27 °C under an ambient atmosphere. After stirring for a specific period, the catalyst was removed by filtration and washed with diethyl ether (ca. 5 mL × 3). The filtrate was concentrated under reduced pressure. To the residue was added 1,1,2,2-tetrachloroethane (52.7 μL, 0.50 mmol) and CDCl3 (ca. 1 mL), and then ^{1}H NMR analysis was conducted using a portion of this solution. The yields were determined by comparison of an integrated value of the peak that corresponds to a proton of silanol with that corresponds to two protons of 1,1,2,2-tetrachloroethane (δ 5.98 ppm).

3.4.2 Recycling run experiment

To a reaction tube equipped with a magnetic stir bar was added Au:F-CAC (0.01 atom%), 1a (0.50 mmol), water (400 mol%), and THF (3 mL). The mixture was stirred at 27 °C under an ambient atmosphere. After stirring for 5 h, the catalyst was removed by filtration and washed with diethyl ether (ca. 5 mL × 3). The spent catalyst was dried at 45 °C under reduced pressure for 12 h, and this was used for the next recycling run.

3.4.3 General procedure for kinetic study of oxidation of hydrosilanes reaction

To a reaction tube equipped with a magnetic stir bar was added Au:F-CAC, triphenylsilane (**1a**, 0.50 mmol), water, and solvent. To the mixture was added n-dodecane (57.5 μL, 0.25 mmol) as an internal standard. The mixture was stirred under an ambient atmosphere. After stirring for a specific period, an aliquot of the reaction mixture was sampled into GC vial and diluted with ethyl acetate. After stirring the mixture vigorously, GC analysis was conducted by using an aliquot of the resulting organic phase. GC conditions for analyses of the oxidation of 1a: Constant linear column flow was adjusted to 50 cm s^{-1}. The temperature of the injector and the detector were held at 270 °C. The GC oven temperature program was set as follows: heated from 50 °C to 200 °C at the rate of 12 °C min^{-1}, and then heated to 270 °C at the rate of 6 °C min^{-1}. Retention times: n-dodecane (10.1 min, internal standard), triphenylsilane (19.4 min, **1a**), triphenylsilanol (21.7 min, **2a**).

3.4.4 Near ambient pressure X-ray photoelectron spectroscopy experiment of Au:PVP under oxygen/water atmosphere

The near ambient pressure X-ray photoelectron spectroscopy (NAP-XPS) experiments were

performed at the BL13B beamline of photon factory (PF) equipped with an APPLE II type undulator[34] under the ring-conditions of 2.5 GeV and 450 mA. X-ray beam energy was tuned to be 630 eV by a Monk-Gillieson-type monochromator.[35] NAP-XPS data was collected at Au 4f and Si 2p core levels with constant analyzer energy (CAE) mode with the energy step size of 0.05 eV at room temperature. The binding energy was corrected using the Si $2p_{3/2}$ signal of a Si substrate to 99.1 eV. The spectra were normalized to exclude the attenuation caused by the introduced gases.

A silicon substrate (P-type, low conductivity, Si(100) facet, Nilaco Co., SI-500440, ca. 10 mm × ca. 10 mm × 0.5 mm) was cleaned by ultrasound irradiation in ethanol for 15 min and dried under ambient atmosphere. 6.8 mg of Au:PVP(K-30) was dissolved in ethanol (20 mL) using a volumetric flask to prepare 3.0 mmol/L Au:PVP(K-30) solution. 0.1 mL of the solution was diluted with 0.9 mL ethanol to afford 0.3 $mmol_{PVP}$/L Au:PVP(K-30) solution. 5 μL of the Au:PVP(K-30) solution (0.3 $mmol_{PVP}$/L) was applied on a Si substrate. After drying, the sample was attached to a sample holder. The sample holder was fixed on a sample bank, and then this was connected to a linear and rotatable manipulator. After the pressure in the load-lock chamber reached less than 1×10^{-7} Torr, the sample was transferred to a main chamber. XPS data were collected under the pressure of 6.8×10^{-9} Torr. Then, oxygen gas was slowly introduced to the main chamber from a gas cylinder connected through a variable leak valve. After the pressure of the main chamber reached 0.1 Torr, NAP-XPS experiments were performed under an oxygen atmosphere. H_2O was purified by the freeze-thaw-pumping method and slowly introduced by a variable leak valve to the main chamber. After the pressure of the main chamber reached 0.2 Torr (p_{oxygen} = 0.1 Torr, p_{water} = 0.1 Torr), NAP-XPS experiments were performed under the oxygen/water atmosphere.

3.4.5 Solution-state X-ray absorption spectroscopy of Au:PVP in water

Au L_3-edge X-ray absorption spectroscopy (XAS) experiments were performed at the BL14B2 beamline of SPring-8 using Si(111) double-crystal monochromatised synchrotron radiation under the ring-conditions of 8.0 GeV and 100 mA. All experiments were carried out using fluorescent method with quick scan technique (QXAFS) at room temperature, otherwise noted. Ionization chambers were used to measure the intensities of the incident (I_0) and transmitted (I_1) X-ray. X-ray fluorescence was monitored using a 19-element Ge solid-state detector (SSD). XAS analysis was conducted using the Demeter package, a comprehensive system for processing and analyzing XAS data.[31] Background removal and normalization of raw data were performed using the cubic spline method using Athena software. E_0 was defined as photon energy at the absorption edge where μT = 0.5 in the normalized XAS spectrum. E_0 values of Au foil were set to 11919 eV for photon energy calibration. Reference samples (Au foil and Au_2O_3) were measured using the transmission method.

Au:PVP(K-30) was dissolved in H_2O to prepare 8.0 $mmol_{Au}$/L solution. The solution was introduced in a polyethylene bag and subjected to XAS experiment. Then, the solution was bubbled with N_2 gas at the flow rate of 60 mL min^{-1} for 15 min to degas the dissolved oxygen. After sealing, XAS experiment was again conducted.

3.4.6 Compound data

Triphenyl silanol (2a)
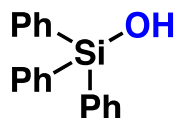
^{1}H NMR (400 MHz, CDCl$_3$) δ 7.65–7.62 (m, 6H), 7.47–7.44 (m, 3H), 7.43–7.37 (m, 6H), 2.46 (s, 1H);

^{13}C NMR (100 MHz, CDCl$_3$) δ 135.10, 134.97, 130.13, 127.92.

The data are consistent with that reported in the literature.[32]

Methyldiphenylsilanol (2b).
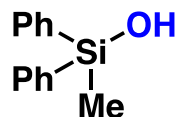
^{1}H NMR (400 MHz, CDCl$_3$) δ 7.62–7.01 (m, 4H), 7.44–7.36 (m, 6H), 2.14 (s, 1H), 0.68 (s, 3H);
^{13}C NMR (100 MHz, CDCl$_3$) δ 137.02, 133.94, 129.91, 127.92, –1.25.

The data are consistent with that reported in the literature.[32]

Dimethylphenylsilan(2c)
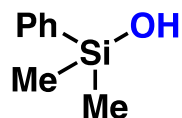
^{1}H NMR (400 MHz, CDCl$_3$) δ 7.61–7.59 (m, 2H), 7.42–7.37 (m, 3H), 2.27 (s, 1H), 0.41 (s, 6H);
^{13}C NMR (100 MHz, CDCl$_3$) δ 139.08, 133.01, 129.59, 127.86, –0.07.

The data are consistent with that reported in the literature.[33]

^{1}H NMR (400 MHz) and ^{13}C NMR (100 MHz) spectra of **2b** (CDCl$_3$)
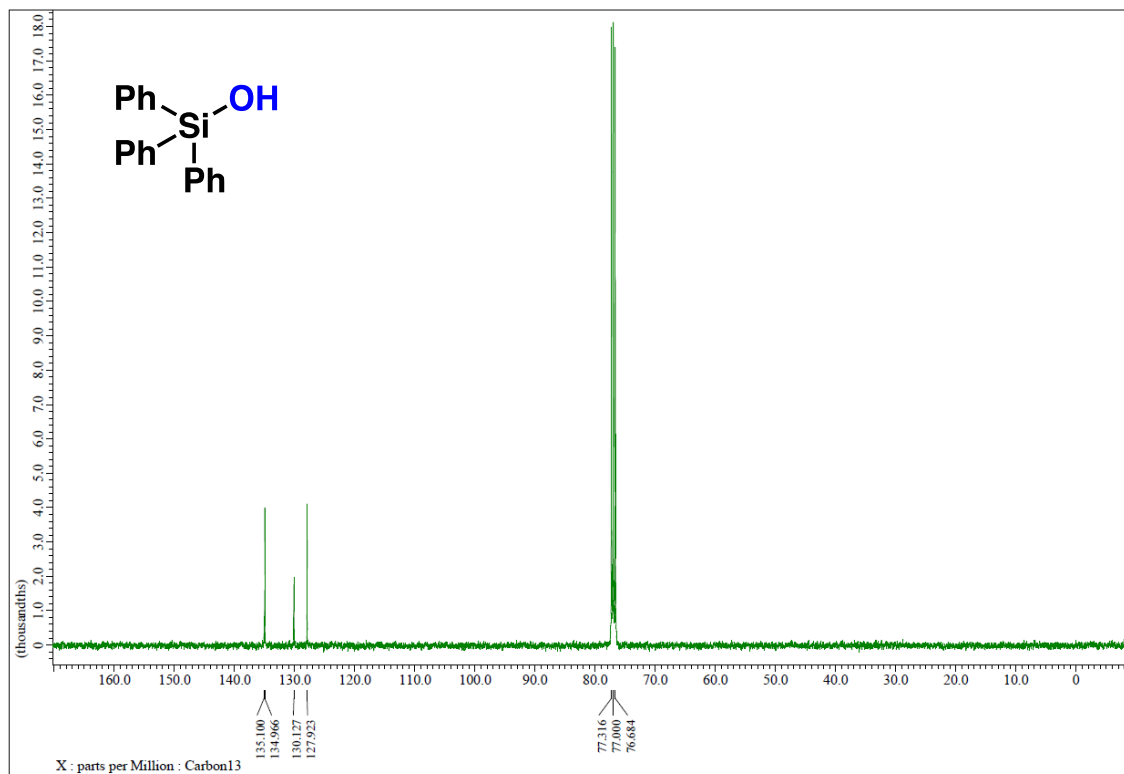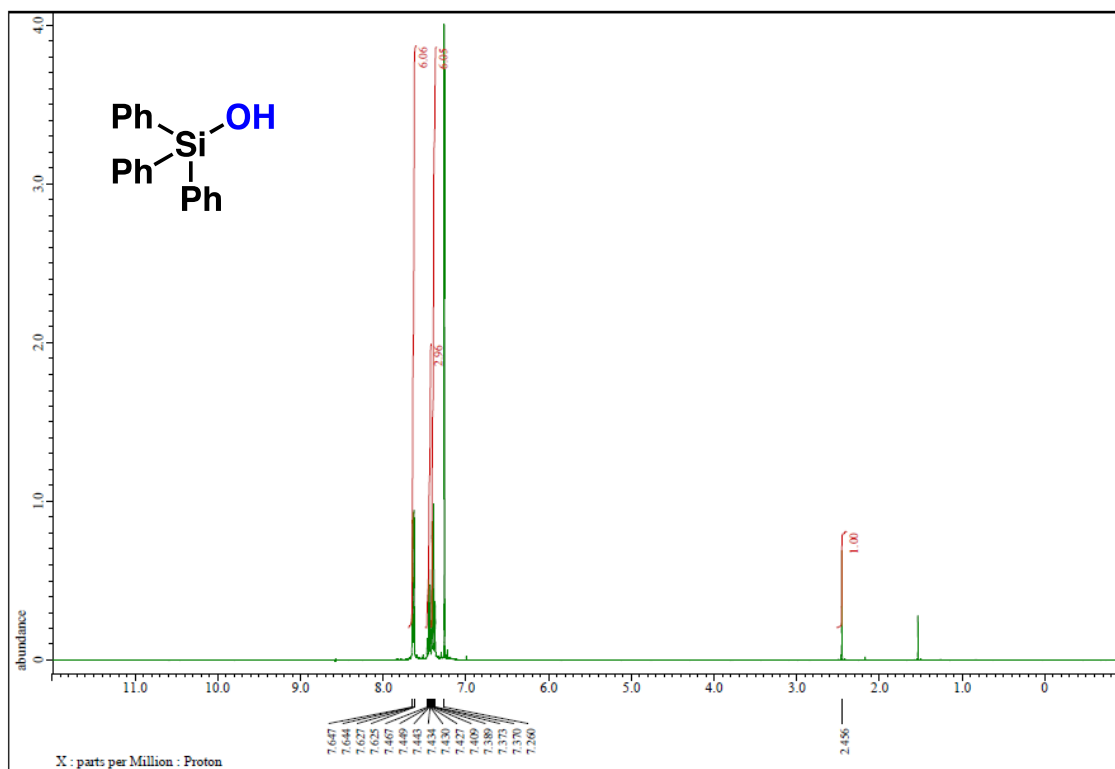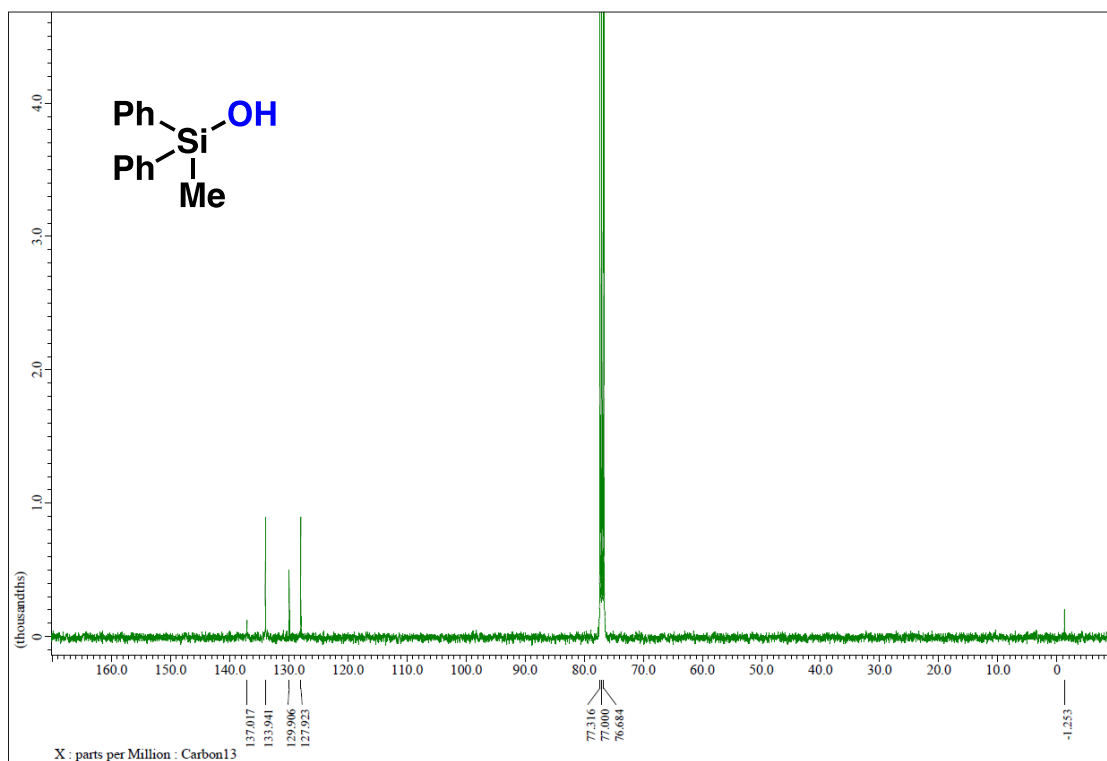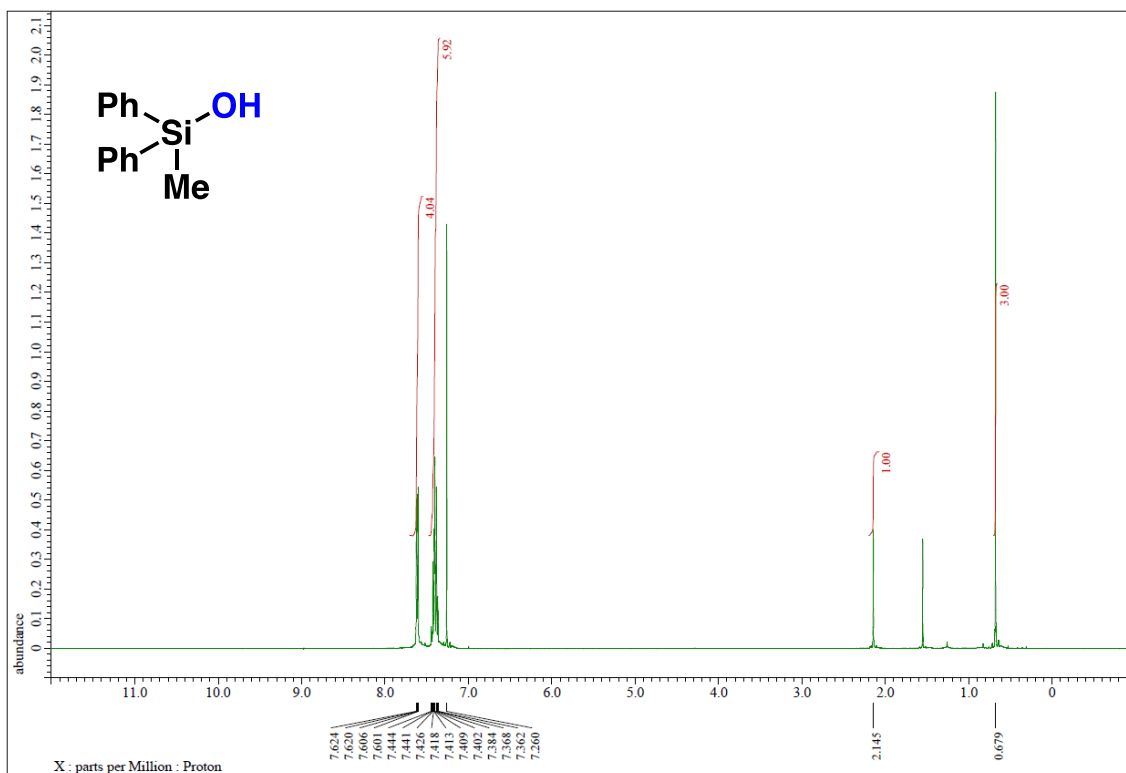
^{1}H NMR (400 MHz) and ^{13}C NMR (100 MHz) spectra of **2c** (CDCl$_3$)
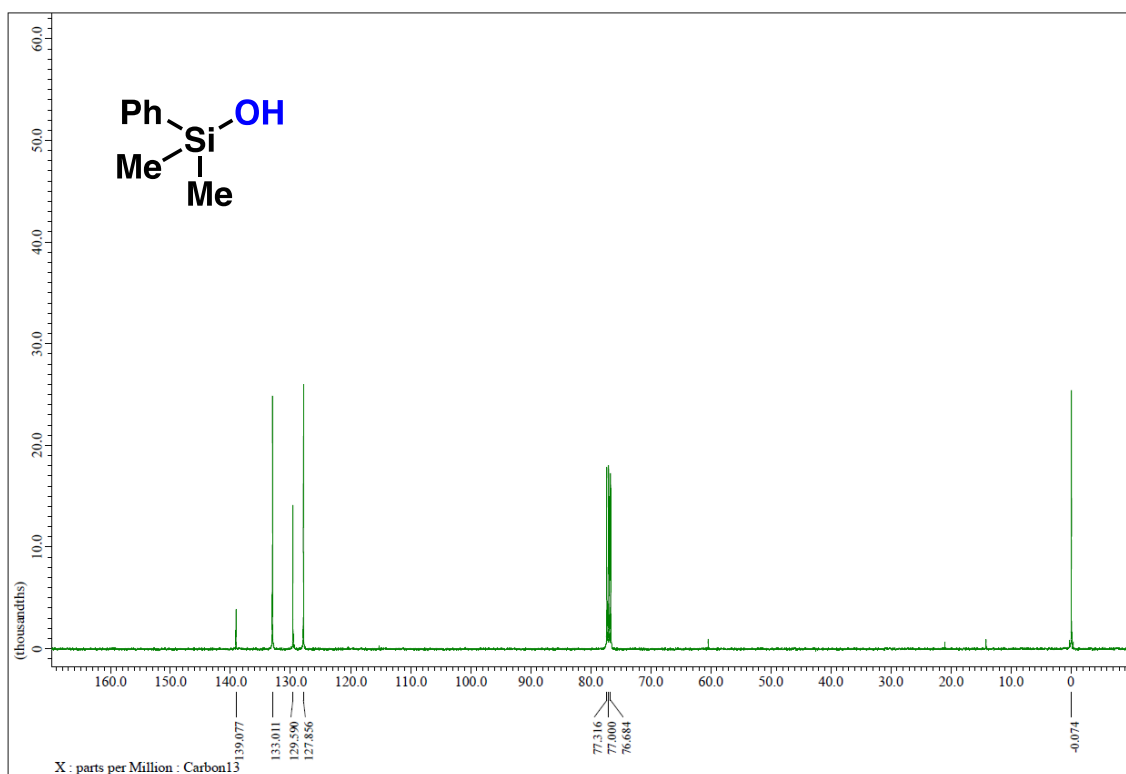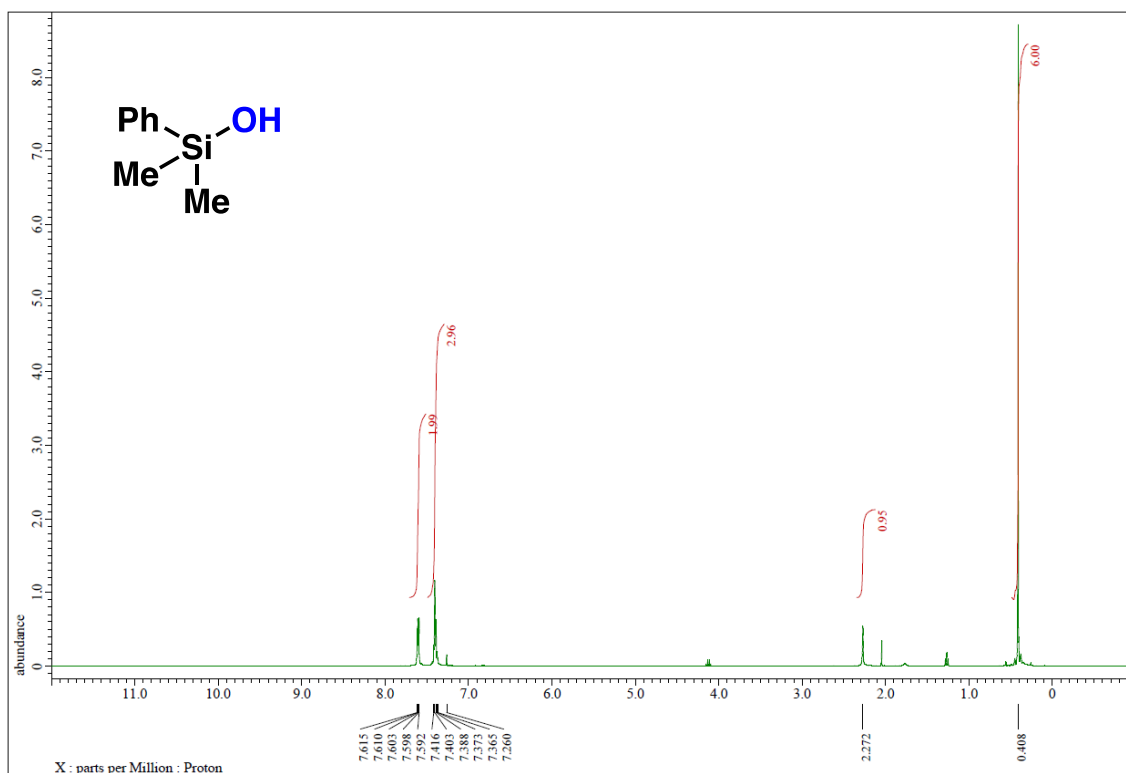
3.5 References

1. R. Pietschnig, Advances and Properties of Silanol-Based Materials, in *Main Group Strategies towards Functional Hybrid Materials*, 2018, pp. 141–162.

2. A. K. Franz, S. O. Wilson, *J. Med. Chem.* **2013**, *56*, 388.

3. S. E. Denmark, S. Fujimori, *J. Am. Chem. Soc.* **2005**, *127*, 8971.

4. P. W. Long, X. F. Bai, F. Ye, L. Li, Z. Xu, K. F. Yang, Y. M. Cui, Z. J. Zheng, L. W. Xu, *Adv. Synth. Catal.* **2018**, *360*, 2825.

5. (a) M. Jeon, J. Han, J. Park, *ACS Catal.* **2012**, *2*, 1539. (b) P. D. Lickiss, R. Lucas, *J. Organomet. Chem.* **1996**, *521*, 229. (c) K. Valliant-Saunders, E. Gunn, G. R. Shelton, D. A. Hrovat, W. T. Borden, J. M. Mayer, *Inorg. Chem.* **2007**, *46*, 5212. (d) B. Yang, Z. X. Wang, *Org. Lett.* **2019**, *21*, 7965. (e) L. H. Sommer, L. A. Ulland, G. A. Parker, *J. Am. Chem. Soc.* **1972**, *94*, 3469. (f) L. Spialter, J. D. Austin, *J. Am. Chem. Soc.* **1965**, *87*, 4406.

6. (a) M. Shi, K. M. Nicholas, *J. Chem. Res*. **1997**, *11*, 400. (b) W. Adam, R. Mello, R. Curci, *Angew.* **1990**, *26*, 890. (c) L. H. Sommer, L. A. Ulland, G. A. Parker, *J. Am. Chem. Soc*. **1972**, *94*, 3469.

7. J. John, E. Gravel, A. Hagege, H. Li, T. Gacoin, E. Doris, *Angew. Chem*. **2011**, *50*, 7533.

8. (a) T. Mitsudome, A. Noujima, T. Mizugaki, K. Jitsukawa, K. Kaneda, *Chem. Commun.* **2009**, 5302. (b) T. Urayama, T. Mitsudome, Z. Maeno, T. Mizugaki, K. Jitsukawa, K. Kaneda, *Chem. Lett.* **2015**, *44*, 1062. (c) L. Ma, W. Leng, Y. Zhao, Y. Gao, H. Duan, *RSC Adv.* **2014**, *4*, 6807. (d) T. Mitsudome, Y. Yamamoto, A. Noujima, T. Mizugaki, K. Jitsukawa, K. Kaneda, *Chem. Eur. J.* **2013**, *19*, 14398. (e) N. Asao, Y. Ishikawa, N. Hatakeyama, Menggenbateer, Y. Yamamoto, M. Chen, W. Zhang, A. Inoue, *Angew. Chem. Int. Ed.* **2010**, *49*, 10093. (f) V. Gitis, R. Beerthuis, N. R. Shiju, G. Rothenberg, *Catal. Sci. Technol.* **2014**, *4*, 2156.

9. (a) T. Liu, F. Yang, Y. Li, L. Ren, L. Zhang, K. Xu, X. Wang, C. Xu, J. Gao, *J. Mater. Chem.* **2014**, *2*, 245. (b) G. M. A. Rahman, D. M. Guldi, E. Zambon, L. Pasquato, N. Tagmatarchis, M. Prato, *J. Nanotechnol.* **2005**, *1*, 527. (c) J. John, E. Gravel, A. Hagège, H. Li, T. Gacoin, T. Gacoin, E. Doris, *Angew. Chem. Int. Ed.* **2011**, *50*, 7533.

10. Z. T. Xie, T. Asoh, Y. Uetake, H. Sakurai, H. Uyama, *Carbohydr. Polym.* **2020**, *247*, 116723.

11. (a) A. G. M. da Silva, C. M. Kisukuri, T. S. Rodrigues, E. G. Candido, I. C. de Freitas, A. H. M. da Silva, J. M. Assaf, D. C. Oliveira, L. H. Andrade, P. H. C. Camargo, *Appl.*

Catal. **2016**, *184*, 35. (b) H. T. Tang, H. Y. Zhou, Y. M. Pan, J. L. Zhang, F. H. Cui, W. H. Li, D. Wang, *Angew. Chem. Int. Ed.* **2024**, *63*, e202315032.

12. (a) X. Cui, A. Ozaki, T. A. Asoh, H. Uyama, *Polym. Degrad. Stab.* **2020**, *175*, 109118. (b) X. Cui, T. Honda, T. A. Asoh, H. Uyama, *Carbohydr. Polym.* **2020**, *230*, 115662.

13. T. Chutimasakul, Y. Uetake, J. Tantirungrotechai, T. Asoh, H. Uyama, H. Sakurai, *ACS Omega* **2020**, *5*, 33206.

14. R. Gupta, S. Paul, R. Gupta, *J. Mol. Catal.* **2007**, *266*, 50.

15. M. Jeon, J. Han, J. Park, *ChemCatChem* **2012**, *4*, 521.

16. E. Villemin, E. Gravel, D. V. Jawale, P. Prakash, I. N. N. Namboothiri, E. Doris, Macromol. *Chem. Phys.* **2015**, *216*, 2398.

17. W. Li, A. Wang, X. Yang, Y. Huang, T. Zhang, *Chem. Commun.* **2012**, *48*, 9183.

18. Y. Sawama, M. Masuda, N. Yasukawa, R. Nakatani, S. Nishimura, K. Shibata, T. Yamada, Y. Monguchi, H. Suzuka, Y. Takagi, H. Sajiki, *J. Org. Chem.* **2016**, *81*, 4190.

19. M. Dhiman, B. Chalke, V. Polshettiwar, *J. Mater. Chem. A* **2017**, *5*, 1935.

20. R. J. Maya, J. John, R. L. Varma, *Chem. Commun.* **2016**, *52*, 10625.

21. Z. Chen, Q. Zhang, W. Chen, J. Dong, H. Yao, X. Zhang, X. Tong, D. Wang, Q. Peng, C. Chen, W. He, Y. Li, *Adv. Mater.* **2018**, *30*, 1704720.

22. H. Li, L. Chen, P. Duan, W. Zhang, *ACS Sustainable Chem. Eng.* **2022**, *10*, 4642.

23. Q. Zhang, M. Peng, Z. Gao, W. Guo, Z. Sun, Y. Zhao, W. Zhou, M. Wang, B. Mei, X. L. Du, Z. Jiang, W. Sun, C. Liu, Y. Zhu, Y. M. Liu, H. Y. He, Z. H. Li, D. Ma, Y. Cao, *J. Am. Chem. Soc.* **2023**, *145*, 4166.

24. H. Kitahara, H. Sakurai, *Chem. Lett.* **2009**, *39*, 46.

25. Y. Uetake, B. Suwattananuruk, H. Sakurai, *Sci. Rep.* **2022**, *12*, 20602.

26. (a) K. Bobuatong, H. Sakurai, M. Ehara, *ChemCatChem* **2017**, *9*, 4450. (b) M. Boronat, A. Leyva-Pérez, A. Corma, *Acc. Chem. Res.* **2014**, *47*, 834. (c) S. Yamazoe, K. Koyasu, T. Tsukuda, *Acc. Chem. Res.* **2014**, *47*, 816. (d) M. Stratakis, H. Garcia, *Chem. Rev.* **2012**, *112*, 4469.

27. M. Palashuddin Sk, C. K. Jana, A. Chattopadhyay, *Chem. Commun.* **2013**, *49*, 8235.

28. H. Tsunoyama, N. Ichikuni, H. Sakurai, T. Tsukuda, *J. Am. Chem. Soc.* **2009**, *131*, 7086.

29. (a) E. M. Simmons, J. F. Hartwig, *Angew. Chem. Int. Ed.* **2012**, *51*, 3066. (b) T. Y. George, T. Asset, A. Avid, P. Atanassov, I. V. Zenyuk, *ChemPhysChem* **2020**, *21*, 469. (c) N. J. F. Christensen, *Synlett* **2015**, *26*, 508.

30. (a) T. Kamachi, K. Shimizu, D. Yoshihiro, K. Igawa, K. Tomooka, K. Yoshizawa, *J. Phys. Chem. C* **2013**, *117*, 22967. (b) C. J. Ennis, S. A. Morton, L. Sun, S. P. Tear, E. M.

McCash, *Chem. Phys. Lett.* **1999**, *304*, 217. (c) D. C. Kershner, J. W. Medlin, *Surf. Sci.* **2008**, *602*, 693.

31. (a) J. J. Rehr, R. C. Albers, *Rev. Mod. Phys.* **2000**, *72*, 621. (b) M. Newville, *J. Synchrotron Radiat.* **2001**, *8*, 322. (c) B. Ravel, M. Newville, *J. Synchrotron Radiat.* **2005**, *12*, 537.

32. P. Lian, K. Wang, H. Liu, R. Li, M. Li, X. Bao, X. Wan, *Org. Lett.* **2023**, *25*, 7984.

33. I. K. Goncharova, R. S. Tukhvatshin, R. A. Novikov, A. D. Volodin, A. A. Korlyukov, V. G. Lakhtin, A. V. Arzumanyan, *Eur. J. Org. Chem.* **2022**, *35*, e202200871.

Chapter 4: Dehydrosilylation of Alcohols Using Gold Nanoparticles Deposited on Citric Acid-modified Fibrillated Cellulose

4.1   Introduction

The use of silane etherification has become a potent approach in the realm of functional organosilicon compounds and organic synthesis.[1] Specifically, the process of silylation for alcohol protection is widely acknowledged and frequently applied in synthetic chemistry. Traditionally, silyl ethers are synthesized by reacting chlorosilanes with alcohols in the presence of a stoichiometric base.[2] However, this method requires the use of corrosive reagents and inevitably produces organic salts as byproducts (**Figure 4-1A**). Consequently, research has focused on alternative methods for silyl ether synthesis, particularly the dehydrogenative coupling of hydrosilanes. This approach stands out for its production of H_2 as the sole byproduct, offering a significant environmental advantage over traditional methods.[4,5]

Extensive research has been dedicated to metal-catalyzed dehydrosilylation (**Figure 4-1B**). Initially, the research has been focused on homogeneous metal catalysts such as using $InBr_3$ as a catalyst under reflux in toluene. This report has demonstrated a highly effective and unprecedented technique for silylating primary and secondary alcohols, phenols, and oximes using hydrosilanes. This technique also produced silyl ethers in good yields with bulky hydrosilanes.[4] Recent attention has shifted towards heterogeneous catalysts, prized for their reusability.[5,6] For example, the modification of gold surfaces with a caged, compact trialkylphosphane (SMAP) was used in chip form for alcohol silylation dehydrogenatively catalyzed by rhodium. Compared to homogeneous Rh catalysts and the comparable surface catalyst with traditional Ph_2P-type coordinating groups, the Rh catalyst [Au]-SMAP-Rh demonstrated remarkable durability and high efficiency in terms of reusability.[5a] However, in many studies, catalytic dehydrosilylation reactions have typically relied on solvents or excessive alcohol amounts, restricting their utility in alcohol protection strategies for organic synthesis. A breakthrough in this area was achieved by Cao et al., who introduced a single-atom cobalt catalyst capable of addressing these limitations.[7] Their catalyst enabled the effective protection of 1 equivalent of alcohols using 2–3 equivalents of hydrosilanes. The developed single-atom cobalt catalyst synthesis of silyl ethers offers advantages over conventional Si-alkoxylation procedures, including increased cost-effectiveness and simpler scalability. Despite this advancement, there remains significant interest in developing novel heterogeneous catalysts that further enhance the efficiency of hydroxy group protection methodologies (**Figure 4-1C**).

Since the initial discovery of dehydrosilylation using Al_2O_3-supported gold nanoparticles (AuNPs), AuNPs have emerged as highly effective catalysts for this reaction, garnering significant

research attention.[5c] Subsequent studies have focused on developing various AuNPs catalysts that demonstrate exceptional efficiency under mild reaction conditions and accommodate a wide range of substrates.[8] These catalysts include self-assembled monolayers capped AuNPs,[8a] hydroxyapatite-supported AuNPs,[8b] silica-supported AuNPs[8c] and graphene supported single-atom Au(I) catalyst.[8d] Despite these advancements, many of these catalysts still require excess alcohol, posing a limitation. In recent years, several reactions have been developed using an AuNPs supported on citric acid-modified fibrillated cellulose (Au:F-CAC).[9] The fibrous structure of F-CAC enhances the surface area, facilitating efficient deposition of metal nanoparticles and ensuring high stability during catalytic reactions.[9,10] In the previous chapter, the author has demonstrated the dehydrogenative oxidation of hydrosilanes under aerobic conditions using Au:F-CAC, revealing that the reaction occurs at cationic Au sites generated through oxygen adsorption.[9c] Building on this foundation, it is hypothesized that Au:F-CAC could also be suitable for the dehydrosilylation of alcohols.

In this chapter, the author aims to apply Au:F-CAC to dehydrogenative coupling under neutral conditions for two types of applications. In the first part, the catalyst is used to functionalize silane compounds. In the latter part, the author focuses on achieving silyl protection of alcohols. In this case, alcohol is a valuable compound that needs to be used in limited quantities. The investigation demonstrated that Au:F-CAC is an efficient catalyst for dehydrosilylation with 1 equivalent of alcohol, offering clean and effective silyl protection.

A. *O*-silylation of alcohols with R₃SiCl
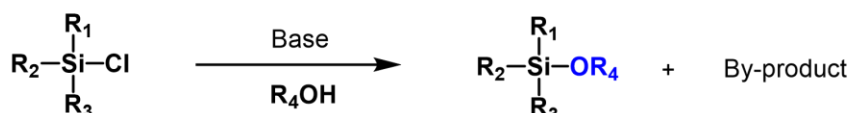
B. Catalytic dehydrogenative coupling of hydrosilanes with alcohols by transition metal
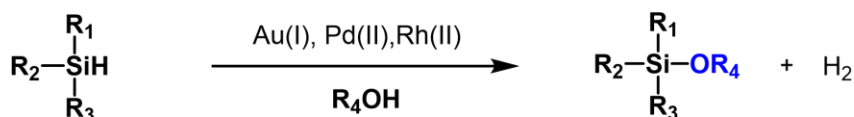
C. Catalytic dehydrogenative coupling of hydrosilanes with alcohols in by heterogeneous catalyst
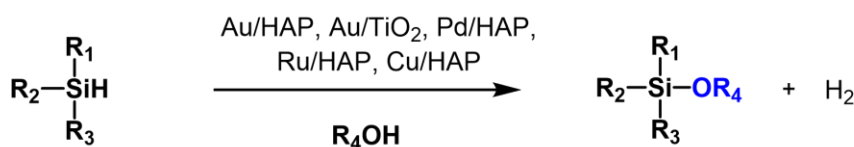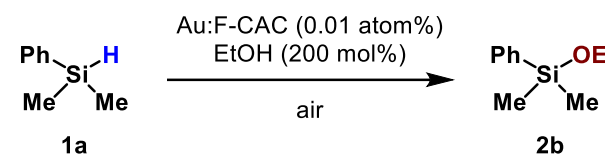
Figure 4-1. Dehydrosilylation of alcohols in various methods

4.2 Result and discussions

4.2.1 Optimization of reaction conditions for functionalize the silane

The preparation of catalyst Au:F-CAC (particle size of Au: 1.7 ± 0.2 nm, 1.7×10^{-3} wt%) is well studied and the optimization condition for preparing is established.[9b] With the catalyst in hand, the investigation began with optimizing the reaction conditions using 1 equivalent of dimethylphenylsilane (**1a**) and an excess amount of ethanol. The dehydrogenative coupling of **1a** was initially performed using ethanol as the solvent, in the presence of 0.01 atom% Au:F-CAC at room temperature under aerobic conditions. This resulted in the conversion of **1a** to ethoxydimethylphenylsilane (**2b**) with a 99% yield, demonstrating that Au:F-CAC catalyzes dehydrogenative coupling of hydrosilane (**Table 4-1**, entry 1). Subsequently, the amount of ethanol was reduced to 2 equivalents, and the reaction was carried out using various organic solvents. Screening these solvents revealed that toluene provided the best result, yielding **2a** in 71% yield (entries 2–5). Although reaction temperature showed negligible effects, slightly extending the reaction time increased the yield to 95% (entries 6 and 7). However, using only 1 equivalent of ethanol reduced the yield to 63% (entry 8).

Table 4-1. Hydroamination of primary amines in various conditions

entry	solvent	time (h)	temp. (°C)	1a (%)	2b (%)
1[a]	EtOH	3	27	0	>99
2	*n*-hexane	3	27	65	30
3	EtOAc	3	27	70	25
4	THF	3	27	60	34
5	toluene	3	27	25	71
6	toluene	3	50	24	73
7	toluene	4	27	0	95
8[b]	toluene	4	27	35	63

[a]EtOH (1 mL) was used as a solvent. [b]100 mol% of EtOH was used.

With the optimized conditions established, the synthesis of silyl ethers was explored using various combinations of silanes and alcohols (**Figure 4-2**). The dehydrogenative coupling of **1a** with primary alcohols such as methanol, ethanol, *n*-propanol, and *n*-butanol yielded silyl ethers (**2a**–**2d**)

in quantitative yields. In contrast, the coupling of 1a with 2-propanol resulted in the desired silyl ether **2e** with only a 50% yield, even with extended reaction time. When diphenylmethylsilane (**1b**) or triphenylsilane (**1c**) were used, a similar trend was observed, although the catalytic activity of **1c** was notably lower with n-butanol and 2-propanol (yielding **2e** and **2k**, respectively). Additionally, no reaction occurred when sterically demanding *tert*-BuOH was used, regardless of extending the reaction time or increasing the temperature.
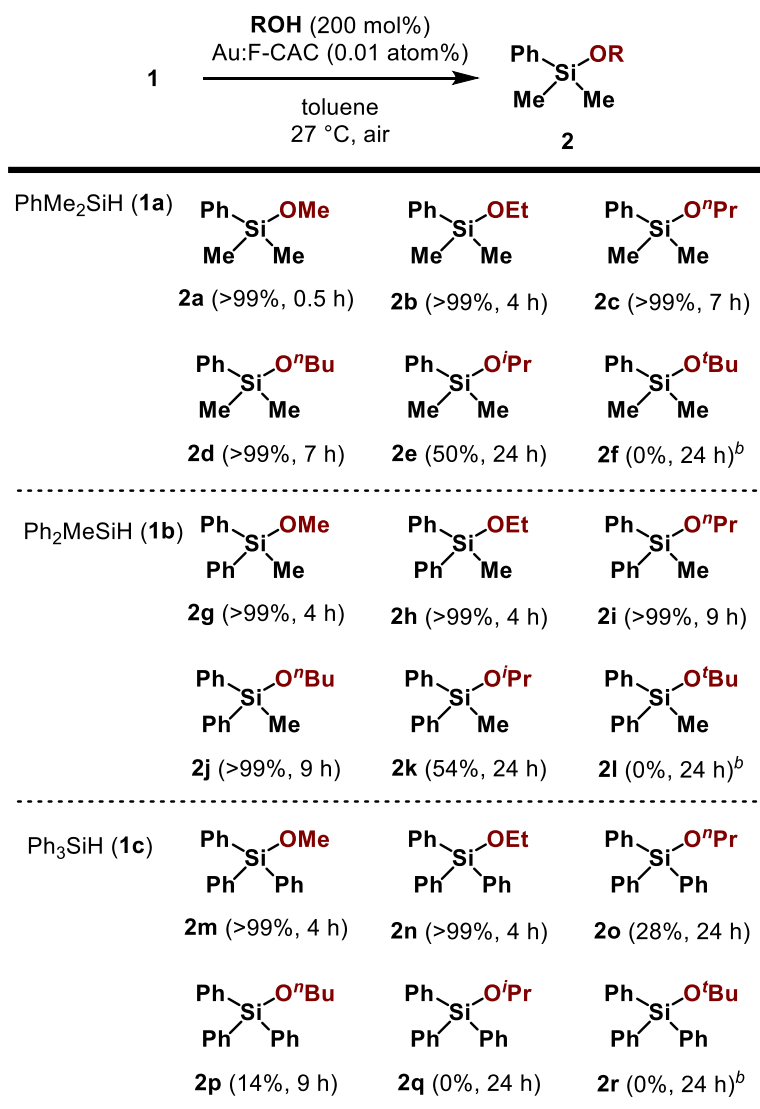
Figure 4-2. Synthesis of silyl ethers from various silanes and alcohols catalyzed by Au:F-CAC[a]
[a]Reaction conditions: hydrosilane (0.5 mmol), alcohol (1 mmol), toluene (3.0 mL). The yields were determined by ^{1}H NMR analysis. [b]50 °C, 24 h.

4.2.2 The durability and reusability of Au:F-CAC

A reusability test was conducted to evaluate the durability of the Au:F-CAC catalyst. The spent catalyst was employed in subsequent recycling runs after recovery without additional treatment. During the first three recycle runs, the dehydrogenative coupling of **1a** proceeded quantitatively (**Figure 4-3a**). Although a slight decrease in catalytic activity was observed after the third cycle, **2a** was still obtained in 80–86% yield, demonstrating the excellent durability of Au:F-CAC in this reaction. Transmission electron microscopy (TEM) observation of the fresh and reused catalysts showed slight aggregation of AuNPs (2.9 ± 0.5 nm) after the 6th cycle, which accounts for the slight loss in yield of **2a** (**Figure 4-3b**).
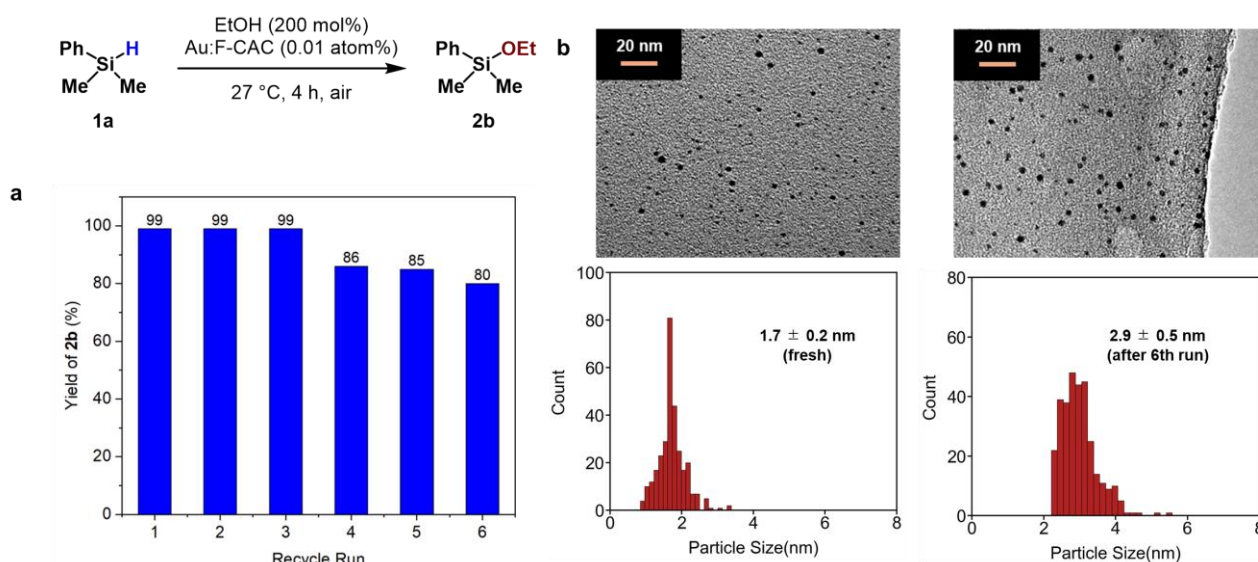
Figure 4-3. Catalytic performance of Au-F-CAC catalyst for dehydrogenative coupling of hydrosilanes. (a) Recycling run experiment. (b) TEM images of the fresh and spent catalyst after the sixth run. Mean diameter and standard deviation are based on the average 300 particles.

In addition, a hot filtration experiment was performed.[11] The Au:F-CAC was filtered to separate the catalyst from the reaction mixture when the yield of **2b** reached 70% (approximately after 3 hours, **Figure 4-4**). The filtrate was subsequently subjected to the same reaction conditions without the catalyst, there was no additional increase in the yield of **2a** observed. Furthermore, inductively coupled plasma-atomic emission spectroscopy (ICP-AES) analysis confirmed the absence of gold species in the filtrate, indicating that the reaction occurred on the gold surface. The sustained catalytic activity indicates the high stability of this catalyst, likely due to the presence of carboxylic acid groups attached to cellulose. This study demonstrated that Au:F-CAC is a highly efficient, stable, and

91

reusable catalyst for the dehydrosilylation of alcohols, offering a clean and mild process suitable for industrial and functional silanol-based material applications.
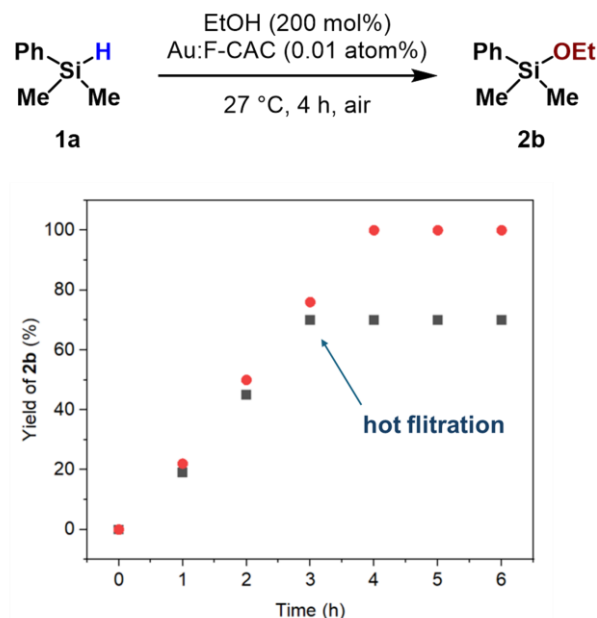
Figure 4-4. Hot filtration experiment

4.2.3 Optimization of reaction conditions for alcohol protection

To apply this reaction to the protection of the hydroxy group, the reaction conditions were reoptimized using one equivalent of 2-propanol as a substrate. In the presence of 0.01 atom% Au:F-CAC and 200 mol% of **1a**, the dehydrogenative coupling between 2-propanol and **1a** proceeded to give silyl ether **2e** in 46% yield (**Table 4-2**, entry 1). The yield increased to 71% when 400 mol% of **1a** was used (entry 2). However, further increasing the amount of **1a** to 600 mol% did not improve the yield of the silyl ether (entry 3). With 400 mol% of **1a**, the Au loading was then optimized. The best result was achieved when 0.1 atom% of Au:F-CAC was used, affording **2e** in an 89% yield (entries 4–6). A thorough search of the relevant literature reveals that this is the first example of the AuNP-catalyzed dehydrogenative silylation of alcohol using a limited amount of hydrosilane.

92

Table 4-2. Optimization of reaction conditions

PhMe$_2$SiH (**x** mol%)
OH → Au:F-CAC (**y** atom%) → OSiMe$_2$Ph
toluene
(1 equiv) 27 °C, 24 h, air
2e

entry	x	Y	yield (%)
1	200	0.01	46
2	400	0.01	71
3	600	0.01	66
4	400	0.05	86
5	400	0.1	89
6	400	0.2	85

4.2.4 The effect of the reaction atmosphere

The high efficiency of Au:F-CAC in dehydrosilylation can be attributed to the cationic Au sites created by oxygen adsorption.[12] Zbořǐl et al. demonstrated that cationic Au serves as the catalytically active species in dehydrogenative silylation using a single-atom Au catalyst.[8d] Previous studies have also experimentally confirmed that oxygen adsorption forms cationic Au sites, using near ambient pressure X-ray photoelectron spectroscopy. The reaction atmosphere was crucial for both this reaction and dehydrogenative oxidation, as evidenced by the yield of **2b** after 1 hour. Yields of **2b** were 55%, 17%, and 3% under oxygen, air, and argon atmospheres, respectively, highlighting the significant role of oxygen in the reaction rate (**Table 4-3**). It is believed that these cationic Au sites facilitate the cleavage of O–H and/or Si–H bonds.[13]

Table 4-3. Effect of atmosphere

EtOH (200 mol%)
Au:F-CAC (0.01 atom%)
toluene
27 °C, **x** h, air

Ph–Si(Me)(Me)–H → Ph–Si(Me)(Me)–OEt
1a → 2a

atmosphere	x	yield (%)^a
O_2	1	55
air	1	17
Ar	1	3
O_2	4	>99
air	4	>99
Ar	24	45

^{a}Determined by ^{1}H NMR

4.2.5 Substrate scope

The dehydrogenative silylation using various primary and secondary alcohols reactions was explored (**Figure 4-5**). Benzyl alcohol (**3a**) underwent dehydrogenative coupling over 6 hours to produce the corresponding silyl ether (**4a**) with an isolated yield of 82%. Benzyl alcohols with methoxy (**3b**), fluoro (**3c**), or bromo (**3d**) substituents on the aromatic ring were successfully converted to silyl ethers **4b** and **4c**, with yields of 78%, and 93% yields, respectively. Under the reaction conditions, benzyl alcohols with electron-withdrawing groups such as esters (**3e**) were well tolerated, producing silyl ethers(**4e**) in an impressive 90% yield. The reaction also proved compatible with substrates containing aldehydes (**3f**) and unprotected amines (**3g**), resulting in the corresponding silyl ethers **4f** and **4g** in 48% and 42% yields, respectively. Notably, despite the moderate yields, there was a significant recovery of starting materials, with 42% recovery for **3f** and 46% for **3g**. Additionally, the reaction was unaffected by the presence of a heteroaromatic ring, such as furan. The silyl ether **4h** was successfully synthesized from **3h** with a yield of 73%. An aliphatic alcohol with an alkene group (**3i**) reacted smoothly, yielding **4i** in 76% without any 1,5-cyclization.

Secondary alcohols were also examined: cyclopentanol (**3j**) and cyclohexanol (**3k**) were silylated to produce **4j** and **4k** in yields of 75% and 83%, respectively. 2-Butanol (**3n**) was converted to its silyl ether (**4n**) in 76% yield. Additionally, secondary benzyl alcohols such as 1-indanol (**3l**) and diphenylmethanol (**3m**) were silylated to give **4l** and **4m** in yields of 76% and 66%, respectively. To further demonstrate the synthetic utility of the Au:F-CAC, the dehydrogenative coupling with

alcohol-containing natural products such as (–) menthol (**3o**) was conducted to yield **4o** in 65% with 27% recovery of **3o**, showcasing synthetic utility of the Au:F-CAC catalyst.

R₁OH **3** (1 equiv) → PhMe₂SiH (400 mol%), Au:F-CAC (0.05 atom%), toluene, 27 °C, air → **4**

Primary alcohol

4a (96% (82%)[a], 6 h) **4b** (93% (78%)[a], 8 h) **4c** (97% (83%)[a], 8 h)

4d (98% (93%)[a], 8 h) **4e** (98% (90%)[a], 8 h) **4f** (51% (48%)[a](42%)[b], 24 h)

4g (49% (42%)[a](46%)[b], 24 h) **4h** (89% (73%)[a], 8 h) **4i** (98% (76%)[a], 6 h)

Secondary alcohol

4j (95% (75%)[a], 8 h) **4k** (92% (83%)[a], 8 h) **4l** (85% (76%)[a], 24 h)

4m (75% (66%)[a], 8 h) **4n** (95% (76%)[a], 8 h) **4o** (71% (65%)[a](27%)[b], 24 h)
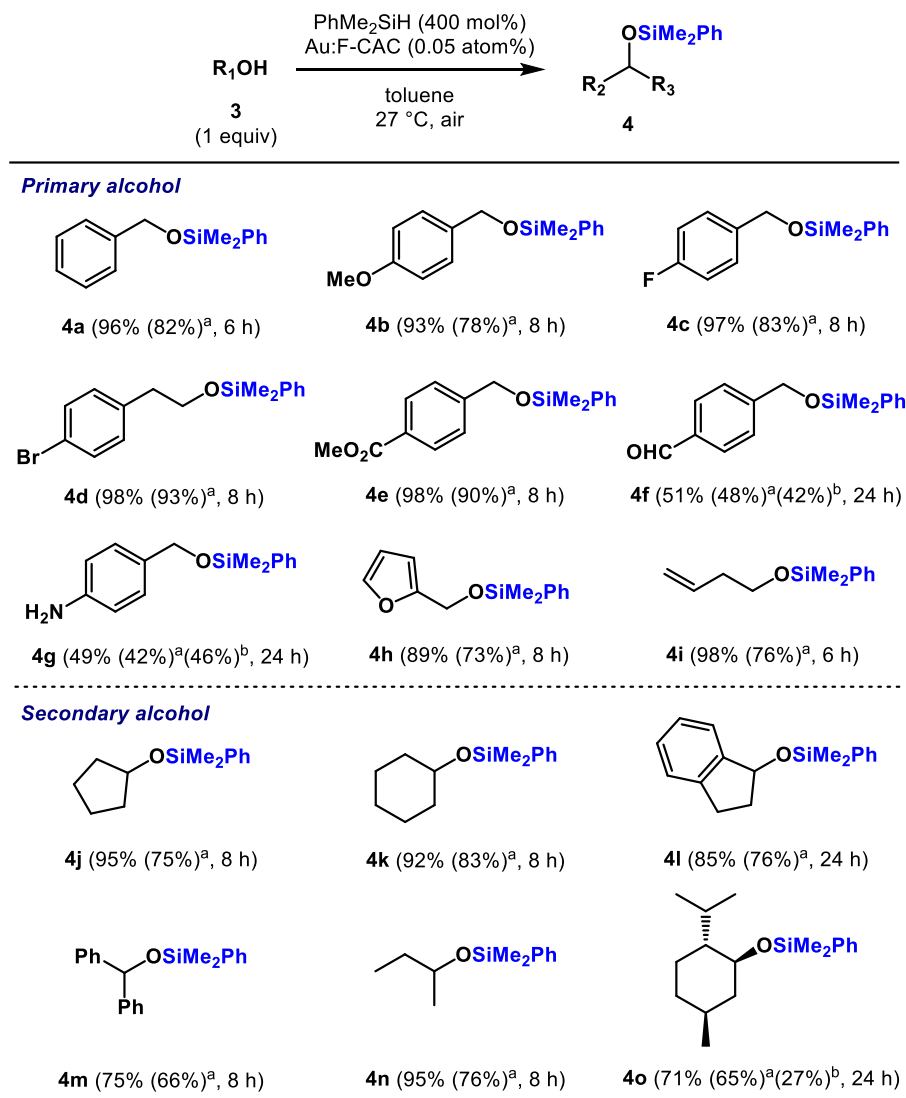
Figure 4-5. Substrate scope. The reactions were conducted on a 0.5 mmol scale in toluene (3 mL). The yields were determined by ^{1}H NMR analysis. [a]Isolated yields, [b]Recovery yields.

According to the effect of atmosphere in **Table 4-3**, a plausible reaction mechanism was shown in **Figure 4-6**. The role of oxygen is crucial in the initial where it adsorbs to form cationic Au surface. It is considered that this cationic Au sites would facilitate the O–H and/or Si–H bonds cleavage, leading to the formation of intermediates **B** and **C**.[13] The silyl intermediate is then attacked via an S_N2-type mechanism by a nucleophile derived from alcohol, generating silyl ethers and intermediate **D**. Finally, reductive elimination from **D** occurs on the Au surface to regenerate **A** or **B** with expelling H₂ thus completing the catalytic cycle. The possibility of transesterification mechanism was

investigated using triphenylsilanol as a substrate and no reaction was observed, indicating that this reaction does not proceed from silanol generated by water remaining in the solvent (**Figure 4-7**).
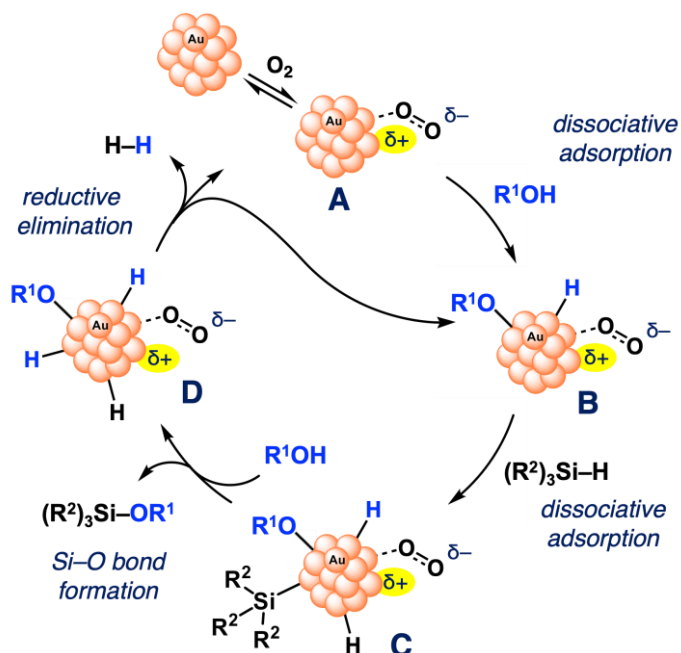
Figure 4-6. Possible reaction mechanism
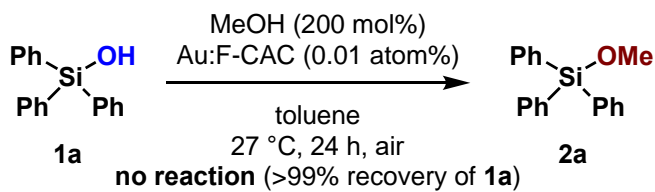
Figure 4-7. Transesterification of triphenylsilanol with methanol

4.3   Conclusion

The Au:F-CAC catalyst demonstrated high catalytic activity for the dehydrogenative coupling with alcohols. The comprehensive optimization and evaluation showed the effectiveness of this catalytic system in introducing silicon functionalities directly into organic molecules under mild conditions. Notably, Au:F-CAC overcomes the limitations of existing Au-based catalysts by eliminating the need for excess alcohol, making it both practical and cost-effective for alcohol protection applications. Reusability tests confirmed the robustness and stability of the Au:F-CAC, highlighting its potential for industrial-scale use. Additionally, the wide range of substrates, including various primary and secondary alcohols, emphasizes the versatility and synthetic utility of the catalytic system.

4.4 Experimental details

4.4.1 General procedure for dehydrosilylation of alcohols

To a reaction tube equipped with a magnetic stir bar were added Au:F-CAC, silane (0.50 mmol), alcohol, and solvent. The mixture was stirred under an ambient atmosphere. After stirring for a specific period, the catalyst was removed by filtration and washed with diethyl ether (ca. 5 mL ×3) The filtrate was concentrated under reduced pressure. To the residue was added 1,1,2,2-tetrachloroethane (52.7 µL, 0.50 mmol) and CDCl$_3$ (ca. 1 mL), and then ^{1}H NMR analysis was conducted using a portion of this solution. The yields were determined by comparison of an integrated value of the peak that corresponds to a proton of silanol with that corresponds to two protons of 1,1,2,2-tetrachloroethane (δ 5.98 ppm).

4.4.2 General procedure for dehydrosilylation of alcohols for alcohol protection

To a reaction tube equipped with a magnetic stir bar were added Au:F-CAC, silane, alcohol (0.5 mmol), and solvent. The mixture was stirred under an ambient atmosphere. After stirring for a specific period, the catalyst was removed by filtration and washed with diethyl ether (ca. 5 mL × 3). The filtrate was concentrated under reduced pressure. To the residue was added 1,1,2,2-tetrachloroethane (52.7 µL, 0.50 mmol) and CDCl$_3$ (ca. 1 mL), and then ^{1}H NMR analysis was conducted using a portion of this solution. The yields were determined by comparison of an integrated value of the peak that corresponds to a proton of silanol with that corresponds to two protons of 1,1,2,2-tetrachloroethane (δ 5.98 ppm).   After ^{1}H NMR analysis, the combined residue was purified by silica-gel column chromatography or preparative TLC to give silyl ether.

4.4.3 Recycling Run experiment

To a reaction tube equipped with a magnetic stir bar was added Au:F-CAC (0.01 atom%), **1a** (0.50 mmol), ethanol (200 mol%), and toluene (3 mL). The mixture was stirred at 27 °C under an ambient atmosphere. After stirring for 4 h, the catalyst was removed by filtration and washed with diethyl ether (ca. 5 mL × 3). The spent catalyst was dried at 45 °C under reduced pressure for 12 h, and this was used for the next recycling run.

4.4.5 Filtration experiment

To a reaction tube equipped with a magnetic stir bar was added Au:F-CAC (0.01 atom%), **1a** (0.50 mmol), ethanol (200 mol%), and toluene (3 mL). The mixture was stirred at 27 °C under an ambient atmosphere. After stirring for 3 h, the catalyst was removed by filtration. The resulting filtrate was further treated under the same reaction conditions in the absence of the filtered catalyst for 6 h. Then,

the filtrate was concentrated under reduced pressure. To the residue was added 1,1,2,2-tetrachloroethane (52.7 μL, 0.50 mmol) and CDCl$_3$ (ca. 1 mL), and then ^{1}H NMR analysis was conducted using a portion of this solution. The yields were determined by comparison of an integrated value of the peak that corresponds to a proton of silanol with that corresponds to two protons of 1,1,2,2-tetrachloroethane (δ 5.98 ppm).

4.4.6 Compound data

Methoxy(dimethylphenyl)silane (2a)
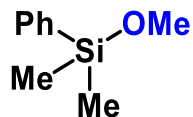
Purified by PTLC (*n*-hexane/EtOAc = 9/1);

^{1}H NMR (CDCl$_3$) δ 7.59–7.57 (m, 2H), 7.40–7.39 (m, 3H), 3.45 (s, 3H), 0.39 (s, 6H);

^{13}C NMR (CDCl$_3$) δ 137.4, 133.4, 129.6, 127.9, 50.7, –2.4.

The data are consistent with that reported in the literature.[7]

Ethoxy(dimethylphenyl)silane (2b)
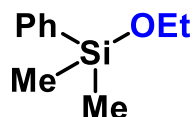
Purified by PTLC (*n*-hexane/EtOAc = 9/1);

^{1}H NMR (CDCl$_3$) δ 7.60–7.57 (m, 2H), 7.40–7.38 (m, 3H), 3.67 (q, *J* = 6.9 Hz, 2H), 1.19 (t, *J* = 6.9 Hz, 2H), 0.38 (s, 6H);

^{13}C NMR (CDCl$_3$) δ 138.1, 133.5, 129.5, 127.8, 58.7, 18.4, –1.7.

The data are consistent with that reported in the literature.[7]

Propoxy(dimethylphenyl)silane (2c)
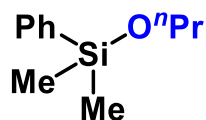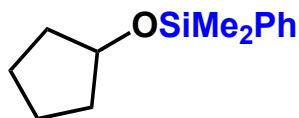

Purified by PTLC (*n*-hexane/EtOAc = 9/1);

^{1}H NMR (CDCl$_3$) δ 7.59–7.57 (m, 2H), 7.40–7.36 (m, 3H), 3.55 (t, *J* = 6.6 Hz, 2H), 1.59–1.50 (m, 3H), 0.87 (t, *J* = 7.5 Hz, 3H), 0.38 (s, 6H);

^{13}C NMR (CDCl$_3$) δ 138.1, 133.5, 129.5, 127.8, 64.8, 25.7, 10.3, –1.8.

The data are consistent with that reported in the literature.[14]

Butoxydimethyl(phenyl)silane (2d)

Ph—Si(Me)(Me)—O^{n}Bu
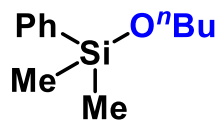
Purified by PTLC (*n*-hexane/EtOAc = 9/1);

^{1}H NMR (CDCl$_3$) δ 7.59–7.56 (m, 2H), 7.40–7.37 (m, 3H), 3.59 (t, *J* = 6.6 Hz, 2H), 1.54–1.49 (m, 2H), 1.33 (qt, *J* = 7.3, 7.8 Hz, 2H), 0.88 (t, *J* = 7.3 Hz, 3H), 0.37 (s, 6H);

^{13}C NMR (CDCl$_3$) δ 138.1, 133.5, 129.5, 127.8, 62.9, 34.7, 18.9, 13.9, –1.8.

The data are consistent with that reported in the literature.[7]

Isopropoxy(dimethylphenyl)silane(2e)

Ph—Si(Me)(Me)—O^{i}Pr
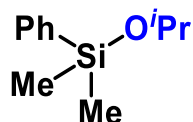
Purified by PTLC (*n*-hexane/EtOAc = 9/1);

^{1}H NMR (CDCl$_3$) δ 7.61–7.58 (m, 2H), 7.41–7.36 (m, 3H), 3.98 (sept, *J* = 6.4 Hz, 1H), 1.14 (d, *J* = 6.4 Hz, 6H), 0.38 (s, 6H);

^{13}C NMR (CDCl$_3$) δ 138.5, 133.5, 129.4, 127.7, 65.3, 25.7, –1.2.

The data are consistent with that reported in the literature.[7]

Methoxy(methyldiphenyl)silane (2g)

Ph—Si(Ph)(Me)—OMe
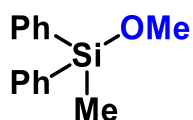
Purified by PTLC (*n*-hexane/EtOAc = 9/1);

^{1}H NMR (CDCl$_3$) δ 7.60–7.58 (m, 4H), 7.42–7.36 (m, 6H), 3.54 (s, 3H), 0.64 (s, 3H);

^{13}C NMR (CDCl$_3$) δ 135.6, 134.3, 129.9, 127.9, 51.3, –3.6.

The data are consistent with that reported in the literature.[15]

Ethoxy(methyldiphenyl)silane (2h)

Ph\
Si—OEt
Ph/ |
     Me
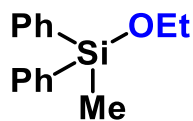
Purified by PTLC (*n*-hexane/EtOAc = 1/9);

^{1}H NMR (CDCl$_3$) δ 7.61–7.59 (m, 4H), 7.42–7.35 (m, 6H), 3.78 (q, *J* = 6.8 Hz, 2H), 1.23 (t, *J* = 6.8 Hz, 3H), 0.65 (s, 3H);

^{13}C NMR (CDCl$_3$) δ 136.2, 134.3, 129.7, 127.8, 59.2, 18.4, –3.0.

The data are consistent with that reported in the literature.[15]

Propoxy(methyldiphenyl)silane (2i)

Ph\
Si—O^{n}Pr
Ph/ |
     Me
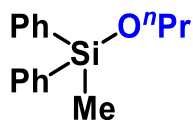
Purified by PTLC (*n*-hexane/EtOAc = 1/9);

^{1}H NMR (CDCl$_3$) δ 7.61–7.59 (m, 4H), 7.43–7.35 (m, 6H), 3.66 (t, *J* = 6.6 Hz, 2H), 1.64–1.55 (m, 2H), 0.90 (t, *J* = 7.3 Hz, 3H), 0.64 (s, 3H);

^{13}C NMR (CDCl$_3$) δ 136.3, 134.3, 129.7, 127.8, 65.2, 25.8, 10.3, –3.0.

The data are consistent with that reported in the literature.[16]

Butoxy(methyldiphenyl)silane (2j)

Ph\
Si—O^{n}Bu
Ph/ |
     Me
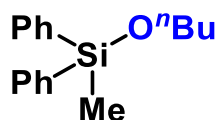
Purified by PTLC (*n*-hexane/EtOAc = 1/9);

^{1}H NMR (CDCl$_3$) δ 7.61–7.59 (m, 4H), 7.42–7.35 (m, 6H), 3.71 (t, *J* = 6.4 Hz, 2H), 1.58–1.53 (m, 2H), 1.37 (qt, *J* = 7.3, 7.8 Hz, 2H), 0.89 (t, *J* = 7.3 Hz, 3H), 0.64 (s, 3H);

^{13}C NMR (CDCl$_3$) δ 136.3, 134.3, 129.7, 127.8, 63.3, 34.7, 19.0, 13.9, –3.0.

The data are consistent with that reported in the literature.[7]

Isopropoxy(methyldiphenyl)silane (2k)

Ph—Si(Ph)(Me)—O^{i}Pr
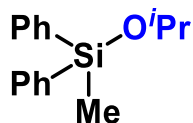
Purified by PTLC (*n*-hexane/EtOAc = 9/1);

^{1}H NMR (CDCl$_3$) δ 7.62–7.59 (m, 4H), 7.40–7.34 (m, 6H), 4.14 (sept, *J* = 6.0 Hz, 1H), 1.18 (d, *J* = 6.0 Hz, 6H), 0.66 (s, 3H);

^{13}C NMR (CDCl$_3$) δ 136.8, 134.3, 129.6, 127.8, 65.8, 25.7, –2.4.

The data are consistent with that reported in the literature.[16]

Methoxy(triphenyl)silane (2m)

Ph—Si(Ph)(Ph)—OMe
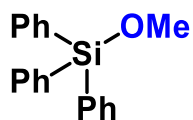
Purified by PTLC (*n*-hexane/EtOAc = 9/1);

^{1}H NMR (CDCl$_3$) δ 7.65–7.62 (m, 6H), 7.46–7.38 (m, 9H), 3.65 (s, 3H);

^{13}C NMR (CDCl$_3$) δ 135.4, 133.9, 130.1, 127.9, 51.9.

The data are consistent with that reported in the literature.[16]

Ethoxy(triphenyl)silane (2n)

Ph—Si(Ph)(Ph)—OEt
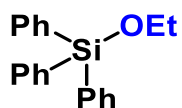
Purified by PTLC (*n*-hexane/EtOAc = 9/1);

^{1}H NMR (CDCl$_3$) δ 7.64–7.62 (m, 6H), 7.44–7.36 (m, 9H), 3.88 (q, *J* = 6.8 Hz, 2H), 1.24 (t, *J* = 6.8 Hz, 3H);

^{13}C NMR (CDCl$_3$) δ 135.4, 134.4, 129.9, 127.8, 59.7, 18.4.

The data are consistent with that reported in the literature.[16]

(Benzyloxy)dimethyl(phenyl)silane (4a)
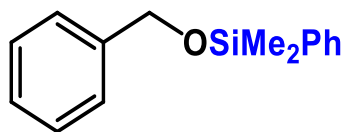
Purified by PTLC (*n*-hexane/EtOAc = 20/1);

^{1}H NMR (CDCl$_3$) δ 7.62–7.60 (m, 2H), 7.42–7.37 (m, 4H), 7.32–7.29 (m, 3H), 7.26–7.24 (m, 1H), 4.70 (s, 2H), 0.41 (s, 6H);

^{13}C NMR (CDCl$_3$) δ 140.7, 137.6, 133.5, 129.7, 128.3, 127.9, 127.1, 126.5, 65.0, –1.7.

The data are consistent with that reported in the literature.[7]

((4-Methoxybenzyl)oxy)dimethyl(phenyl)silane (4b)
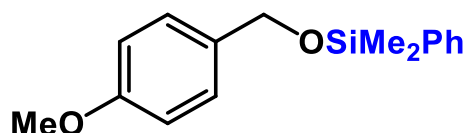
Purified by MPLC (*n*-hexane/EtOAc = 30/1);

^{1}H NMR (CDCl$_3$) δ 7.61–7.58 (m, 2H), 7.41–7.36 (m, 3H), 7.22–7.20 (AA′BB′, 2H), 6.86–6.84 (AA′BB′, 2H), 4.62 (s, 2H), 3.80 (s, 3H), 0.39 (s, 6H);

^{13}C NMR (CDCl$_3$) δ 158.8, 137.7, 133.6, 132.9, 129.6, 128.2, 127.9, 113.7, 64.7, 55.3, –1.7.

The data are consistent with that reported in the literature.[7]

(4-Fluorobenzyl)oxy)dimethyl(phenyl)silane (4c)
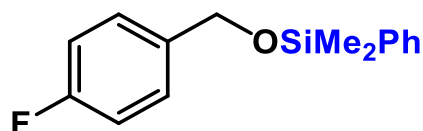
Purified by PTLC (*n*-hexane/EtOAc = 9/1);

^{1}H NMR (CDCl$_3$) δ 7.60–7.58 (m, 2H), 7.41–7.38 (m, 3H), 7.27–7.23 (AA′BB′X, 2H), 7.01–6.97 (AA′BB′X, 2H), 4.64 (s, 2H), 0.41 (s, 6H);

^{13}C NMR (CDCl$_3$) δ 163.2, 160.8, 137.4, 136.4, 133.5, 129.7, 128.3, 128.2, 127.9, 115.2, 114.9, 64.3, –1.8.

The data are consistent with that reported in the literature.[7]

(4-Bromophenethoxy)dimethyl(phenyl)silane (4d)
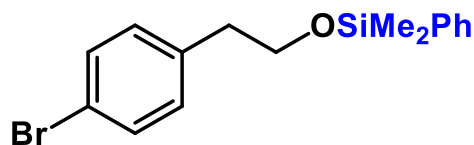
Purified by MPLC (n-hexane/EtOAc = 9/1);

93% yield;

^{1}H NMR (CDCl$_3$) δ 7.48 (dd, J = 7.3, 1.4 Hz, 2H), 7.41–7.33 (m, 5H), 7.04–7.01 (AA′BB′, 2H), 3.76 (t, J = 6.9 Hz, 2H), 2.76 (t, J = 6.9 Hz, 2H), 0.31 (s, 6H);

^{13}C NMR (CDCl$_3$) δ 138.0, 137.5, 133.4, 131.3, 130.8, 129.6, 127.8, 119.9, 63.8, 38.6, –1.9.

The data are consistent with that reported in the literature.[17]

Methyl 4-((((dimethyl(phenyl)silyl)oxy)methyl)benzoate (4e)
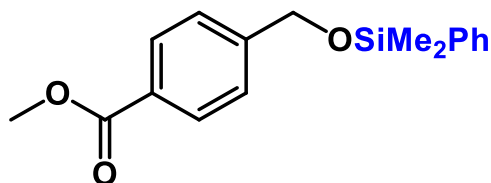
Purified by MPLC (n-hexane/EtOAc = 9/1);

90% yield;

^{1}H NMR (CDCl$_3$) δ 8.00–7.98 (AA′BB′, 2H), 7.60 (dd, J = 7.3, 1.8 Hz, 2H), 7.42–7.36 (m, 5H), 4.74 (s, 2H), 3.91 (s, 3H), 0.42 (s, 6H);

^{13}C NMR (CDCl$_3$) δ 167.0, 146.1, 137.2, 133.5, 129.8, 129.6, 128.9, 127.9, 126.1, 64.4, 52.0, –1.8.

The data are consistent with that reported in the literature.[18]

4-((((Dimethyl(phenyl)silyl)oxy)methyl)benzaldehyde (4f)
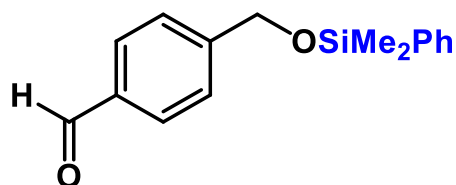
Purified by MPLC (n-hexane/EtOAc = 9/1);

48% yield;

^{1}H NMR (CDCl$_3$) δ 9.99 (s, 1H), 7.86–7.81 (AA′BB′, 2H), 7.60 (dd, J = 7.9, 1.8 Hz, 2H), 7.49–7.43 (AA′BB′, 2H), 7.42–7.37 (m, 3H), 4.77 (s, 2H), 0.44 (s, 6H);

^{13}C NMR (CDCl$_3$) δ 192.1, 147.9, 137.1, 135.4, 133.5, 129.9, 129.8, 128.0, 126.6, 64.4, –1.8;

IR (diamond, cm^{-1}) 3069, 2957, 2846, 2733, 1696, 1607, 1578, 1427, 1303, 1251, 1206, 1164, 1116,

1082, 1015, 845, 826, 784, 728, 698, 648, 618, 470;

HRMS (EI$^+$) m/z 270.1082 (270.1076 calcd for C$_{16}$H$_{18}$O$_2$Si, M$^{+\bullet}$).

4-(((Dimethyl(phenyl)silyl)oxy)methyl)aniline (4g)
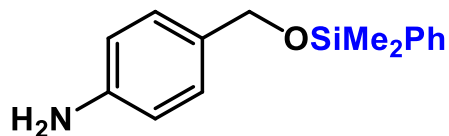
Purified by MPLC (n-hexane/EtOAc = 3/7);

42% yield;

^{1}H NMR (CDCl$_3$) δ 7.59 (dd, J = 7.1, 2.1 Hz, 2H), 7.43–7.34 (m, 3H), 7.11–7.05 (AA′BB′, 2H), 6.67–6.61 (AA′BB′, 2H), 4.57 (s, 2H), 3.63 (s, NH$_2$), 0.38 (s, 6H);

^{13}C NMR (CDCl$_3$) δ 145.6, 137.8, 133.6, 130.8, 129.6, 128.4, 127.8, 115.0, 65.0, –1.6;

IR (diamond, cm^{-1}) 3450, 3359, 3225, 3019, 2954, 2862, 1623, 1517, 1427, 1375, 1252, 1214, 1173, 1116, 1046, 844, 823, 782, 727, 697, 642, 536, 493, 470;

HRMS (EI$^+$) m/z 257.1236 (257.1230 calcd for C$_{15}$H$_{19}$NOSi, M$^{+\bullet}$).

(Furan-2-ylmethoxy)dimethyl(phenyl)silane (4h)
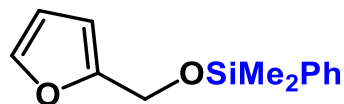
Purified by MPLC (n-hexane/EtOAc = 1/9);

73% yield;

^{1}H NMR (CDCl$_3$) δ 7.59–7.57 (m, 2H), 7.40–7.36 (m, 4H), 6.30 (dd, J = 3.2, 1.8 Hz, 1H), 6.18 (d, J = 3.2 Hz, 1H), 4.59 (s, 2H), 0.39 (s, 6H);

^{13}C NMR (CDCl$_3$) δ 153.6, 142.3, 137.3, 133.6, 129.7, 127.9, 110.2, 107.8, 57.7, –1.8.

The data are consistent with that reported in the literature.[7]

(But-3-en-1-yloxy)dimethyl(phenyl)silane (4i)
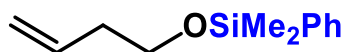
Purified by PTLC (n-hexane/EtOAc = 9/1);

76% yield;

^{1}H NMR (CDCl$_3$) δ 7.59–7.57 (m, 2H), 7.40–7.37 (m, 3H), 5.78 (ddt, J = 17.1, 10.3, 6.9 Hz, 1H), 5.08–5.00 (m, 2H), 3.64 (t, J = 6.9 Hz, 2H), 2.29 (ddt, J = 13.7, 6.9, 1.4 Hz, 2H), 0.38 (s, 6H);

^{13}C NMR (CDCl$_3$) δ 137.9, 135.2, 133.5, 129.6, 127.8, 116.5, 62.6, 37.1, –1.8.

The data are consistent with that reported in the literature.[7]

(Cyclopentyloxy)dimethyl(phenyl)silane (4j)

Purified by PTLC (*n*-hexane/EtOAc = 1/9);

75% yield;

^{1}H NMR (CDCl$_3$) δ 7.59–7.57 (m, 2H), 7.38–7.36 (m, 3H), 4.22 (tt, *J* = 5.0, 5.0 Hz, 1H), 1.71–1.67 (m, 4H), 1.56–1.45 (m, 4H), 0.36 (s, 6H);

^{13}C NMR (CDCl$_3$) δ 138.7, 133.5, 129.4, 127.7, 74.7, 35.5, 23.1, –1.1.

The data are consistent with that reported in the literature.[7]

(Cyclopentyloxy)dimethyl(phenyl)silane (4k)
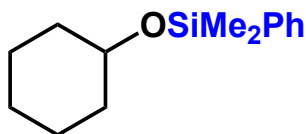
Purified by PTLC (*n*-hexane/EtOAc = 9/1);

83% yield;

^{1}H NMR (CDCl$_3$) δ 7.61–7.58 (m, 2H), 7.39–7.35 (m, 3H), 3.59 (ddd, *J* = 13.7, 9.6, 4.1 Hz, 1H), 1.78–1.68 (m, 4H), 1.50–1.11 (m, 6H), 0.37 (s, 6H);

^{13}C NMR (CDCl$_3$) δ 138.8, 133.5, 129.4, 127.7, 71.4, 35.9, 25.5, 24.3, –1.0.

The data are consistent with that reported in the literature.[17]

(Cyclopentyloxy)dimethyl(phenyl)silane (4l)

Purified by PTLC (*n*-hexane/EtOAc = 9/1);

76% yield;

^{1}H NMR (CDCl$_3$) δ 7.67–7.65 (m, 2 H), 7.41–7.39 (m, 3 H), 7.24–7.23 (m, 1H), 7.19–7.18 (m, 3H), 5.25 (dd, *J* = 6.5, 6.5 Hz , 1H), 2.98 (ddd, *J* = 16.0, 8.7, 3.7 Hz, 1H), 2.72 (ddd, *J* = 16.0, 7.8, 7.8 Hz,

1H), 2.31 (dddd, J = 15.6, 7.8, 6.5, 3.7 Hz, 1H), 1.95 (dddd, J = 15.6, 8.7, 7.8, 6.5 Hz), 0.48 (s, 3H), 0.47 (s, 3H);

^{13}C NMR (CDCl$_3$) δ 145.1, 142.7, 138.1, 133.6, 129.6, 127.9, 127.8, 126.4, 124.6, 124.2, 36.2, 29.7, –1.0, –1.1.

The data are consistent with that reported in the literature.[17]

(Benzhydryloxy)dimethyl(phenyl)silane (4m)

Ph__OSiMe$_2$Ph
|
Ph
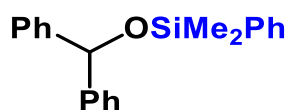
Purified by PTLC (*n*-hexane/EtOAc = 9/1);

66% yield;

^{1}H NMR (CDCl$_3$) δ 7.53–7.51 (m, 2H), 7.40–7.25 (m, 11H), 7.22–7.18 (m, 2H), 5.74 (s, 1H), 0.28 (s, 6H);

^{13}C NMR (CDCl$_3$) δ 144.7, 137.8, 133.7, 129.6, 128.2, 127.8, 127.1, 126.6, –1.0.

The data are consistent with that reported in the literature.[17]

(Benzhydryloxy)dimethyl(phenyl)silane (4n)

OSiMe$_2$Ph
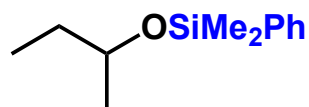
Purified by PTLC (*n*-hexane/EtOAc = 9/1);

76% yield;

^{1}H NMR (CDCl$_3$) δ 7.61–7.58 (m, 2H), 7.39–7.35 (m, 3H), 3.76–3.69 (m, 1H), 1.47–1.40 (m, 2H), 1.10 (d, J = 5.9 Hz, 3H), 0.84 (t, J = 7.3 Hz, 3H), 0.38 (s, 6H);

^{13}C NMR (CDCl$_3$) δ 138.6, 133.5, 129.4, 127.7, 70.4, 32.2, 23.2, 10.2, –1.0, –1.2.

The data are consistent with that reported in the literature.[14]

(((1*R*,2*S*,5*R*)-2-Isopropyl-5-methylcyclohexyl)oxy)dimethyl-(phenyl)silane (4o)

OSiMe$_2$Ph
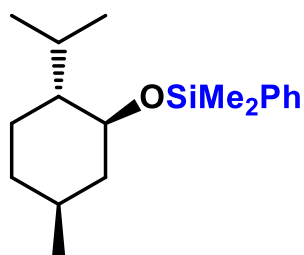
Purified by MPLC (*n*-hexane/EtOAc = 9/1);

65% yield;

^{1}H NMR (CDCl$_3$) δ 7.61−7.58 (m, 2H), 7.38–7.34 (m, 3H), 3.42 (ddd, *J* = 10.3, 10.3, 4.6 Hz, 1H), 2.18 (dddd, *J* = 20.9, 13.9, 7.0, 2.5 Hz, 1H), 1.82 (dddd, *J* = 12.1, 5.5, 1.8, 1.8 Hz, 1H), 1.65−1.52 (m, 2H), 1.37−1.25 (m, 1H), 1.17 (dddd, *J* = 11.7, 9.8, 3.0, 3.0 Hz, 1H), 1.02 (ddd, *J* = 12.1, 12.1, 10.5 Hz, 1H), 0.96−0.75 (m, 2H), 0.88 (d, *J* = 6.9 Hz, 3H), 0.86 (d, *J* = 6.9 Hz, 3H), 0.61 (d, *J* = 6.9 Hz, 3H), 0.394 (s, 3H), 0.386 (s, 3H);

^{13}C NMR (CDCl$_3$) δ 138.6, 133.5, 129.4, 127.7, 72.8, 50.1, 45.3, 34.5, 31.6, 25.2, 22.8, 22.3, 21.3, 15.7, –0.7, –0.9.

The data are consistent with that reported in the literature.[19]

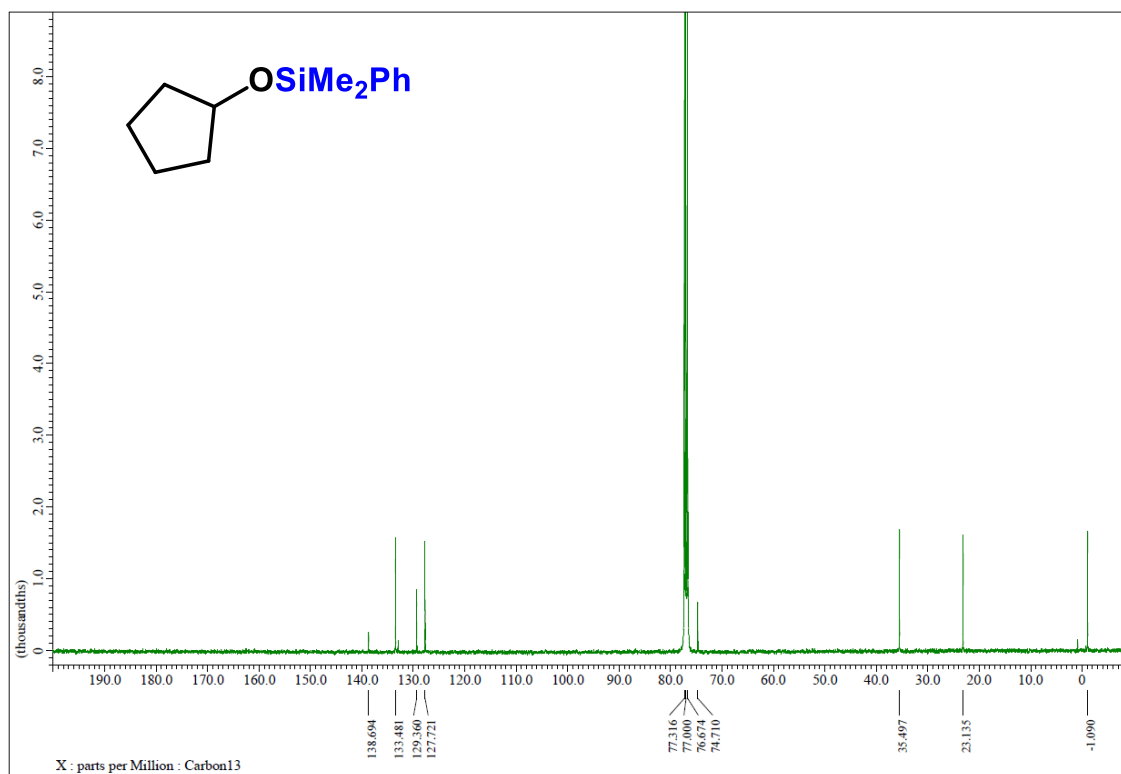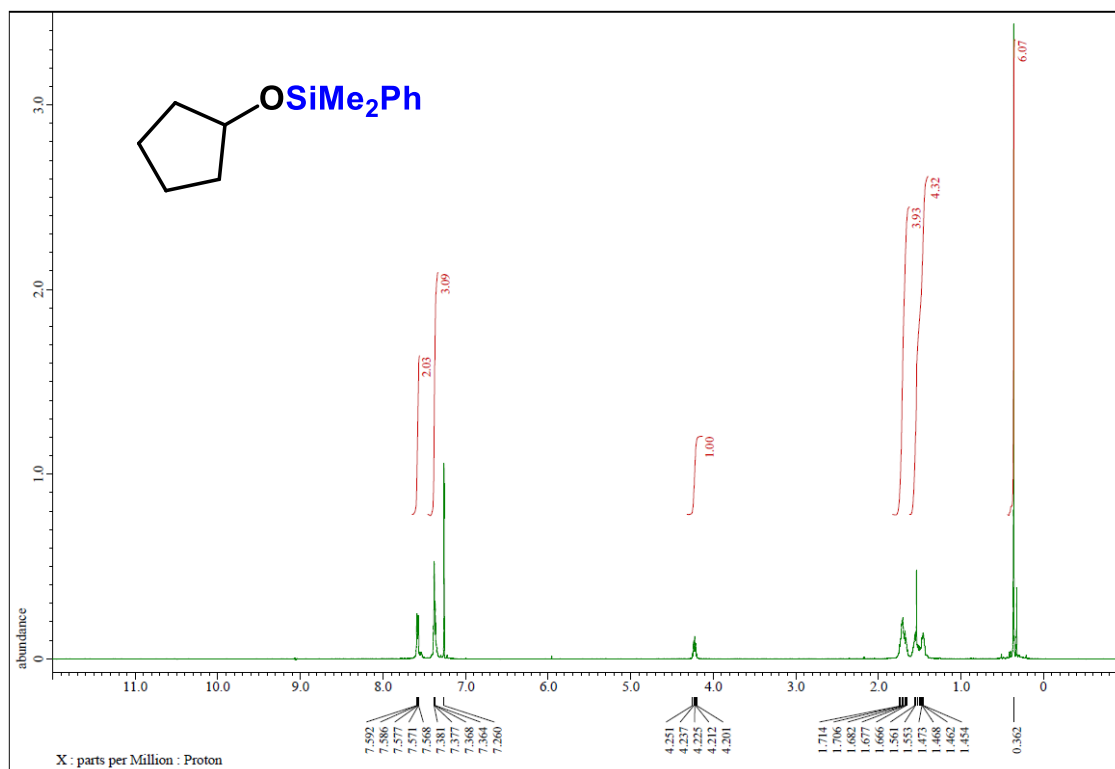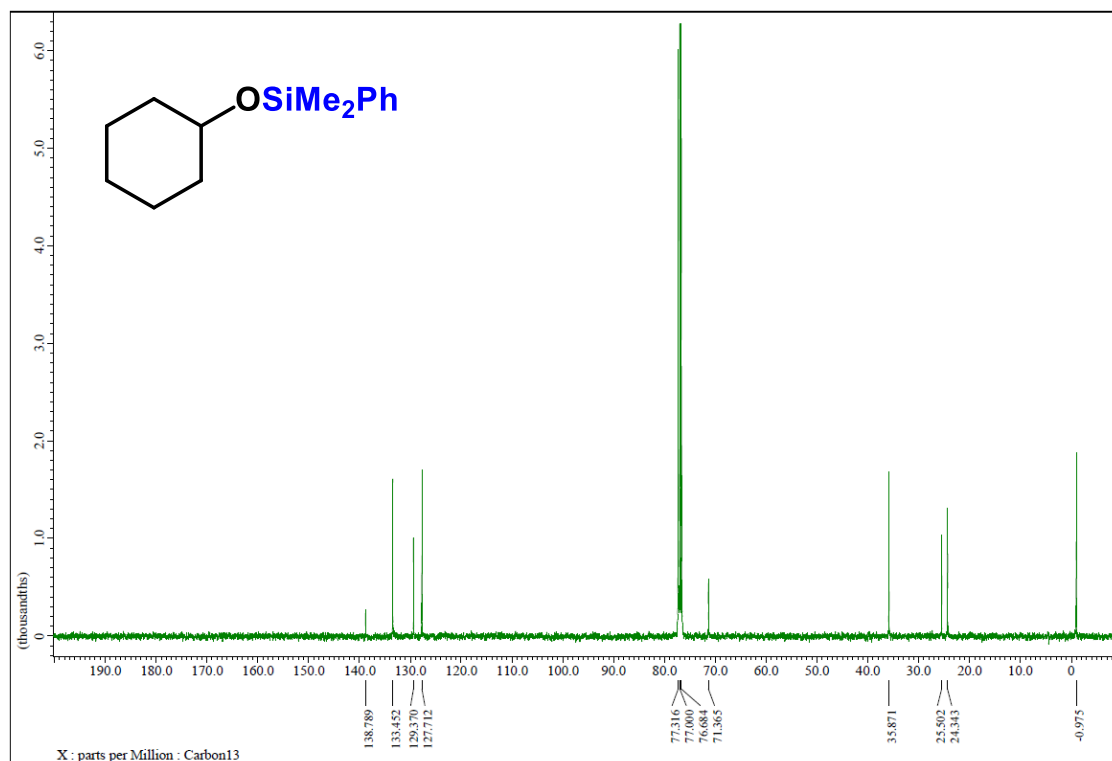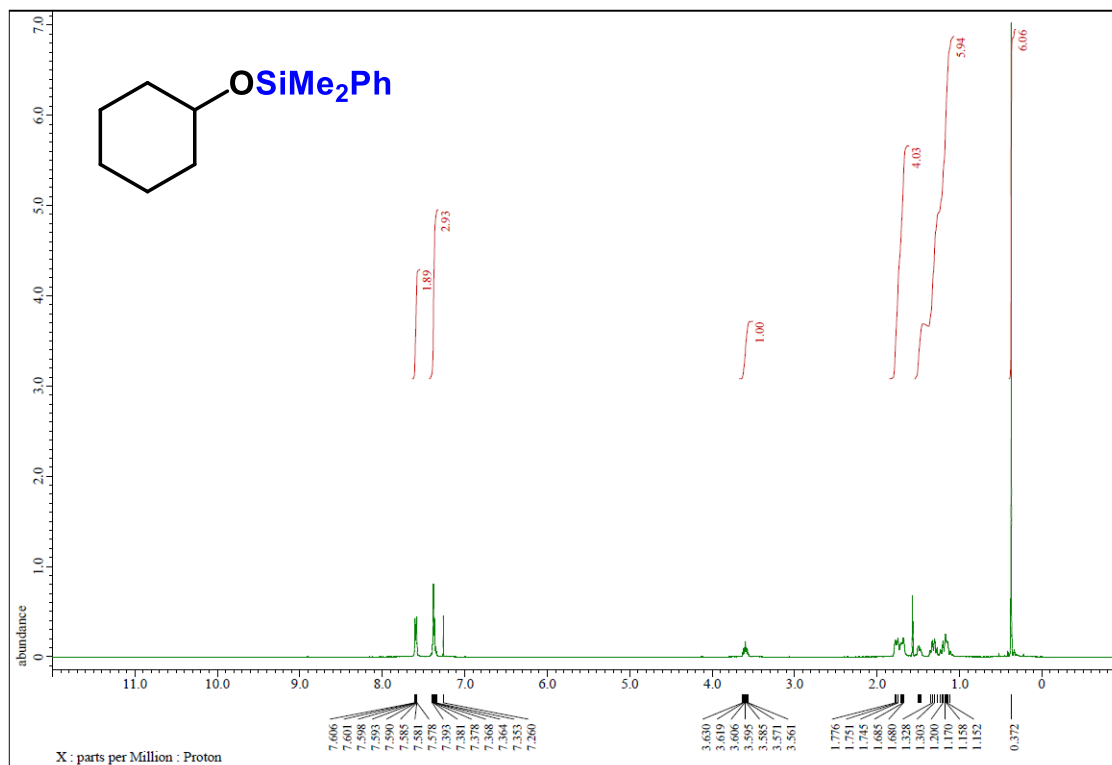¹H NMR (400 MHz) and ¹³C NMR (100 MHz) spectra of **2a** (CDCl₃)
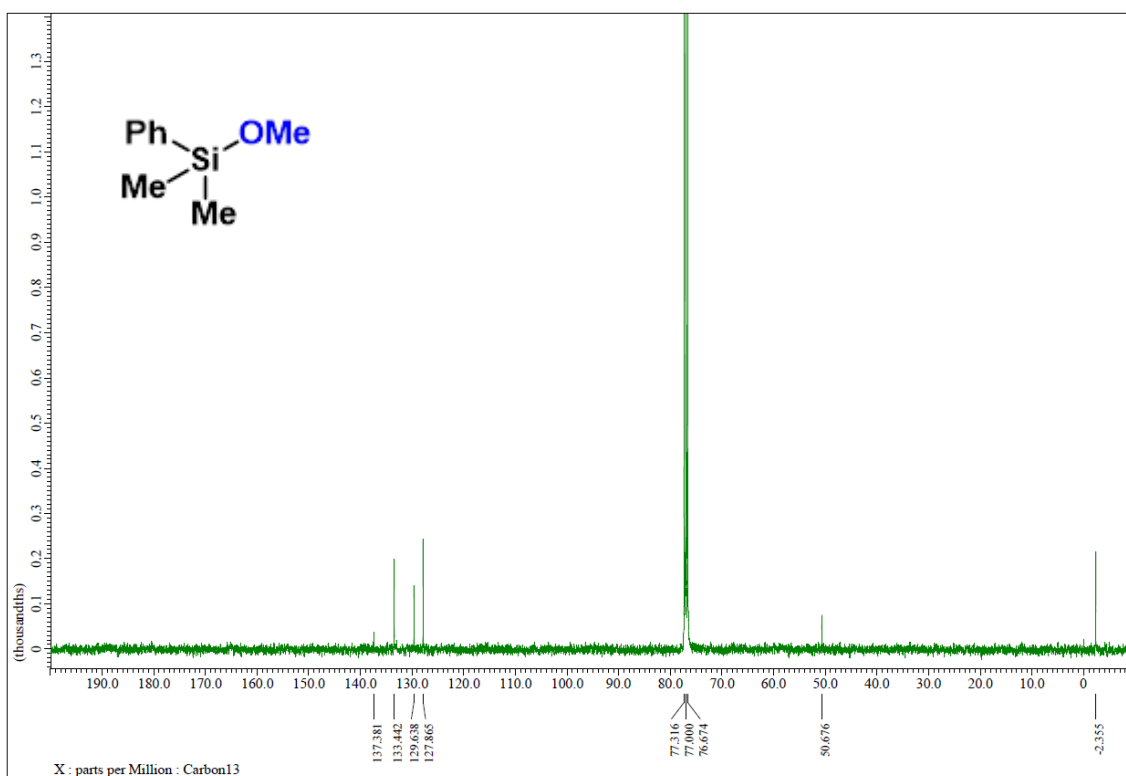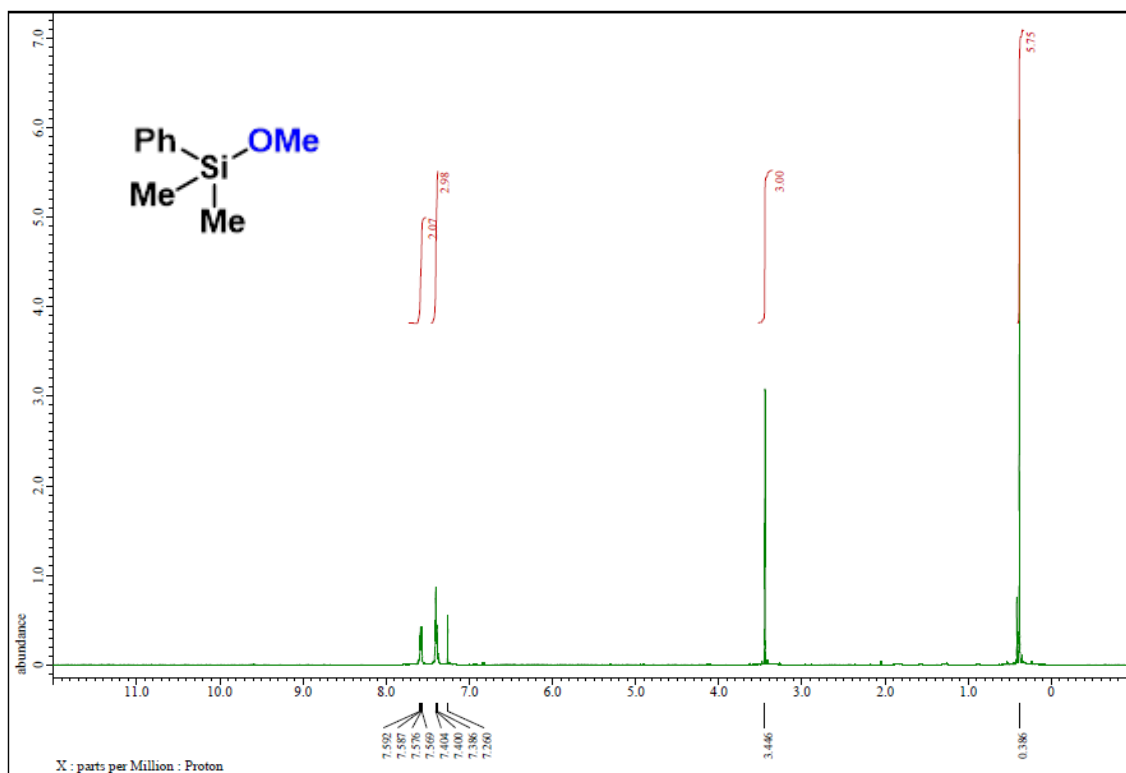
¹H NMR (400 MHz) and ¹³C NMR (100 MHz) spectra of **2b** (CDCl₃)
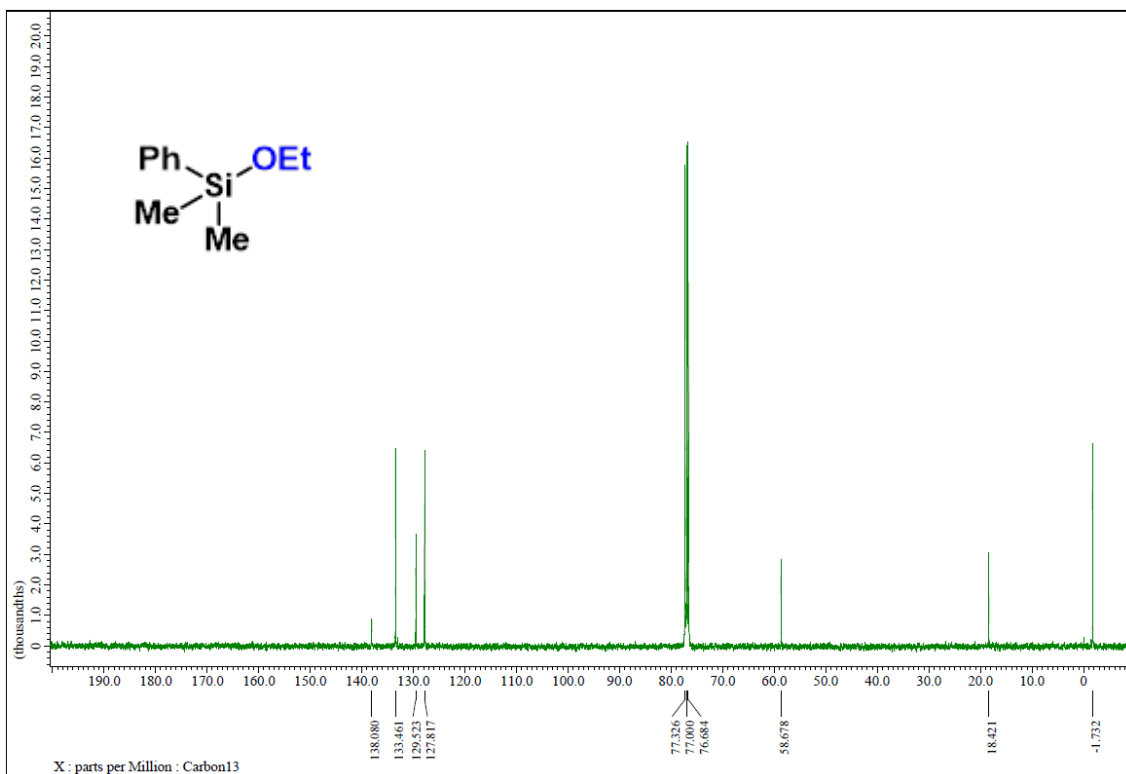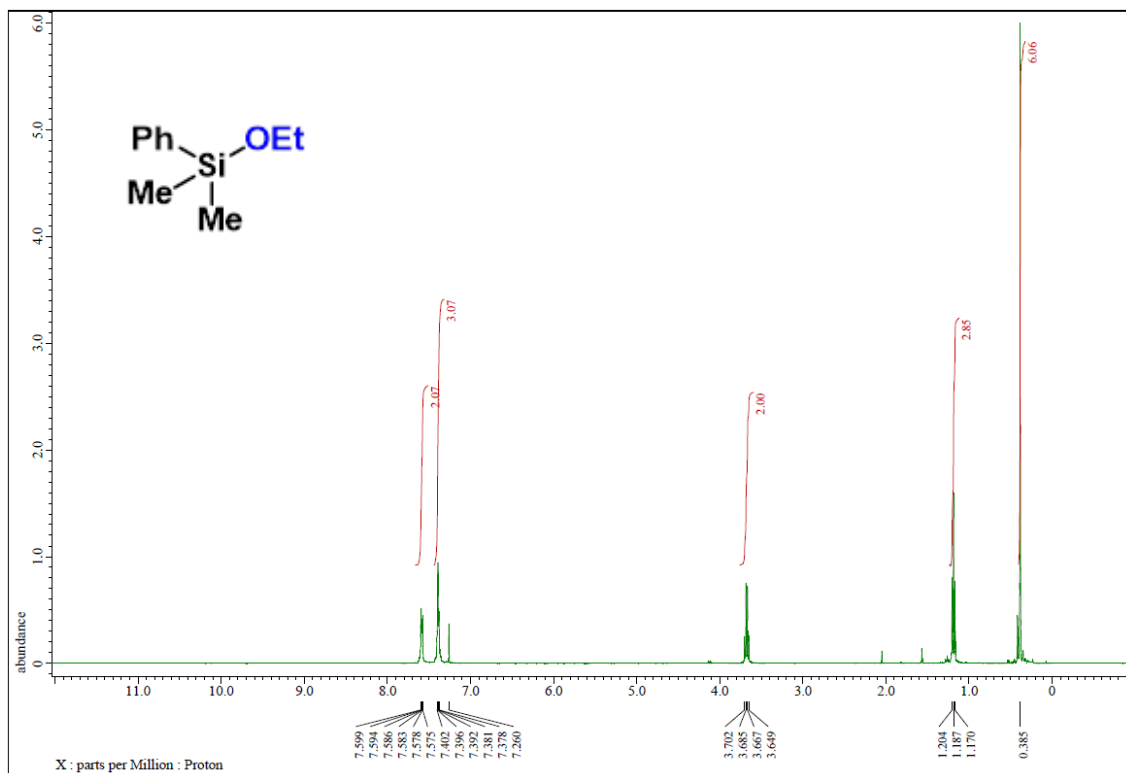
¹H NMR (400 MHz) and ¹³C NMR (100 MHz) spectra of **2c** (CDCl₃)
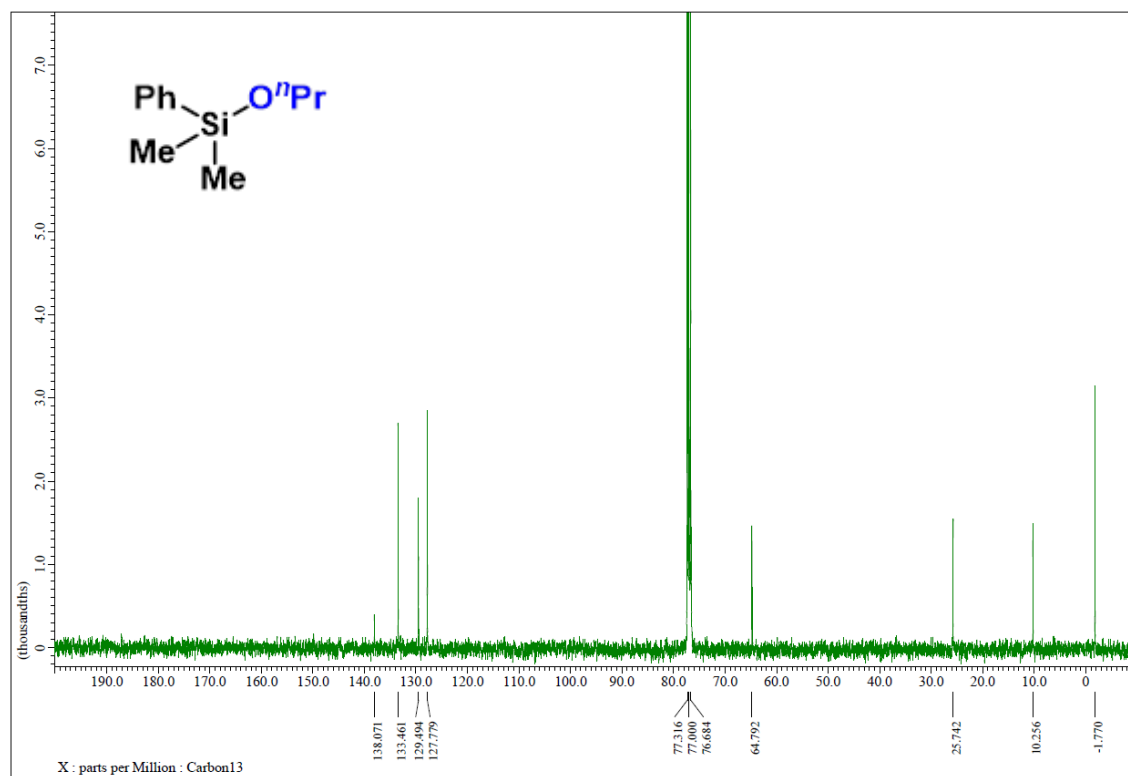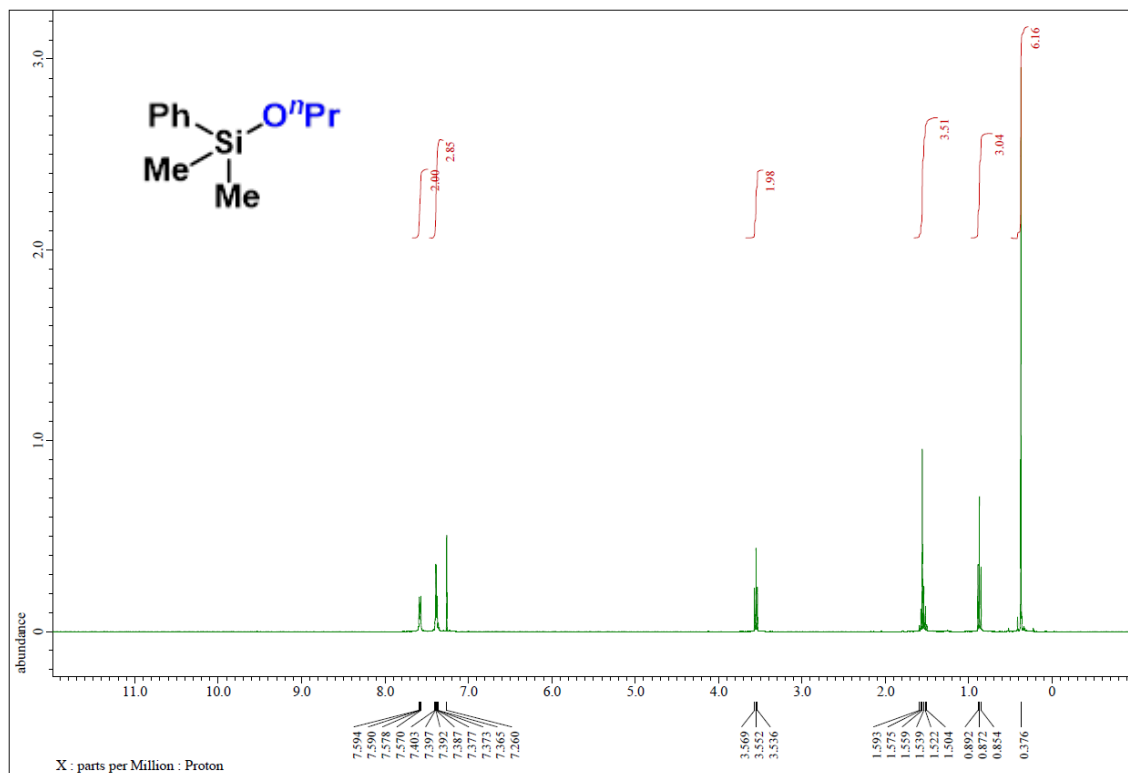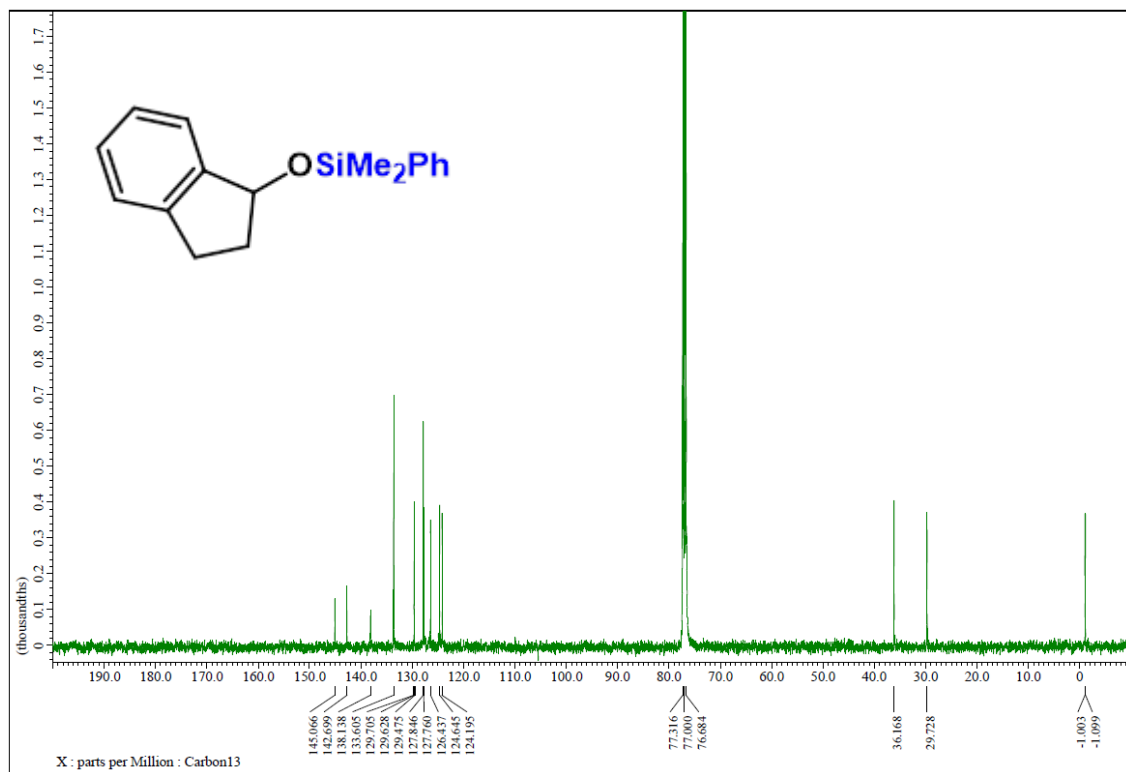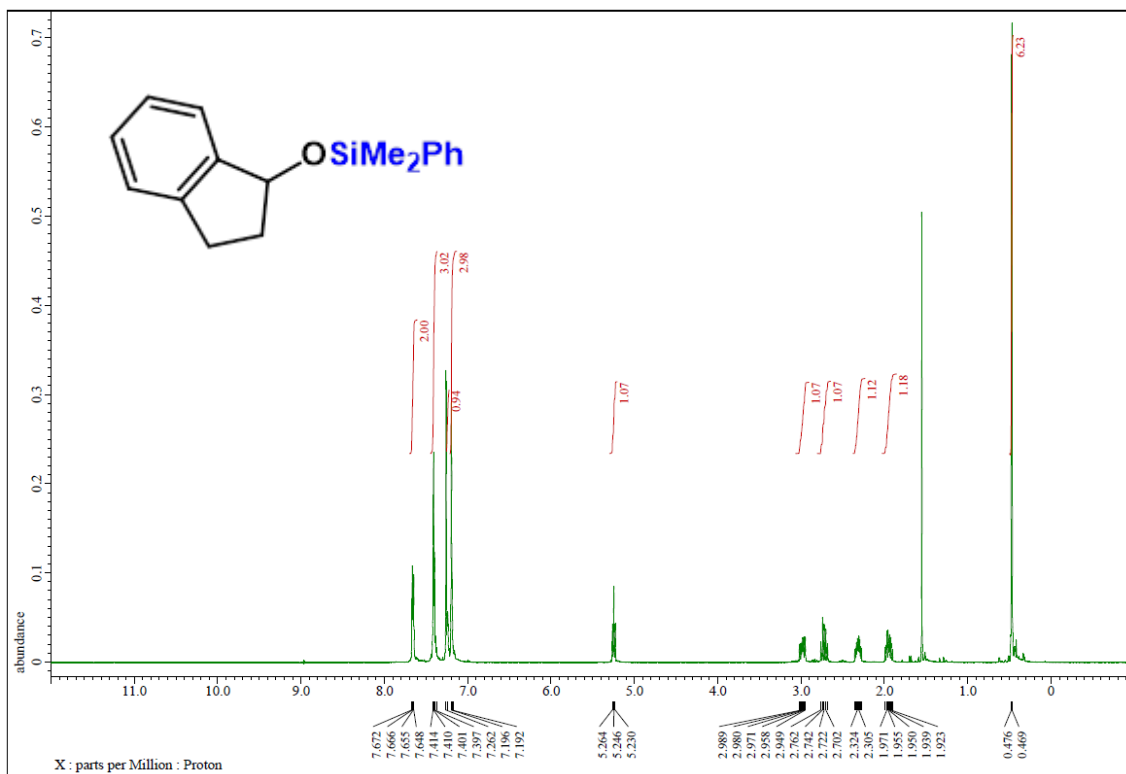
¹H NMR (400 MHz) and ¹³C NMR (100 MHz) spectra of **2d** (CDCl₃)
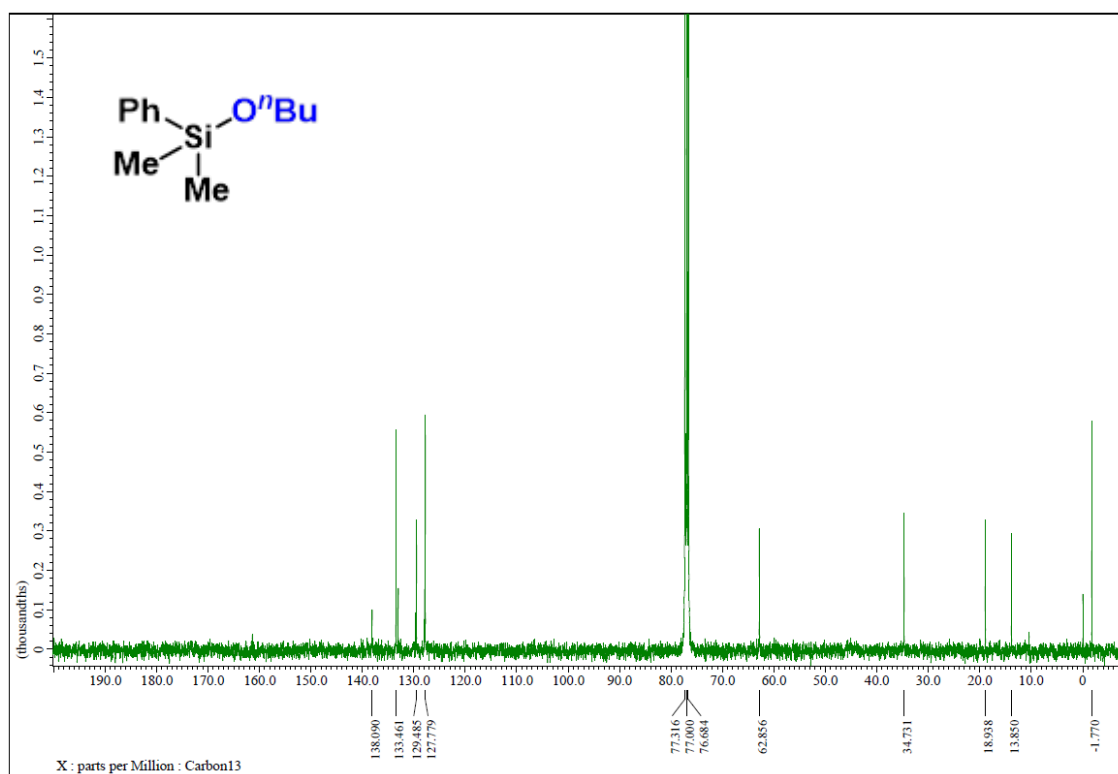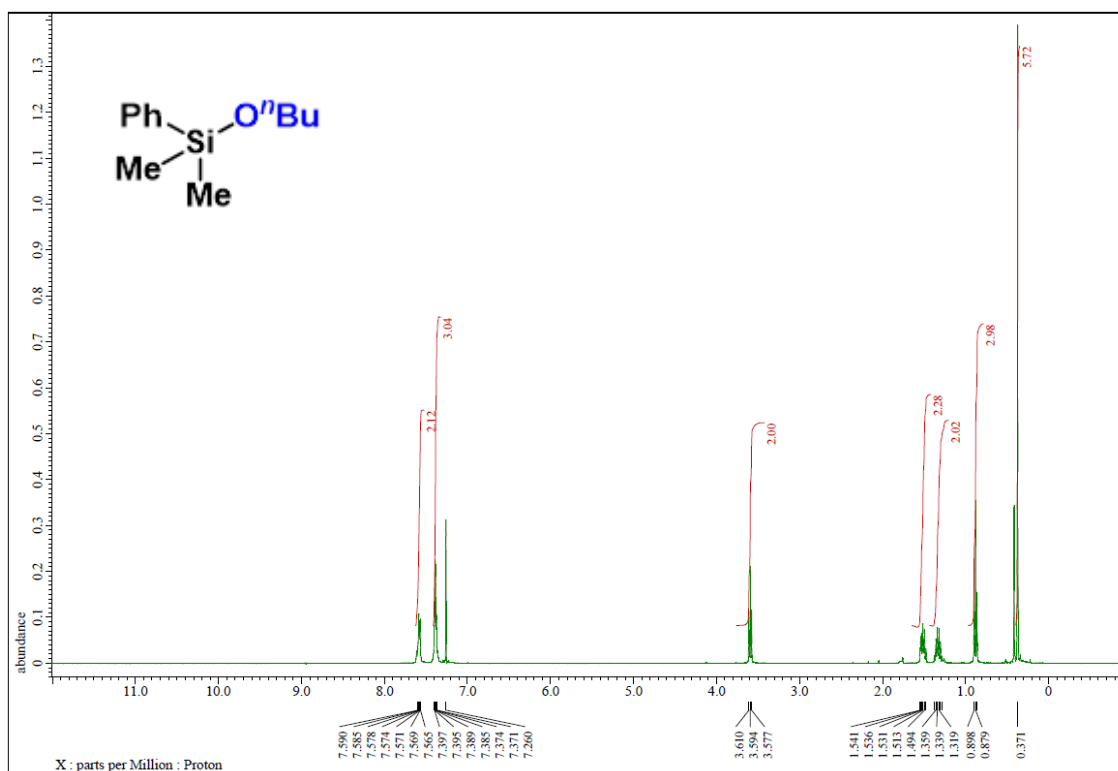
¹H NMR (400 MHz) and ¹³C NMR (100 MHz) spectra of **2e** (CDCl₃)
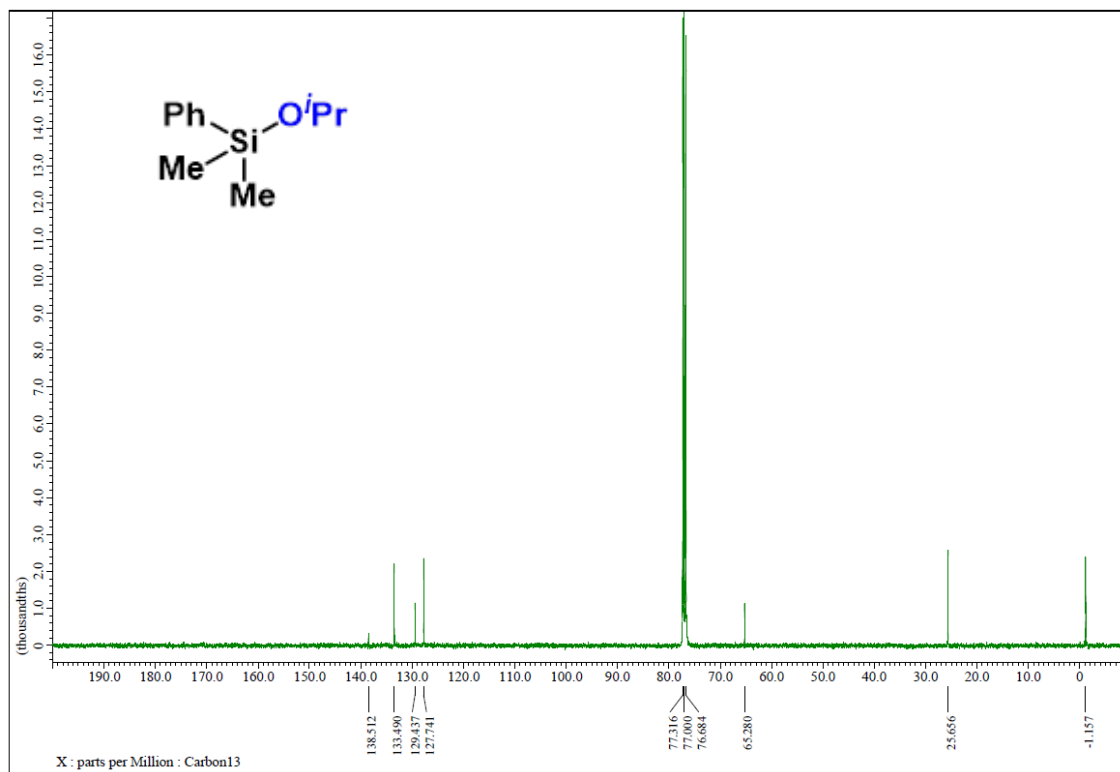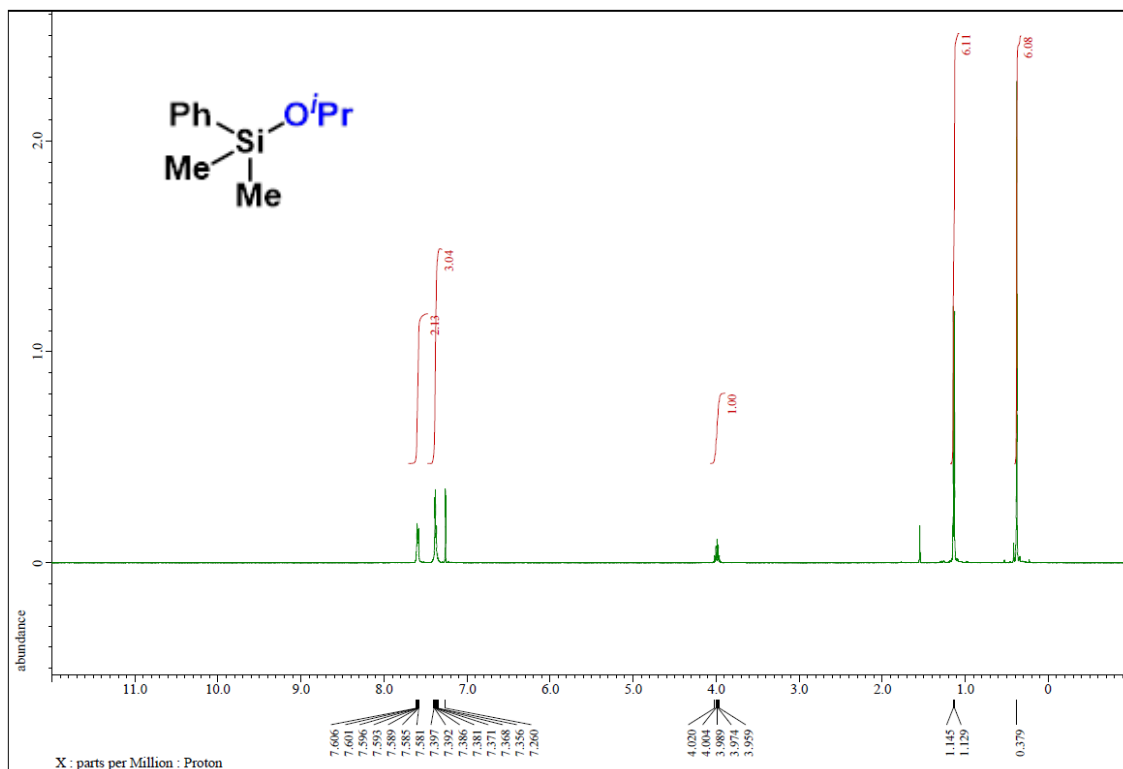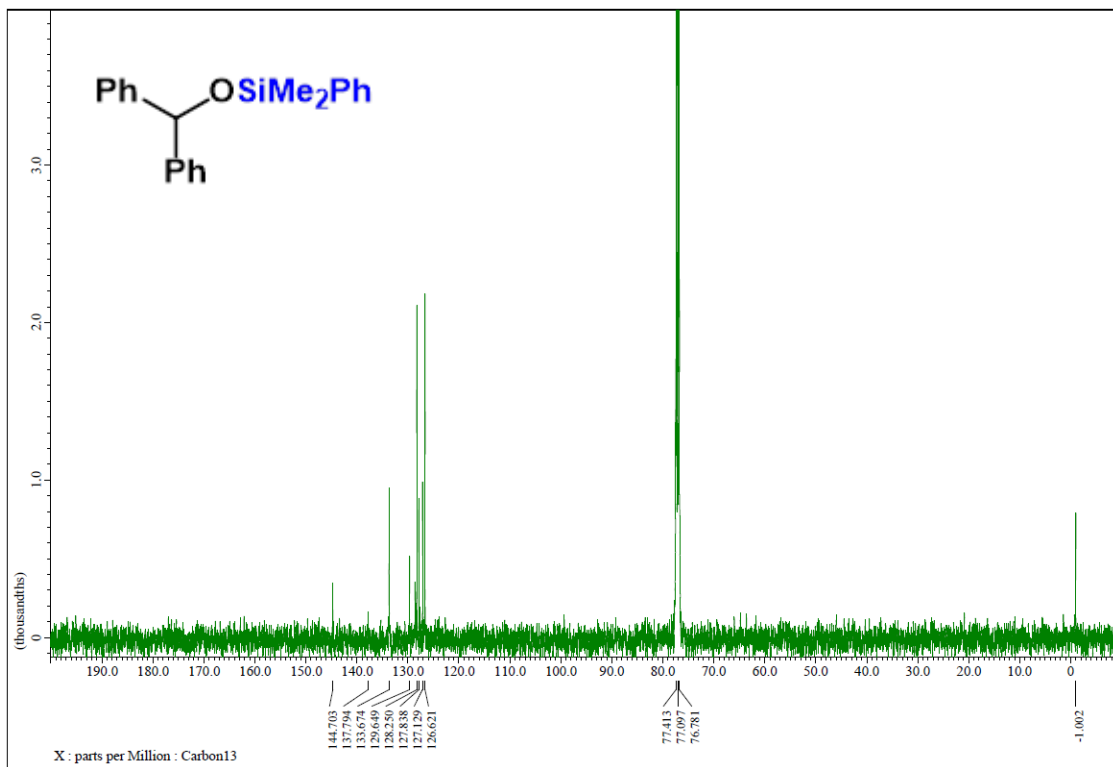
¹H NMR (400 MHz) and ¹³C NMR (100 MHz) spectra of **2g** (CDCl₃)
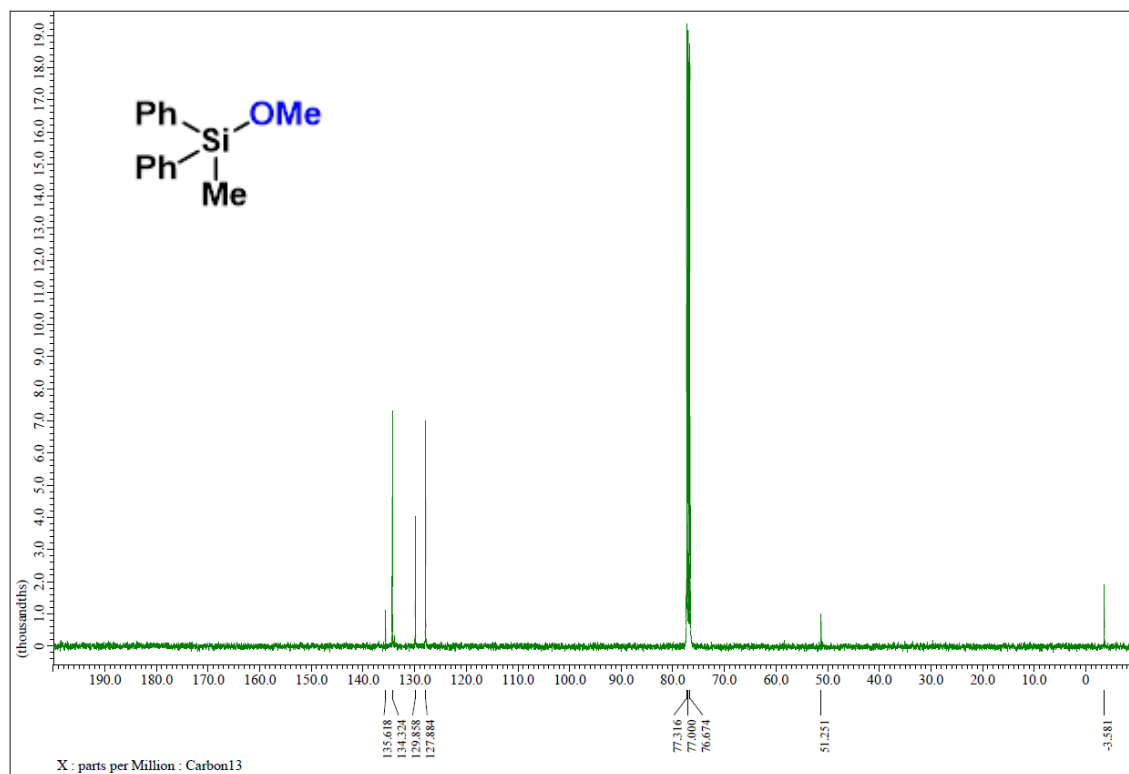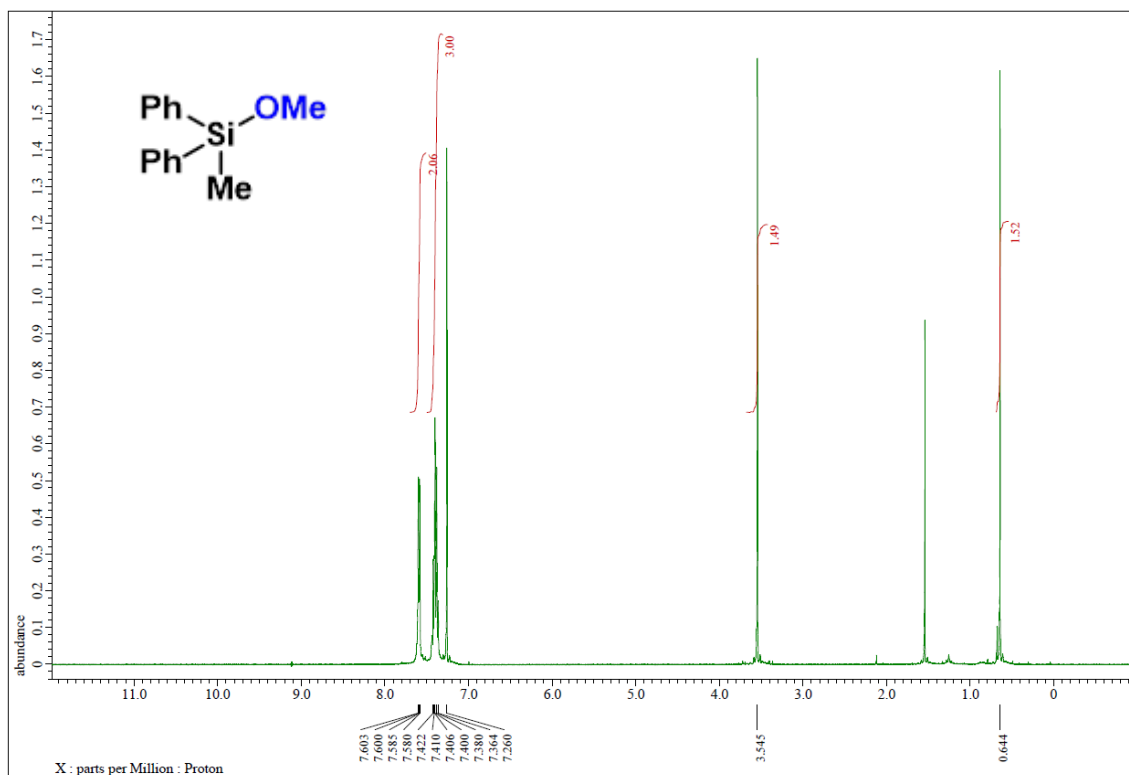
¹H NMR (400 MHz) and ¹³C NMR (100 MHz) spectra of **2h** (CDCl₃)
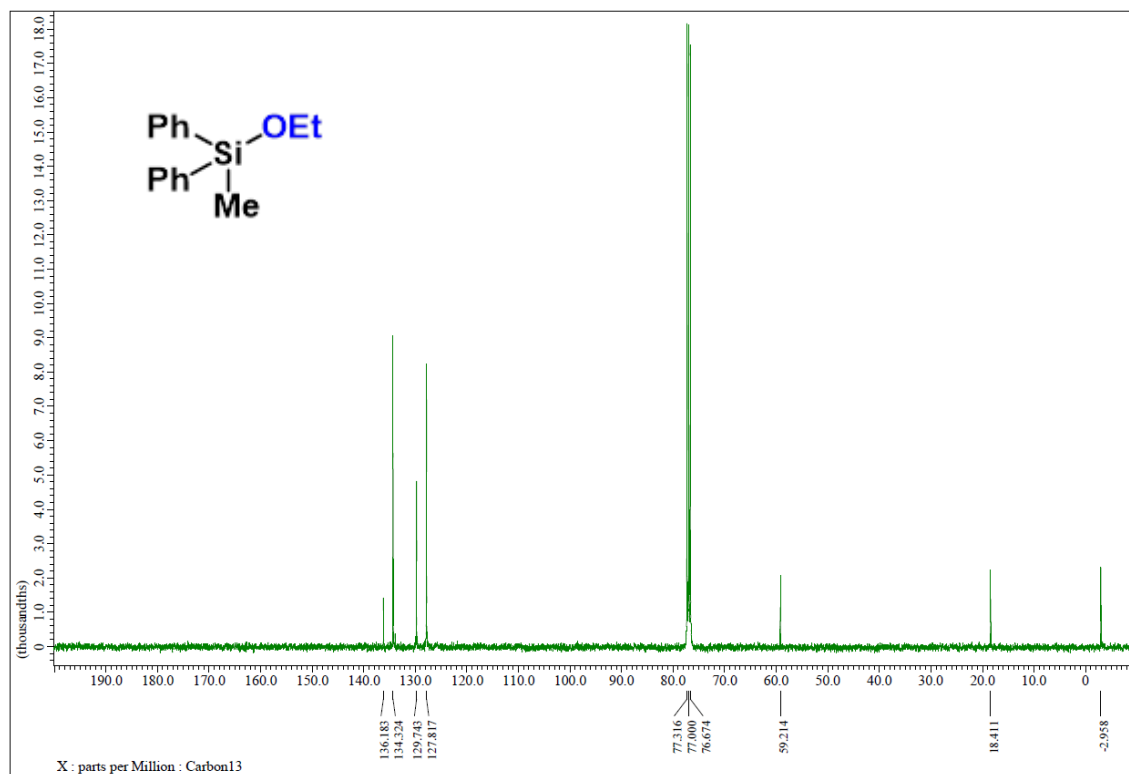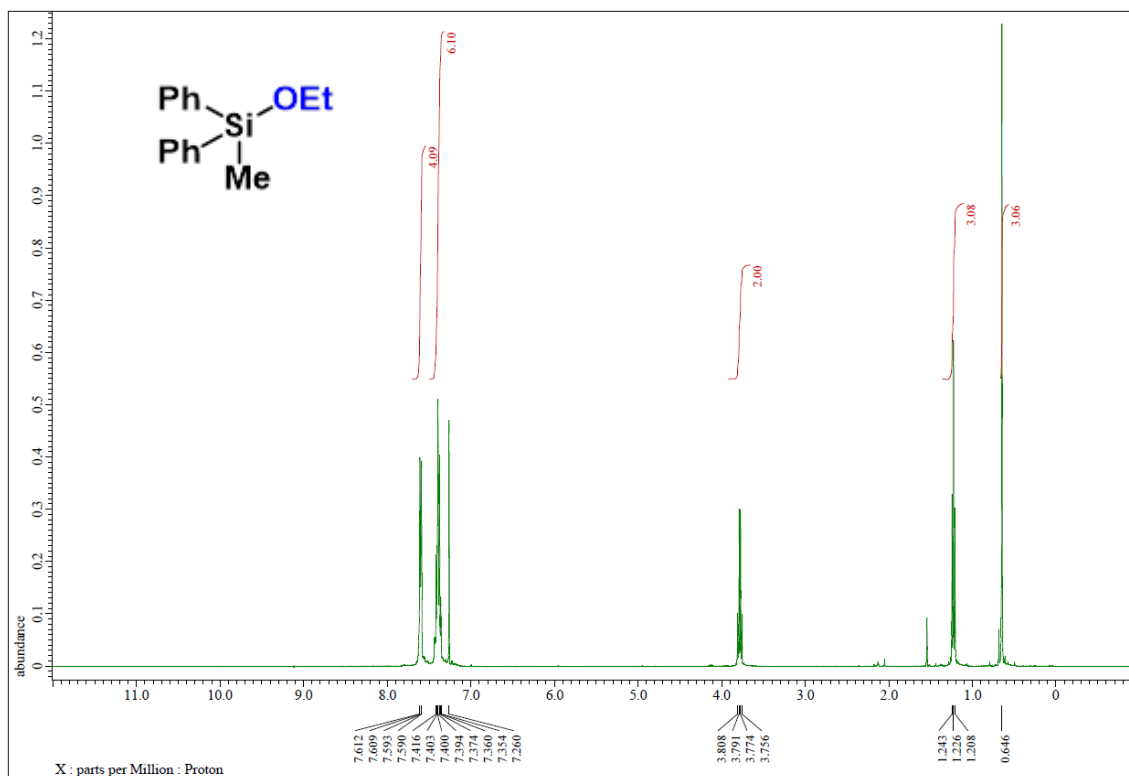
¹H NMR (400 MHz) and ¹³C NMR (100 MHz) spectra of **2i** (CDCl₃)
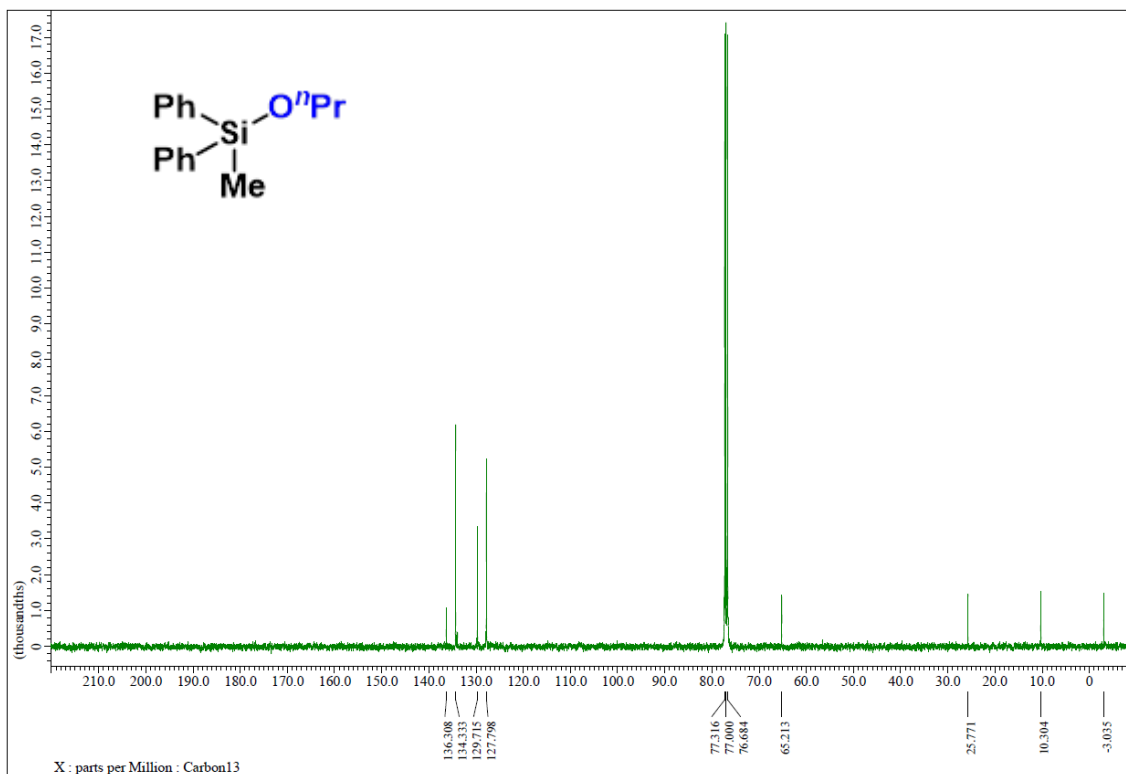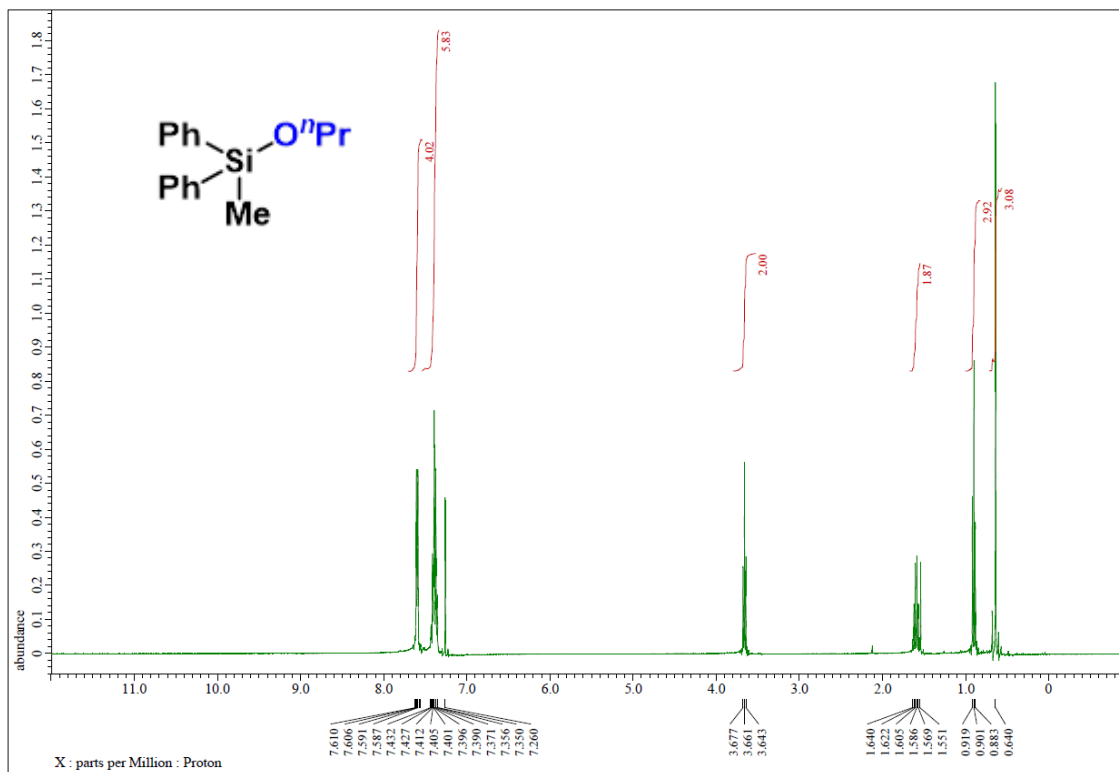
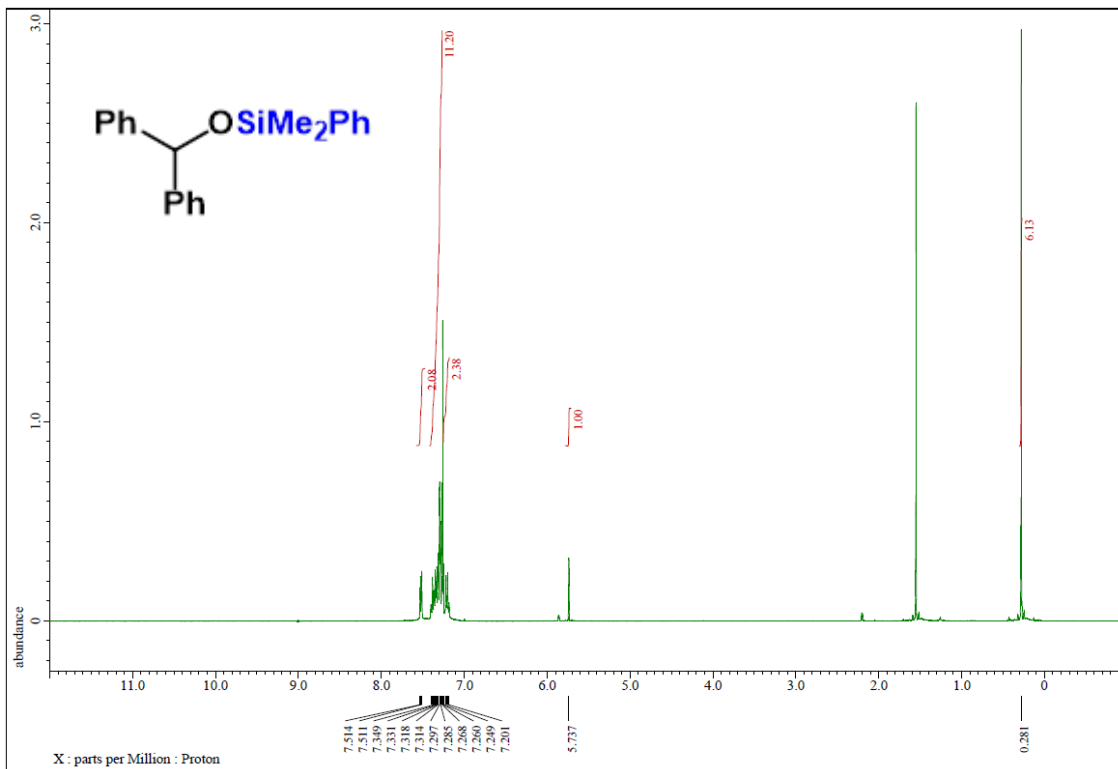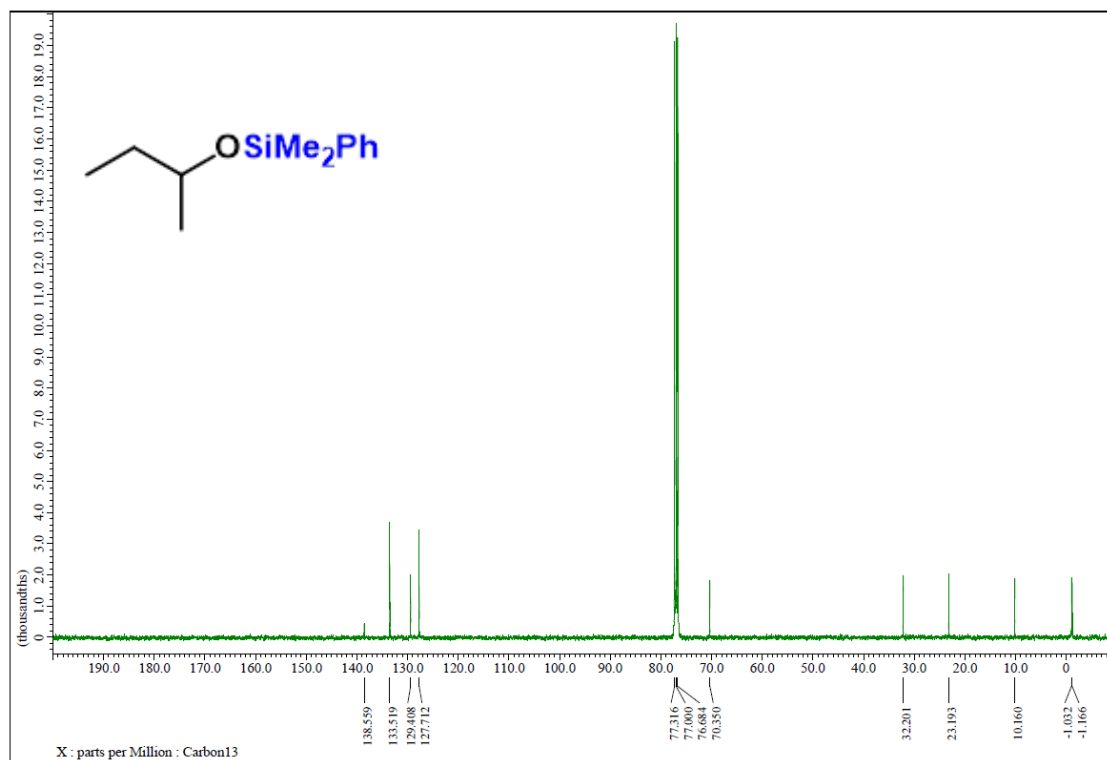¹H NMR (400 MHz) and ¹³C NMR (100 MHz) spectra of **2j** (CDCl₃)
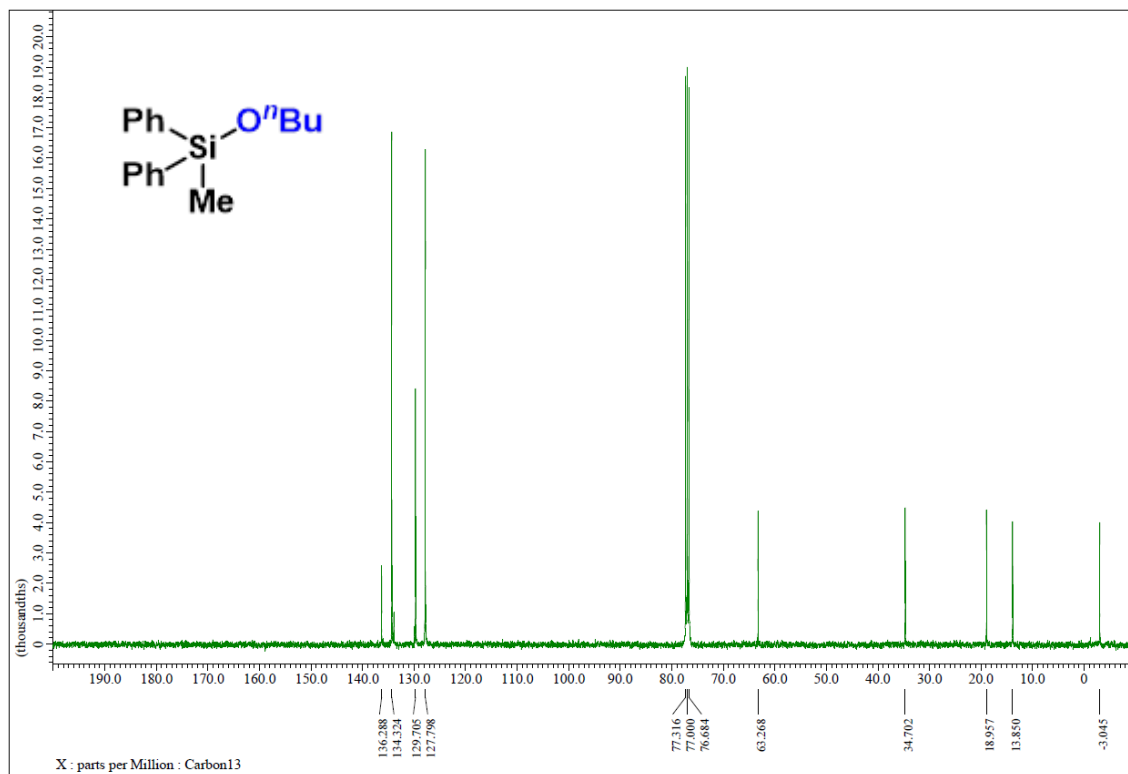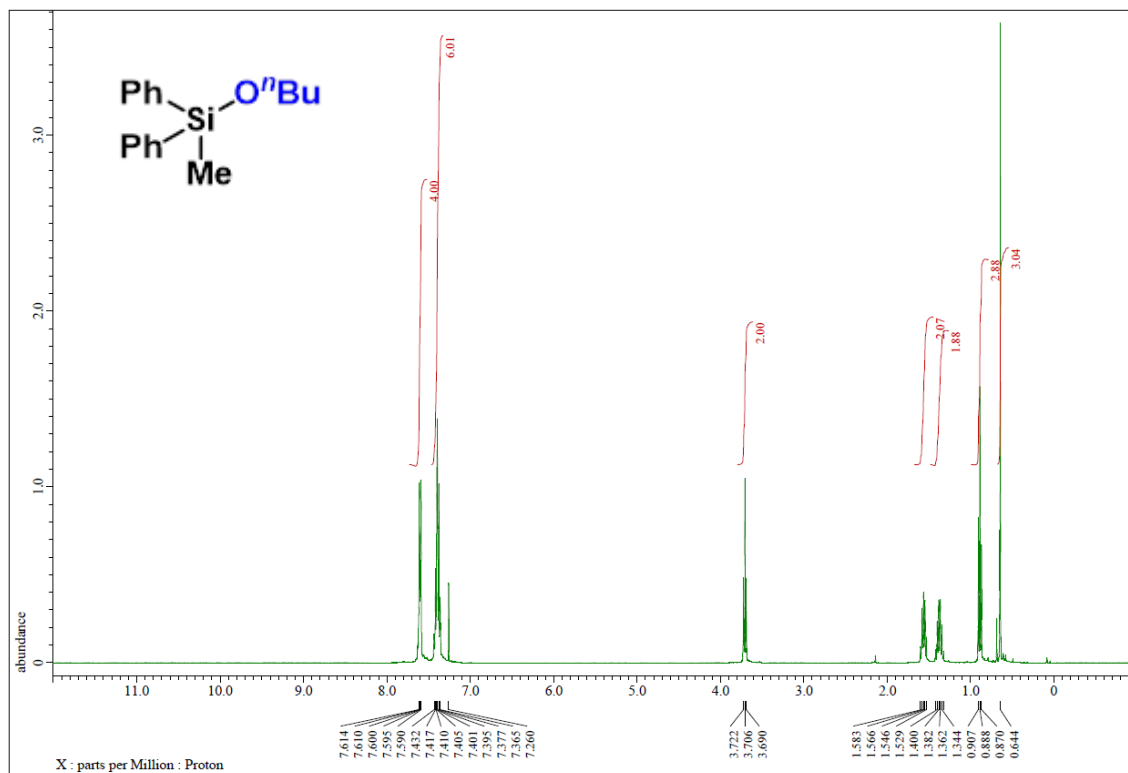
118
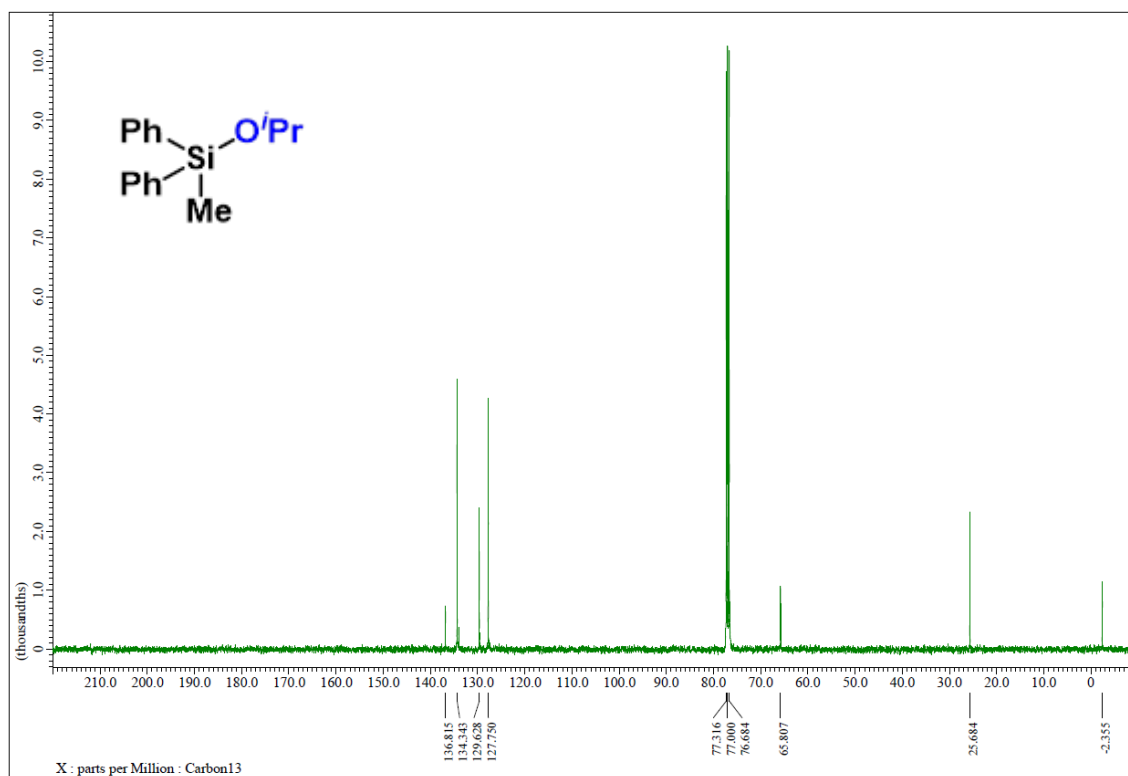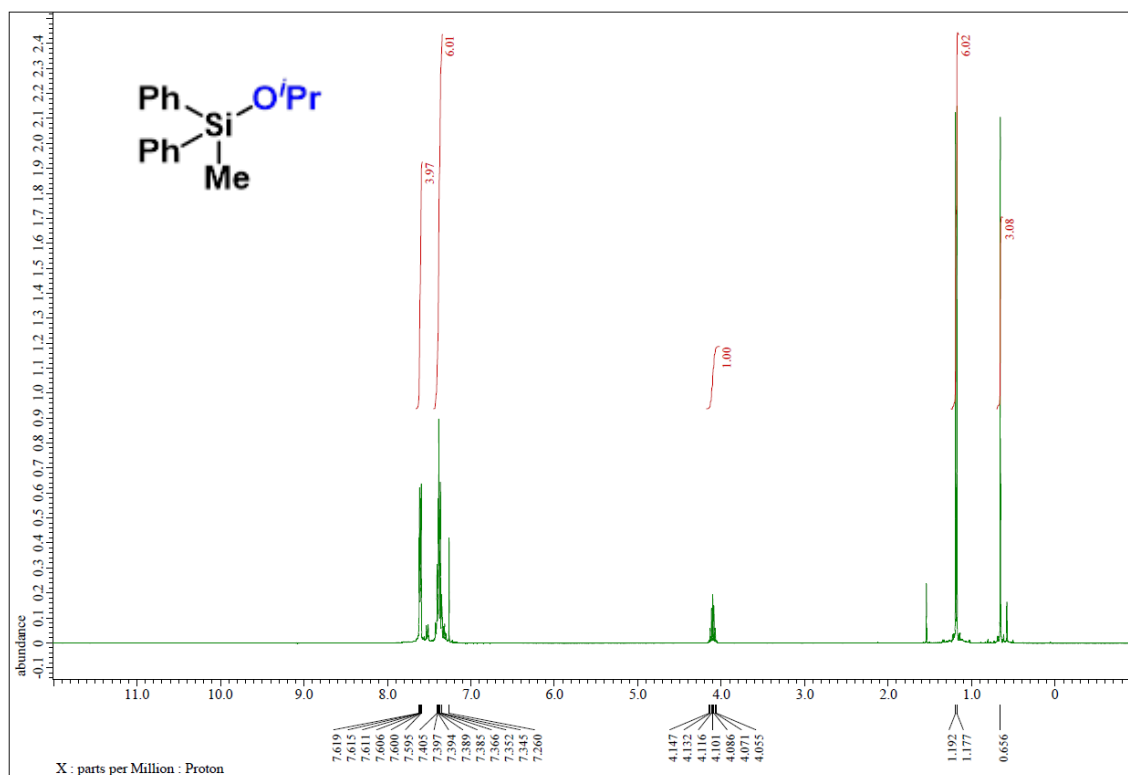
¹H NMR (400 MHz) and ¹³C NMR (100 MHz) spectra of **2m** (CDCl₃
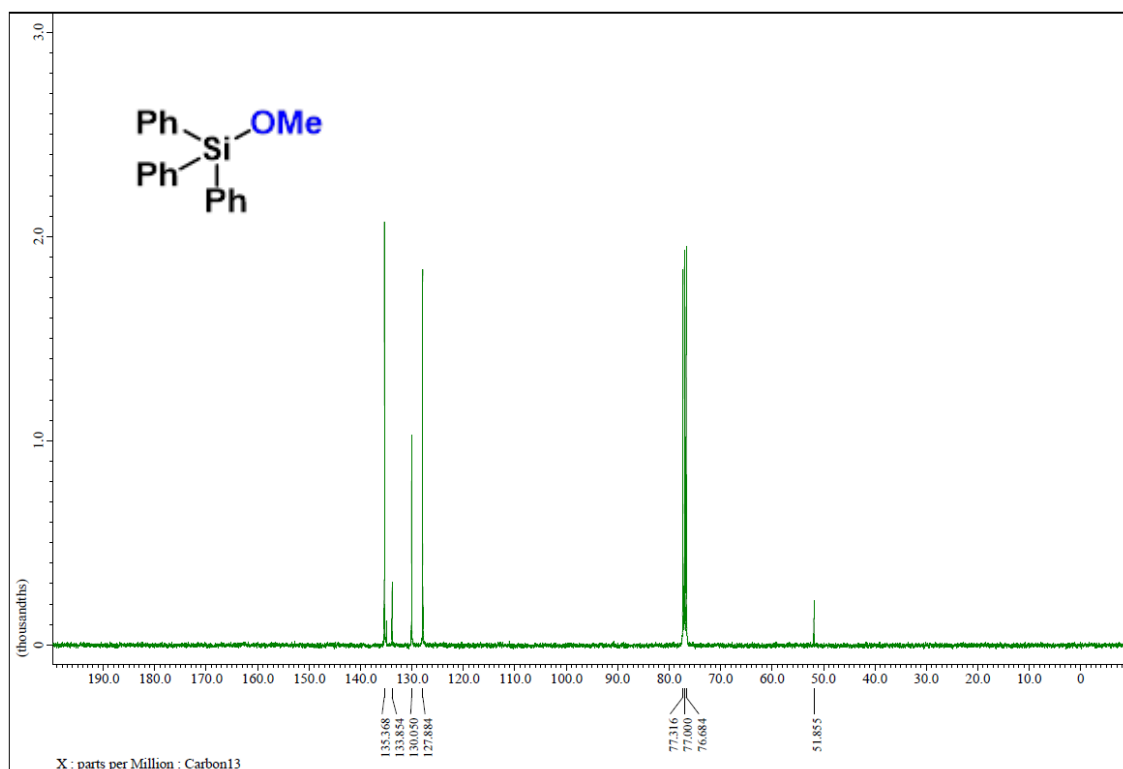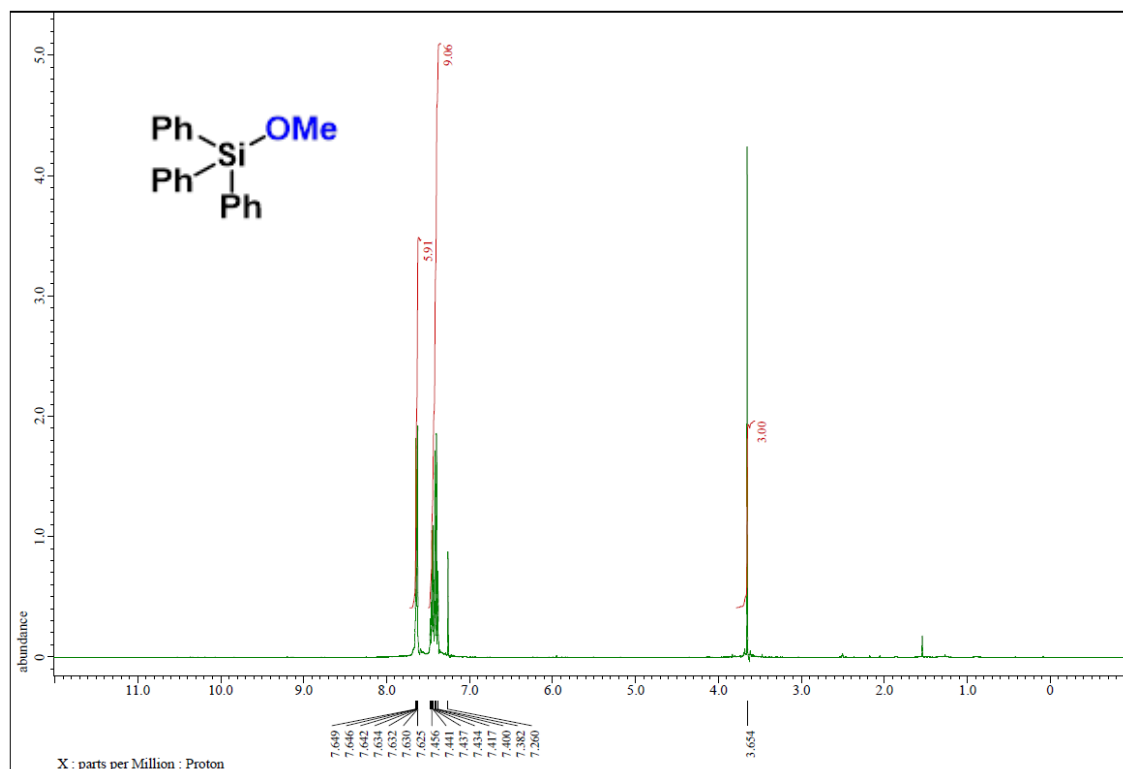
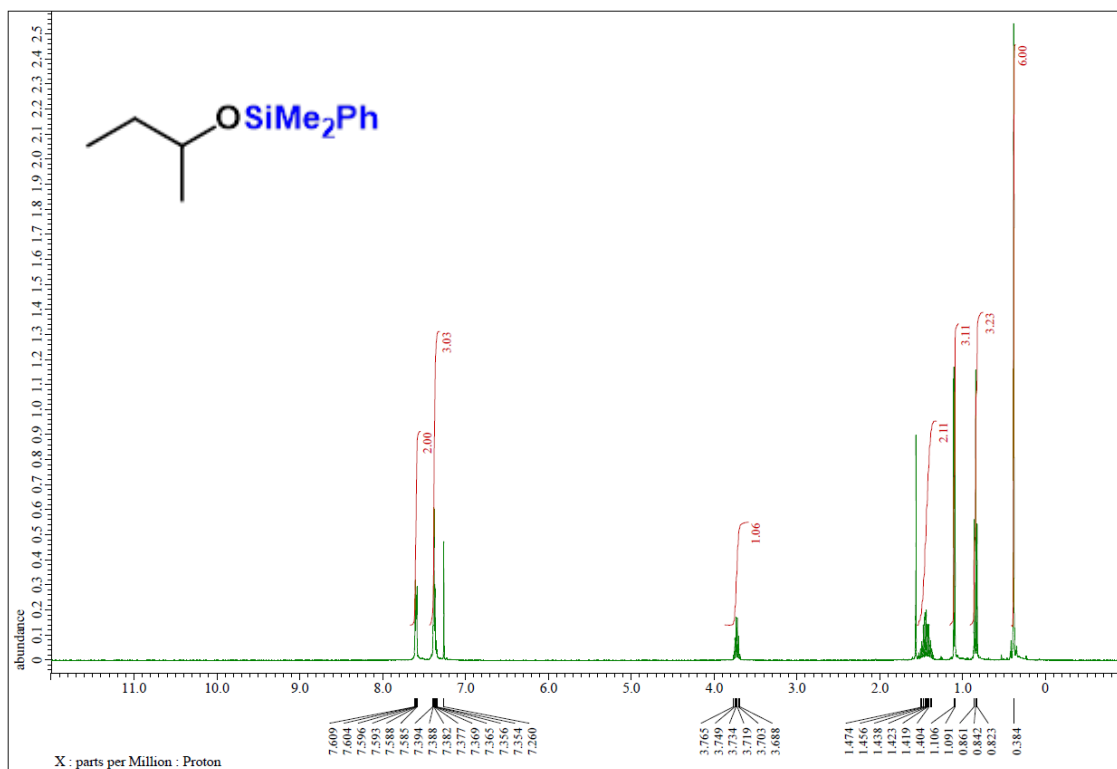¹H NMR (400 MHz) and ¹³C NMR (100 MHz) spectra of **2n** (CDCl₃)
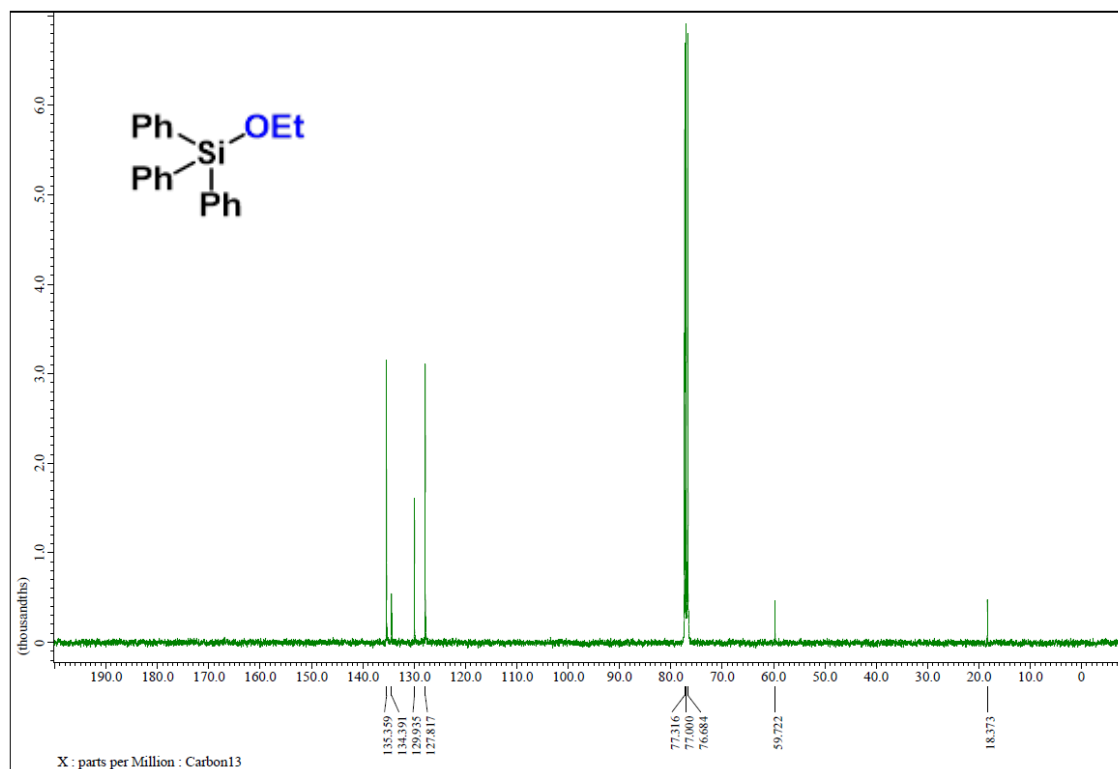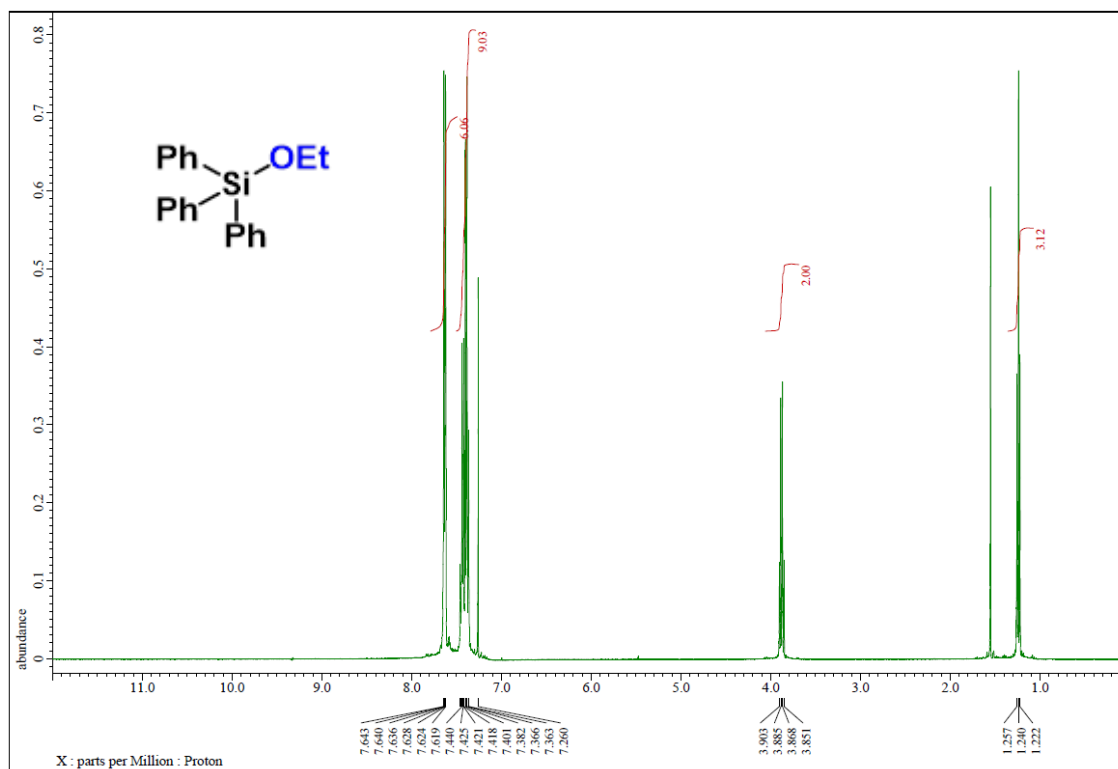
¹H NMR (400 MHz) and ¹³C NMR (100 MHz) spectra of **4a** (CDCl₃)
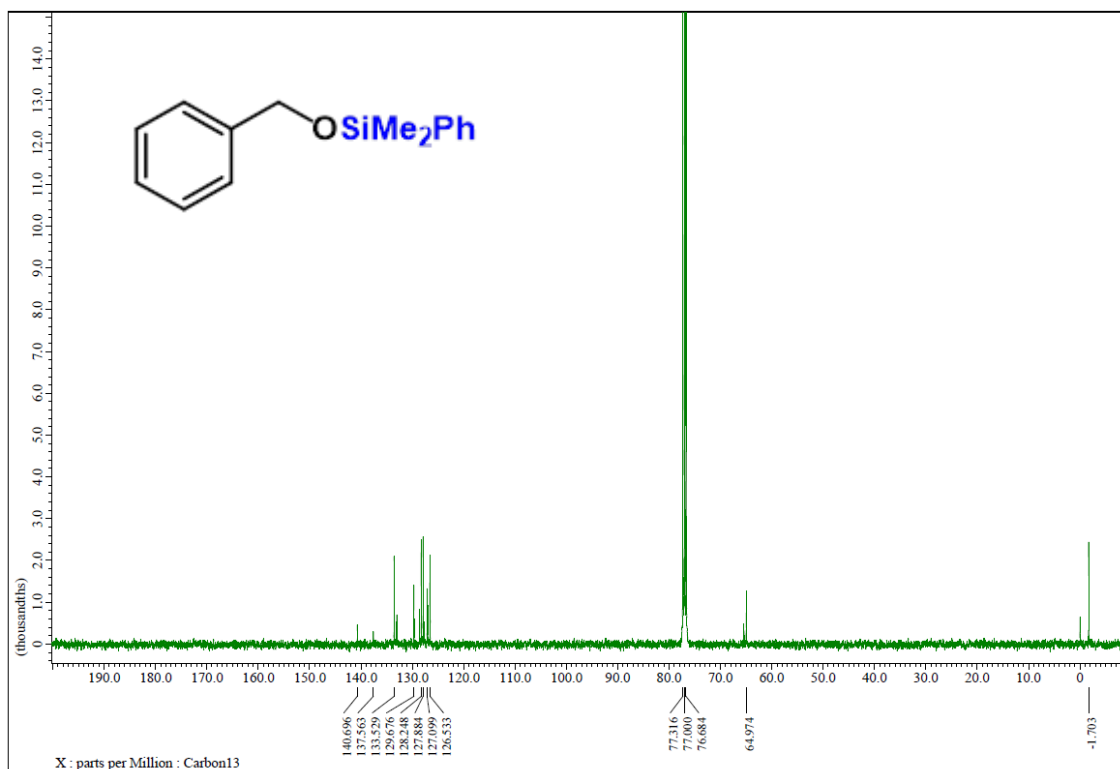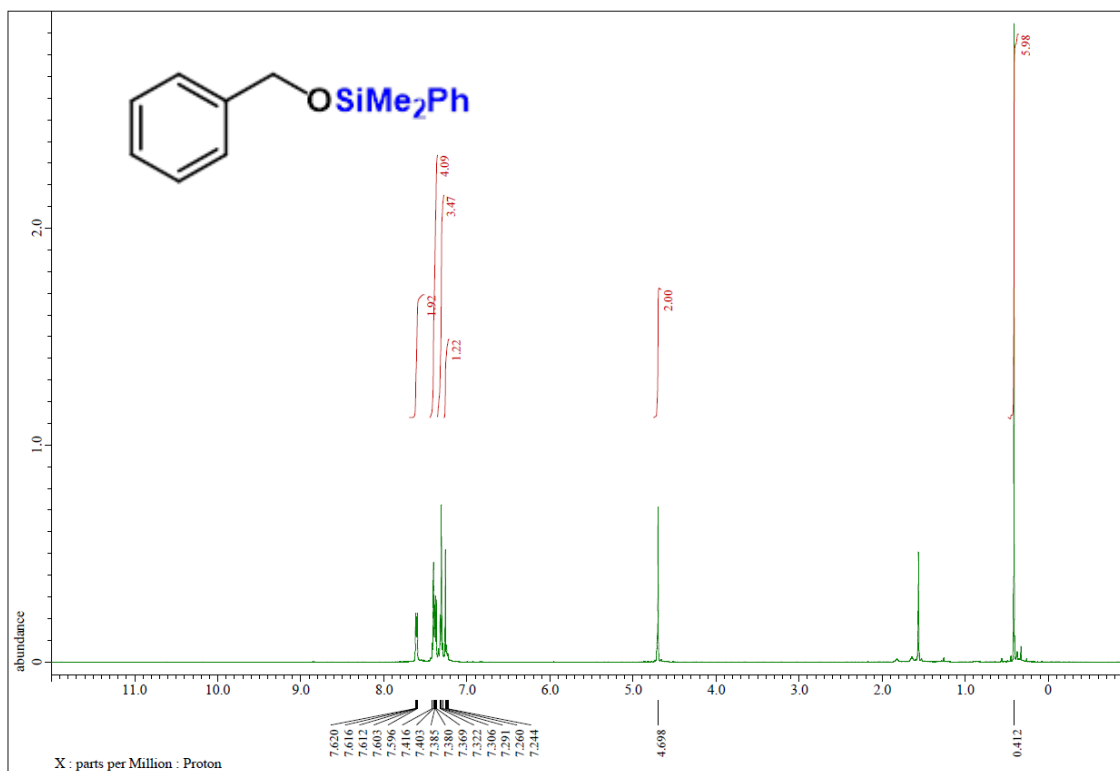
^{1}H NMR (400 MHz) and ^{13}C NMR (100 MHz) spectra of **4b** (CDCl$_3$)
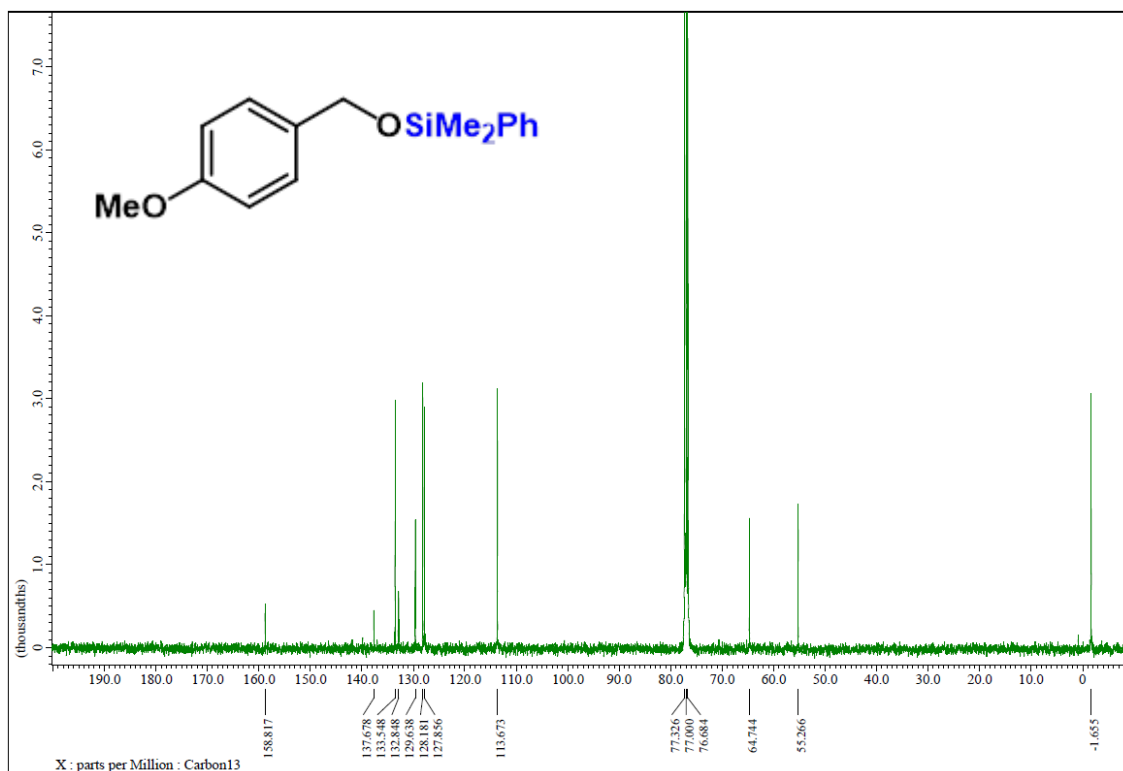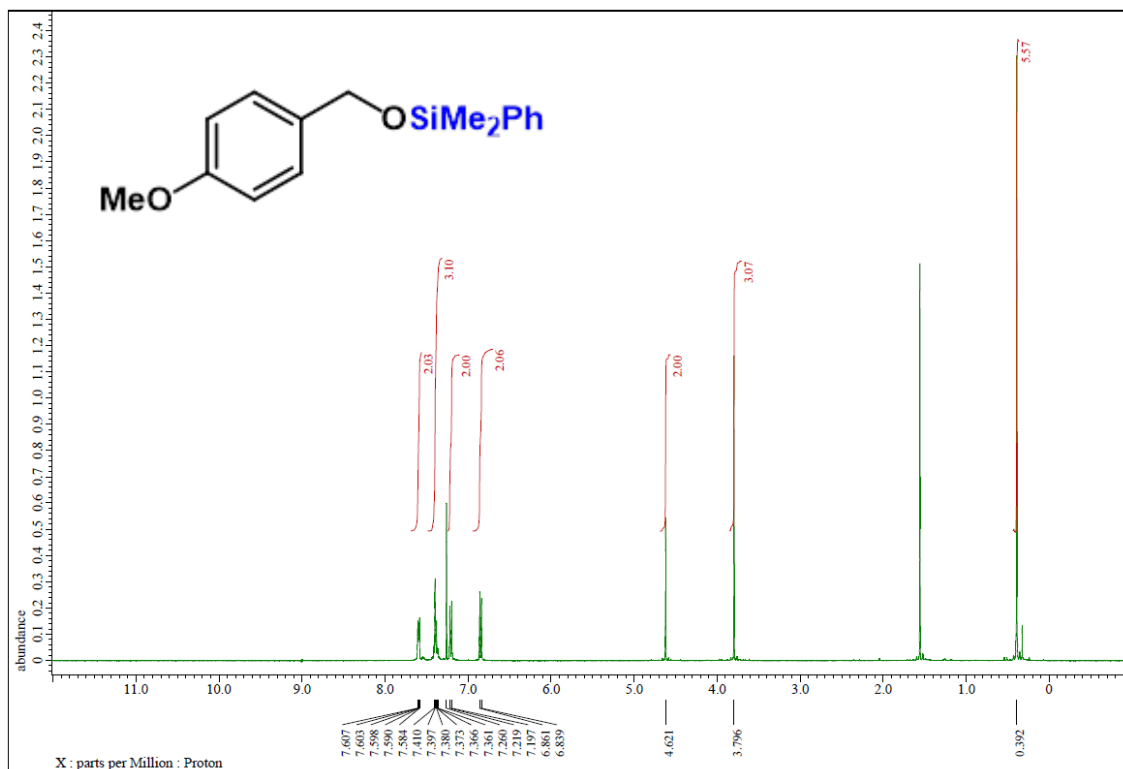
¹H NMR (400 MHz) and ¹³C NMR (100 MHz) spectra of **4c** (CDCl₃)

124
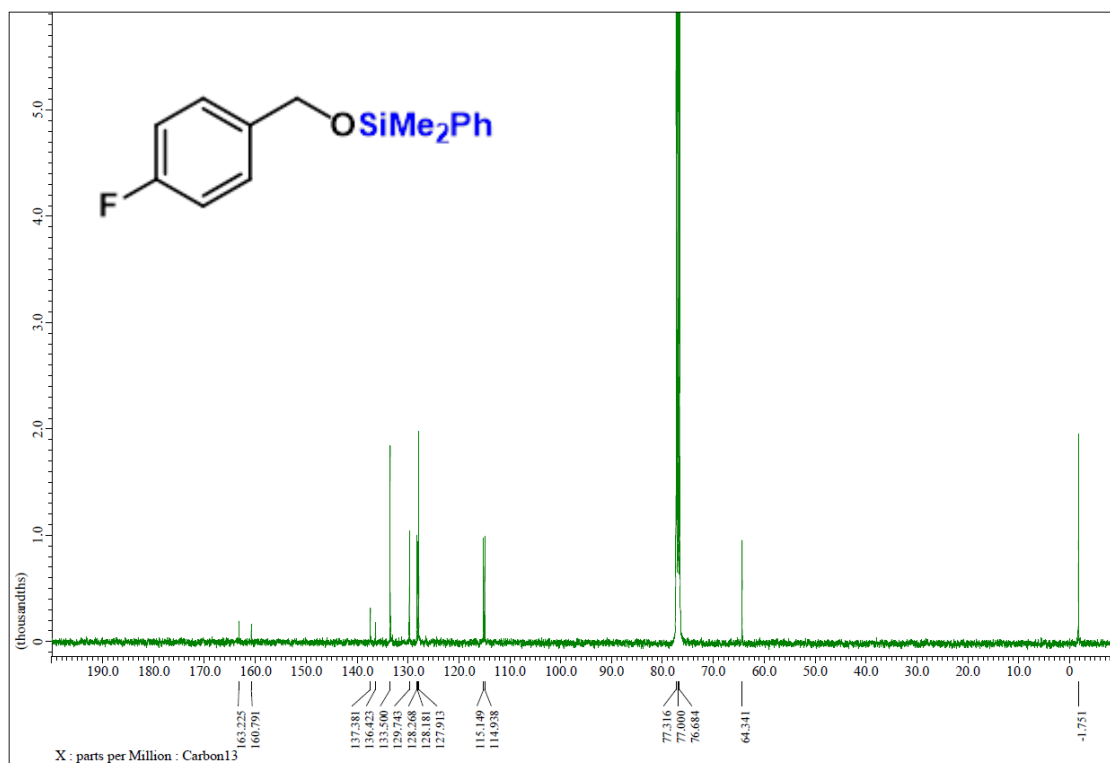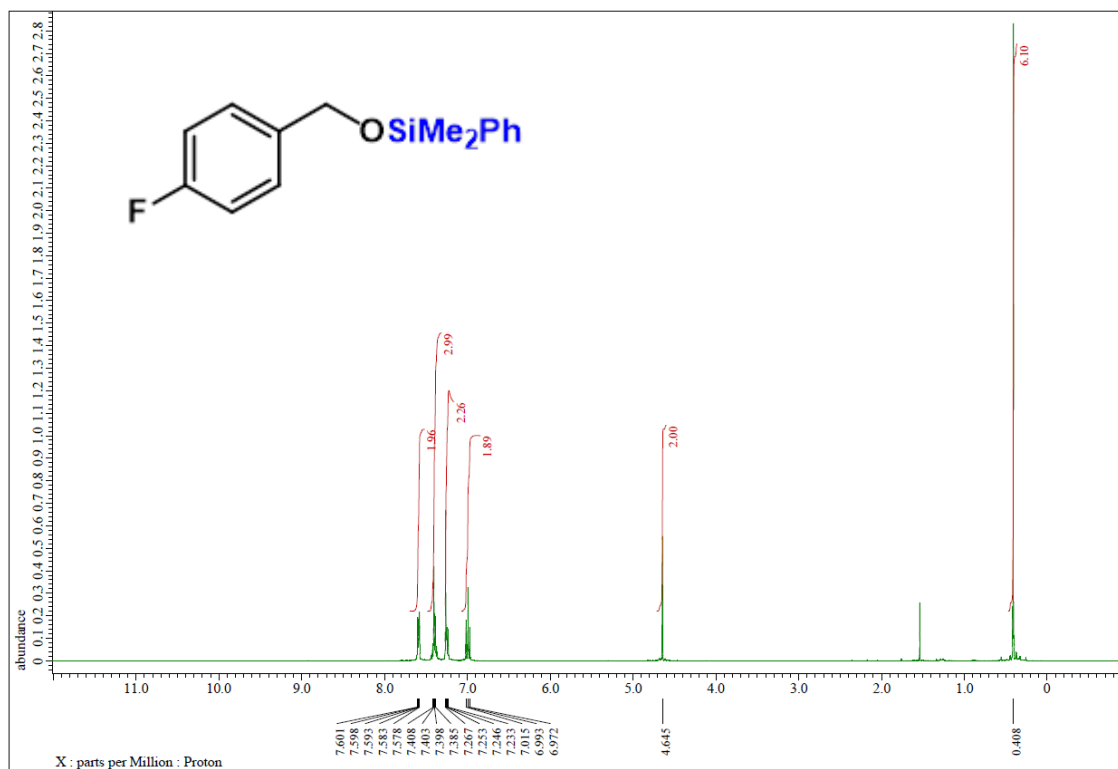
^{1}H NMR (400 MHz) and ^{13}C NMR (100 MHz) spectra of **4d** (CDCl$_3$)
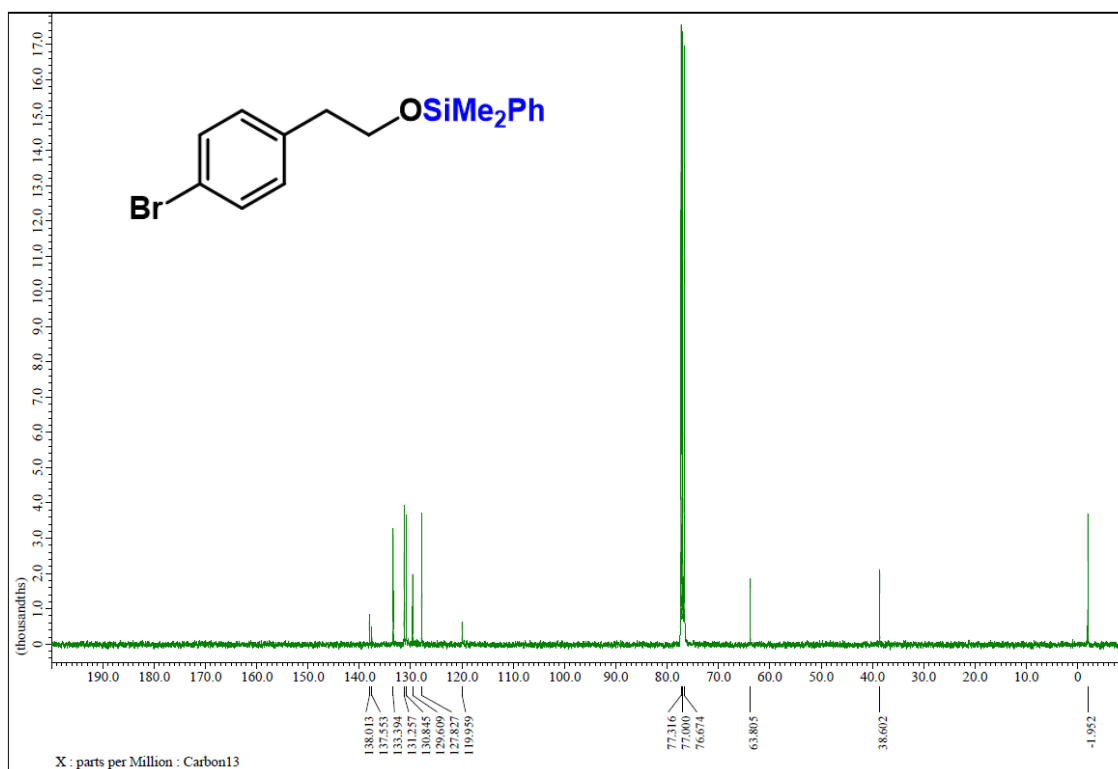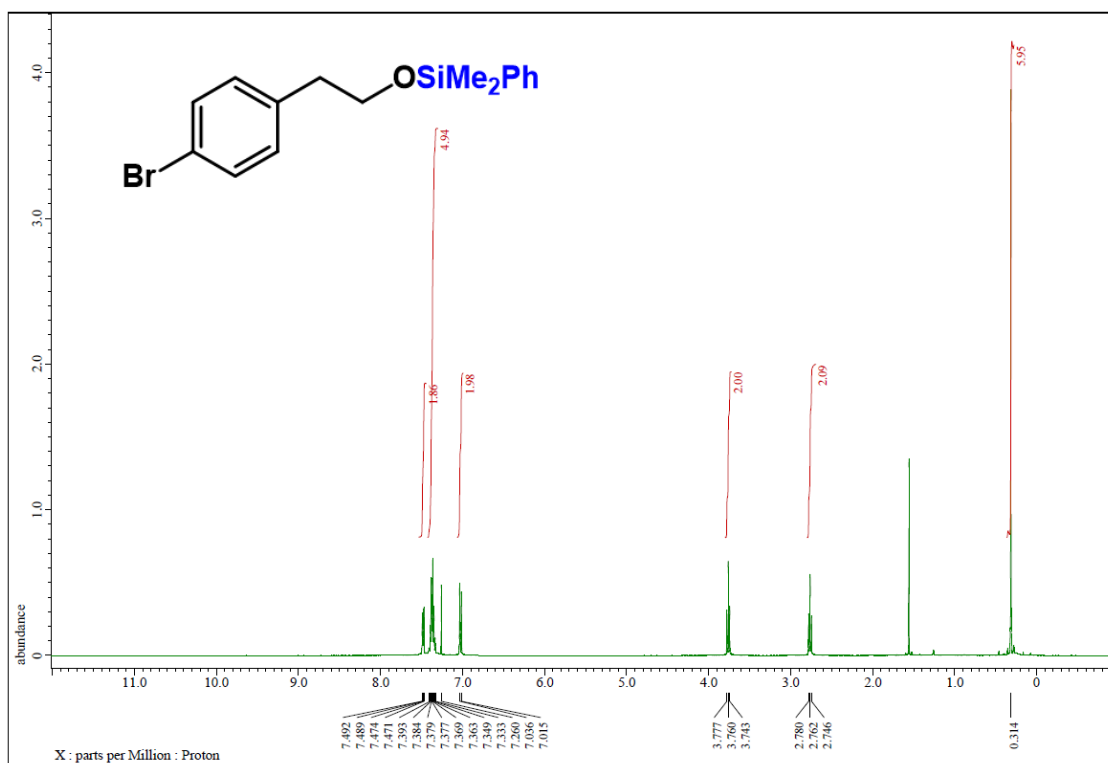
¹H NMR (400 MHz) and ¹³C NMR (100 MHz) spectra of **4e** (CDCl₃)
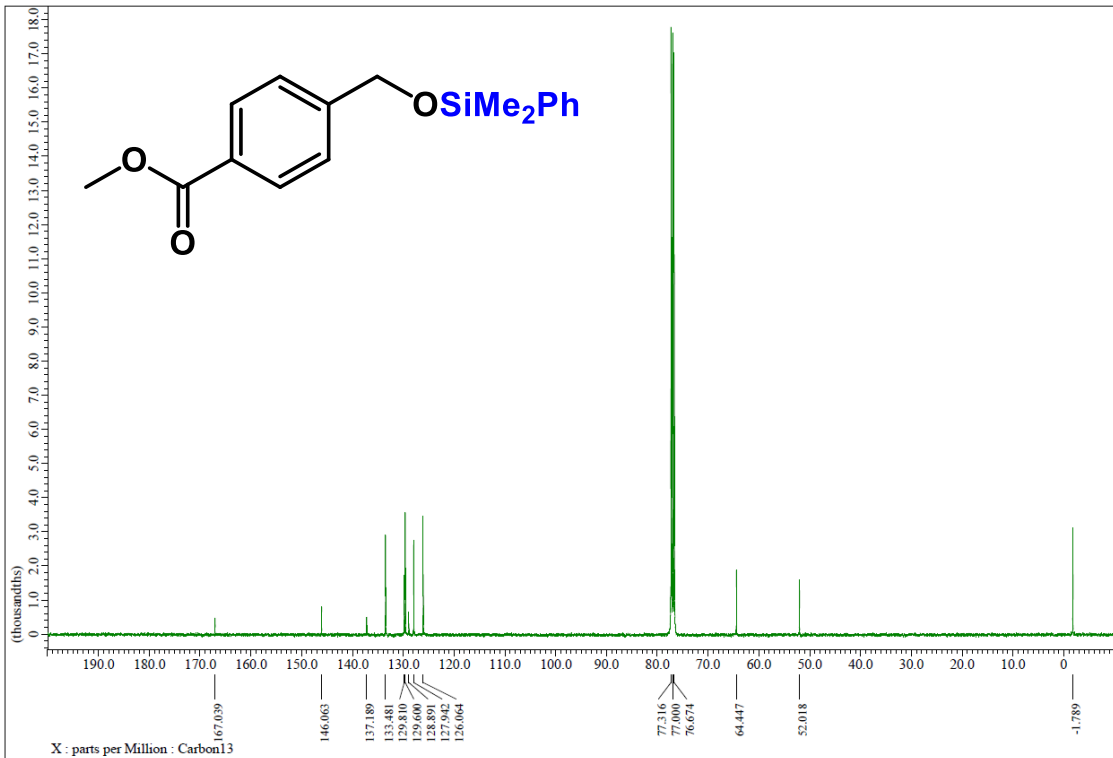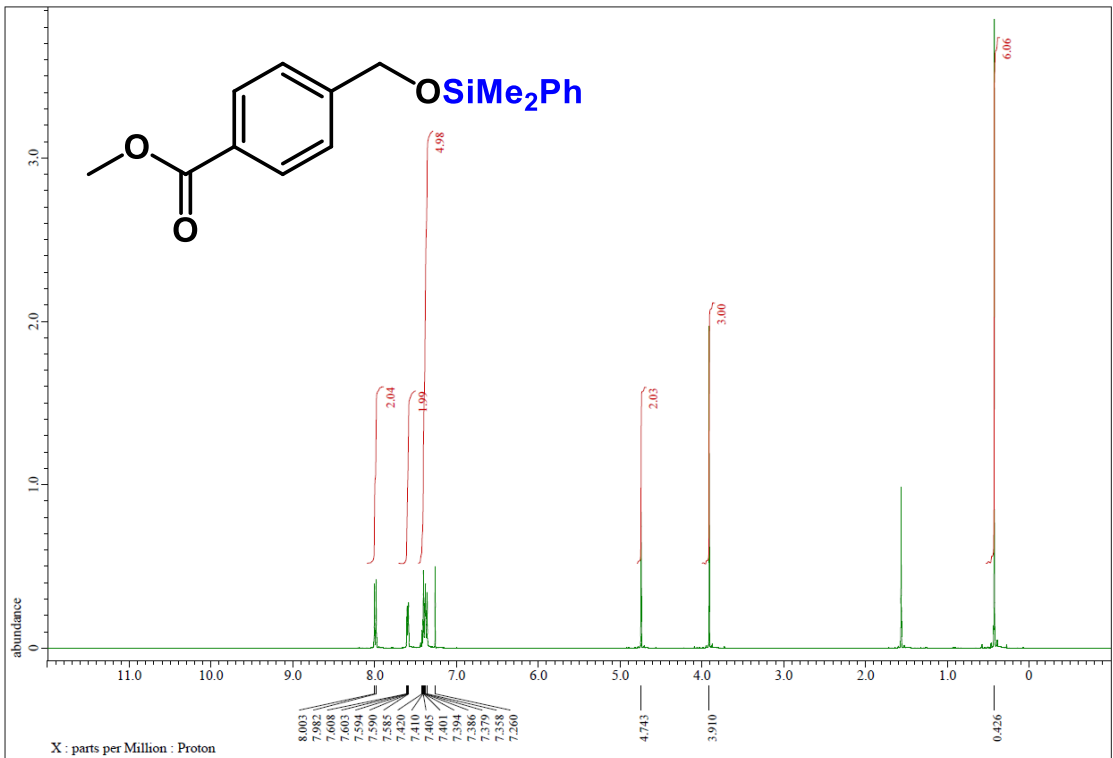
¹H NMR (400 MHz) and ¹³C NMR (100 MHz) spectra of **4f** (CDCl₃)
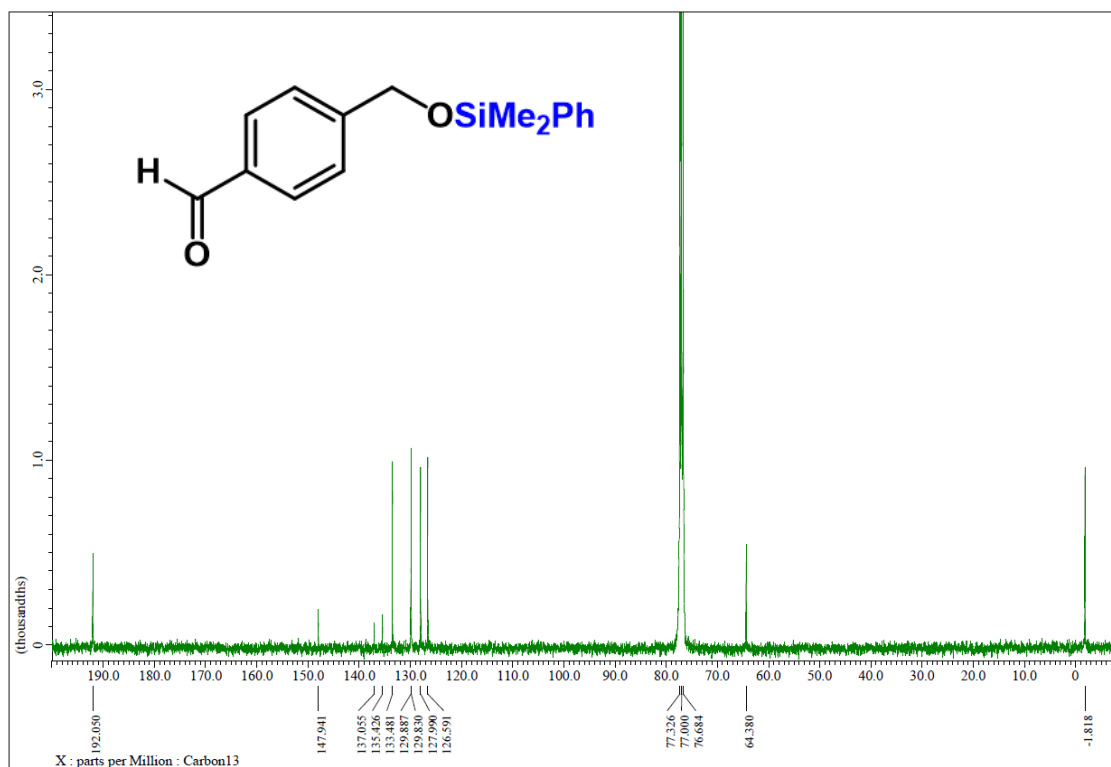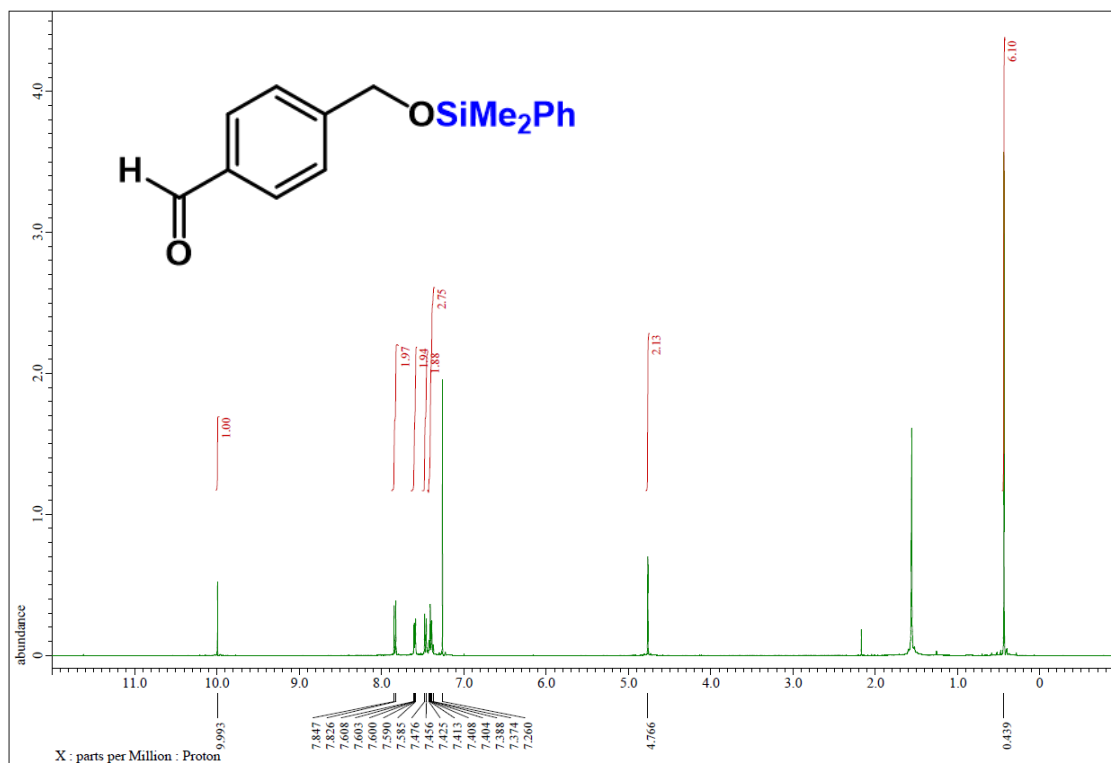
^{1}H NMR (400 MHz) and ^{13}C NMR (100 MHz) spectra of **4f** (CDCl₃)
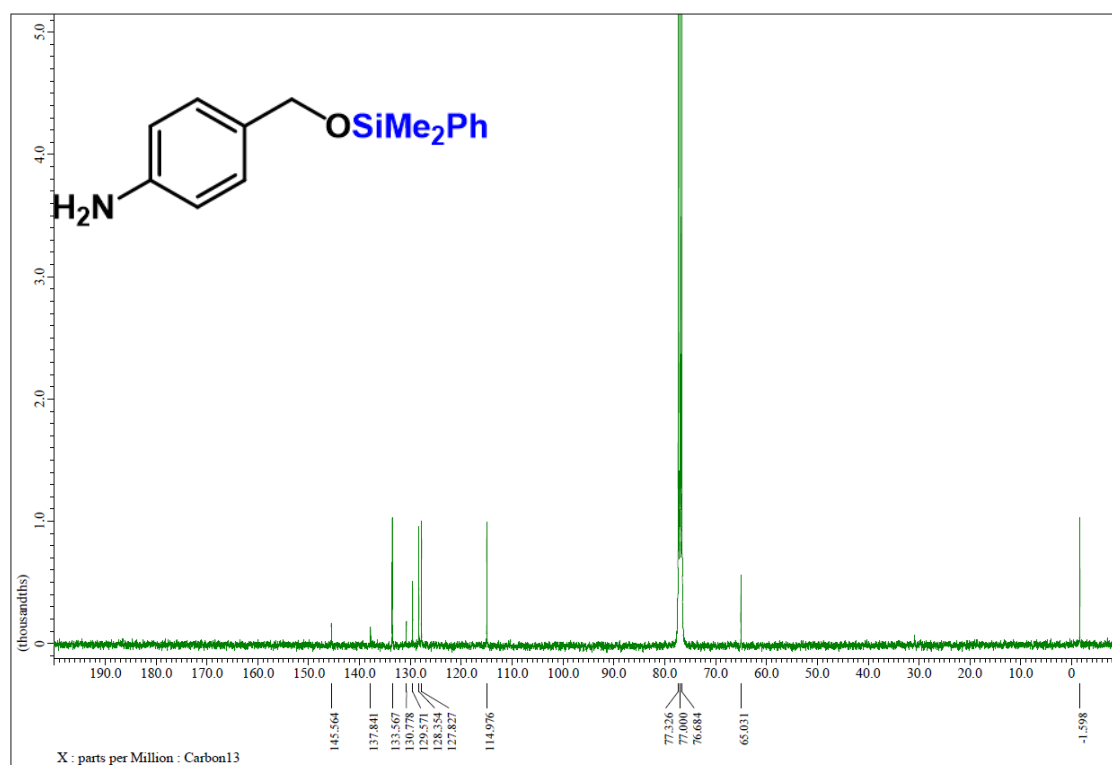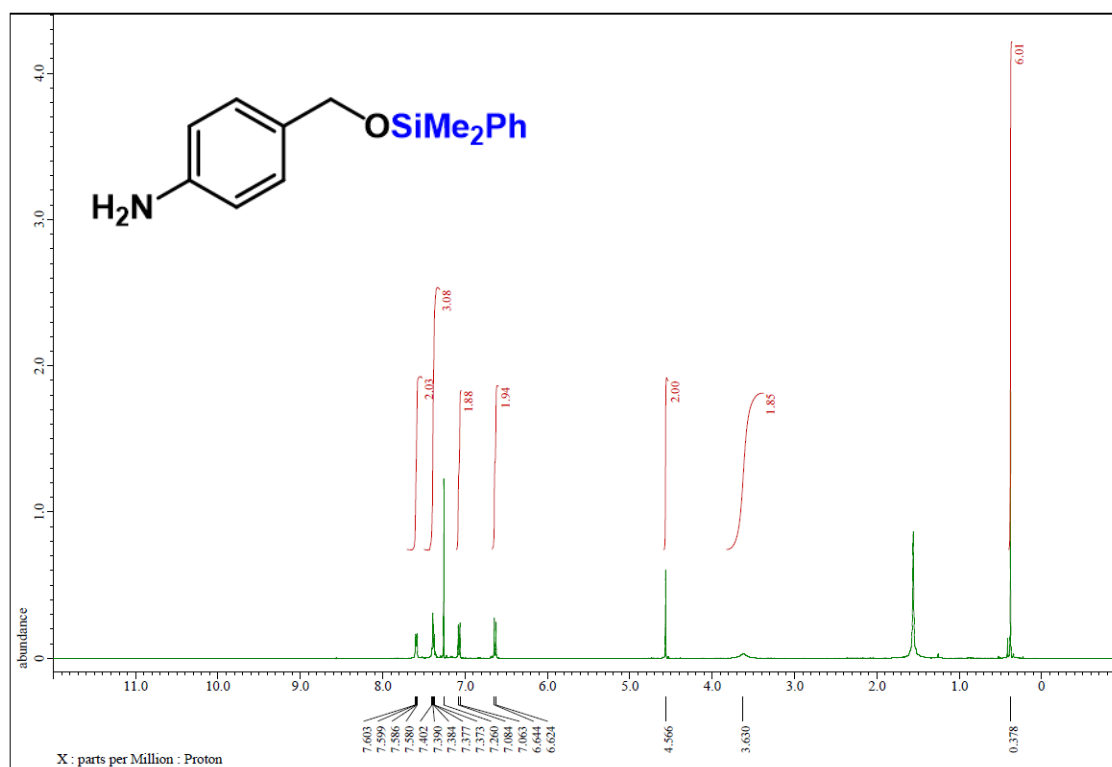
¹H NMR (400 MHz) and ¹³C NMR (100 MHz) spectra of **4h** (CDCl₃)
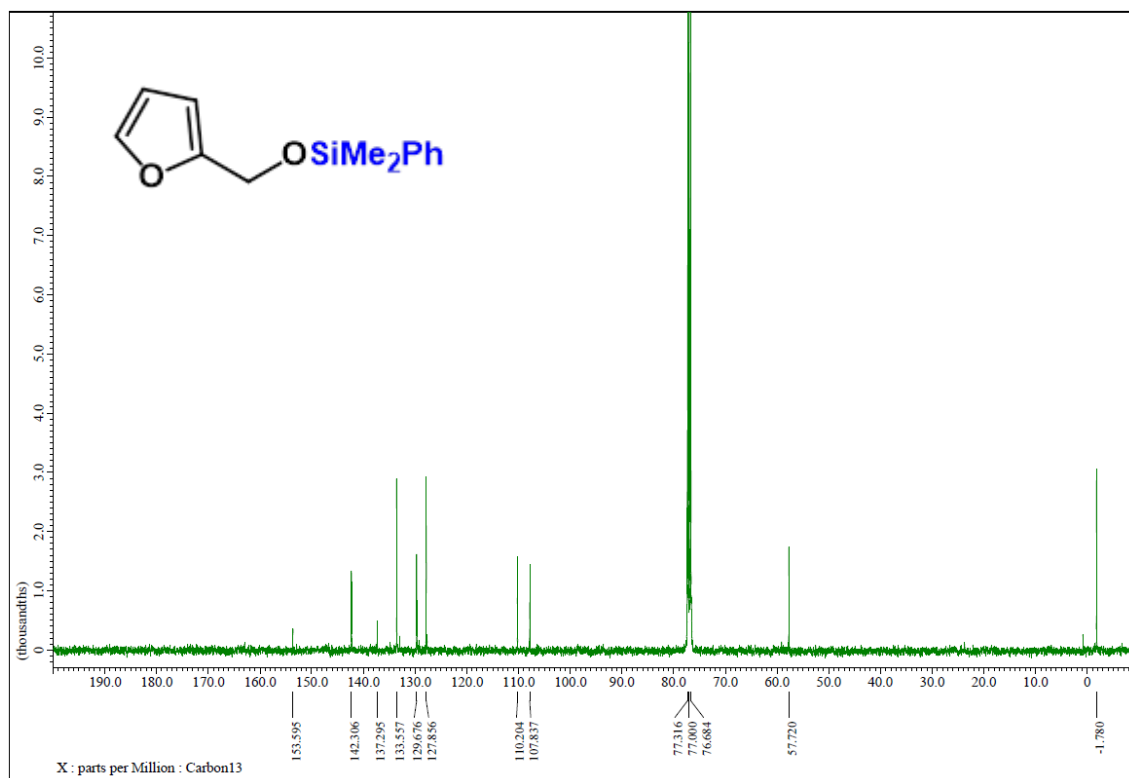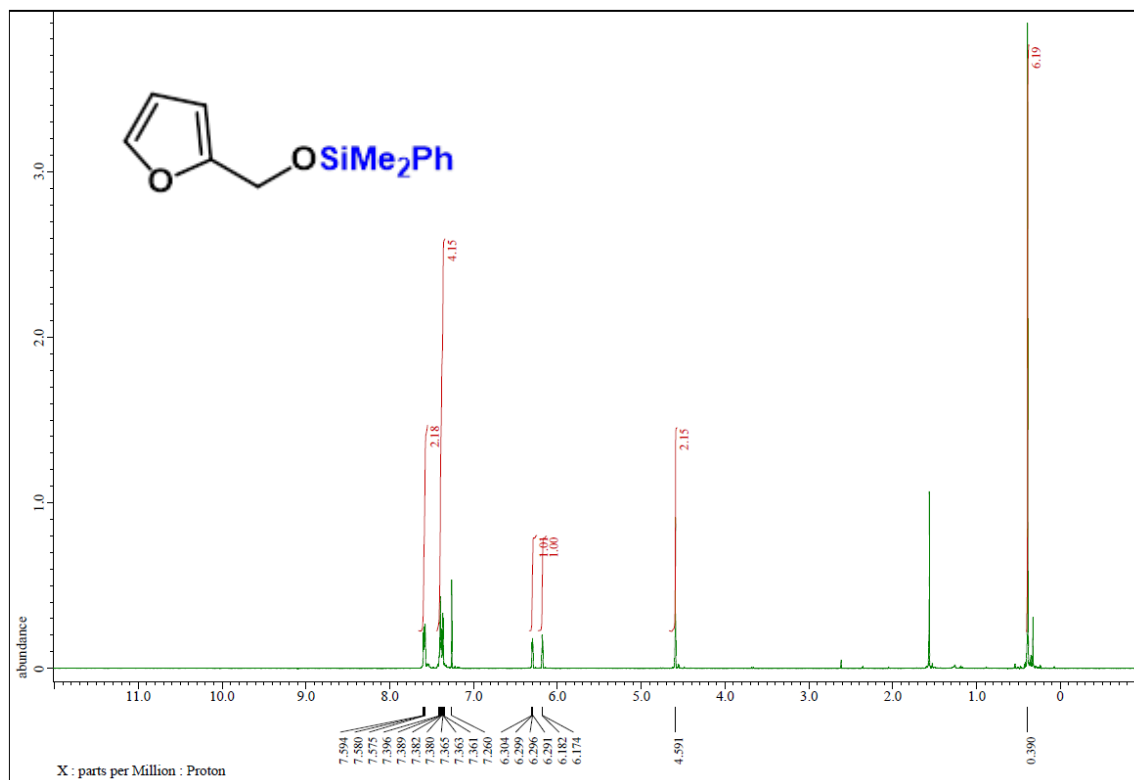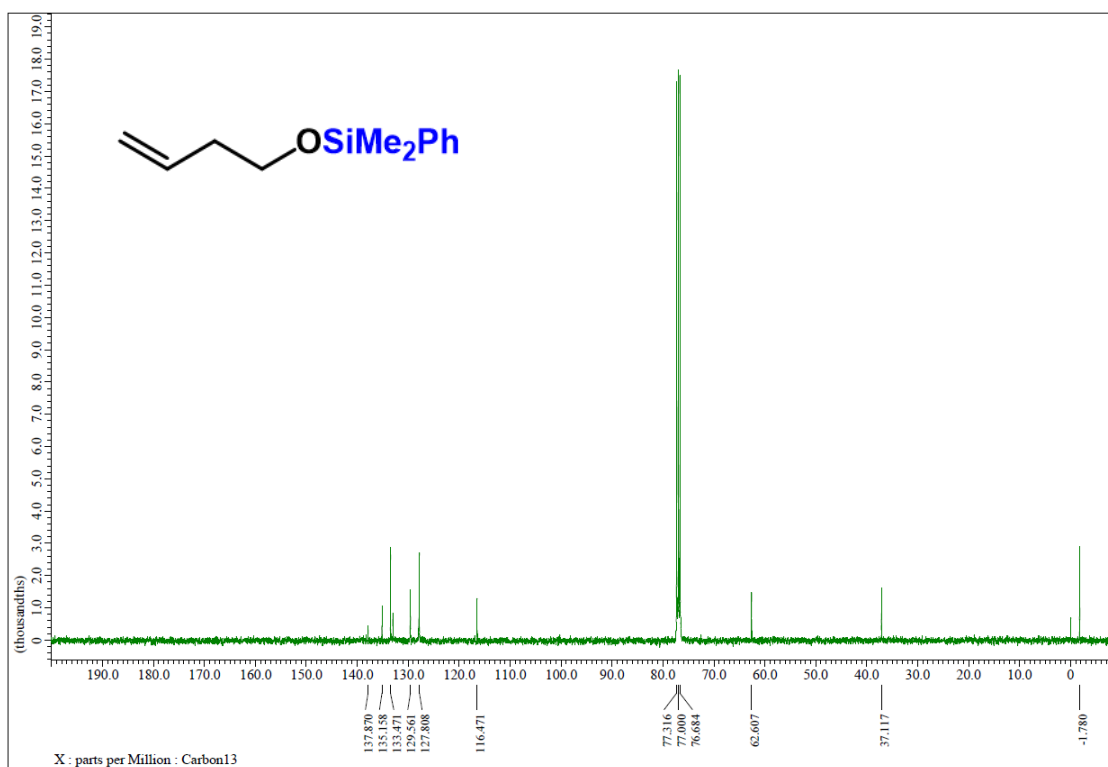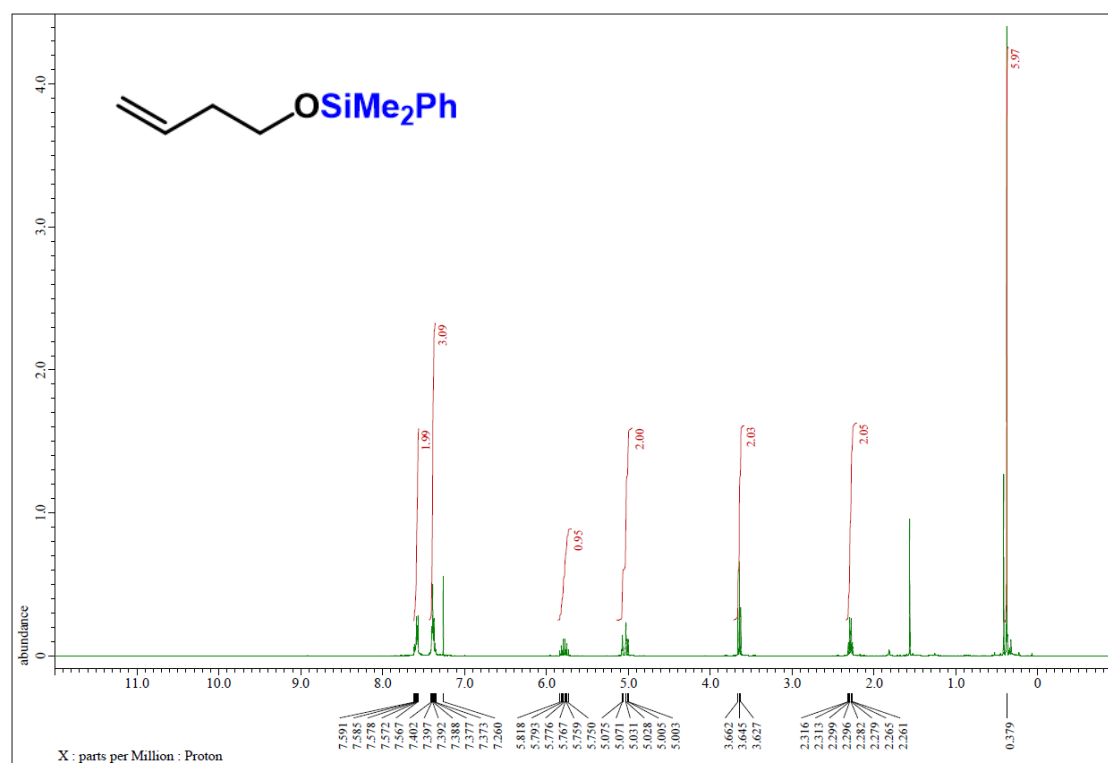
¹H NMR (400 MHz) and ¹³C NMR (100 MHz) spectra of **4j** (CDCl₃)

¹H NMR (400 MHz) and ¹³C NMR (100 MHz) spectra of **4k** (CDCl₃)

^{1}H NMR (400 MHz) and ^{13}C NMR (100 MHz) spectra of **4l** (CDCl₃)

¹H NMR (400 MHz) and ¹³C NMR (100 MHz) spectra of **4m** (CDCl₃)

<superscript>1</superscript>H NMR (400 MHz) and <superscript>13</superscript>C NMR (100 MHz) spectra of **4n** (CDCl<subscript>3</subscript>)

H NMR (400 MHz) and ^{13}C NMR (100 MHz) spectra of **4o** (CDCl$_3$)
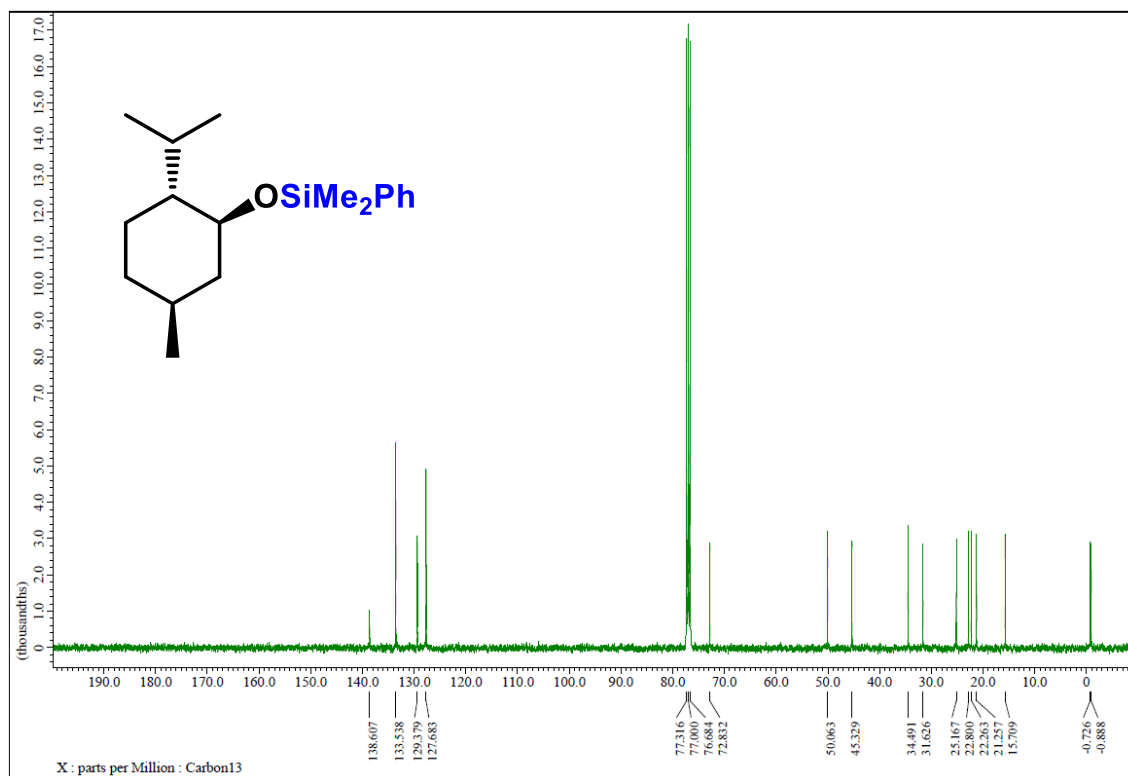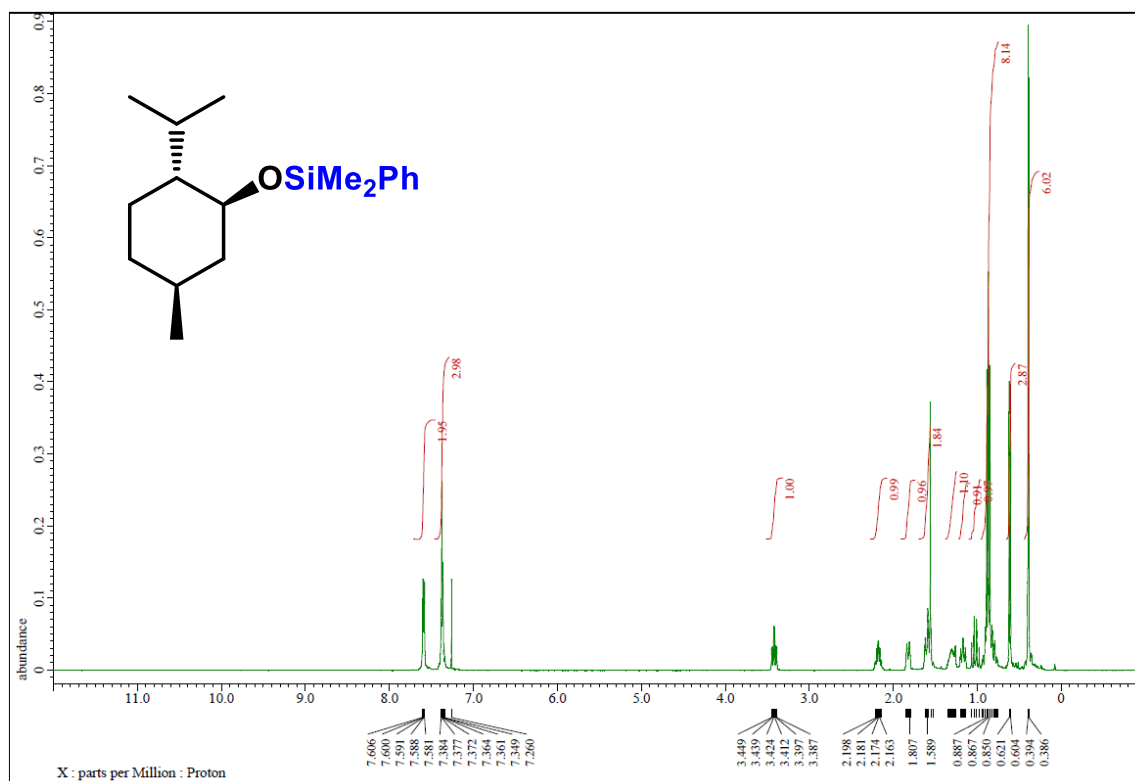
4.5 References

1. (a) J. Pietrasik, M. Zaborski, *Polym. Int.* **2005**, *54*, 1119. (b) M. C. Parrott, J. C. Luft, J. D. Byrne, J. H. Fain, M. E. Napier, J. M. Desimone, *J. Am. Chem. Soc.* **2010**, *132*, 17928. (c) K. Karki, A. Materny, D. Roccatano, *J. Appl. Polym. Sci.* **2011**, *13*, 11864.

2. T. W. Greene, P. G. M. Wuts, Protective groups in organic synthesis, third ed.; John Wiley & Sons: New York, 1991.

3. (a) E. Lukevics, M. Dzintara, *J. Organomet. Chem.* **1985**, *295*, 265. (b) B. Hatano, S. Toyota, F. Toda, *Green Chem.* **2001**, *3*, 140.

4. (a) W. Caseri, P. S. Pregosin, *Organometallics* **1988**, *7*, 1373. (b) H. Ito, K. Takagi, T. Miyahara, M. Sawamura, *Org. Lett.* **2005**, *7*, 3001. (c) X. Dong, A. Weickgenannt, M. Oestreich, *Nat. Commun.* **2017**, *8*, 15547. (d) M. Sridhar, J. Raveendra, B. C. Ramanaiah, C. Narsaiah, *Tetrahedron Lett.* **2011**, *52*, 5980.

5. (a) K. Hara, R. Akiyama, S. Takakusagi, K. Uosaki, T. Yoshino, H. Kagi, M. Sawamura, *Angew. Chem., Int. Ed.* **2008**, *47*, 5627. (b) J. F. Blandez, A. Primo, M. Alvaro, H. Garcia, *Angew. Chem., Int. Ed.* **2014**, *53*, 12581. (c) P. Raffa, C. Evangelisti, G. Vitulli, P. Salvadori, *Tetrahedron Lett.* **2008**, *49*, 3221. (d) Z. Li, C. Zhang, J. Tian, Z. Zhang, X. Zhang, Y. Ding, *Catal. Commun.* **2014**, *53*, 53. (e) Z. Li, S. Lin, L. Ji, Z. Zhang, X. Zhang, Y. Ding, *Catal. Sci. Technol.* **2014**, *4*, 1734.

6. R. J. White, R. Luque, V. L. Budarin, J. H. Clark, D. J. Macquarrie, *Chem. Soc. Rev.* **2009**, *38*, 481.

7. Q. Zhang, M. Peng, Z. Gao, W. Guo, Z. Sun, Y. Zhao, W. Zhou, M. Wang, B. Mei, X.-L. Du, Z. Jiang, W. Sun, C. Liu, Y. Zhu, Y.-M. Liu, H.-Y. He, Z.-H. Li, D. Ma, Y. Cao, *J. Am. Chem. Soc.* **2023**, *145*, 4166.

8. (a) T. Taguchi, K. Isozaki, K. Miki, *Adv. Mater.* **2012**, *24*, 6462. (b) T. Mitsudome, Y. Yamamoto, A. Noujima, T. Mizugaki, K. Jitsukawa, K. Kaneda, *Chem. Eur. J.* **2013**, *19*, 14398. (c) C. Wang, X. Lin, Y. Ge, Z. H. Shah, R. Lu, S. Zhang, *RSC Adv.* **2016**, *6*, 102102. (d) R. G. Kadam, M. Medved', S. Kumar, D. Zaoralová, Z. Zoppellaro, Z. Bad'ura, T. Montini, A. Bakandritsos, E. Fonda, O. Tomanec, M. Otyepka, R. S. Varma, M. B. Gawande, P. Fornasiero, R. Zbořil, *ACS Catal.* **2023**, *13*, 16067.

9. (a) T. Chutimasakul, Y. Uetake, J. Tantirungrotechai, T. Asoh, H. Uyama, H. Sakurai, *ACS Omega* **2020**, *5*, 33206. (b) Y. Uetake, B. Suwattananuruk, H. Sakurai, *Sci. Rep.* **2022**, *12*, 20602. (c) B. Suwattananuruk, Y. Uetake, R. Ichikawa, R. Toyoshima, H. Kondoh, H. Sakurai, *Nanoscale* **2024**, *16*, 12474.

10. (a) X. Cui, A. Ozaki, T. A. Asoh, H. Uyama, *Polym. Degrad. Stab.* **2020**, *175*, 109118. (b) X. Cui, T. Honda, T. A. Asoh, H. Uyama, *Carbohydr. Polym.* **2020**, *230*, 115662.

11. R. Gupta, S. Paul, R. Gupta, *J. Mol. Catal.* **2007**, *266*, 50.

12. (a) T. Mitsudome, A. Noujima, T. Mizugaki, K. Jitsukawa, K. Kaneda, *Chem. Commun.* **2009**, 5302. (b) K. Bobuatong, H. Sakurai, M. Ehara, *ChemCatChem* **2017**, *9*, 4450. (c) M. Boronat, A. Leyva-Pérez, A. Corma, *Acc. Chem. Res.* **2014**, *47*, 834. (d) S. Yamazoe, K. Koyasu, T. Tsukuda, *Acc. Chem. Res.* **2014**, *47*, 816. (e) M. Stratakis, H. Garcia, *Chem. Rev.* **2012**, *112*, 4469.

13. A. G. M. da Silva, C. M. Kisukuri, T. S. Rodrigues, E. G. Candido, I. C. de Freitas, A. H. M. da Silva, J. M. Assaf, D. C. Oliveira, L. H. Andrade, P. H. C. Camargo, *Appl. Catal. B* **2016**, *184*, 35.

14. R. González-Fernández, P. Crochet, V. Cadierno, *Dalton Trans.* **2020**, *49*, 210.

15. Y. R. Jorapur, T. Shimada, *Synlett* **2012**, *23*, 1064.

16. Y.-q. Yuan, P. S. Kumar, S.-r. Guo, *Synlett* **2017**, *28*, 1620.

17. H. Lv, R. D. Laishram, J. Chen, R. Khan, Y. Zhu, S. Wu, J. Zhang, X. Liu, B. Fan, *Chem. Commun.* **2021**, *57*, 3660.

18. A. A. Toutov, K. N. Betz, M. C. Haibach, A. M. Romine, R. H. Grubbs, *Org. Lett.* **2016**, *18*, 5776.

19. B. Wang, Z. Yin, Y. Li, T.-X. Yang, X.-B. Meng, Z.-J. Li, *J. Org. Chem.* **2011**, *76*, 9531.

Concluding remarks

In this doctoral thesis, the author demonstrated the remarkable catalytic capabilities of gold nanoparticles (AuNPs) supported on citric acid-modified cellulose (F-CAC) in various organic reactions. The innovative approach of utilizing F-CAC as a support has proven to enhance the stability and catalytic activity of AuNPs.

In chapter 1, the author successfully prepared Au:F-CAC, although achieving reproducibility proved challenging. The efficiency of transferring AuNPs from PVP to F-CAC dropped significantly, highlighting the need for a reproducible synthesis method. Key factors affecting reproducibility were identified and optimized: the amount of citric acid on F-CAC, the form of the carboxylic group on citric acid, surface morphology influenced by the fibrillation process, and the method of transferring AuNPs. Establishing a reproducible procedure for synthesizing Au:F-CAC.

In chapter 2, the author demonstrates the effective use of Au:F-CAC in intramolecular hydroamination under slightly acidic conditions. The catalyst successfully catalyzed the cycloamination of amines to unactivated alkenes, yielding pyrrolidine derivatives with only 0.2 atom% Au loading. The high sensitivity of Au:F-CAC to the substitution pattern of alkenes allowed for unique chemoselective cycloamination, resulting in the formation of new compounds. The study underscores the catalyst's efficiency, reusability, and practical applicability in hydroamination reactions.

In chapter 3, the dehydrogenative oxidation of hydrosilanes was explored using Au:F-CAC in organic solvents, taking advantage of the catalyst's high tolerance to such environments. Various AuNPs sizes were prepared and studied, with significant catalytic activity observed in producing silanols with high turnover frequency. Mechanistic studies revealed the formation of catalytically active cationic Au sites through molecular oxygen adsorption. These findings provide new insights into the reaction mechanism and demonstrate the catalyst's versatility and stability in organic solvents.

In chapter 4, the author extends the findings from Chapter 3. In this chapter, the author explores the dehydrosilylation of alcohols using Au:F-CAC. The catalyst exhibited remarkable catalytic activity under mild conditions with minimal Au loading, efficiently forming silyl ethers with excellent yields. This study highlights the high catalytic activity of Au:F-CAC, overcoming the limitations of requiring excess alcohol for silyl alcohol protection applications. The work represents a significant

advancement in dehydrosilylation catalysis, offering a sustainable, efficient, and environmentally friendly approach for synthesizing functional silanol-based materials and alcohol protection applications.

These findings underscore the potential of Au:F-CAC catalysts in promoting green chemistry by enabling reactions under mild conditions with environmentally friendly aspects. The successful application of Au:F-CAC to a broad range of substrates further emphasizes their versatility and practical utility in synthetic organic chemistry. This research has laid a strong foundation for the ongoing development of AuNPs-based catalysts, demonstrating their potential to revolutionize catalytic processes with enhanced efficiency, selectivity, and environmental compatibility.

List of Publications

The content of this thesis has been published in the following papers.

1. Intramolecular hydroamination catalysed by gold nanoparticles deposited on fibrillated cellulose
Yuta Uetake, **Butsaratip Suwattananuruk**, Hidehiro Sakurai
Sci. Rep. **2022**, *12*, 20602.
DOI: 10.1038/s41598-022-24955-3

2. Dehydrogenative Oxidation of Hydrosilanes Using Gold Nanoparticle Deposited on Citric Acid-Modified Fibrillated Cellulose: Unveiling the Role of Molecular Oxygen
Butsaratip Suwattananuruk, Yuta Uetake, Rise Ichikawa, Ryo Toyoshima, Hiroshi Kondoh, Hidehiro Sakurai
Nanoscale **2024**, *16*, 12474–12481.
DOI: 10.1039/d4nr01184h

3. Dehydrosilylation of Alcohols Using Gold Nanoparticles Deposited on Citric Acid-modified Fibrillated Cellulose
Butsaratip Suwattananuruk, Yuta Uetake, Hidehiro Sakurai
Synlett **2024**,
DOI: 10.1055/a-2379-9191

Acknowledgements